Equilibrium and Transient Morphologies of River Networks: Discriminating Among Fluvial Erosion Models

by

Nicole Marie Gasparini

Submitted to the Department of Civil and Environmental Engineering
in partial fulfillment of the requirements for the degree of

Doctor of Philosophy

at the

MASSACHUSETTS INSTITUTE OF TECHNOLOGY

September 2003

Author .....
Department of Civil and Environmental Engineering
August 15, 2003

Certified by .....
Rafael L. Bras
Bacardi and Stockholm Water Foundations Professor
Thesis Supervisor

Accepted by .....
Heidi Nepf
Chairman, Department Committee on Graduate Students

Equilibrium and Transient Morphologies of River Networks: Discriminating Among Fluvial Erosion Models

by

Nicole Marie Gasparini

Submitted to the Department of Civil and Environmental Engineering
on August 15, 2003, in partial fulfillment of the
requirements for the degree of
Doctor of Philosophy

Abstract

We examine the equilibrium and transient morphology of alluvial and bedrock river networks. We apply analytical methods and an iterative model to solve for equilibrium slope-area and texture-area (in alluvial networks) relationships under different tectonic and climatic forcings. Transient morphology resulting from a change in uplift or precipitation rate is simulated using the CHILD landscape evolution model.

In alluvial networks, it is well recognized that both channel slope and mean grain size usually decrease downstream. These variables play an important role in determining sediment transport rates, and their mutual adjustment to a change in the forces that drive erosion can yield surprising results. Adjustments in grain size can lead to spatially variable channel concavity and larger transport rates on shallower slopes. As a consequence, equilibrium channel slopes may decrease under higher uplift conditions (or, similarly, faster base-level lowering). Selective erosion and deposition can cause transient channel slopes to both increase and decrease and surface texture to both coarsen and fine, all in response to a single change in forcing.

In bedrock rivers, increasing attention has been given to the role of sediment flux on incision processes. We find that all applied erosion rules (stream-power and three sediment-flux models) produce similar equilibrium morphologies, although some details lead to differences in sensitivity. On the other hand, the transient response can be much more complicated than a simple knickpoint migration when the integrated response of the sediment flux is considered. Both increasing and decreasing channel slopes can result from a single change in forcing.

Although some of the processes described by the different erosion models in this study represent conditions in very different types of rivers, two important common principles hold. First, concave graded river profiles appear to be a robust element of the landscape and fairly insensitive to the details of the erosion process. However, downstream variations in channel erodibility can alter equilibrium sensitivity to boundary conditions in ways that had not previously been considered. And second, transient conditions in the main channel are highly dependent on the entire network response. The results can be complex and counter-intuitive, highlighting that rivers are not independent of the tributaries that feed them.

Thesis Supervisor: Rafael L. Bras
Title: Bacardi and Stockholm Water Foundations Professor

Acknowledgments

My work was funded by the US Army Construction Engineering Research Laboratory (DACA 88-95-R-0020), the Italian National Research Council, the NSF Hydrology Fellowship and the NASA Earth System Science Fellowship.

I am most grateful for the never-ending patience and support of my advisor, Rafael Bras. He always had faith in me, even when I had none in myself.

It has always been my pleasure to work with Greg Tucker. He has been a great mentor and a source of constant encouragement. John Grotzinger has always been enthusiastic about my different projects and given me good perspective. Keeping up with Kelin Whipple, both in the field (running) and in discussion has been a great challenge and learning experience. His interest in my work kept me motivated. I wouldn't be a geormorphologist today without the guidance of Athol Abrahams.

Rafael always has amazing people working for him, and I have received much inspiration from all of my fellow research group-members. Of special note is Daniel Collins, whose spirit, creativity, insight, and friendship have helped me through research snafus and successes, and through New Zealand.

Many friends have helped me through this process. Thank you Rachel Adams, Steve Margulis, Guiling Wang, Karen Friedman, Mary Conway, Anke Hildebrandt, Freddi Eisenberg, Joel Johnson, Simon Brocklehurst, John MacFarlane and Sheila Frankel. Thank you Dee Siddalls for many celebrations, talks, and for always having a smile. Thank you Gretchen Jehle for being a super friend that never judges and always remembers me with a card or a call. Thank you Elaine Pagliarulo for reminding me about the important things in life and your too kind words. Thank you Vicki Murphy for listening to my problems, solving my problems, and for always having chocolate. Thank you Susan Dunne for monitoring my sanity, not letting me take things too seriously and taking me out when I needed it. Thank you Giacomo Falorni for letting me complain and reminding me it wasn't so bad. Thank you Neda Farahbakhshazad for making me feel not crazy, for making me have fun, and for so much support. Thank you Jenny Jay and Anand Patel for giving me a home, lots of love, and making me part of your family.

Thanks to my brother for making me laugh. I thank my parents for teaching me to be humble and grateful and to enjoy life.

Contents

List of Figures

List of Tables

Chapter 1

Introduction

This work investigates how the mechanics of river erosion influence the form and dynamics of a drainage basin. We consider two very different settings: rivers that are incising into bedrock and rivers with a bed and banks composed of sediment. In both settings, there are numerous theories that can be used to predict fluvial erosion rates. This study looks for the differences and similarities among landscapes produced using different erosion models. We examine the morphology of river networks which have both spatially uniform erosion rates (equilibrium conditions) and spatially variable erosion rates (transient conditions). Both analytical methods and a numerical landscape evolution model are used to investigate landscape morphology. Although all of the results presented here are theoretical and do not represent a specific location, the hope is that we can find some differences and identifying features of landscapes that are sculpted by different fluvial processes. The insights gained from this study can be applied when looking at real landscapes and interpreting past conditions or when making predictions about future conditions.

Geomorphologists have often idealized rivers into two categories: alluvial and bedrock. Alluvial rivers are formed in sediment or easily-weathered rock, and erosion rates are generally thought to be limited by the amount of material the river can transport (e.g. Gilbert (1877); Howard (1997)). For this reason, alluvial rivers are often termed transport-limited. On the other hand, bedrock rivers are actively incising into rock. Although there may be sediment in the channel, erosion rates are generally

thought to be limited by the rate at which a river can erode through bedrock. These rivers are often termed detachment-limited (e.g. Howard (1994)).

Alluvial rivers have been studied more extensively than bedrock rivers. Two important general characteristics of alluvial rivers were observed by Sternberg (1875): (1) rivers are generally concave up, that is channel slope decreases downstream, and (2) the median grain size on the channel bed generally decreases downstream. Along with Sternberg and many others, Yatsu (1955) and Hack (1957) conducted important early studies linking channel slope with grain size in alluvial rivers.

The properties of hydraulic geometry are a general unifying principle in alluvial rivers as well. Hydraulic geometry refers to the relationship between fluvial discharge and channel width, depth, slope, roughness, suspended load and velocity. All of these channel properties have been found to vary with fluvial discharge both downstream and "at-a-station"- with discharge variations at a given location. Among the pioneering studies are those published by Leopold and Maddock (1953), Wolman (1955), and Leopold et al. (1964). The theory behind hydraulic geometry is that alluvial rivers are able to shape their own channel and floodplain. These concepts are often applied but we still grapple with exactly why they hold. Specifically, the relationship between channel width and discharge was referred to by Parker (1997) as "the holy grail of river mechanics".

The rate of sediment entrainment and transport in alluvial rivers has been studied by many (e.g. Meyer-Peter and Müller (1948); Einstein (1950); Engelund and Fredsoe (1976); Milhous (1973); Bagnold (1980); Bridge and Dominic (1984) Church (1985); Lisle (1989); Parker (1990); Buffington and Montgomery (1999); Wilcock (2001)) and all data seem to support that sediment transport rates are highly dependent on the grain-size distribution of the channel bed. Sediment grains are immobile below a threshold value of applied fluvial shear stress. Above the threshold, or critical shear stress, grains are set in motion. On a bed with uniform grain sizes, the critical shear stress is well described by the Shields' curve (Shields 1936) and increases with the grain diameter. However, in a heterogeneous mixture of grain sizes, the threshold for entrainment is much more difficult to describe. One model is that of equal mobility,

which has been observed in gravel bed streams with a coarse pavement. Under flow conditions that permit entrainment of the pavement, all of the exposed grain sizes are entrained at the same critical shear stress (Parker and Klingeman (1982) and Parker et al. (1982)). Under different conditions, the interactions between different grain sizes can add a great deal of complexity to the individual threshold values. It is often observed that relatively smaller grains in a mixture become harder to entrain (in comparison with a homogeneous bed), and relatively larger grains become easier to entrain (e.g. Komar (1987); Wilcock (1998)). These details are very important in some of the results that we will present.

The processes that control fluvial incision into bedrock have not been studied in the same depth as sediment transport in alluvial rivers. Gilbert (1877) was probably the first to describe some of the important variables that control bedrock erosion and recent attention has focused on some of Gilbert's ideas. The most commonly mentioned controls on bedrock incision are: (1) quarrying or plucking, which refers to removal of large blocks from the channel bed; (2) abrasion resulting from the impact of bedload and suspended load hitting the channel bed and walls; (3) solution, or chemical weathering of bedrock; and (4) cavitation, which is the implosion of vapor bubbles due to pressure changes in the flow in regions such as waterfalls and rapids. (Some descriptions of these processes can be found in Morisawa (1968); Baker (1973); Foley (1980); Wohl (1993); Hancock et al. (1998); Sklar and Dietrich (1998); Wohl (1998); Whipple, Hancock and Anderson (2000); Hartshorn et al. (2002)). Obviously some of these processes work together. For example, plucking occurs along fractures in the bedrock. These fractures could be natural regions of weakness in the rock that are further weakened through chemical weathering and hydraulic wedging - the enhancement of joints as bedload clasts get wedged into cracks (Hancock et al. (1998)). The rate of incision into bedrock is thus a function of many variables, such as lithology, degree of jointing, sediment supply and local weathering processes.

An outstanding geomorphic question is whether or not the hydraulic geometry relationship between channel width and fluvial discharge holds in bedrock rivers. Hydraulic geometry is implicit in erosion models such as the stream-power rule, which

is often applied to estimate rates of incision into bedrock (e.g. Seidl and Dietrich (1992); Howard (1994); Rosenbloom and Anderson (1994); Tucker and Slingerland (1996); Stock and Montgomery (1999); Roe et al. (2002); Snyder et al. (2002)). The stream-power rule models incision into bedrock as a power law function of both channel drainage area and slope. The relationship between the incision rate and drainage area is derived assuming that the channel width varies directly with fluvial discharge. However, channel width often decreases locally in regions of more resistant bedrock. Overall, studies suggest that the power-law relationship between channel width and drainage does apply in bedrock channels; although width may not increase as quickly downstream as it does in alluvial rivers (Montgomery and Gran (2001); Snyder et al. (2003a); Tomkin et al. (2003); Whipple (n.d.)).

More and more, geomorphologists are finding that the division between transport-limited and detachment-limited rivers may not be so clear. In fact, some bedrock rivers may be highly influenced by the amount of sediment moving through them (e.g. Sklar and Dietrich (1998)). Thresholds for motion appear to be important in all types of fluvial channels and recent studies suggest that their role in landscape evolution can not be ignored (e.g Baldwin et al. (2003); Snyder et al. (2003b); Tucker (2003)). Further, many equilibrium models of detachment-limited and transport-limited fluvial processes predict steep bedrock channels with a higher concavity in the upper reaches of a drainage network, in comparison with the lower portions of a network that contain less concave alluvial rivers (e.g. Whipple and Tucker (2002)). However, disequilibrium conditions can result in sediment clogged channels upstream from bedrock channels (observed in the San Gabriel Mountains, California). These complications - the mechanics of erosion in transport-limited and detachment-limited channels and differences between equilibrium and disequilibrium morphologies produced using different erosion models - are explored in this thesis.

A large part of this work focuses on steady-state or equilibrium landscapes. The idea stems from a graded channel, or one that has adjusted its profile in order to transport all of its load (e.g. Mackin (1948)). When applied to the landscape, it refers to a regional balance between inputs and outputs, between erosion rates and

uplift rates, between erosion rates and base-level lowering rates, or between erosion and deposition. Equilibrium serves as a useful test for models since we have some idea about what steady-state topographies should look like.

For example, the power-law relationship between channel slope and drainage area, resulting in concave channel networks, holds in many natural drainage networks (e.g. Flint (1974); Tarboton et al. (1989); Tucker and Whipple (2002)). This relationship can be derived analytically assuming a spatially uniform erosion rate (e.g. Whipple and Tucker (1999)). Under a wide range of applied erosion processes, numerical models are able to produce realistic concavities at steady-state.

Steady-state is also a useful state to consider because it is easily defined (flux in equals flux out) and comparisons between different landscapes that are in the same state can be fairly made. However, one may question whether or not any landscapes ever reach steady state. Given the length of time that it takes for a landscape to evolve, is it reasonable to think that boundary conditions, such as climatic and tectonic forcings, can remain steady over such time-scales?

Some regions are thought to be in steady-state. For example, studies have suggested that the Central Range of Taiwan has reached a balance between long-term uplift rates and erosion rates measured through sediment records (e.g. Li (1976); Liew et al. (1990); Hovius et al. (2000)). Whipple (2001) calculated the time-scale of response to tectonic perturbation in the Central Range of Taiwan and found that is reasonable for channel profiles to have reached a "quasi-steady-state" form. Erosion rates estimated through sediment load on the whole appear to balance uplift rates in the Southern Alps of New Zealand (e.g. Adams (1985)). It is also proposed that the European Alps have reached a steady rate of exhumation, measured through fission-track dating (Bernet et al. (2001)). So there is evidence that steady-state can be reached, making it a useful case to consider but not the only case.

We will explore how the details of different fluvial processes influence landscape morphology, both at steady-state and during transitions between steady-states. Specifically, we include a two-grain size sediment transport model to describe alluvial river networks, and we include three different sediment-flux models to calculate incision

into bedrock. We solve for the equilibrium network form (slope-area relationship) resulting from different erosion models. In some cases, equilibrium sensitivity to the uplift and precipitation rates varies between erosion models (Chapters 3 and 5). Even though some of the models predict spatial variability in concavity, it is still difficult to discern between fluvial processes based on network concavity alone.

We focus a fair amount of attention on disequilibrium channels. Because equilibrium channel form is not necessarily a good indicator of process, transient landscapes might be able to tell us more about the mechanics of river erosion. Further, many landscapes are not thought to be in equilibrium. We hope to gain some insight into how networks might respond to a change in forcing so that we can better interpret the clues about the past that still remain in the landscape we see today.

Numerical experiments with the heterogeneous sediment transport model illustrate that variations in surface texture and slope can be quite complex in response to a single change in forcing (chapter 4). Similarly, when sediment flux is considered in the bedrock incision model, erosion rates vary both spatially and temporally in response to an increase in uplift rate (chapter 5). In essence, all of the transient numerical experiments allow for a spatially and temporally variable erodibility. This seemingly small consideration has important implications for landscape evolution.

Before we present the results, a brief description of CHILD, the numerical landscape evolution model used in this study (Tucker, Lancaster, Gasparini and Bras (2001); Tucker, Lancaster, Gasparini, Bras and Rybarczyk (2001)), is given in Chapter 2. Chapter 3 details the equilibrium sensitivity of transport-limited alluvial networks with multiple grain sizes using two different erosion models. We discuss the transient response in a sand and gravel alluvial network using the CHILD model in Chapter 4. In Chapter 5, we discuss both the equilibrium sensitivity and transient conditions using three different sediment-flux erosion rules to determine incision rates. All of the results are summarized in Chapter 6, and avenues for further research are presented.

Chapter 2

CHILD Model Description

Part of this thesis explores the predicted transient network response to a change in forcing; all of these results are obtained using the CHILD numerical landscape evolution model. Chapter 4 looks at changes in a heterogeneous alluvial network; the details of the sediment transport equations are given in chapter 3. Chapter 5 describes three different sediment-flux erosion rules contained in CHILD and looks at their influence on transient erosion rates and network form. In this chapter, we briefly discuss the algorithms used to model fluvial erosion.

Details of the landscape representation and some of the flow and erosion algorithms are described by Tucker, Lancaster, Gasparini, Bras and Rybarczyk (2001). Many of the processes contained in CHILD and how they shape the landscape are illustrated in Tucker, Lancaster, Gasparini and Bras (2001). The model has grown since these publications and includes a great deal of complexity that is not described in this study. For example, CHILD contains a model for lateral channel migration; its role in landscape evolution is described by (Lancaster 1998). An algorithm to model the growth of vegetation and its destruction through erosion was applied by (Collins 2002). Diffusive hillslope processes and landsliding (calculated based on the factor of safety equation (Teles et al. 2002)) are both contained in CHILD. Precipitation can be modeled simply as a constant rainfall rate, or the Poisson rectangular pulse rainfall model of Eagleson (1978) can be used (Tucker 2003). CHILD has also been expanded to explore the lateral advection of rock in fault-bend folds (Miller et al.

2002). We encourage the reader to explore these other references to fully appreciate this model.

2.1 General Description of Landscape

In CHILD, the landscape is represented by set of nodes which can be in any configuration, as opposed to a grid of regularly spaced nodes. This provides freedom to resolve the landscape at multiple resolutions, but adds some complication in determining connections between the nodes. The mesh, which refers to all of the edges that connect the nodes, is a Triangular Irregular Network (TIN) (Braun and Sambridge (1997); Tucker, Lancaster, Gasparini, Bras and Rybarczyk (2001)). Figure 2-1 illustrates a small part of a TIN. The lines between the nodes are the edges. Connectivity is determined by the Delaunay triangulation, and a mesh is constructed in which a circle connecting three points of any of the triangles in the mesh does not contain any other nodes (e.g. Du (1996)).

Every node has an elevation (z) and a surface area (a). The elevation (z) is a simple attribute assigned to every node. The area associated with a node is not as straightforward, especially in comparison with a regular grid. A node's area is determined by its voronoi cell or polygon. This is the area around a node formed by the perpendicular bisectors of all the edges connected to a node. The relationship between nodes, edges, and voronoi cells is illustrated in figure 2-1. Just as elevation can change through time, a nodes area can change in time if nodes are moving in the landscape. We do not apply this capability in any of the simulations presented here.

A landscape can be illustrated by its mesh (figure 2-2A) or by its set of voronoi cells (figure 2-2B). Many figures in this work use the mesh representation because it is able to simultaneously illustrate the topography (through the mesh) and one other landscape variable (through shading). However one should keep in mind that the variables illustrated in our figures apply to the voronoi cells and not the triangles.

Flow of water and sediment is along the steepest edge from a node (figure 2-1). The slope (S) between a node and one of its neighbors is simply the difference in

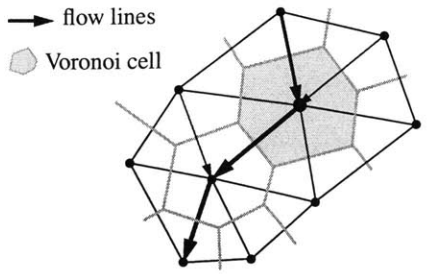

Figure 2-1: Example of TIN connectivity. The nodes are the black dots; the edges are the black lines (some with arrows) and the voronoi cell is the gray shaded area formed by the perpendicular bisectors of the edges (gray lines).

elevation between the nodes divided by the length of the connective edge. Water and sediment only flow from higher elevations to lower elevations in all of the examples we will illustrate. (CHILD has an algorithm to route flow from pits in the landscape, but this is not used in our numerical experiments.)

The drainage area (A) of a node follows from the flow directions and is computed as the sum of the voronoi cell areas of the upstream nodes, including a nodes own voronoi area. The precipitation rate (P) is constant in space and time in all of our examples. Fluvial discharge (Q) is calculated from the drainage area as:

$$Q = PA \tag{2.1}$$

Every node contains a number of other attributes which apply to this study. The parameters related to the sediment transport rate (K_t) and bedrock incision rate (K) are associated with each node. These parameters could vary in space, although they do not in this study. Information on the grain-size distribution of the surface and layers of sediment below is also specific to each node. The last section of this chapter details the algorithm which is used to track the composition of sediment layers.

2.2 Fluvial Erosion

As water flows across the landscape, it imparts a shear stress on the channel bed which can detach and transport sediment. Following other studies (e.g. Howard

(A)

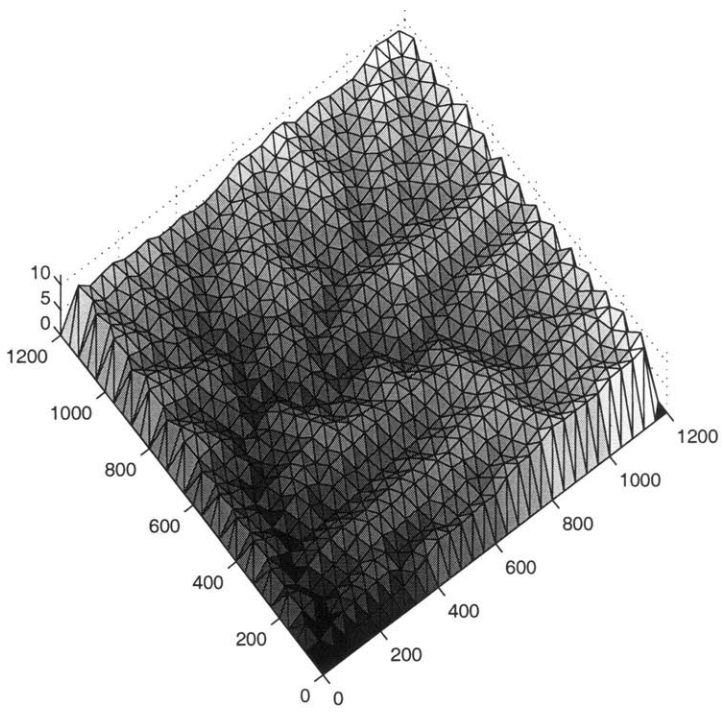

(B)

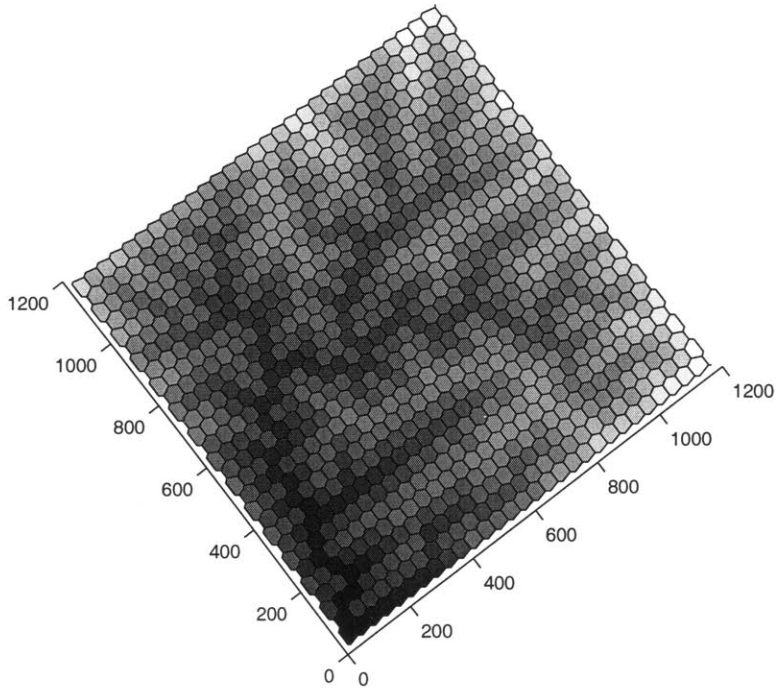

Figure 2-2: The same landscape illustrated by its mesh (A) and its voronoi cells (B). In both cases shading is by elevation.

(1994); Whipple and Tucker (1999)) we assume the following relationships hold in order to calculate the bed shear stress:

Velocity is calculated from the Manning Equation (e.g. Chow (1959)) (N is the roughness coefficient and D is channel depth):

$$V = N^{-1} D^{\frac{2}{3}} S^{\frac{1}{2}}. \tag{2.2}$$

Channel width (W) is described by hydraulic geometry (e.g. (Leopold and Maddock 1953)):

$$W = k_w Q^{0.5}. \tag{2.3}$$

Flow is steady and uniform (ρ is water density and g is gravitational acceleration):

$$\tau = \rho g D S. \tag{2.4}$$

Conservation of mass applies:

$$Q = VWD. \tag{2.5}$$

Equations 2.1- 2.5 can be rearranged to solve for the bed shear stress as a function of drainage area and slope.

$$\tau = \rho g \left(\frac{N}{k_w}\right)^{0.6} (PA)^{0.3} S^{0.7} \tag{2.6}$$

In some cases, we will calculate bed shear stress exactly as written in equation 2.6 to determine sediment transport rates. In other cases (chapter 5) we just assume that the bed shear stress follows a power law of drainage area and slope,

$$\tau = K A^m S^n, \tag{2.7}$$

and appropriate values of K, or erodibility, m, and n are explored.

Sediment transport rates are calculated for each grain size class and are a function

of the bed shear stress and surface texture properties which set the critical shear stress (τ_c). We assume that the sediment transport rate is zero when the bed shear stress is less than the critical shear stress ($\tau < \tau_c$). The details of the critical shear stress calculations and sediment transport formulas are given for each application in the following chapters. For now, the following expression for sediment transport rate is sufficient:

$$Q_{si} = f(A, S, d_i, d_{50}), \tag{2.8}$$

where Q_{si} is the volumetric sediment load of the i-th grain-size class; d_i is the representative grain size of the i-th class; and d_{50} is the median grain size or an appropriate representation of the grain-size distribution on the channel bed. We assume that once the bed shear stress surpasses the critical shear stress, sediment is easily removed from the bed and erosion rates are limited by the amount of sediment that can be transported. Erosion rates of each grain-size class are calculated individually assuming continuity of mass; this results in the following equation for the total change in elevation from transport-limited erosion:

$$\frac{\partial z}{\partial t}_{trans} = U - \frac{\sum_{i=1}^{n_d} (Q_{si}^{in} - Q_{si}^{out})}{a}, \tag{2.9}$$

where U is the uplift rate (uniform in space for all simulations); Q_{si}^{in} is the volumetric sediment load of the i-th grain-size class coming into a node; and n_d is the number of grain size classes. Erosion rates are calculated from the uppermost parts of the network downstream. In the nodes which only drain themselves, $Q_{si}^{in} = 0$. Any sediment eroded is sent downstream and both the total volume and the composition of the sediment load are tracked. Note that it is possible for erosion of one grain-size class and deposition of another to occur.

The details of the incision equations are given in chapter 5. Although the total erodibility in some of the incision equations varies as a function of the total incoming sediment load (Q_s^{in}), K is constant in space. Again, we only give a flavor for the

erosion equation here:

$$\frac{\partial z}{\partial t}_{detach} = f(A, S, Q_s^{in}). \tag{2.10}$$

Here $\frac{\partial z}{\partial t}_{detach}$ represents the erosion rate when incision into bedrock is the limiting process.

Even when erosion is considered to be detachment-limited, the sediment load is still tracked throughout the network. In all cases, both the detachment-limited erosion rate (equation 2.10) and the transport-limited erosion rate (equation 2.9) at a node are calculated and the modeled erosion rate is the minimum of the two. It's possible for a channel to be detachment-limited in some regions and transport-limited in others.

In all of the examples with multiple grain-size alluvial channels (chapter 4) the parameters used to calculate the detachment rate are set, and therefore the incision rates are very high, so that the channel is always limited by what it can transport.

2.2.1 Layering Algorithm

The texture of alluvial layers must be tracked in order to correctly model erosion and deposition of multiple grain sizes. Each node in the numerical model is composed of a number of sediment layers; sediment of each grain size can be eroded from or deposited into these layers. The top layer is the active mixing layer within which particles are entrained or deposited. Models of particle sorting on very short time scales typically define the active layer depth as a few grain diameters (e.g., Parker (1991); van Niekerk et al. (1992); Cui et al. (1996); and Hoey and Ferguson (1997)). However, this definition is inappropriate for our study because we consider average transport rates over days or years. Over longer time spans, a typical river presumably has access to significantly more near-surface sediment stored on the bed and in bars, an observation which led Paola and Seal (1995) to suggest that active layer depth scales with channel depth. Here, the depth of the active layer is simply held constant in space and time at a value much larger than the median grain diameter. We will refer to the active layer in this model as the surface layer, since its depth is held fixed

(although its texture varies in space and time). More discussion on the importance of the active layer depth and how it affects the numerical results is given in chapter 4.

Whenever sediment is eroded from the surface layer depleting it by a depth dz, the layer below is also depleted by a depth dz and this material replenishes the surface layer to its original thickness (Figure 2-3). The sediment that replenishes the surface layer has the texture of the sediment layer below. (All layers are assumed to be well mixed.) Similarly, when a depth of sediment dz is deposited into the surface layer, sediment of depth dz is first moved out of the surface layer into the layer below (Figure 2-4). The sediment moved out of the surface layer has the texture of the surface layer before deposition. (The layers below the surface layer have a maximum depth, and once this depth is reached deposition creates a new layer below the surface layer). Through selective erosion and deposition, the texture of the surface layer changes in time and space. The bottom-most layer of sediment, referred to here as the substrate, is essentially infinitely deep. The texture of the substrate does not vary spatially in any of the numerical experiments, but it does vary between experiments.

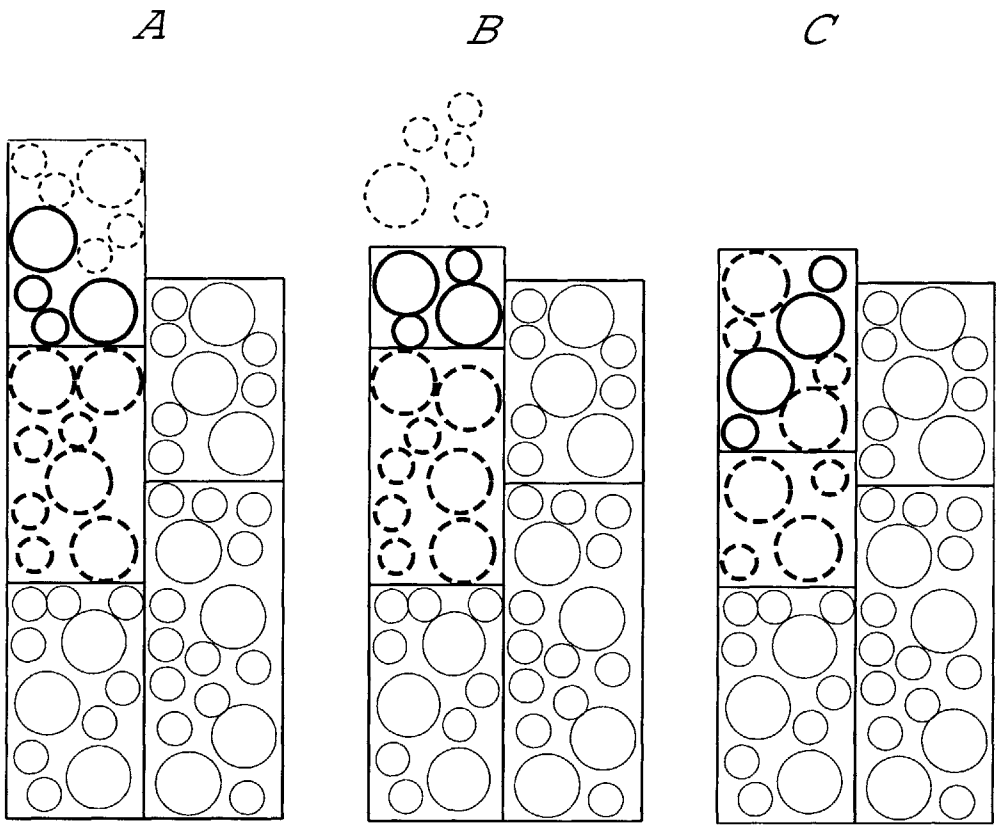

Figure 2-3: Cartoon example of erosion at a single grid cell. First the amount of material to be eroded (drawn with the thin dashed line) is calculated, shown in A. In B, the material is eroded away and becomes part of the sediment load. The surface layer is depleted. Finally, in C the surface layer is replenished with material from the layer below, drawn with a thick dashed line.

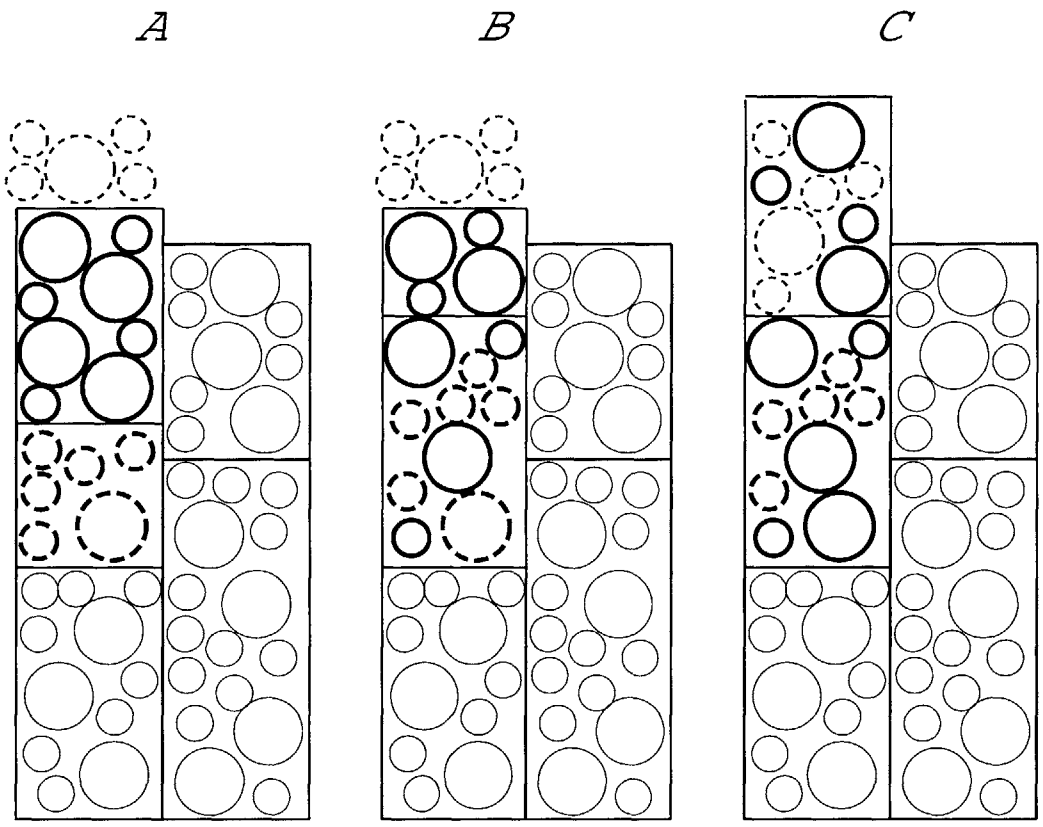

Figure 2-4: Cartoon example of deposition. Part A shows the initial condition before any changes to the layers have been made. The depth of deposited material has been calculated. The material to be deposited, shown with thin dashed lines, is not yet part of a layer. In B material has been moved out of the surface layer to make room for the new material to be deposited. The surface layer is replenished with the deposited material in C.

Chapter 3

Equilibrium Conditions in Transport-Limited Alluvial Rivers

3.1 Motivation

How does the uplift rate affect the equilibrium concavity and downstream texture patterns in a drainage network? What role does the precipitation rate play in setting equilibrium slopes and surface texture? How does grain size affect downstream fining and network concavity? How does subsurface texture affect downstream fining and network concavity? In this chapter we explore these questions using an iterative solution of the sediment transport equations to solve for the equilibrium slope-area and texture-area relationships. We investigate whether trends previously found by Gasparini et al. (1999) and Gasparini et al. (2003) hold over a wide range of parameter values. The sensitivity of these trends to the sediment-transport rule and critical shear stress rule is also explored.

Before exploring the equilibrium results produced by different multiple grain-size models, we present a general overview on equilibrium conditions in transport-limited alluvial rivers. A quick overview of the sensitivity of the slope-area relationship in alluvial networks with a single grain size (homogeneous networks) is given. The bulk of this chapter focuses on the equilibrium predictions of different multiple grain-size sediment transport models, focusing on their sensitivity to boundary conditions.

3.2 Homogeneous Sediment Transport

Entrainment and transport of sediment in rivers is a classic problem which has been studied for many years by numerous researchers (e.g. Shields (1936); Meyer-Peter and Müller (1948); Einstein (1950); Yalin (1963); Parker (1979); Bagnold (1980); Bridge and Dominic (1984); Wilcock and McArdell (1993)). Sediment transport has important consequences for many engineering applications, such as the construction of dams, dikes, and bridges. Thus the literature in this area is rich and numerous theories and equations have been put forth. Even so, the field is still full of unanswered questions and there is much to be learned.

A full background into sediment transport cannot be given in this thesis. This section is meant to familiarize the reader with some of the basic concepts in sediment transport. All equations given here refer to bedload transport; suspended load transport will not be discussed. This chapter concentrates on the relationship between sediment texture and channel slope. The texture of the channel bed is an important variable in determining bedload transport rates. However, suspended sediment flushes through the system and has less contact with the bed and therefore not much influence on the texture of the channel bed.

A general form for dimensionless bedload transport used by many researchers (e.g. Meyer-Peter and Müller (1948); Wilson (1966); Fernandez Luque and van Beek (1976)) is:

$$q_s^* = \alpha_b \left(\tau^* - \tau_c^*\right)^{p_b} . \tag{3.1}$$

In this equation, the $*$ superscript refers to dimensionless values; q_s is the volumetric sediment transport rate per unit channel width; τ is bed shear stress; τ_c is the critical shear stress value which must be surpassed for sediment transport to occur; α_b is a dimensionless, positive coefficient; and p_b is a dimensionless, positive exponent. The values of α_b and p_b vary between studies. In equation 3.1, the sediment transport rate is non-dimensionalized as:

$$q_s^* = \frac{q_s}{\sqrt{Rgd_{50}}d_{50}} \tag{3.2}$$

where R is the submerged specific gravity, equal to $(\frac{\rho_s}{\rho} - 1)$, where ρ_s and ρ are the densities of sediment and water, respectively; g is the acceleration of gravity; and d_{50} is the median grain size. τ is non-dimensionalized as:

$$\tau^* = \frac{\tau}{\rho R g d_{50}}. \tag{3.3}$$

Note that the sediment transport equation has been described in other forms. For example (e.g. Ashida and Michiue (1972); Engelund and Fredsoe (1976); Bridge and Dominic (1984)):

$$q_s^* = \alpha_b \left(\tau^* - \tau_c^*\right) \left(\sqrt{\tau^*} - \lambda_b \sqrt{\tau_c^*}\right), \tag{3.4}$$

where λ_b is a positive dimensionless coefficient. Although equations 3.1 and 3.4 are slightly different, there are two important similar points about these equations. (1) Sediment transport is proportional to an increasing function of bed shear stress. (2) There exists a threshold shear stress, below which no sediment transport takes place. These characterize the general behavior of sediment transport equations.

In this chapter, we focus on the case of dynamic equilibrium. The idea is analogous to a graded stream, implying a channel that has adjusted its profile so that, on average, all sediment transported into the channel is transported out (e.g. Mackin (1948)). If we extend this idea to a transport-limited alluvial drainage network, dynamic equilibrium requires that the sediment transport rate at any location must equal the sediment supply. Dynamic equilibrium defines a useful end-member case from which to compare model results and is often used in numerical modeling studies (e.g., Willgoose et al. (1991); Howard (1994); Tucker and Bras (1998); Ellis et al. (1999); Snyder et al. (2000)).

In this chapter we will always refer to equilibrium channels as channels in which the erosion rate is balanced by the uplift rate. An analogous way of thinking of the problem is to consider a constant-base level fall. This setting might be more appropriate when thinking about graded alluvial river networks. In this case, the erosion rate throughout the network keeps pace with the erosion rate of the channel into which the network drains. For the problem we present, uplift could be replaced

with base-level fall without changing the results we see.

Given the equilibrium condition that the transport rate at every location in the network must be just large enough to transport all of the material eroded upstream, the following equation must hold:

$$Q_s = \beta U A \ , \tag{3.5}$$

where U represents the vertical uplift rate (for all examples in this chapter uplift is constant in space) and Q_s is the volumetric sediment transport rate ($Q_s = W q_s$, where W is channel width). β represents the proportion of material entrained from the bed that is carried as bedload (versus suspended load) and equals one for all cases discussed here. Our goal is to describe the network concavity, or in other words, find the relationship between channel slope and drainage area,

$$S \propto A^{-\theta}, \tag{3.6}$$

where θ is the concavity value. The value of θ is easily found by plotting channel slope as a function of drainage area in log-log space and measuring the gradient of this relationship. Concavity has been measured in different drainage networks controlled by different fluvial processes, and its value is fairly robust, in most cases ranging between 0.4-0.7 (see Tucker and Whipple (2002) for an overview).

We rearrange equation 3.1 in the following manner to examine its expected equilibrium behavior:

$$q_s = \alpha_b \sqrt{R g d_{50}} d_{50} \left(\frac{1}{\rho R g d_{50}} \right)^{p_b} (\tau - \tau_c)^{p_b} \ . \tag{3.7}$$

The threshold term (τ_c) is now in its dimensional form and increases with grain size, as expected from Shields (1936). From herein, a value of 1.5 is used for p_b (e.g. Meyer-Peter and Müller (1948); Wilson (1966); Fernandez Luque and van Beek (1976)).

Tucker and Bras (1998) and Tucker (2003) showed that basin concavity (θ) varies directly with the threshold for entrainment. Therefore, given Shield's (1936) relation-

ship, we expect that a larger effective grain size produces a more concave basin. We illustrate this concept by investigating the end-member cases of a very small and a very large threshold for entrainment using equation 3.7, and include in the discussion sensitivity of the slope-area relationship to uplift and precipitation rates.

Equation 3.7 is expressed below in terms of volumetric sediment transport rate (Wq_s), including only the terms which contain channel slope (S), drainage area (A), and precipitation rate (P, a single mean annual precipitation rate is applied):

$$Q_s \propto W\left(\tau - \tau_c\right)^{p_b}. \tag{3.8}$$

If we assume that channel width follows the hydraulic geometry equation (equation 2.3), then

$$W \propto (PA)^{0.5}. \tag{3.9}$$

The bed shear stress relationship (equation 2.6) can be expressed as:

$$\tau \propto (PA)^{0.3} S^{0.7}. \tag{3.10}$$

Substituting equations 3.9, and 3.10 into the sediment transport relationship expressed in 3.8 gives the following expression for sediment transport rate as a function of slope, drainage area, and precipitation rate:

$$Q_s \propto (PA)^{0.5}\left((PA)^{0.3} S^{0.7} - \tau_c\right)^{p_b}. \tag{3.11}$$

This relationship can now be substituted into the equilibrium condition expressed in equation 3.5 (letting $\beta = 1$):

$$S \propto U^{0.95} P^{-0.9} A^{0.048} + \tau_c^{1.43} P^{-0.43} A^{-0.43}. \tag{3.12}$$

Although the exact values of the exponents can change in this equation depending on assumptions made about hydraulic geometry, channel velocity, and the sediment transport equation used, the trends are all similar when reasonable assumptions are

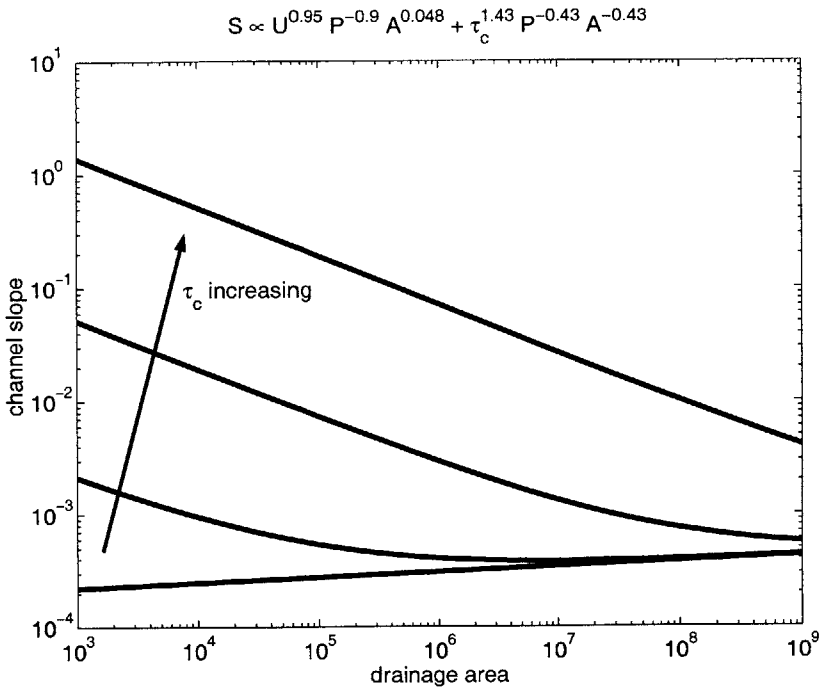

Figure 3-1: Sensitivity of the slope-area relationship for homogeneous sediment (given in equation 3.12) to variable critical shear stress values. Uplift rate and precipitation rate does not vary between the lines.

made. We express this relationship with actual values only so that magnitudes and signs of the exponents can be compared and the general trends examined. The relationship in equation 3.12 is plotted in figure 3-1. The precipitation and uplift values are the same for each line in this plot, and only the value of τ_c varies between the lines. These lines do not represent actual slope values, as many constants have been left out of equation 3.12, but the concavity trends represent those expected using a sediment transport equation of the form given in equation 3.1.

To understand figure 3-1, consider first the case when the bed shear stress is very large, and/or the critical shear stress term is very small. In this case, the first set of terms in equation 3.12 dominates:

$$S \propto U^{0.95} P^{-0.9} A^{0.048} \tag{3.13}$$

This expression describes channel profiles that are slightly convex-up (nearly straight,

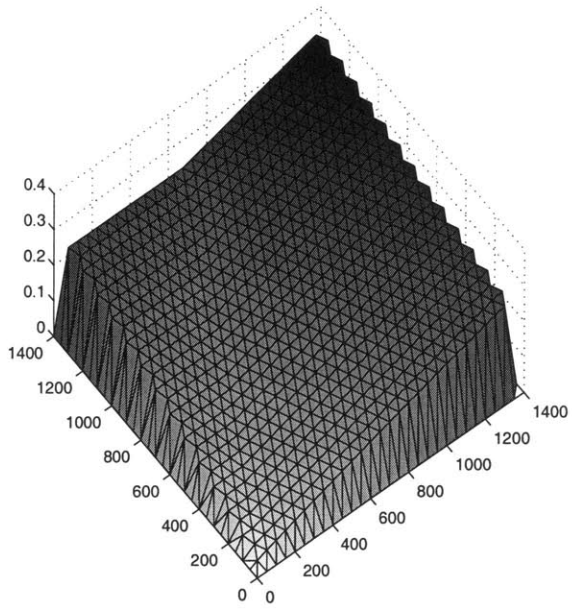

Figure 3-2: Topography evolved using the Meyer-Peter and Müller (1948) equation with no critical shear stress. The shading is by elevation. Note that this topography has no network structure, because it is actually slightly convex ($\theta = -0.038$). The concavity value is not exactly as predicted, most likely because of the scatter in the data. Because the topography is convex, no channel network exists, and flow directions are changing often.

see the bottom line in figure 3-1) and does not seem sensible when referring to eroding equilibrium channels. It does not create topographies with a network structure (Figure 3-2). Remember that this equilibrium expression represents the case when the critical shear stress is essentially zero. We expect this to be the least concave case (Tucker and Bras 1998).

All else being equal, the relationship in equation 3.13 predicts that equilibrium slopes will be steeper in drainage basins with greater uplift rates (figure 3-3A) and/or smaller precipitation rates (figure 3-3B). In the case of greater uplift rates, the equilibrium condition (equation 3.5) states that sediment transport rates need to be greater (for a given drainage area). It is intuitive then that slopes should steepen with uplift rate because more sediment needs to be transported through the network. On the other hand, if the precipitation rate increases but the uplift rate remains the same, the

same amount of sediment still needs to be transported through the network. However, the effective discharge increases (equation 2.1), therefore slopes can actually decrease in this case. The sensitivity of equilibrium slopes to variability in uplift rates and precipitation predicted by equation 3.13 seems sensible. The magnitude of change in uplift rate and precipitation rate is the same in figures 3-3A & B, and the variability in absolute slope value is also nearly the same. This is because the exponents on U and P in equation 3.13 are nearly the same (although the signs differ).

Now, consider the case when the critical shear stress dominates the equilibrium relationship in equation 3.12. This results in:

$$S \propto \tau_c^{1.43} P^{-0.43} A^{-0.43}. \tag{3.14}$$

Here channels are concave-up (top line in figure 3-1). This case produces a value of θ well in the range of concavities of real channels. When the critical shear stress is non-negligible in comparison with the bed shear stress value, we expect more concave channels than in the case when the critical shear stress is negligible, as shown by Tucker and Bras (1998).

Equation 3.14 also predicts that equilibrium channel slopes should increase with the critical shear stress value, or equivalently, grain size, as shown in figure 3-1. In other words, steeper slopes are required to transport larger grain sizes. And similarly to equation 3.13, equilibrium slopes are predicted to decline as effective precipitation increases (figure 3-4), however, slopes are less sensitive to precipitation rates when the critical shear stress term dominates (compare the exponents on P in equations 3.13 and 3.14 and figures 3-3B and 3-4). Most surprising is that the uplift rate is not contained in the equilibrium slope-area relationship expressed in equation 3.14, implying that slopes are insensitive to uplift rate. As discussed previously, one would expect slopes to increase with uplift rate. Remember that equation 3.14 represents an end-member case, however the result is still curious and deserves further attention.

Between the end-member cases, that is when critical shear stress is non-negligible (in comparison with shear stress) but not dominating, the network exhibits behavior

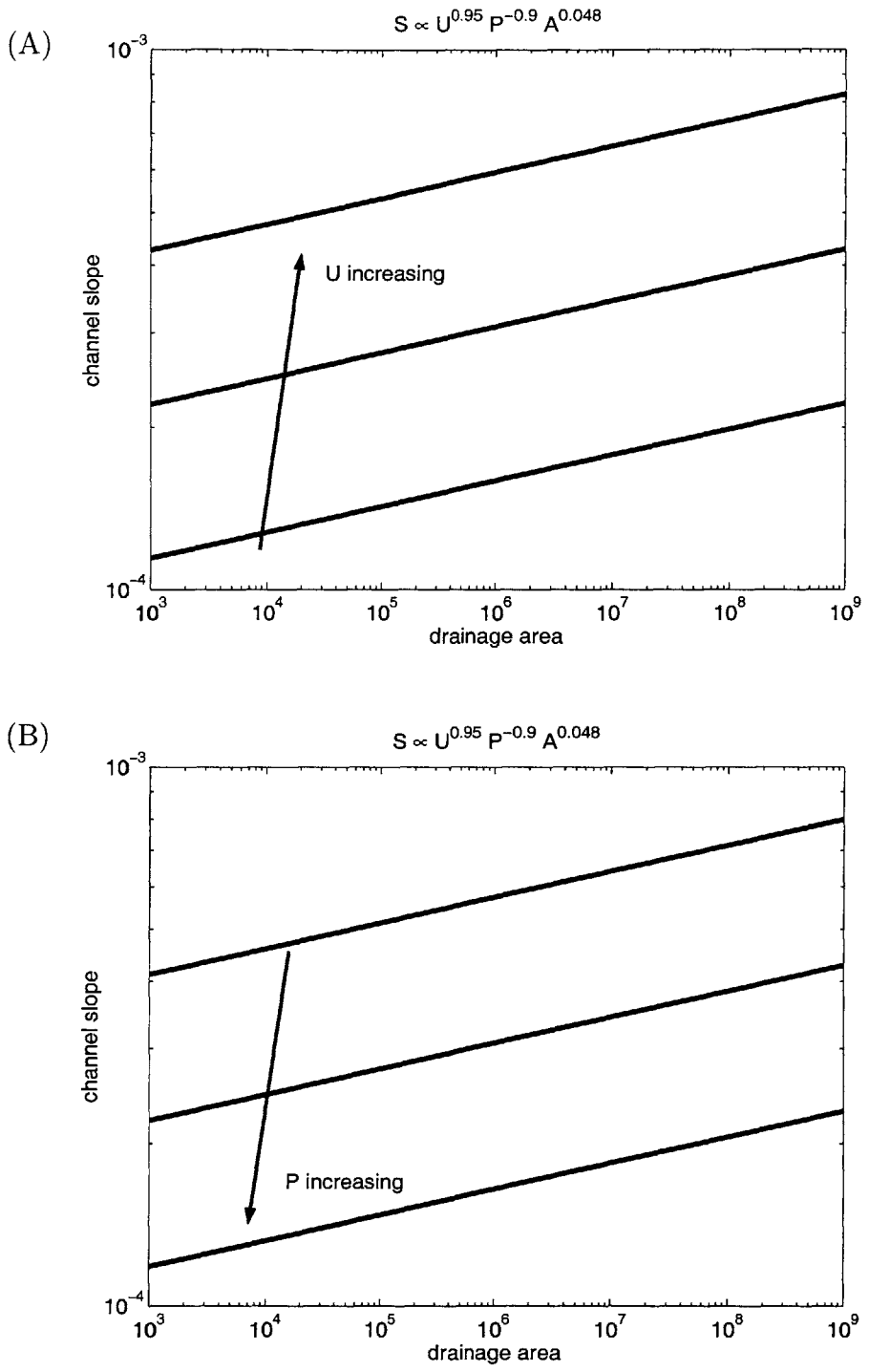

Figure 3-3: Sensitivity to uplift rate (A) and precipitation rate (B) of the equilibrium slope-area relationship when shear stress is much greater than critical shear stress (equation 3.13)

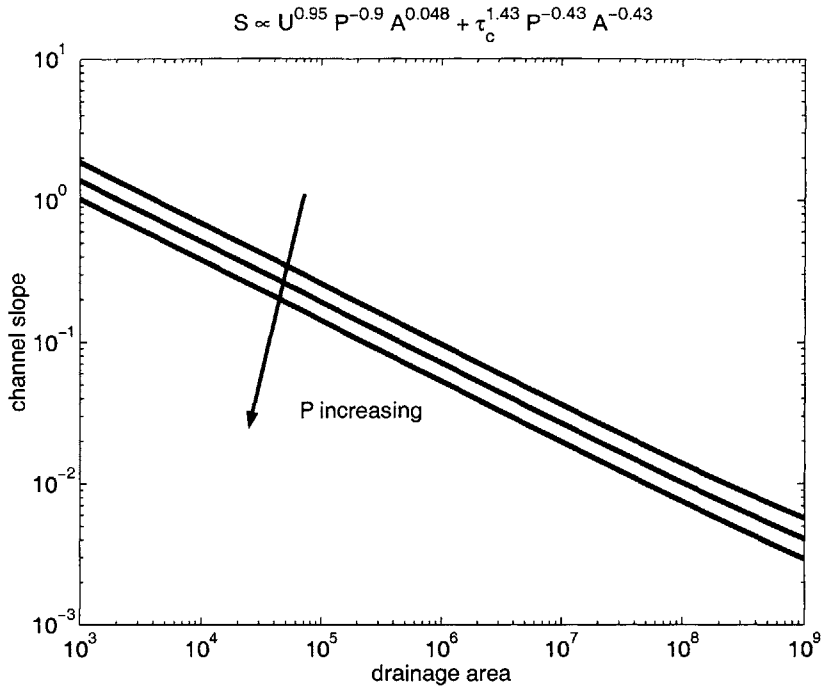

Figure 3-4: Sensitivity to precipitation rate of the slope-area relationship for homogeneous sediment (given in equation 3.12) when the critical shear stress value is large.

of both end-members and channel concavity is not constant throughout the network. For example, the middle lines in figure 3-1 exhibit decreasing slopes with drainage area at smaller values of drainage area, but tend to zero concavity at high drainage areas. This makes sense given equation 3.12. At small drainage areas, the factor containing τ_c (equation 3.14) dominates and the channels are concave, whereas at large drainage areas, the term without τ_c (equation 3.13) dominates, and channels are nearly straight. The importance of each term in equation 3.12 depends on the magnitude of the critical shear stress value, as well as the uplift and precipitation values.

3.3 Equilibrium in a Heterogeneous Sediment Mixture

In the previous sections we described sediment transport of a single grain size and the conditions which hold under uniform erosion rates in a homogeneous transport-

limited drainage network. In the next sections we expand this theory to transport of multiple grain sizes. In all cases we consider only two grain sizes. We are not able to solve for the slope-area relationship analytically; a description of our method used to arrive at the equilibrium relationship between slope and drainage area (as well as the downstream changes in grain size) is given.

Interactions between grain sizes makes transport of sediment mixtures much more complex than that of homogeneous sediment. Studies have shown that larger grains often become easier to entrain (the critical shear stress value decreases in comparison with the homogeneous value) in the presence of smaller grains because they stand-out above the bed. Similarly, smaller grains become harder to entrain (the critical shear stress value increases in comparison with the homogeneous value) in the presence of larger grains because they can get hidden amongst the larger sediment (e.g. Komar (1987), Wilcock (1998)). How exactly the critical shear stress varies in a mixture depends on the distribution of grain sizes on the bed. Just as there is no single sediment transport equation, there is no universal method for determining the critical shear stress for entrainment of sediment mixtures.

In the results presented here, we consider the case of a two grain-size mixture. The basic idea of equilibrium remains the same, that is, in a transport-limited river network equilibrium conditions require the sediment transport rate at every location to be just large enough to carry both the sediment being fed in upstream of a location and the sediment being eroded at that location. The rate of sediment eroded at every location must be exactly equal to the uplift rate in order for equilibrium to hold. This condition is expressed in equation 3.5 for the homogeneous case and is generalized to a sediment mixture in the following expression:

$$Q_s^{total} = \beta U A, \tag{3.15}$$

where Q_s^{total} is the total volumetric sediment transport rate, or

$$Q_s^{total} = \sum_{i=1}^{n} Q_{si}, \tag{3.16}$$

where the index i describes the i-th grain-size class. We assume from this point forth that $\beta = 1$. We have no method for portioning this term for each grain size. One might assume that the proportion of material carried as bedload would be higher for larger grain sizes, in comparison with smaller grain sizes that are more likely to get suspended. However, we do not tackle this problem in our study.

In order to proceed, we need an equilibrium condition for each value of Q_{si}. We consider only the case where the texture of the substrate material does not vary spatially. This implies that the composition of the material feeding the channel, and therefore the composition of the material which must be eroded and transported at every location in the network, must be that of the substrate. Given this condition, the equilibrium sediment transport relationship for each grain-size class is expressed as

$$Q_{si} = f_{subi} UA, \tag{3.17}$$

where f_{subi} refers to the proportion of the i-th grain-size class in the substrate material. In the case of two grain sizes, there are two equilibrium equations which must hold:

$$Q_{s1} = f_{sub1} UA \quad \text{and} \tag{3.18}$$

$$Q_{s2} = (1 - f_{sub1}) UA \ . \tag{3.19}$$

Q_{si} is a function of bed shear stress (which is itself a function of drainage area and local slope) and surface texture (exact equations for Q_{si} are given in the following sections). Ideally, these two equations could be rearranged to solve for slope and surface texture as a function of drainage area. However, the presence of a variable threshold makes it impossible to solve these relationships analytically. Instead, we rearrange equations 3.18 and 3.19 to get the following equation:

$$\frac{Q_{s2}}{1 - f_{sub1}} = \frac{Q_{s1}}{f_{sub1}} \ . \tag{3.20}$$

Using equations 3.18, 3.19, and 3.20, along with the bed shear stress equation (equation 2.6) and the particular sediment transport and critical shear stress rules being

used, we have developed a method to iteratively solve for the equilibrium downstream slope and texture relationships. The steps of our method are described below.

1. An appropriate range of surface texture values are defined. Surface texture is expressed as f_1, which represents the proportion of the first grain-size class in the surface layer. Equilibrium conditions do not exist for the entire range of surface textures, that is $0.0 \leq f_1 \leq 1.0$. The range over which f_1 is defined varies depending on the parameters used. (In all of the cases, we find this range through trial and error.)

2. Given the surface texture, the critical shear stress to entrain each sediment grain size (τ_{ci}) is found.

3. The chosen erosion equation, as a function of shear stress, can be substituted into equation 3.20. The equilibrium condition can be rearranged to find an expression for the bed shear stress as a function of surface texture (chosen in step 1) and critical shear stress for each grain size class (calculated in step 2). We can now calculate the bed shear stress value, given the surface-texture, that satisfies the equilibrium conditions in equation 3.20. (For an example of an equilibrium shear-stress relationship, see equation 3.25.)

4. Bed shear stress (step 3) and surface texture (step 1) provide the sediment transport rate. Once the sediment transport rate is known equation 3.18 or 3.19 can be used to calculate the drainage. **We now have the relationship between surface texture and drainage area.**

5. The drainage area and equilibrium bed shear stress at that drainage area are now known. Finally, we rearrange the shear stress equation 2.6 to solve for local slope, given the drainage area and bed shear stress:

$$S = \left(\frac{\tau}{\rho g (\frac{n}{k_1})^{0.6} (P)^{0.3} (A)^{0.3}} \right)^{\frac{1}{0.7}}. \tag{3.21}$$

The relationship between local slope and drainage area is now defined.

In the sections below, we plug actual sediment transport equations into this method to test their equilibrium sensitivity to uplift rate, precipitation rate, and grain size.

3.4 Meyer-Peter Müller with Komar Hiding Function

We have already introduced the non-dimensional form of the Meyer-Peter Müller transport equation (equation 3.1). As stated, this equation is based on homogeneous sediment transport. For homogeneous sediment transport, $\alpha_b = 8$, $\tau_c^* = 0.047$, and $p_b = 1.5$. The difficulty in applying this equation to a mixture of grain sizes is in defining τ_c. To describe the critical shear stress in the Meyer-Peter Müller equation, we use results from a study by Komar (1987). In his study, Komar looks at sediment entrainment data from a number of studies of gravel-bed rivers and sand-bed rivers containing some fine gravel (data from Milhous (1973); Carling (1983); Hammond et al. (1984); Egiazaroff (1965); and Day (1980)). Komar found that the threshold for motion of the median-grain size (d_{50}) was approximately the same as if the median-grain size were on a homogeneous bed and followed the Shields curve (Shields 1936). Grains larger than the median-grain size were entrained at smaller shear stress values than if they were on a homogeneous bed, and grains smaller than the median-grain size were entrained at larger shear stress values than if they were on a homogeneous bed. He developed an expression for the non-dimensional shear stress for entrainment of each grain size (here referred to as τ_{ci}^*, referred to as θ_{ti} by Komar (1987)). The relationship for τ_{ci}^* found by Komar is

$$\tau_{ci}^* = a\left(\frac{d_i}{d_{50}}\right)^b, \tag{3.22}$$

where a and b are parameters dependent on the mixture properties. The critical shear stress is non-dimensionalized as in equation 3.3, except that d_{50} is replaced with d_i, the grain size for which entrainment is calculated. Komar (1987) found that in the

studies of gravel bed rivers (Milhous (1973); Carling (1983); Hammond et al. (1984)), b varied between -0.71 and -0.68 and $a = 0.045$. In the sand-bed studies (flume data from Day (1980)), b varied between -0.66 and -0.53, and a varied between 0.026 and 0.047. In all the results presented in this section, we consider only gravel-grain sizes and use values of $b = -0.7$ and $a = 0.045$. We found that the trends in the results were not sensitive to these values, as long as $b \neq -1$, which gives the result that τ_{ci} is no longer a function of d_i.

Plugging the expression for critical shear stress into the Meyer-Peter Müller equation (3.7) (with the parameter values stated above) and converting it into a volumetric sediment transport rate we get the following expression:

$$Q_{si} = \frac{8W f_i}{\rho^{1.5} Rg} \left(\tau - \tau_{ci}\right)^{1.5}, \tag{3.23}$$

where

$$\tau_{ci} = (\rho R g d_{50}) a \left(\frac{d_i}{d_{50}}\right)^b. \tag{3.24}$$

With these expressions, we proceed to the equilibrium solution. (Note that d_{50} is calculated in a standard way by interpolation using the log of the grain sizes (phi scale).)

In all examples we use two grain-size fractions. In order to obtain an equilibrium solution, we need to define the texture of the substrate; that is we need values for d_1, d_2, and f_{sub1}. (d_1 is the coarser grain size and each grain size is calculated as the geometric mean of a grain size range.) Following the procedures outlined in section 3.3, over the range of possible surface textures (based on the contents of the substrate material), we calculate the critical shear stress for entrainment of each grain size using equation 3.24 (step 2). With this information, (substrate texture, surface texture, and critical shear stress values) we can calculate surface shear stress, given a precipitation rate (step 3). The relationship for equilibrium shear stress using the

Meyer-Peter Müller equation is:

$$\tau = \frac{\left(\frac{f_1}{f_{sub1}}\right)^{2/3} \tau_{c1} - \left(\frac{f_2}{f_{sub2}}\right)^{2/3} \tau_{c2}}{\left(\frac{f_1}{f_{sub1}}\right)^{2/3} - \left(\frac{f_2}{f_{sub2}}\right)^{2/3}}. \tag{3.25}$$

This equation is obtained by substituting the Meyer-Peter Müller sediment transport equation (3.23) and the critical shear stress relationship (3.24) into the equilibrium relationship expressed in equation 3.20; this relationship is rearranged to solve for bed shear stress as it is expressed in equation 3.25. Solving for the equilibrium bed shear stress using equation 3.25, we combine this value with the surface texture to calculate a sediment transport rate, and therefore, the drainage area (step 4). Once the drainage area is known, we have the relationship between median grain size and drainage area. Finally, we calculate the slope from the drainage area and shear stress values, to describe the network morphology.

Sensitivity of the equilibrium slope-area and texture-area relationships is explored below. All of the results shown are found using the iterative solution. We do not show results from numerical simulations using the CHILD model, but all of the simulations that we have performed with CHILD agree with the predictions from the iterative model.

3.4.1 Equilibrium Network Sensitivity to Uplift Rate/Erosion Rate

In this section we use the equilibrium relationships described above for the Meyer-Peter Müller equation with two grain sizes to explore the effect of uplift rate on the equilibrium morphology and surface texture of drainage networks. (At equilibrium, higher uplift rates, or faster base-level fall rates, imply higher erosion rates. This is worth bearing in mind as the results are presented.) All of the results shown in this section solve for the slope-area and d_{50}-area relationships using the iterative method. In all of the results, a precipitation rate of 1.0m/yr falling over 100 days was used. The texture of the subsurface varies between the examples.

In all cases, the equilibrium solution for only a finite range of sediment transport rates. Because the sediment transport rates correspond to different drainage areas for different uplift rates (or base-level lowering rates), the equilibrium solution exists over larger drainages areas for lower uplift values. This is a result of equation 3.15, which states that for a given drainage area, as uplift rates increase, sediment transport rates increase. Therefore, the same sediment transport rate can be the equilibrium solution for a large drainage area with low uplift rates, or for a smaller drainage area with larger uplift rates. Therefore, equilibrium solutions for different uplift rates do not entirely overlap in drainage area space. Comparisons between networks are only made where the solutions exist at the same drainage area.

The first example shows the sensitivity to uplift rate of the slope-area and d_{50}-area relationships for a network with a substrate composed of a mixture of 20% grains in the 150-100mm range (d_1=123mm) and 80% grains in the 100mm-50mm range (d_2=71mm) (figure 3-5). With this grain size composition, at smaller drainage areas, the slope is essentially unaffected by changes in uplift rate (figure 3-5A). At larger drainage areas, channel slope increases with uplift rate (figure 3-5A). However, for all drainage areas, a larger uplift rate always implies a smaller median grain size (figure 3-5B). In all of the networks, median grain size decreases downstream, even though the composition of the transported load is the same everywhere in the network and equal to the composition of the substrate material.

The sensitivity of the slope-area relationship in figure 3-5A is predicted from the sensitivity of the Meyer-Peter Müller equations with a single grain size (described in section 3.2). The homogeneous analysis predicted that when the critical shear stress plays an important role in determining the sediment transport rate, the equilibrium slope-area relationship is not dependent on uplift rates, because the entrainment criterion dominates the transport criterion. Figure 3-6 illustrates the equilibrium bed shear stress and critical shear stress values for the solution with U=0.5mm/yr. (This relationship follows the same pattern for each uplift value.) In the smaller drainage areas, the value of τ and τ_{c1} are very similar (figure 3-6). In this region equilibrium slopes do not vary with uplift rates. However, in larger drainage areas, the required

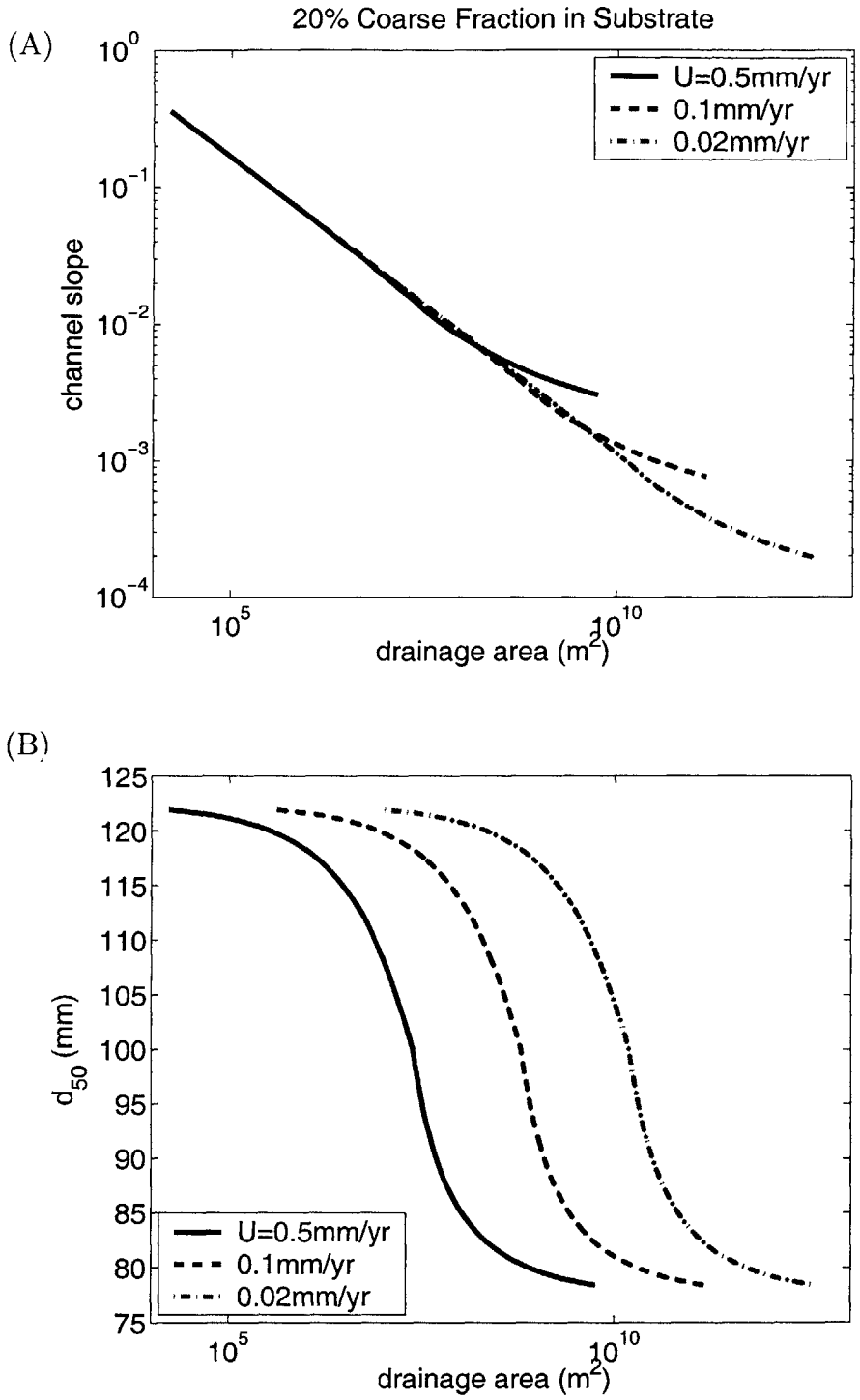

Figure 3-5: Sensitivity of equilibrium slope-area relationship (A) and d_{50}-area relationship (B) to different uplift values (see legend) for networks with 20% of the coarsest fraction in their substrate. Meyer-Peter Müller sediment transport equation with Komar critical shear stress rule is used. (Precipitation rate = 1m/yr falling over 100 days; coarse fraction=150-100mm; fine fraction=100-50mm)

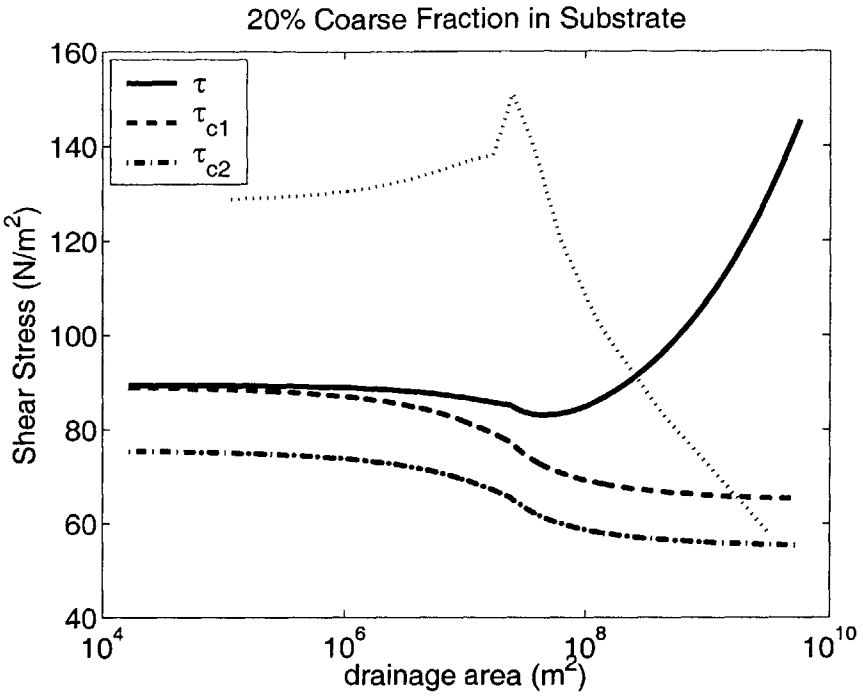

Figure 3-6: Equilibrium bed shear stress and critical shear stress values for the example shown in the figure 3-5 with uplift=0.5mm/yr. Concavity values are scaled to show on figure and range between 0.2 to 0.5 - see solid line in figure 3-7 for exact concavity values.

increase in sediment transport rate is accomplished by drastically increasing bed shear stress and the value of the critical shear stress is no longer important (figure 3-6). In this region equilibrium channel slope does increase with uplift rate (figure 3-5A).

Figure 3-7 illustrates changes in network concavity for the same data shown in figure 3-5A. As explained, the iterative method first chooses a surface texture, and then calculates equilibrium bed shear stress, drainage area, and slope based on that surface texture (and other set parameters). Because all calculations are based on surface texture, calculation of concavity is also made over surface texture regions. This allows for an equivalent comparison between changes in network concavity as uplift rate varies. Figure 3-7 illustrates downstream changes in concavity. We calculate θ over regions in the network which have the same range in median grain size. The trend in concavity is exactly the same for each value of uplift, and is only shifted in drainage area space.

Channel concavity is closely linked to the difference between bed shear stress and

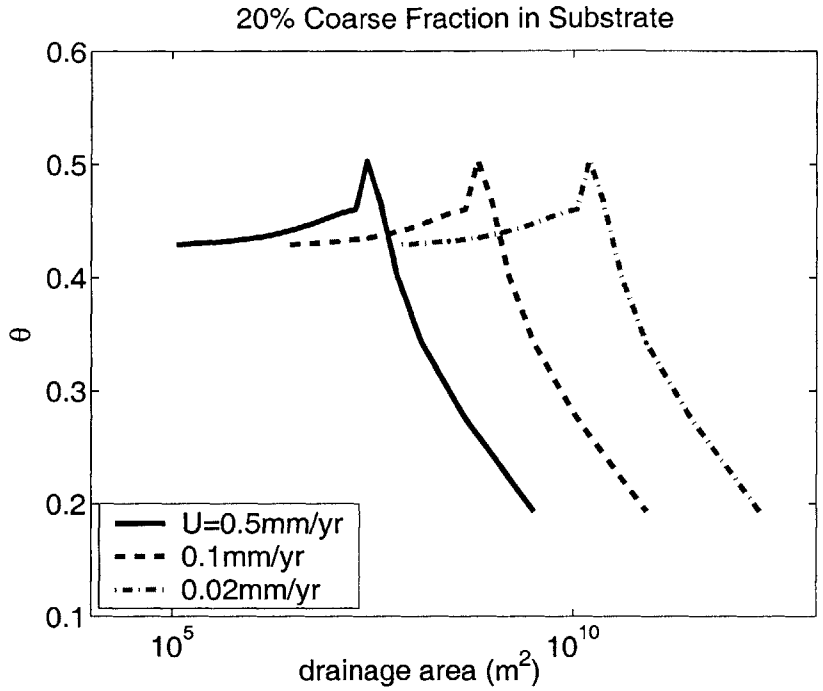

Figure 3-7: Variation in concavity of the slope-area relationships shown in figure 3-5A.

critical shear stress, as expected from the homogeneous theory given in section 3.2. The dotted line in figure 3-6 shows the pattern of change in θ for this example. (This dotted line is the same as the solid line in figure 3-7 except that in figure 3-6 the concavity is scaled so that the trend can be seen on the shear stress plot.) In smaller drainage areas, both bed shear stress and critical shear stress are decreasing downstream, and their values are similar. In this region, channel concavity is slightly increasing, and remains relatively high (see figure 3-7 for actual concavity values). The region in which critical shear stress declines most rapidly in figure 3-6 corresponds to the region of rapid change in d_{50} (figure 3-5). Because critical shear stress is decreasing, slopes can decrease more rapidly, causing channel concavity to increase (peak in concavity values, or dotted-line, in figure 3-6). However, at larger drainage areas, bed shear stress starts increasing while critical shear stress is still decreasing. As previously discussed, in this region the critical shear stress does not have as much influence on the sediment transport rate, so channel concavity decreases and channels slopes are influenced by the uplift rate (figure 3-5A).

The sensitivity of the network properties are not dependent on the value of the

uplift rate. We have explored different magnitudes of change in uplift rate, and the same trends in slope changes, concavity, and grain size result.

The concavity of the network is somewhat affected by the grain size ranges, and this affects changes in slope with uplift rate. Figure 3-8 is similar to figure 3-5, except that the range of coarser grain sizes is expanded, therefore making d_1 larger (158mm). This causes concavity to increase to a larger value (figure 3-10) than in the first example (figure 3-7). Where the concavity is high, channel slopes are decreasing rapidly (figure 3-8A) and there is a small region in which channel slope actually increases with decreasing uplift values. This is a very surprising result and only possible because of the decrease in critical shear stress downstream (figure 3-9). We realize this is a very local result and that the increase in channel slope with decrease in uplift rate is not very extreme. However, given that the result is so unexpected, we feel it is worth pointing out.

When the substrate is composed of more coarse material (f_1 is larger), and therefore more coarse material needs to be transported at equilibrium, the results are similar to the cases already discussed. Figure 3-11 illustrates the network morphology and texture changes in a network exactly the same as that in the first example, except that in this case the substrate contains 50% (versus 20% in figure 3-5) of the coarser material. The equilibrium solution is defined for a smaller range in grain sizes as the amount of coarse material in the substrate increases (figure 3-5B versus figure 3-11B).

In the drainage network transporting coarser material, changes in channel slope with uplift rate are as expected given the previous examples. There is a region in which channel slope does not vary with uplift rate (smaller drainage areas in figure 3-11A), and this is the region in which bed shear stress and critical shear stress have similar values (figure 3-12). In this case there is no region in which bed shear stress declines downstream, and there is also no region in which channel concavity increases downstream (figure 3-13).

As the last example in this section, we illustrate changes in a network which needs to transport 80% of the coarse fraction. Figure 3-14A illustrates that for this very

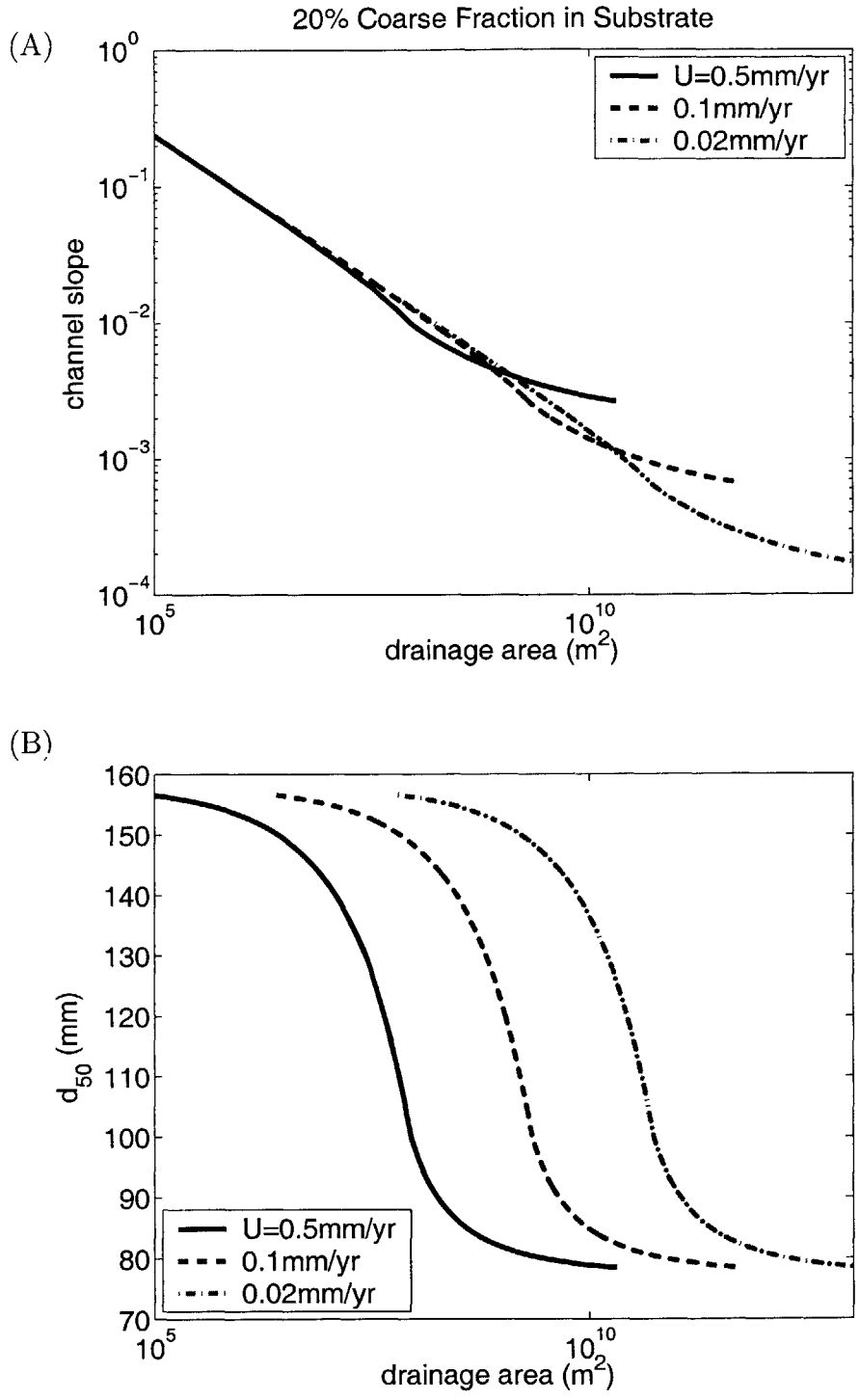

Figure 3-8: This figure is almost identical to figure 3-5 except that here the coarsest fraction varies between 250mm and 100mm.

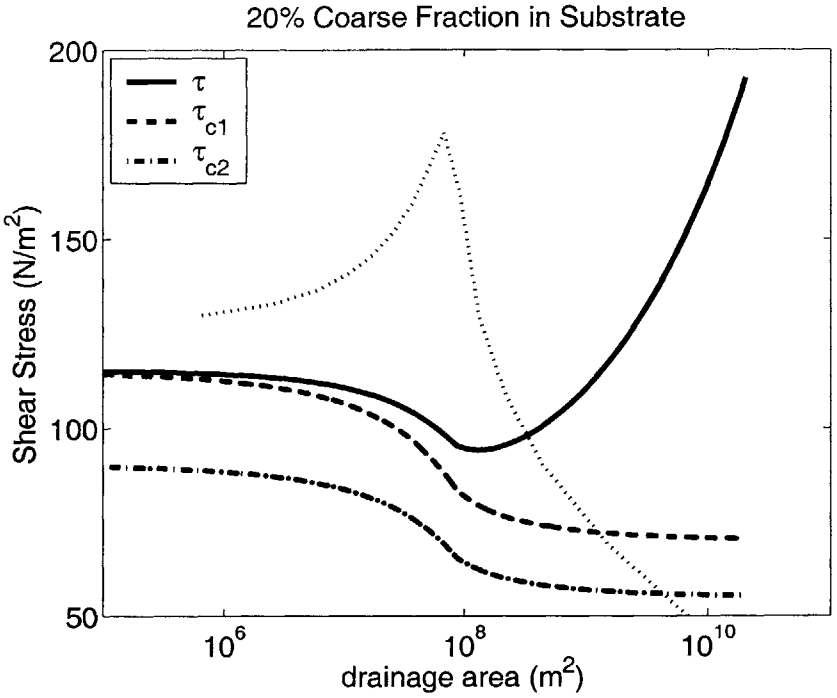

Figure 3-9: Equilibrium bed shear stress and critical shear stress values for the example shown in the figure 3-8 with uplift=0.5mm/yr. Dotted line illustrates the trend in concavity values. See solid line in figure 3-10 for exact concavity values. Here they are scaled to show on figure, but actual values range between 0.15 and 0.6.

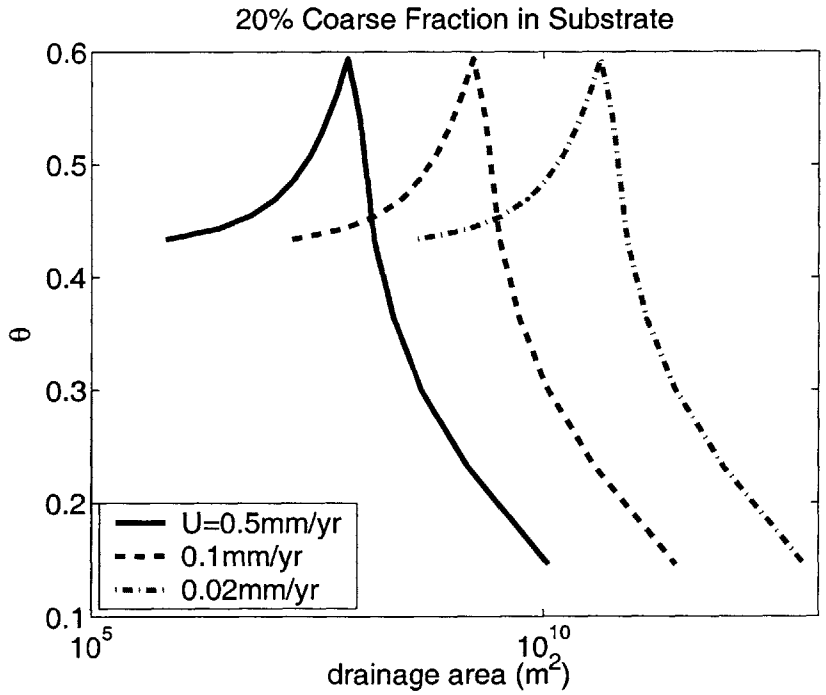

Figure 3-10: Variation in concavity (θ) for the slope-area relationships shown in figure 3-8A. See text for details of calculation.

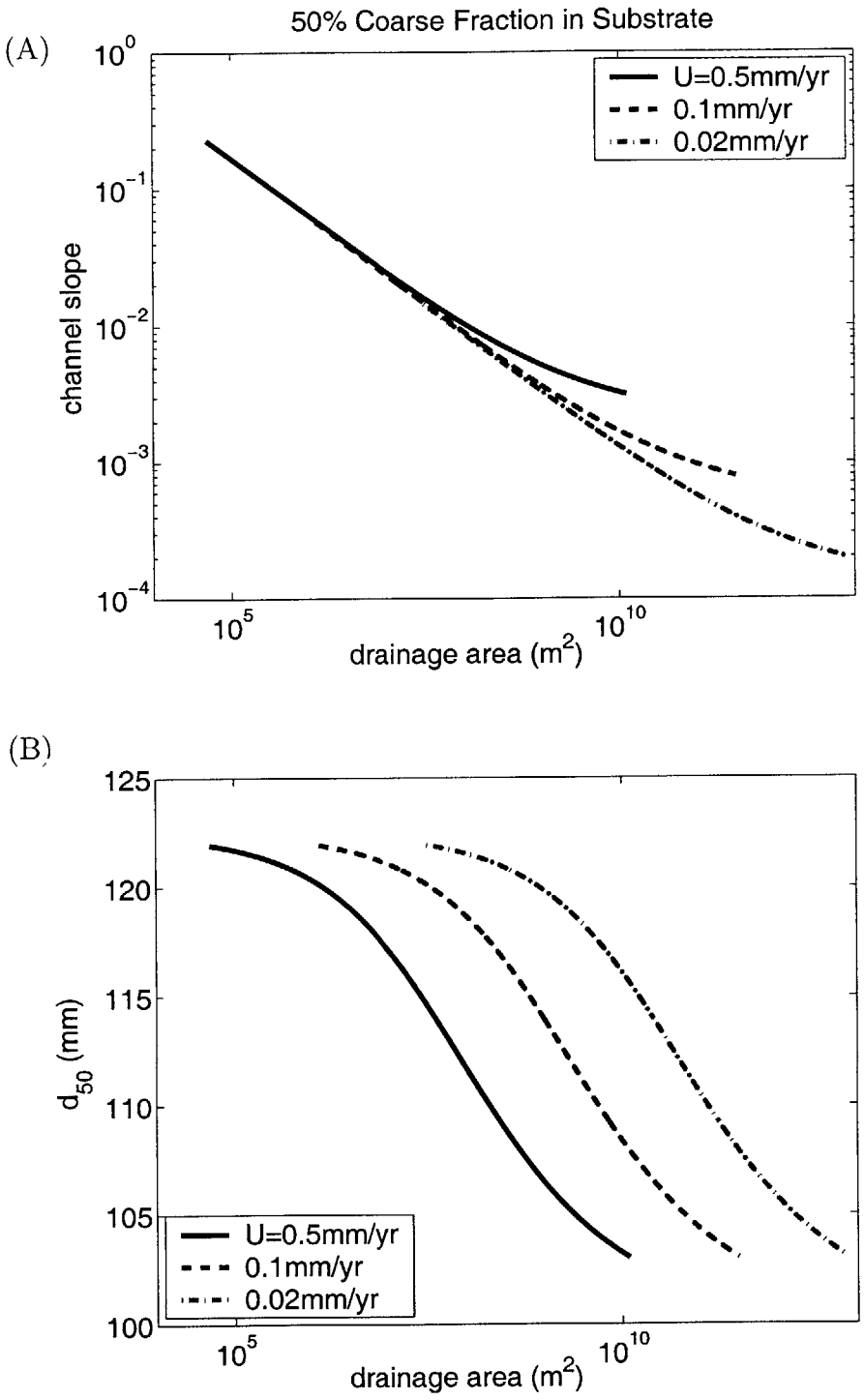

Figure 3-11: Sensitivity of equilibrium slope-area relationship (A) and d_{50}-area relationship (B) to different uplift values (see legend) for networks with 50% of the coarsest fraction in their substrate. Meyer-Peter Müller sediment transport equation with Komar critical shear stress rule is used. (Precipitation rate = 1m/yr falling over 100 days; coarse fraction=150-100mm; fine fraction=100-50mm)

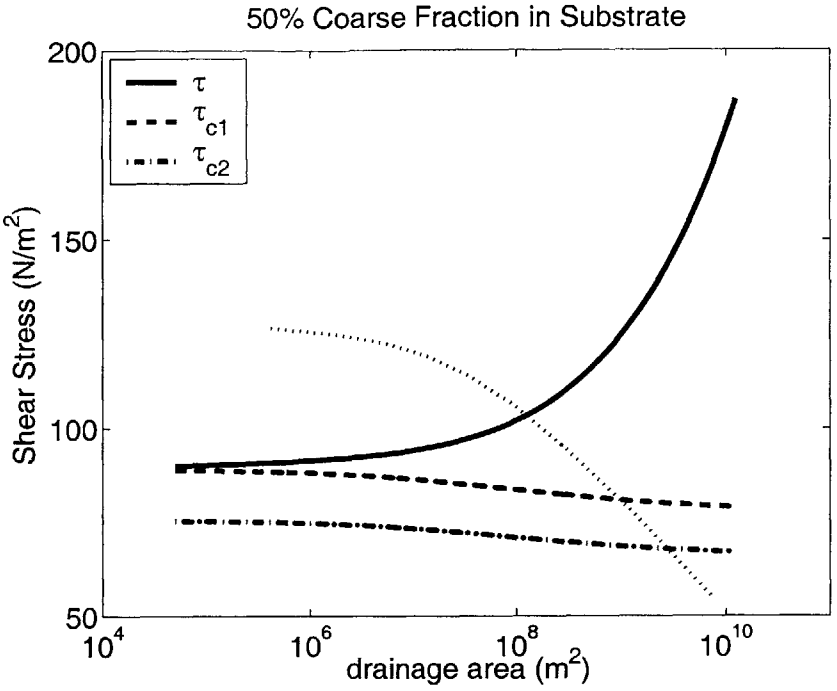

Figure 3-12: Equilibrium bed shear stress and critical shear stress values for the example shown in the figure 3-11 with uplift=0.5mm/yr. Dotted line illustrates the trend in concavity values which is shown as a solid line in figure 3-13. Concavity values are scaled to show on this figure, but actual values range between 0.18 and 0.42.

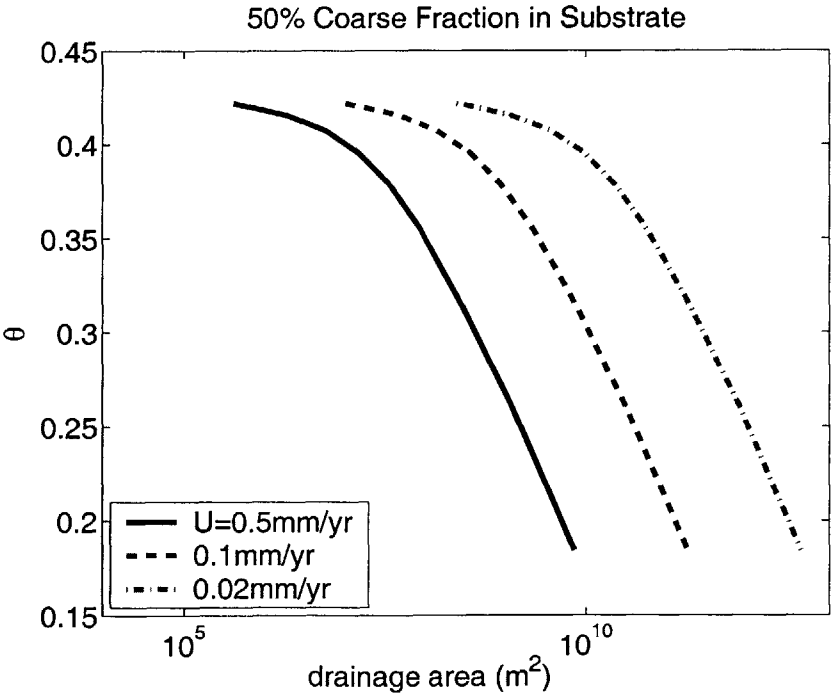

Figure 3-13: Variation in concavity (θ) for the slope-area relationships shown in figure 3-11A. See text for details of calculation.

coarse example, in all cases channel slope increases with uplift rate. The bed shear stress is diverging from the critical shear stress for all drainage area values in this solution (figure 3-15), and therefore the variation in channel slope with uplift rate agrees with the trends already illustrated. In this case, the equilibrium solution is defined for an even smaller range of grain sizes (figure 3-14B) than in the case with 50% coarse material in the substrate (figure 3-11B).

3.4.2 Sensitivity to Precipitation Rate

Variation in precipitation does not have any surprising results on equilibrium morphology or channel bed texture. Figure 3-16 illustrates sensitivity to precipitation rate in a basin with 20% coarse material in the substrate (d_1=123mm; d_2=71mm). For a given drainage area, channel slope decreases with increasing precipitation rate (figure 3-16A). Fluvial discharge increases with the precipitation rate, and if the slope remained the same (ignoring grain-size changes for a moment), this would cause bed shear stress to increase and more material to be transported. However, equilibrium transport rates do not change with changes in precipitation rate, therefore to compensate for the increase in fluvial discharge, channel slopes decrease. The amount of change in slope for different precipitation values is somewhat dampened by the change in surface texture (figure 3-16B). The channel bed coarsens (d_{50} increases) as precipitation increases. Coarsening of the channel bed increases the critical shear stress and therefore limits transport rates. However, the change in critical shear stress (see figure 3-6, which has the same trend in τ and τ_c as this example) is not great enough to significantly dampen changes in slope with precipitation rate in comparison with the homogeneous case, in which critical shear stress doesn't change.

Slopes vary slightly more with precipitation rate at larger drainage areas (figure 3-16), as is predicted by the homogeneous theory. When the critical shear stress is small (higher drainage areas), the first term in the homogeneous slope-area equation (3.12) is more important in determining channel slopes and this term is more sensitive to precipitation rate.

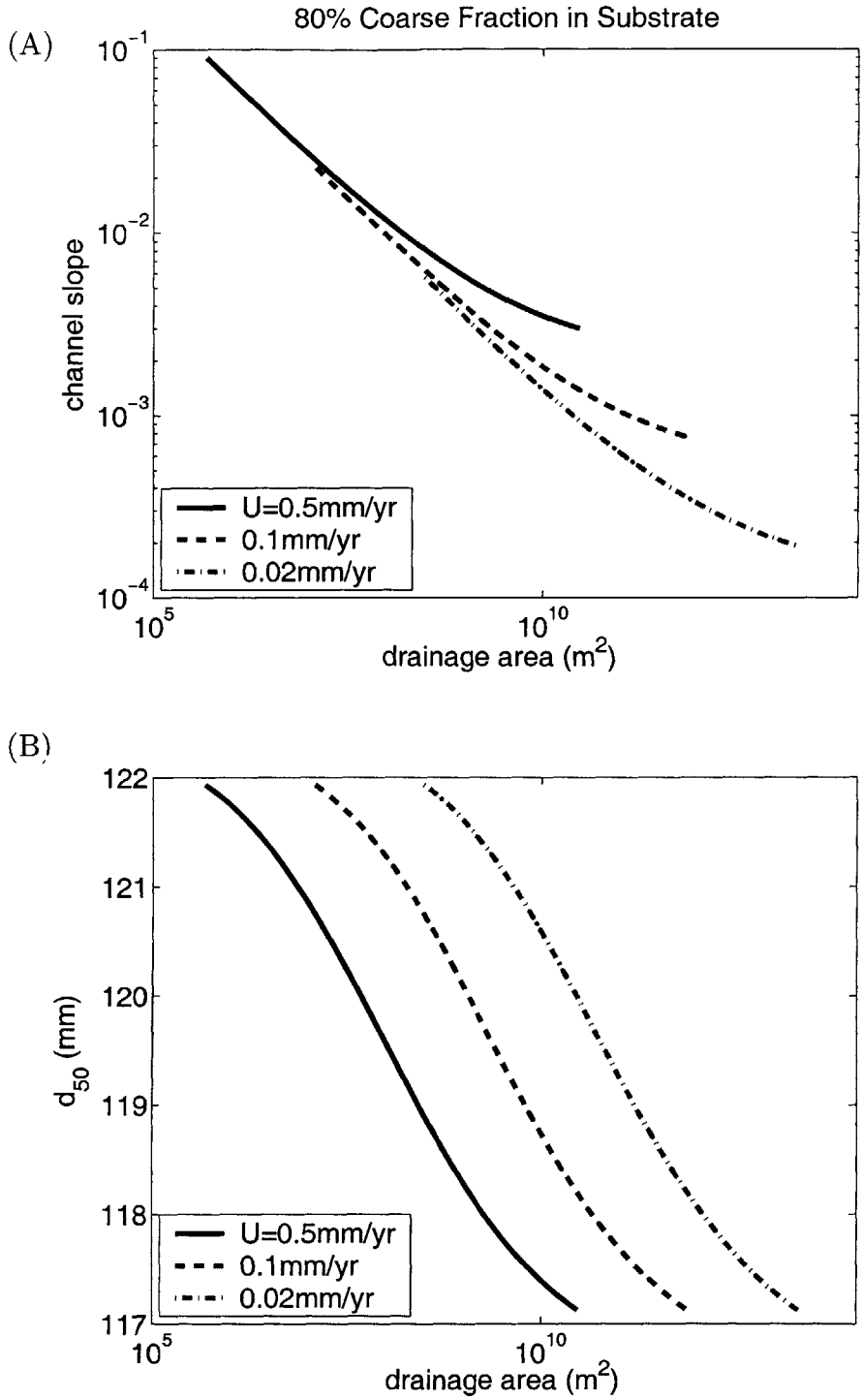

Figure 3-14: Sensitivity of equilibrium slope-area relationship (A) and d_{50}-area relationship (B) to different uplift values (see legend) for networks with 80% of the coarsest fraction in their substrate. Meyer-Peter Müller sediment transport equation with Komar critical shear stress rule is used. (Precipitation rate = 1m/yr falling over 100 days; coarse fraction=150-100mm; fine fraction=100-50mm)

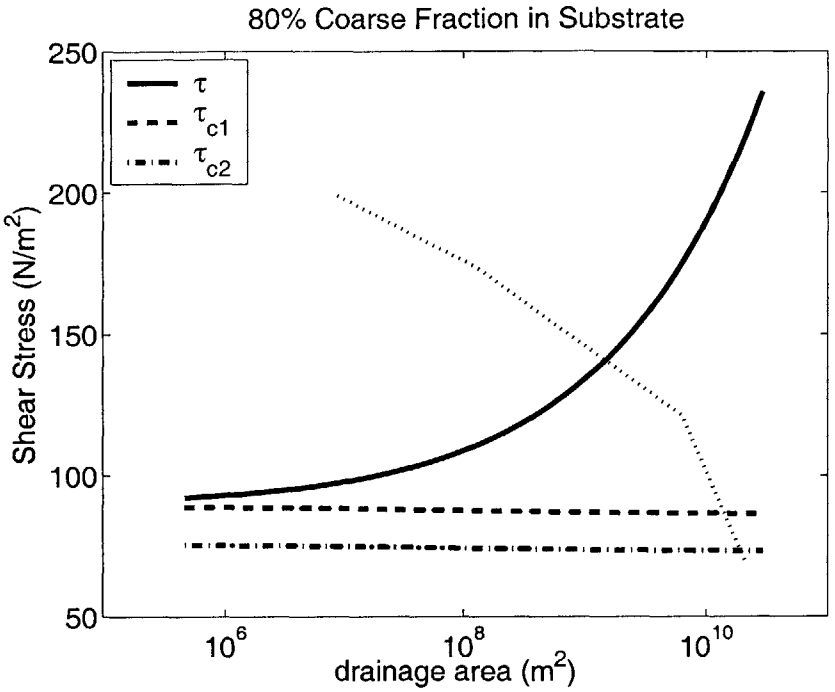

Figure 3-15: Equilibrium bed shear stress and critical shear stress values for the example shown in the figure 3-14 with uplift=0.5mm/yr. Dotted line illustrates the trend in concavity values (concavity values are scaled to show on figure).

3.4.3 Sensitivity to Grain Size

Finally, using the Meyer-Peter Müller sediment transport equation with the Komar critical shear stress rule, we explore the effects that grain size has on network morphology. In section 3.4.1 we showed that an increase in d_1 increased local concavity. Here we explore changes in d_1 and d_2 further.

Figure 3-17A illustrates the effects of variation of the coarser gravel fraction on the equilibrium slope-area relationship. (The finer gravel-grain size is 71mm, the uplift rate is 0.1mm/yr, and the precipitation rate is 1m/yr falling over 100 days in all cases in figure 3-17.) In the smaller drainage areas, the network with the coarsest gravel-grain size has the steepest slopes. When the coarser fraction is made up of larger grain sizes (figure 3-17B), the critical shear stress to entrain these grains is larger (equation 3.22), resulting in larger equilibrium slopes. In larger drainage areas, the median grain size is relatively smaller and is effectively not changing (figure 3-17B). In this region, the critical shear stress has decreased and no longer plays an important role in determining the transport rates. In this region the channel slopes are similar

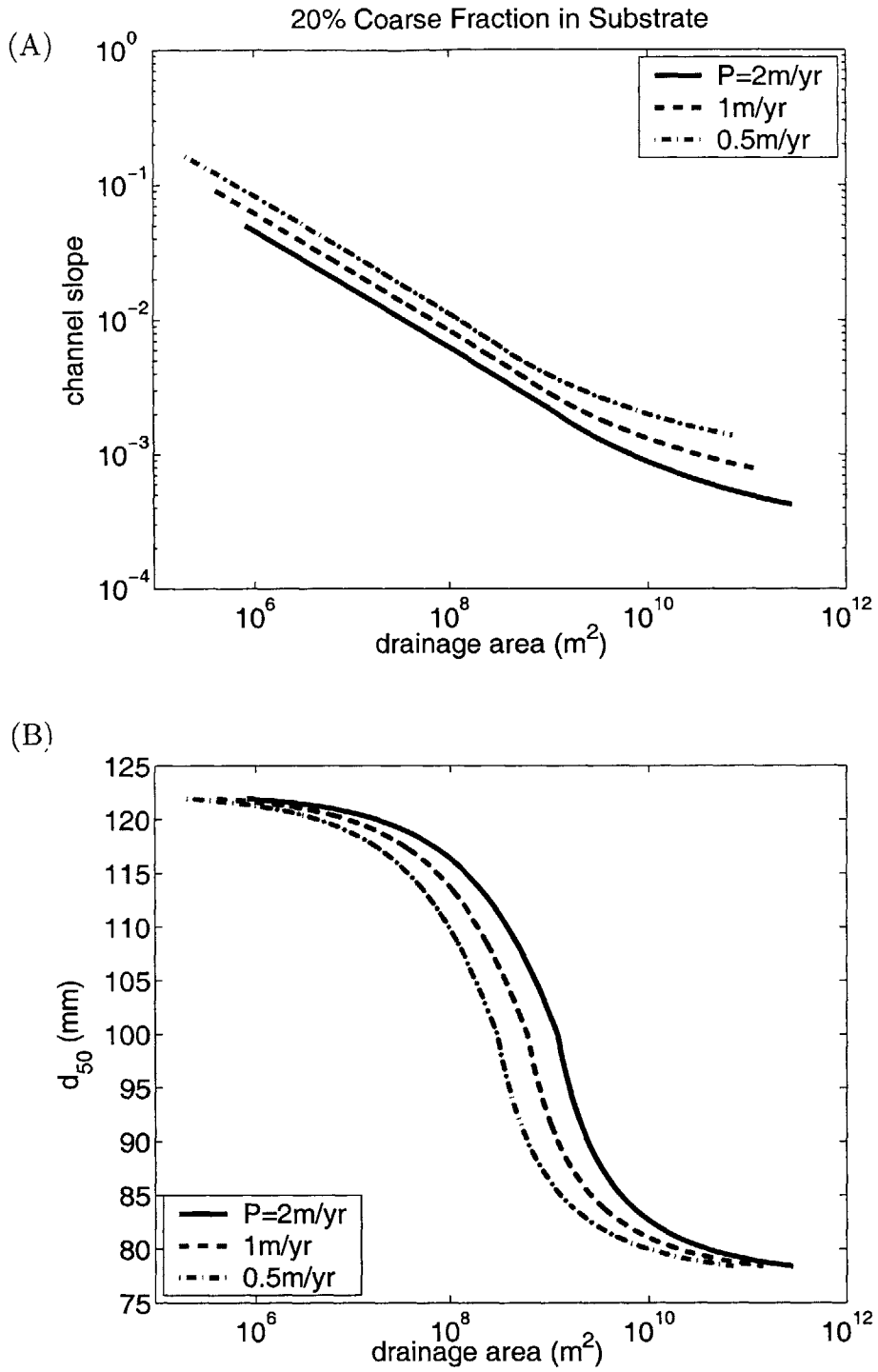

Figure 3-16: Sensitivity of equilibrium slope-area relationship (A) and median-grain size/area relationship (B) to different precipitation values (see legend) for networks with 20% of the coarsest fraction in their substrate. Meyer-Peter Müller sediment transport equation with the Komar critical shear stress rule is used. (Precipitation falls over 100 days; uplift rate=0.1mm/yr; coarse fraction=150-100mm; fine fraction=100-50mm). Note that the dashed lines in this figure are the same as the dashed lines in figure 3-5.

and concavity is at its lowest value (figure 3-18). The rapid change in grain size in the network with the largest variation in the coarse fraction creates a region with very large concavity (figure 3-18). The decline in median-grain size allows for a large decrease in critical shear stress, and therefore a rapid decrease in slopes.

Variation in the range of finer-grain sizes causes channel slopes in the larger drainage areas to decrease (figure 3-19A), while channel slopes in the smaller drainage areas are essentially unaffected. The median-grain size in the smaller drainage areas (figure 3-19B) is not affected by changing the range of finer sizes and therefore the coarser critical shear stress is nearly the same in all three networks shown (see equation 3.22). However, in the larger drainage areas, where d_{50} does vary between the networks, channel slopes are smaller in the network with the finest material. In other words, the coarse fraction controls the entrainment-limited upper reach while the finer fraction controls the transport-limited lower reach, so changes in the fine fraction only influence the latter. Again, the network which has more of a range in grain sizes has the highest local concavity value (figure 3-20).

Variation in both d_1 and d_2 affects channel slopes and concavity in all parts of the network as a combination of the simpler examples shown here. (These results are not shown.)

3.5 Wilcock Sand-Gravel Model

In this section we explore the equilibrium form of channel networks composed of a sand and gravel mixture. Based on field data (Oak Creek, Oregon (Milhous 1973); East Fork River, Wyoming (Emmett (1980), Emmett et al. (1980), Emmett et al. (1985)); Jacoby Creek, California (Lisle 1989); and Goodwin Creek, Mississippi (Kuhnle 1992)) and flume data (Wilcock and McArdell 1993), Wilcock (2001) showed that the sediment transport rates in sand and gravel mixtures could be calculated using only the median sand and gravel grain sizes. Here, we use the equations which he developed:

$$Q_{sg} = \frac{11.2 W f_g}{(s-1)g} \left(\frac{\tau}{\rho}\right)^{1.5} \left[1 - \frac{\tau_{cg}}{\tau}\right]^{4.5} \tag{3.26}$$

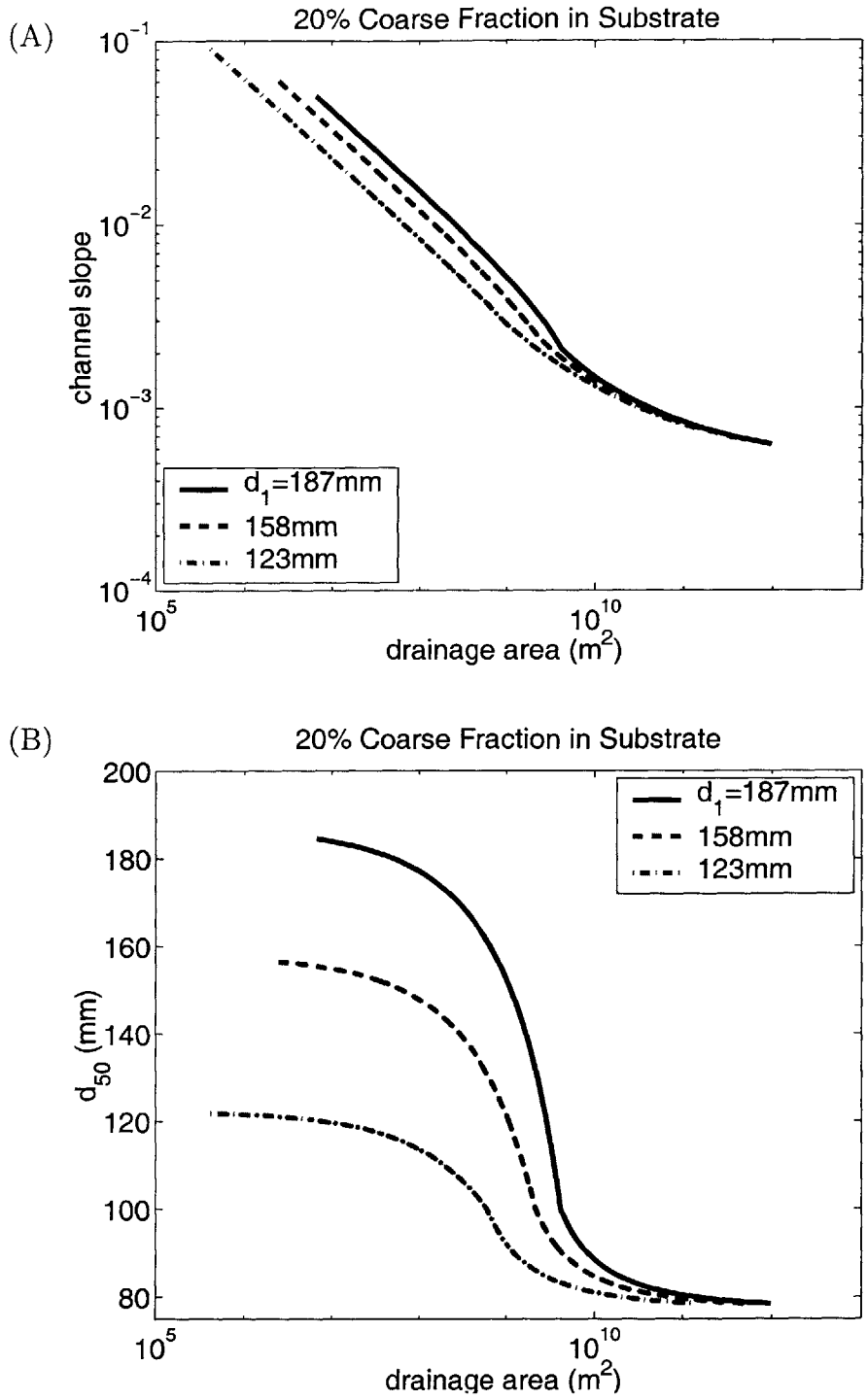

Figure 3-17: Change in equilibrium channel slope (A) and median grain size (B) with variation in coarse grain size. Here the coarser fraction ranges from 350-100mm (solid line), 250-100mm (dashed line) and 150-100mm (dash-dot line). The finer fraction range is 100-50mm (d_2=71mm), uplift rate is 0.1mm/yr, and precipitation rate is 1mm/yr falling over 100 days in all cases.

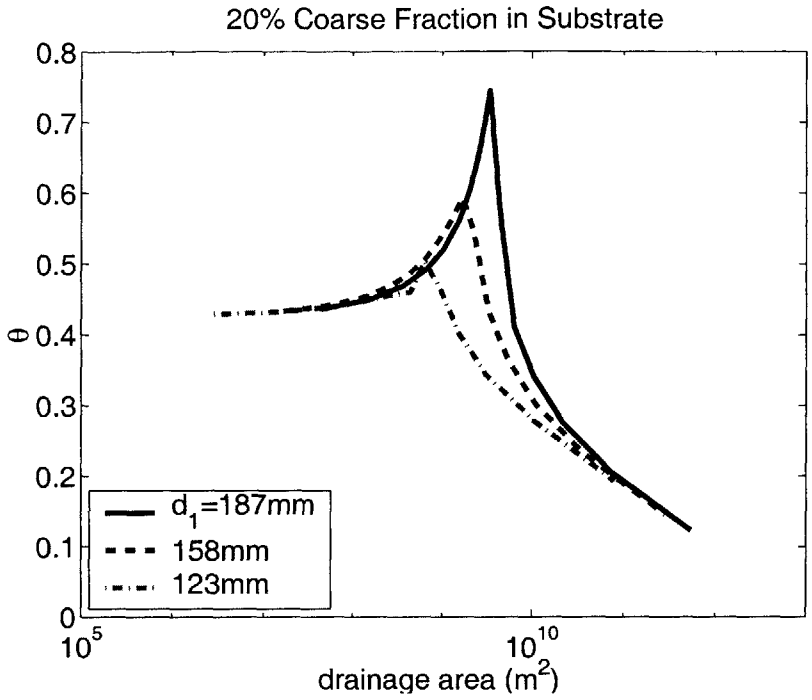

Figure 3-18: Change in equilibrium concavity. Parameters are as stated in the figure 3-17.

and

$$Q_{ss} = \frac{11.2 W f_s}{(s-1)g} \left(\frac{\tau}{\rho}\right)^{1.5} \left[1 - \sqrt{\frac{\tau_{cs}}{\tau}}\right]^{4.5} , \tag{3.27}$$

where Q_{sg} and Q_{ss} are the volumetric load of gravel and sand, respectively, per unit time ; f_g and f_s are the proportion of gravel and sand, respectively, on the channel bed (for modeling purposes, f_g and f_s refer to the proportion of gravel and sand, respectively, in the active layer); s is the ratio of sediment density (ρ_s) to water density (ρ); g is gravitational acceleration; τ_{cg} and τ_{cs} are the critical shear stress values for entrainment of gravel and sand, respectively; and 11.2 is a dimensionless parameter.

The critical shear stresses for entrainment of gravel and sand are calculated from the data of Wilcock (1998). Figures 3-21 (a) and (b) illustrate the relationships used in this study between the dimensionless reference shear stress of gravel (τ^*_{rg}) and sand (τ^*_{rs}) and the proportion of sand on the bed (here calculated as proportion of sand in the surface layer), along with Wilcock's data. Reference shear stress is defined as the shear stress necessary to produce a small reference transport rate; critical shear stress

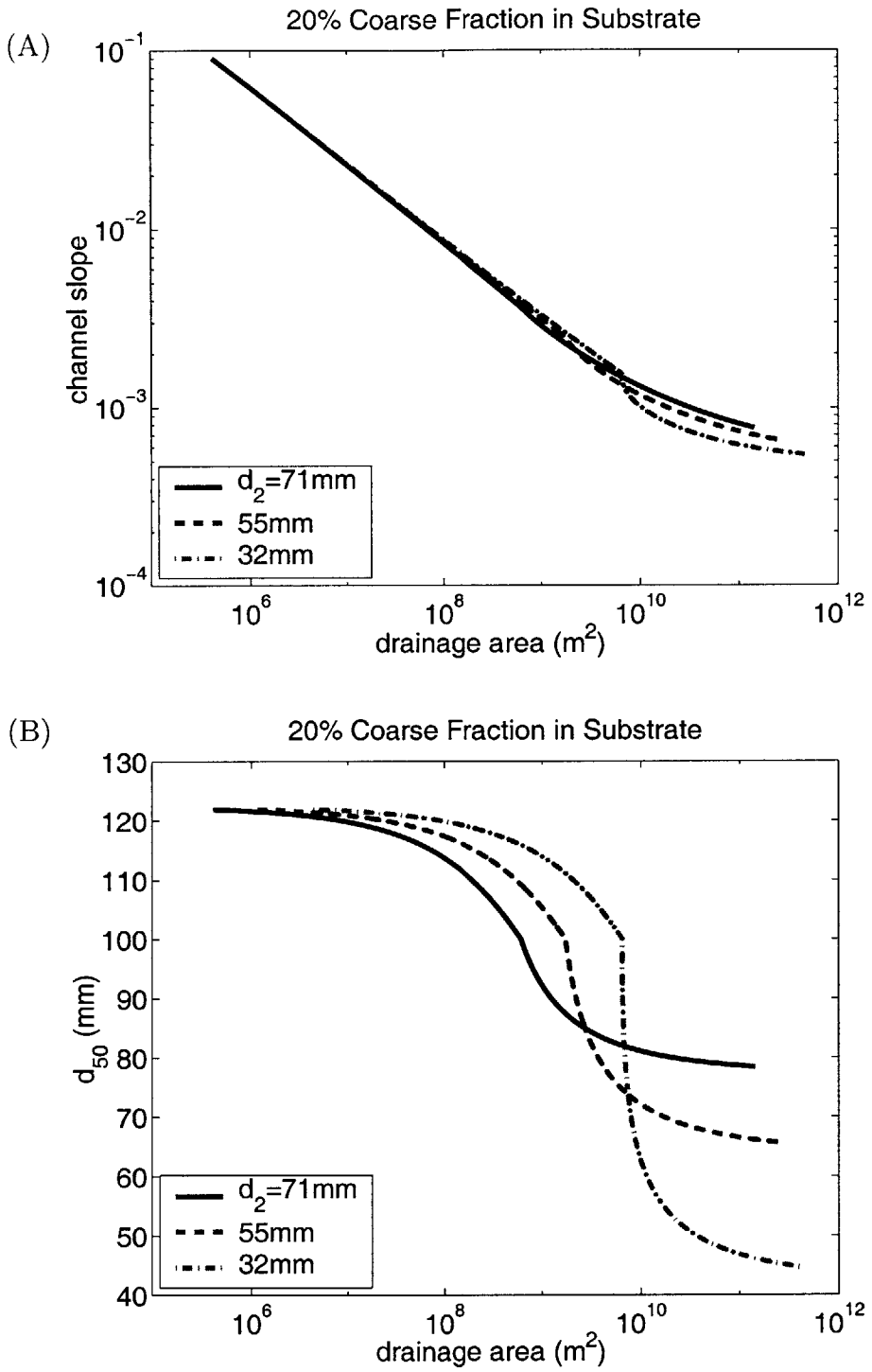

Figure 3-19: Change in equilibrium channel slope (A) and median-grain size (B) with variation in finer grain size. Here the fine fraction ranges from 100-50mm (solid line), 100-30mm (dashed line) and 100-10mm (dash-dot line). The coarse fraction range is 150-100mm (d_1=123mm), uplift rate is 0.1mm/yr, and precipitation rate is 1mm/yr falling over 100 days in all cases.

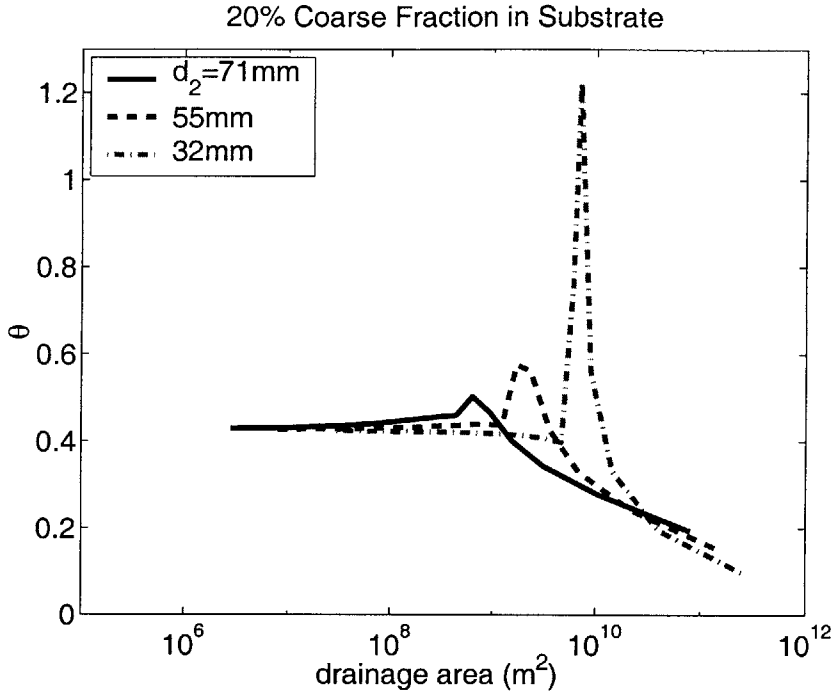

Figure 3-20: Change in equilibrium concavity. Parameters are as stated in the figure 3-19.

is assumed to be a constant fraction of reference shear stress. On a sand-poor bed (< 10% sand), the interlocked gravel framework dominates and inhibits entrainment of both sand and gravel (referred to herein as the gravel-dominated region). The value of τ^*_{rg} remains at a constant value of 0.04, which is the value for a homogeneous bed. The value of τ^*_{rs} also remains constant, but its value depends on the grain sizes present on the bed. The relation $\tau^*_{rs} = \left(0.8\frac{d_g}{d_s}\right)\tau^*_{cg}$ is used to determine the critical shear stress for entrainment of sand when there is less than 10% sand on the bed (d_g and d_s are the median gravel- and sand-grain size, respectively). As the bed becomes sandier, the gravel framework is broken. Gravel particles are spread apart and become easier to entrain because they protrude above the bed, while the sand particles become easier to entrain since they are less prone to hiding within the interstices of the larger particles. In the transitional regime between framework-dominated and matrix-dominated (modeled here as between 10% and 40% sand in the active layer, figure 3-21, and referred to as the transitional region), both τ^*_{rg} and τ^*_{rs} decrease as the proportion of sand on the bed increases. This decrease in the entrainment threshold for both sand and gravel is modeled according to the linear fit shown in Figure 3-21. In

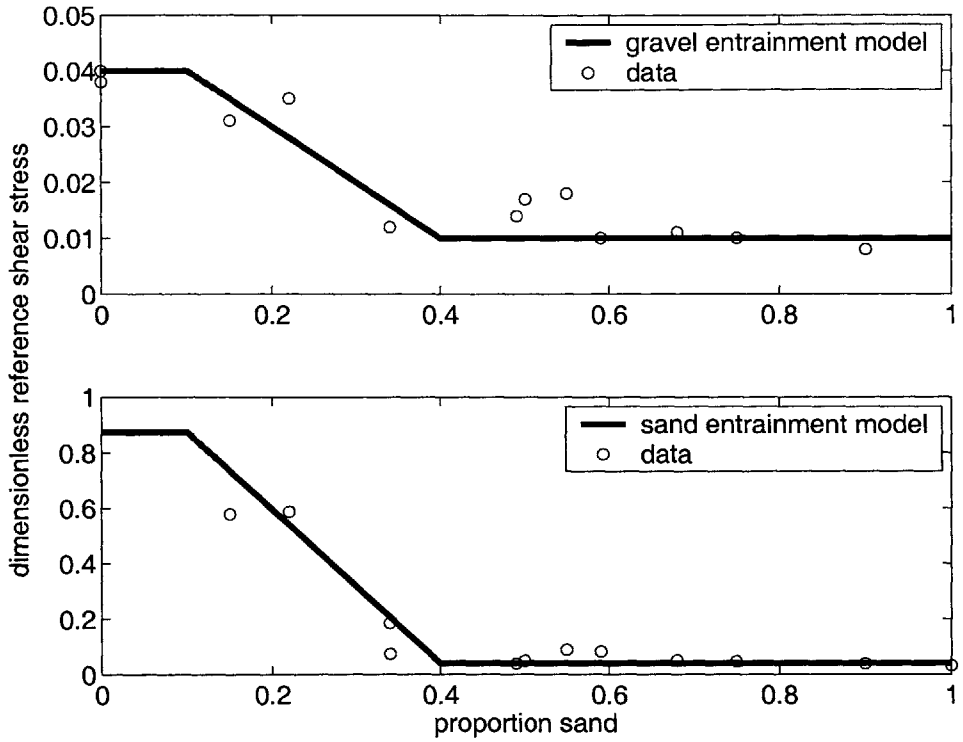

Figure 3-21: Dimensionless reference shear stress for transport of gravel and sand as a function of the volumetric proportion of sand (vs. gravel) on the bed. The data (circles) are from a flume and field studies and were compiled by Wilcock (1998). The lines drawn are the fit which was used for this study.

mixtures containing more than about 40% sand the bed becomes matrix-dominated, and critical shear stress becomes largely insensitive to variations in the relative proportions of sand and gravel; in this regime, the dimensionless reference shear stress for gravel and sand remain constant at 0.01 and 0.04, respectively (referred to as the sand-dominated region). Other heterogeneous sediment entrainment studies support a similar relationship, that is the presence of finer particles enables entrainment of the coarser particles and the presence of coarser particles hinders entrainment of the finer particles (e.g., Andrews (1983); Church (1985); Komar (1987); Kuhnle (1993)).

One could easily argue that there are a number of fits which could be used for the data shown in figure 3-21. However, the data strongly support a region in which critical shear stress decreases with increasing sand content in the surface layer. We have chosen to use a linear fit between 10% and 40% sand content in the surface. We have explored linear fits over different regions on surface sand content, and although

some details may change, the trends in the data do not change. The important aspect of these data is that critical shear stress decreases with increasing sand content, and this is what drives the trends we see. We argue that the general trends in the results we present do not depend on the details of how this declining trend in critical shear stress is described but only that a declining trend exists.

We can now proceed with the equilibrium solution. For each equilibrium example, a substrate texture (sand- and gravel-grain size, and proportion sand in substrate), uplift rate, and precipitation rate are chosen. Following the procedures outlined in section 3.3, over the range of possible surface textures (based on the contents of the substrate material), we calculate the critical shear stress for entrainment of both gravel and sand using the relationship shown in figure 3-21 (step 2). With this information (substrate texture, surface texture, and critical shear stress values), we can calculate surface shear stress (step 3). The relationship for equilibrium surface shear stress (obtained from substituting equations 3.26 and 3.27 into equation 3.20 and rearranging) is

$$\left[\left(\frac{f_s^{sub}}{1-f_s^{sub}}\frac{1-f_s}{f_s}\right)^{\frac{1}{4.5}}-1\right]\tau+\sqrt{\tau_{cs}}\sqrt{\tau}-\left(\frac{f_s^{sub}}{1-f_s^{sub}}\frac{1-f_s}{f_s}\right)^{\frac{1}{4.5}}\tau_{cg}=0\ . \qquad (3.28)$$

This is the equilibrium expression for shear stress as a function of surface texture (remember that the sand and gravel critical shear stress values are a function of f_s and the gravel- and sand-grain sizes) (Gasparini et al. 2003). Figure 3-22 illustrates the equilibrium shear stress relationship for a drainage basin with 50% sand in its substrate. Three important points arise from the equilibrium shear stress relationship: (1) there are two solutions to this equation (only one is shown in Figure 3-22) (2) there is a region of surface texture for which no equilibrium solution exists, and this region is a function of the proportion of sand in the substrate and the median gravel- and sand-grain sizes and (3) shear stress can both increase and decrease with increasing proportion of sand on the bed, and, therefore, because this is a continuous function (in the region over which it is defined), shear stress alone does not uniquely determine the equilibrium surface texture.

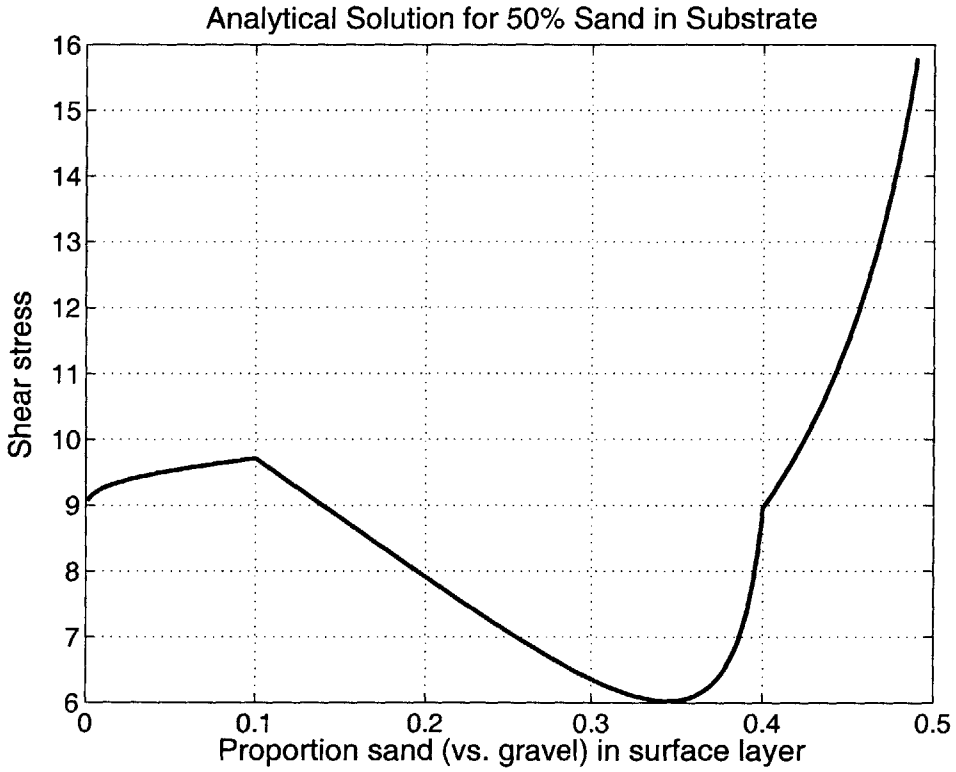

Figure 3-22: One solution to the equilibrium shear stress equation (3.28) using Wilcock's (2001) model for a mixture with 50% sand in the substrate. Shear stress values are in N/m^2.

We now have the equilibrium shear stress given the surface and substrate composition, and we can plug this information back into equation 3.26 (or, equivalently, equation 3.27) to obtain a sediment transport rate, which uniquely defines a drainage area (given the uplift rate, see step 4 from section 3.3 and equations 3.18 and 3.19). This defines the relationship between surface texture and drainage area. Finally, from equation 3.21 (step 5 from section 3.3) we can solve for channel slope and describe the equilibrium morphology of the network.

We present below the equilibrium sensitivity of network morphology and downstream surface texture changes to different uplift rates, and precipitation rates, and substrate textures (sand and gravel grain size, and composition). Surface texture changes are shown in this section as changes in the proportion of sand (versus gravel) in the surface layer. The results we present are obtained using the iterative solution described above. The Wilcock (2001) equations are part of the CHILD model and can be used to evolve transport-limited networks to equilibrium. In all cases, the CHILD model predictions agree exactly with the iterative solution (see later section). (The same result was found by Gasparini et al. (2003) using the GOLEM model (e.g. Tucker and Slingerland (1996)).) Using CHILD to model multiple-grain size sediment transport over geologic time scales is computationally intensive, which is why we developed the iterative method to describe equilibrium landscapes. While the iterative method has the speed advantage, it can obviously only be used for looking at equilibrium relations. The CHILD model can describe both equilibrium conditions as well as the transient conditions between equilibrium states, as illustrated in Chapter 4.

3.5.1 Equilibrium Network Sensitivity to Uplift Rate/Erosion Rate

All of the results in this section look only at the effects of uplift rates; all other parameters (precipitation rate, grain-size variables) are constant in each example. Sensitivity to uplift is somewhat dependent on the proportion of sand in the substrate, and these differences are illustrated between plots. The effective precipitation rate

does not change equilibrium sensitivity to uplift rates, and therefore the precipitation rate in all figures is the same (1m/yr of rain falling over 100 days). Also, the trends do not vary for different values of gravel- and sand-grain size, and these values are held constant at 40mm and 1.5mm, respectively. As discussed in section 3.4.1, the equilibrium solution is defined for larger drainage areas with lower uplift rate values, and comparisons are only made where solutions are defined for the same drainage area. (Remember that higher uplift rates imply higher erosion rates.)

For all of the parameters we investigated, the equilibrium solutions are defined over the widest range of drainage areas and surface textures when the substrate contains 90% sand. We begin our discussion with this case. Figure 3-23 shows the change in the slope-area relationship (A) and texture-area relationship (B) as a function of uplift rate (varying by a factor of 5). (Note that texture is now expressed as f_s and larger values imply more sand (vs. gravel) and therefore finer mixtures.) Figure 3-24 is almost identical to figure 3-23 except that in figure 3-24 uplift rates vary by two orders of magnitude. We show these two figures only to illustrate that differences with uplift rate in the equilibrium slope-area and texture-area relationships are general and do not depend on the magnitude of change in uplift rate.

Looking at a single line in figure 3-23A, one immediately notices that the nature of the slope-area relationship changes with drainage area, and this change corresponds with the surface texture (figure 3-23B). The slope-area and sand-area relationships are highly affected by the nature of changes in critical shear stress. That is, the slope-area and sand-area relationships are distinct in the regions where there is less than 10% sand in the surface layer (region in which the critical shear stress for entrainment of sand and gravel remains constant with proportion sand in the surface, figure 3-21), where there is greater than 10% sand but less than 40% sand in the surface layer (region in which the critical stress for entrainment of both sand and gravel decreases with increasing surface sand content, figure 3-21), and where there is greater than 40% sand in the surface layer (the critical shear stress for entrainment of both sand and gravel again remains constant with increasing surface sand content, figure 3-21). In the region of decreasing shear stress, or the transitional area ($0.1 < f_s < 0.4$), the

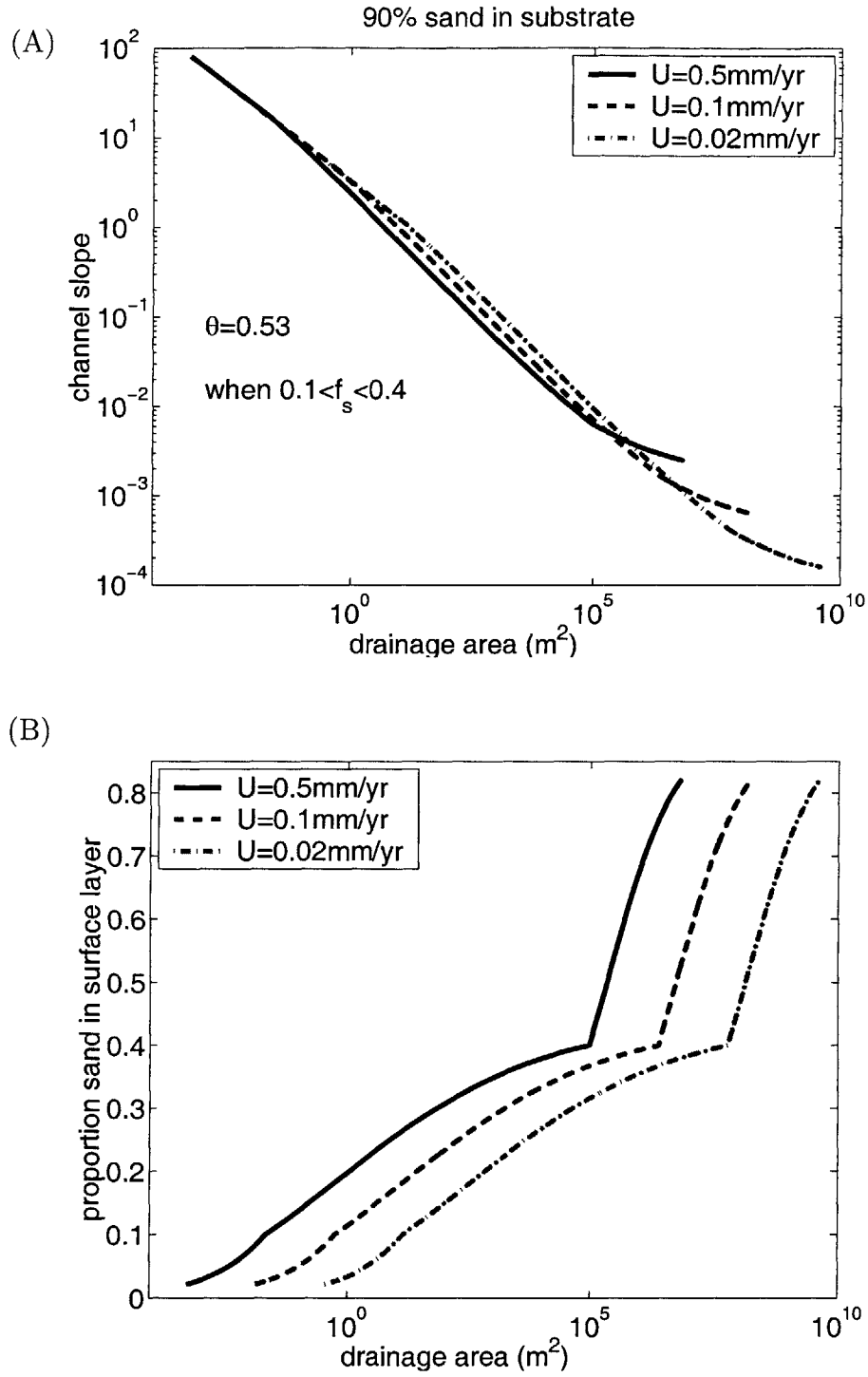

Figure 3-23: Sensitivity of equilibrium slope-area relationship (A) and surface texture-area relationship (B) to different uplift values (see legend) for networks with 90% sand in their substrate. Wilcock (2001) equations are used. (Precipitation rate = 1m/yr falling over 100 days; d_g = 40mm; d_s = 1.5mm)

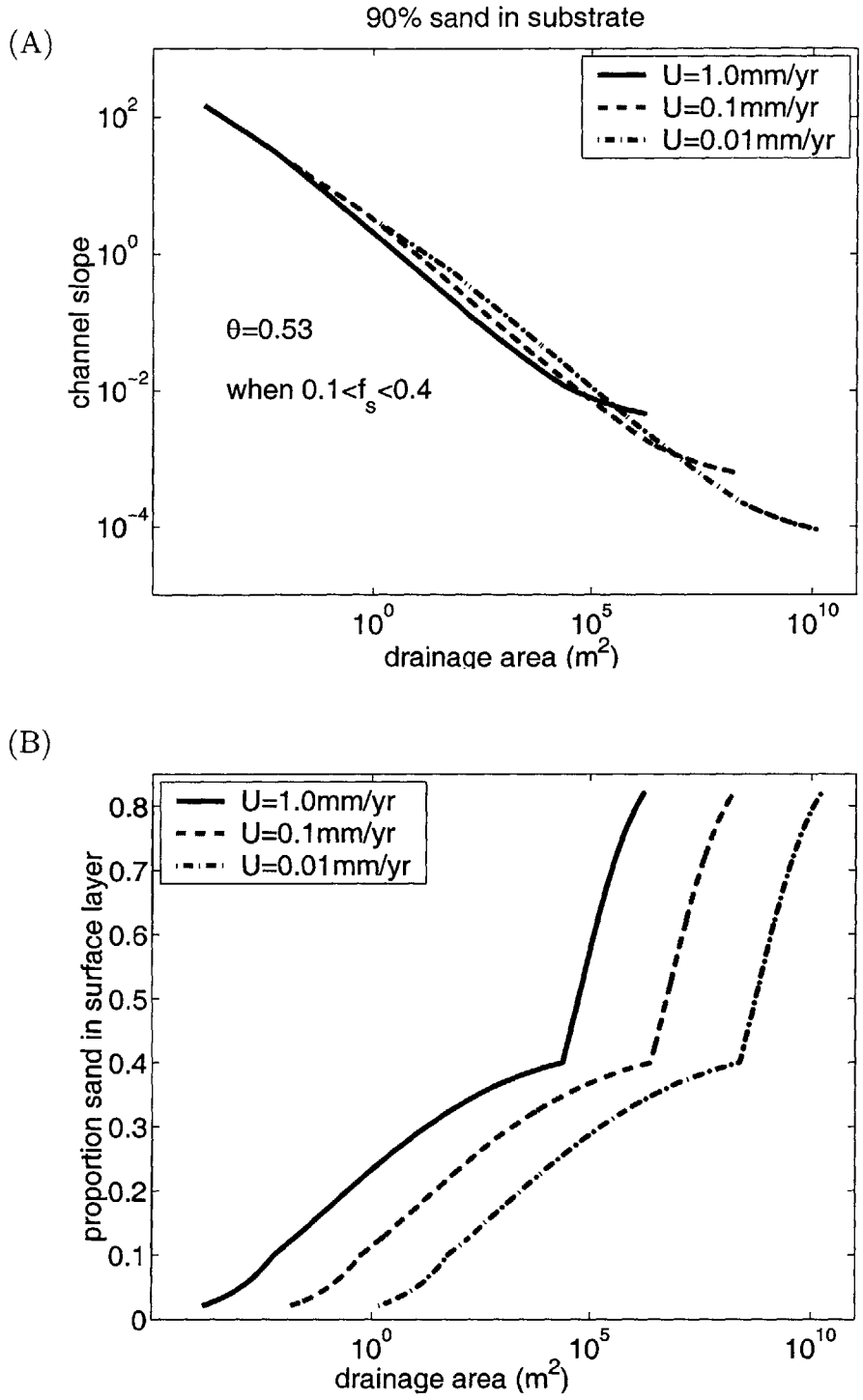

Figure 3-24: Sensitivity of equilibrium slope-area relationship (A) and surface texture-area relationship (B) to different uplift values (see legend) for networks with 90% sand in their substrate. Wilcock (2001) equations are used. The only difference between this figure and the last (figure 3-23) is that uplift values vary by a factor of 10 (versus a factor of 5 for figure 3-23).

concavity is nearly constant, and $\theta = 0.53$ for all uplift values. With these grain size parameters, the assumption of nearly constant theta is reasonable given the concavity variation in the transitional region: $\theta = 0.52$ when $0.1 < f_s < 0.2$; $\theta = 0.54$ when $0.2 < f_s < 0.3$; $\theta = 0.51$ when $0.3 < f_s < 0.4$ (see table 3.1). In this transitional region, channel slope is able to decrease rapidly because critical shear stress is also decreasing, enabling higher transport rates. In the regions in which critical shear stress is constant ($f_s < 0.1$ and $f_s > 0.4$), the concavity is lower, that is slope is not decreasing as rapidly with drainage area ($\theta = 0.42$ when $f_s < 0.1$; $\theta = 0.23$ when $f_s > 0.4$). When the critical shear stress is constant, downstream increases in transport rate are all compensated by increases in bed shear stress, and channel slope is not able to decrease as rapidly, leading to smaller concavity values. This result is similar to the results found using the Meyer-Peter Müller sediment transport equation with the Komar critical shear stress rule, that is when the critical shear stress plays less of a role in determining the transport rate, the concavity decreases.

	$f_{sub} = 90\%$	$f_{sub} = 50\%$	$f_{sub} = 10\%$
$f_s < 0.1$	0.42	0.42	0.40
$0.1 < f_s < 0.4$	0.53	0.47	0.41
$f_s > 0.4$	0.23	0.11	-
$0.1 < f_s < 0.2$	0.52	0.50	0.42
$0.2 < f_s < 0.3$	0.54	0.50	0.37
$0.3 < f_s < 0.4$	0.51	0.40	-

Table 3.1: Concavity values (θ in different parts of three networks with different substrate composition ($d_g = 40mm$, $d_s = 1.5mm$, results not sensitive to uplift rate or precipitation rate).

Now that we understand the nature of the slope-area relationship we examine how uplift rates affect channel slopes. For a given drainage area, one notices that there are regions in which channel slope decreases with increasing uplift rates; in figure 3-23A, this region is roughly for drainage areas between $1m^2$ and 10^5m^2. This is quite surprising, given that transport rates need to increase with increasing uplift rates. How is it possible that higher transport rates can occur on shallower slopes? As was the case with the examples using the Meyer-Peter Müller sediment transport

equation, the answer lies in changes in surface texture. The surface content always becomes finer (contains more sand) with increasing uplift rates (figure 3-23B). In the transitional region, a finer surface implies a smaller critical shear stress, and therefore larger transport rates. Even though the transport rate must increase with uplift rate, the adjustment of surface texture actually allows for shallower slopes at higher uplift rates. In the regions in which critical shear stress remains constant and the concavity of the channels is greatly reduced, channel slope increases with uplift rate as expected.

The surprising result that channel slope can increase with decreasing uplift rates also holds in networks with 50% sand in their substrate (figure 3-25). In this example, we again see that the most concave part of the network are the areas with a transitional surface texture ($\theta = 0.42$ when $f_s < 0.1$; $\theta = 0.47$ when $0.1 < f_s < 0.4$; $\theta = 0.11$ when $f_s > 0.4$, table 3.1). The patterns in surface texture changes (figure 3-25B) are also the same as in the case with 90% sand in the substrate (figure 3-23B), and again it is the fining of the surface that allows for the surprising slope results. In the larger drainage areas, concavity greatly decreases and channel slopes increase with increasing uplift rate. In the smaller drainage areas, channel slopes are very similar (when they overlap) for all cases. This result is more obvious in the case of a network with 10% sand in its substrate (figure 3-26). This case is not defined over a wide range of surface textures, and therefore drainage areas; we show it only to highlight that there is a region in which channel slope is nearly constant with uplift rate.

3.5.2 Sensitivity to Precipitation Rate

The sensitivity of equilibrium channel slope and surface texture to changes in precipitation are as one would predict. Higher precipitation rates produce shallower slopes (figure 3-27A) and have no effect on network concavity (concavity values are exactly the same as those given in the variable uplift examples, table 3.1). This seems logical because as precipitation rates increase the fluvial discharge increases, but there is no required change in transport rates (at a given drainage area). Shallower slopes can produce the same bed shear stress with a higher fluvial discharge. Higher precip-

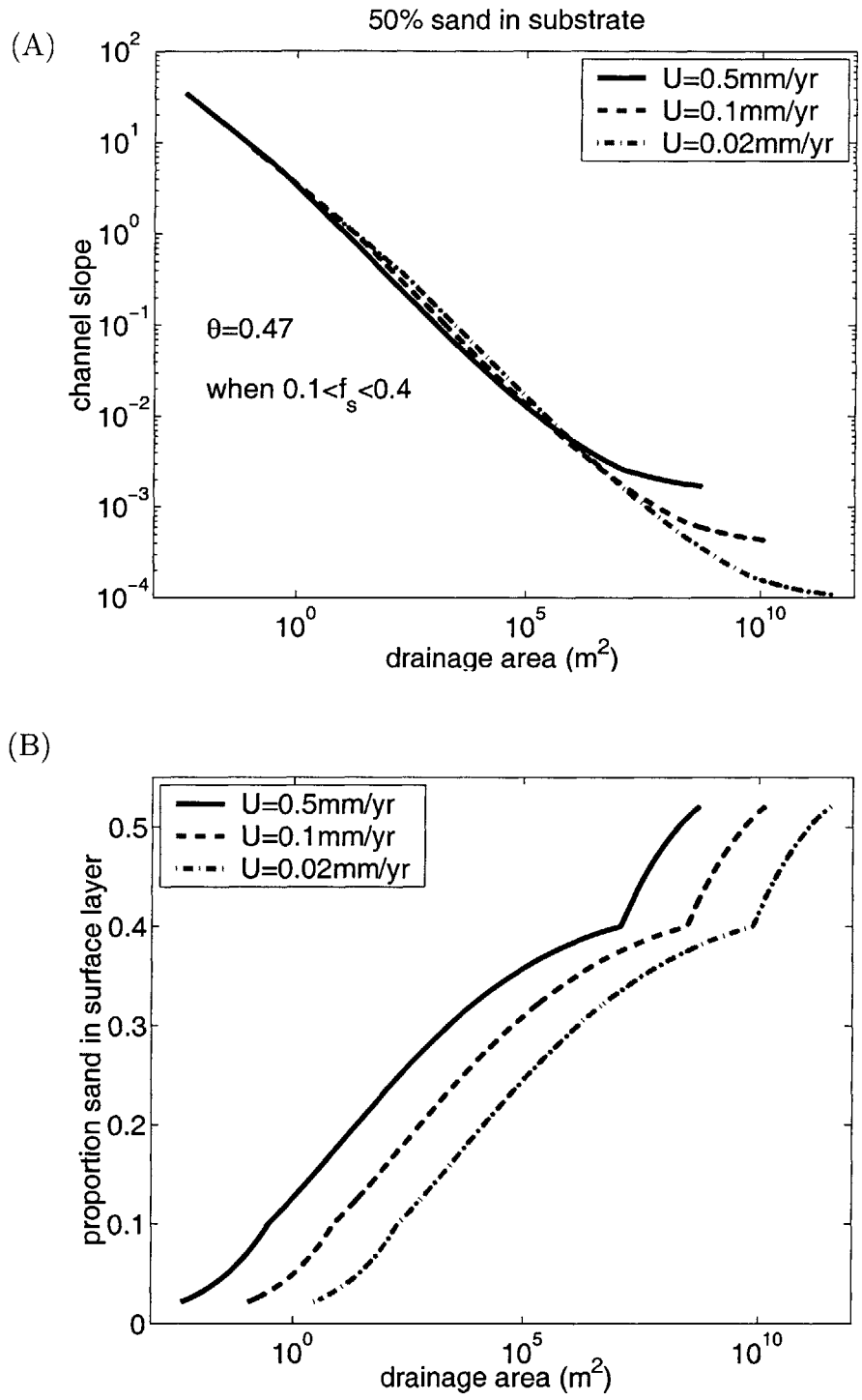

Figure 3-25: Sensitivity of equilibrium slope-area relationship (A) and surface texture-area relationship (B) to different uplift values (see legend) for networks with 50% sand in their substrate. Wilcock (2001) equations are used. (Precipitation rate = 1m/yr falling over 100 days; d_g = 40mm; d_s = 1.5mm)

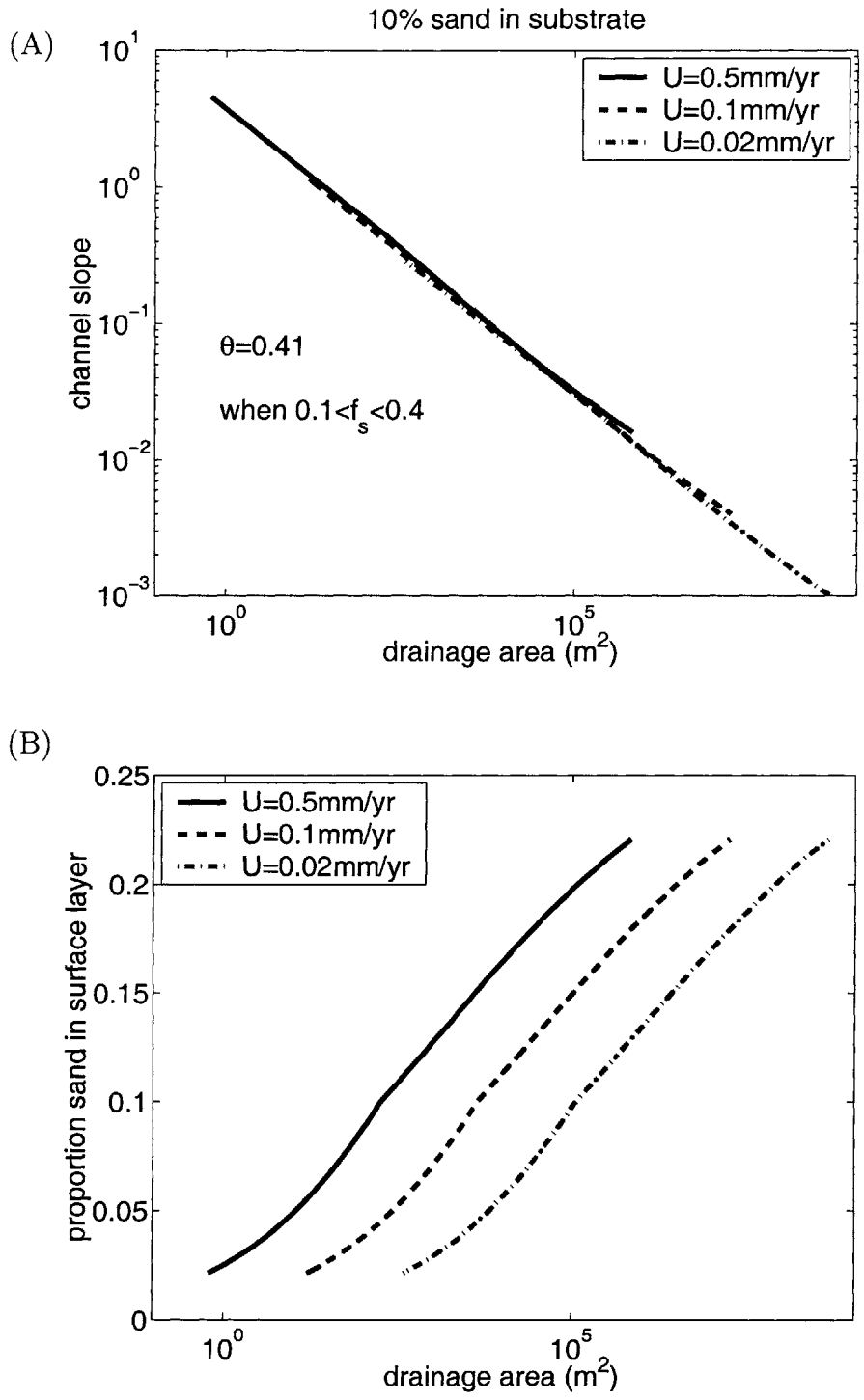

Figure 3-26: Sensitivity of equilibrium slope-area relationship (A) and surface texture-area relationship (B) to different uplift values (see legend) for networks with 10% sand in their substrate. Wilcock (2001) equations are used. (Precipitation rate = 1m/yr falling over 100 days; d_g = 40mm; d_s = 1.5mm)

itation rates also produce coarser surfaces (figure 3-27B), which seems logical. As fluvial discharge increases, the surface coarsens to inhibit transport rates. We only show one illustration of the sensitivity to precipitation rate, because all of the figures look exactly the same.

3.5.3 Sensitivity to Texture and Grain Size

In this section we make comparisons between basins with different substrate sand contents and gravel-grain sizes. Changes in sand grain size do not have a noticeable affect on the equilibrium results.

For the most part basins with a greater gravel content have the steeper slopes (figure 3-28A). Remember that in equilibrium the texture of the material in transport is that of the substrate. At a given drainage area in figure 3-28 all of the networks are transporting the same total load, but the composition of the load changes between the networks. So the drainage network with 10% sand in its substrate needs to transport a mixture containing more gravel than either the network with 50% sand or 90% sand in its substrate. In order to transport the greater gravel load, the slopes are steeper.

Figure 3-28B shows the sensitivity of surface sand content to subsurface sand content. For a given drainage area, the surface sand content is higher for basins which contain more sand in their substrate. Our method does not produce an equilibrium solution for large surface sand contents in a network with 10% sand in its substrate. One might point to availability of gravel for transport as the reason for this. On the other hand, the critical shear stress to entrain gravel also decreases with surface sand content, so one might expect the basin with a high gravel content in its substrate to at least be defined over the entire range of surface sand contents for which gravel critical shear stress is decreasing. However, the gravel transport rate is also proportional to the amount of gravel available on the bed, so as surface sand content increases, there are opposing factors controlling the gravel transport rate. It is probably these competing factors which set the range over which the equilibrium solution is defined.

The sensitivity of the equilibrium networks to changes in gravel-grain size is illustrated in figure 3-29. In this figure all parameters remain the same except for

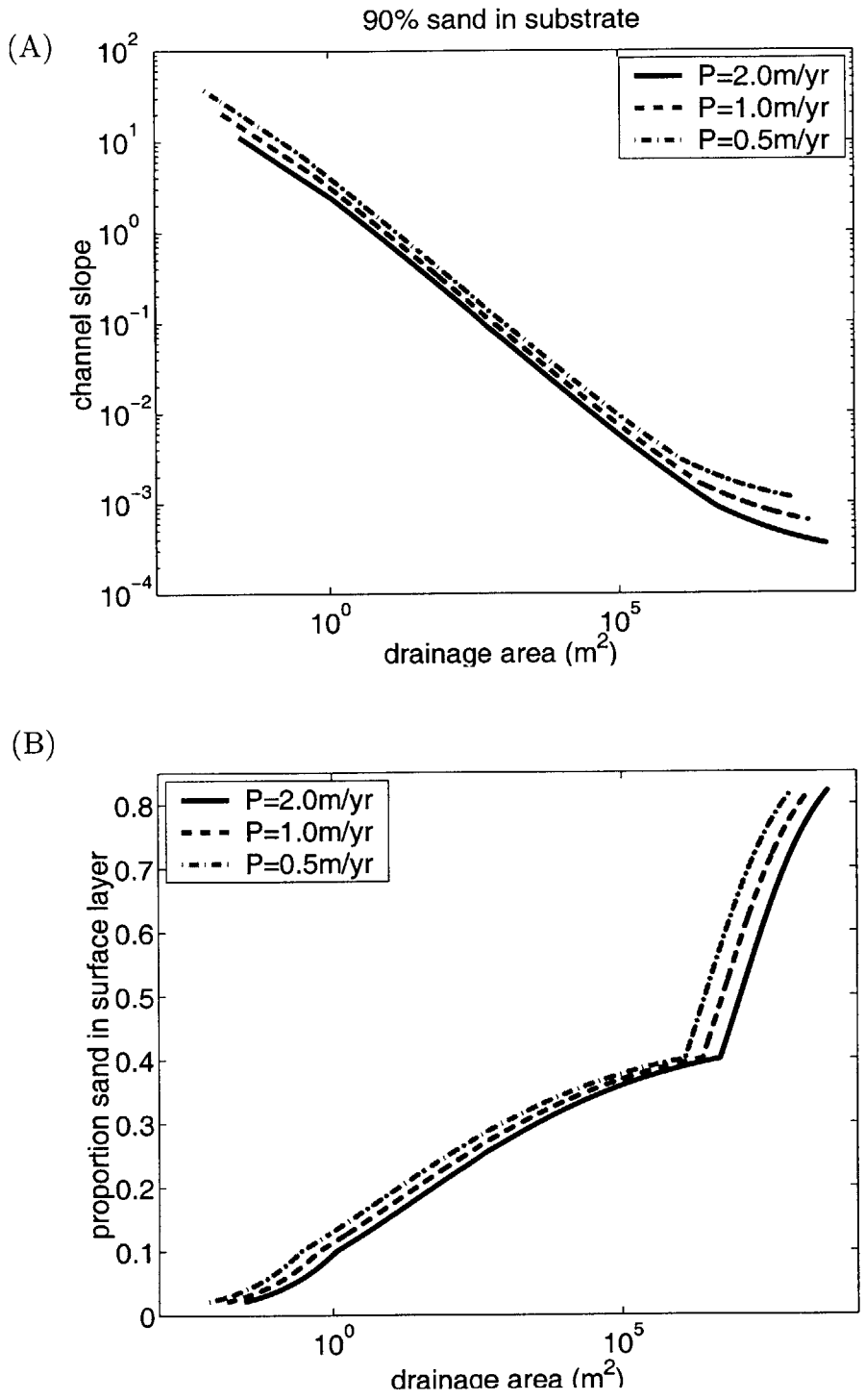

Figure 3-27: Sensitivity of equilibrium slope-area relationship (A) and surface texture-area relationship (B) to different precipitation rates (falling over 100 days a year) for networks with 90substrate. Wilcock (2001) equations are used. (Uplift rate = 0.1mm/yr; $d_g = 40$mm; $d_s = 1.5$mm)

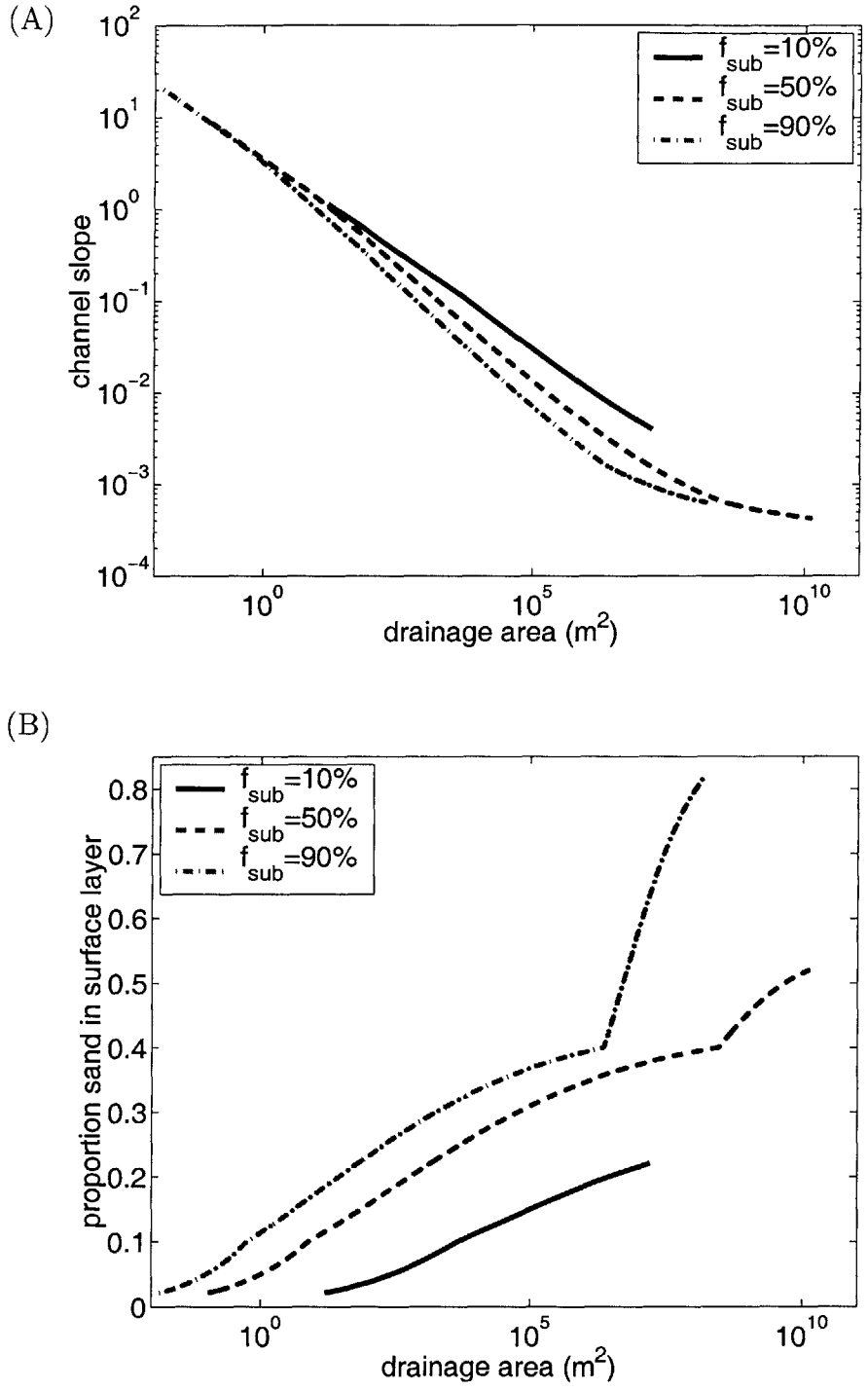

Figure 3-28: Sensitivity of equilibrium slope-area relationship (A) and surface texture-area relationship (B) to the composition of the substrate. Wilcock (2001) equations are used. (Uplift rate = 0.1mm/yr; Precipitation rate = 1m/yr falling over 100 days; d_g = 40mm; d_s = 1.5mm)

the gravel-grain size. Where the solutions overlap in drainage area, the basin with the largest gravel-grain size has the steepest slopes. This is as expected, since larger grain sizes have larger critical shear stresses, and therefore steeper slopes are needed to transport the material. In this figure, for a given drainage area, not only are the total transport rates the same but so are the sand- and gravel-transport rates.

$f_{sub} = 90\%$	d_g=10mm	d_g=20mm	d_g=40mm	d_g=160mm
$f_s < 0.1$	0.42	0.42	0.42	0.42
$0.1 < f_s < 0.4$	0.73	0.56	0.53	0.51
$f_s > 0.4$	0.35(0.33)	0.25(0.24)	0.18(0.17)	0.10
$0.1 < f_s < 0.2$	0.63	0.54	0.52	0.51
$0.2 < f_s < 0.3$	0.75	0.57	0.54	0.53
$0.3 < f_s < 0.4$	0.74	0.55	0.51	0.48

Table 3.2: Sensitivity of concavity values (θ) to gravel-grain size in different parts of the network ($f_{sub} = 0.90$, d_s=1.5mm, uplift rate is 0.1mm/yr, and precipitation rate is 1m/yr falling over 100 days). All concavity values are calculated over the same surface texture range (minimum $f_s = 0.02$, maximum $f_s = 0.90$), except for those in parentheses, which are calculated to the largest surface sand content possible given the parameters.

The drainage network with the smallest gravel-grain size is defined over the smallest range of drainage areas (figure 3-29) but the largest range of surface sand contents (figure 3-29 illustrates solutions over the definable range for d_g=160mm). The reason for the smaller range in drainage areas in the network with the smallest gravel-grain size is that the surface sand content increases much faster in the transitional region in this network (figure 3-29B). This rapid increase in surface sand content corresponds to a greater concavity in the transitional region (table 3.2). Concavity greatly varies between the basins with different gravel-grain sizes in the transitional region and also in the sand-dominated region with ($f_s > 0.4$). In the gravel-dominated region ($f_s < 0.1$) concavity does not vary. The inter-comparison of concavity values is a bit surprising. Given the results presented using a single grain size (section 3.2) one would expect the concavity of a networks with a larger gravel-grain size (and therefore the larger critical shear stress) to be larger. However, the result is exactly the opposite in both the transitional region and in the sand-dominated region, that is the

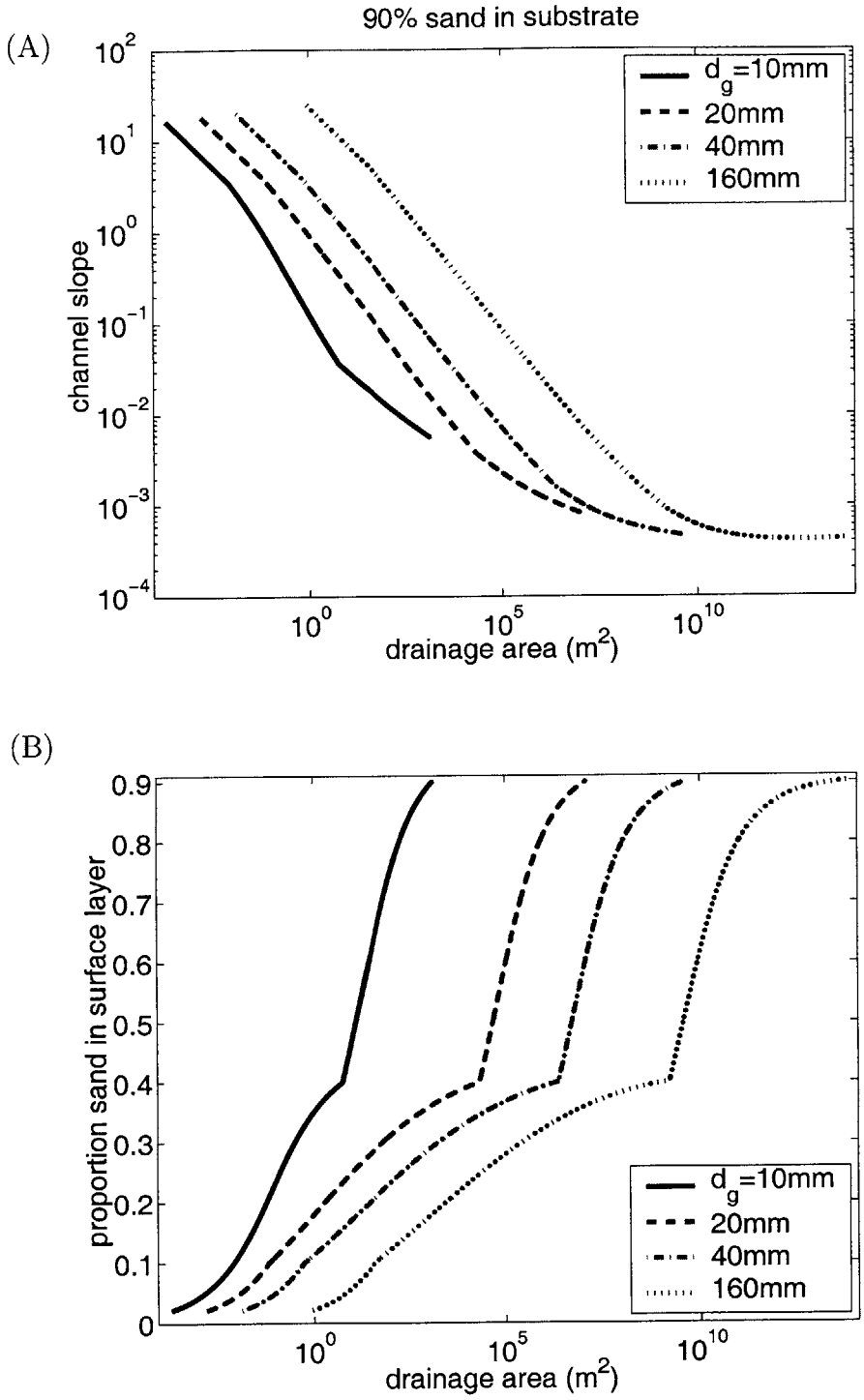

Figure 3-29: Sensitivity of equilibrium slope-area relationship (A) and surface texture-area relationship (B) to the gravel grain size. Wilcock (2001) equations are used. (Uplift rate = 0.1mm/yr; Precipitation rate = 1m/yr falling over 100 days; d_s = 1.5mm)

concavity increases with decreasing gravel-grain size (and therefore decreasing critical shear stress). Note that for the parameter space explored here, the change in concavity in these regions is quite significant (for example in the transitional region $\theta = 0.73$ in the network with d_g=10mm, and $\theta = 0.51$ in the network with d_g=160mm, see table 3.2).

In table 3.2, there are two values for concavity in the sand-dominated region; the values not in parentheses are calculated over the maximum range for the network with d_g=160mm. The equilibrium solutions is defined for larger surface sand contents as the gravel-grain size decreases. When the concavity is calculated over the maximum range of surface sand contents (values in parentheses in table 3.2), the concavity value is slightly reduced, but the same trend still results. Concavity varies depending on the range of surface contents over which it is calculated because concavity is changing in this region (curved slope-area lines).

Figure 3-30 shows the sensitivity of network morphology and surface texture to gravel-grain size in a basin containing 50% sand in its substrate. The results are similar to the basin with 90% sand in its substrate. For a given drainage area, slopes are steeper in the network which has a larger gravel-grain size. Concavity in the transitional and sand-dominated regions also increases with decreasing gravel-grain size (table 3.3), and the increase in concavity is linked to faster changes in surface texture with drainage area as gravel-grain size decreases (figure 3-30B). As with the case of $f_{sub} = 0.90$, concavity values in the sand-dominated region were calculated in two ways: up to the same maximum f_s, which is also the maximum definable surface sand content for the basin with d_g=160mm, and up to the maximum surface sand content for each gravel-grain size. Regardless of the method, we see that concavity in the sand-dominated region increases with decreasing gravel-grain size. Note that the channels are essentially straight in the sand-dominated region when d_g=160mm (figure 3-30A and table 3.3).

It is surprising that concavity does not vary with gravel-grain size in the gravel-dominated region but does in the sand dominated region given the way that critical shear stress is calculated. In the gravel-dominated region, the critical shear stress to

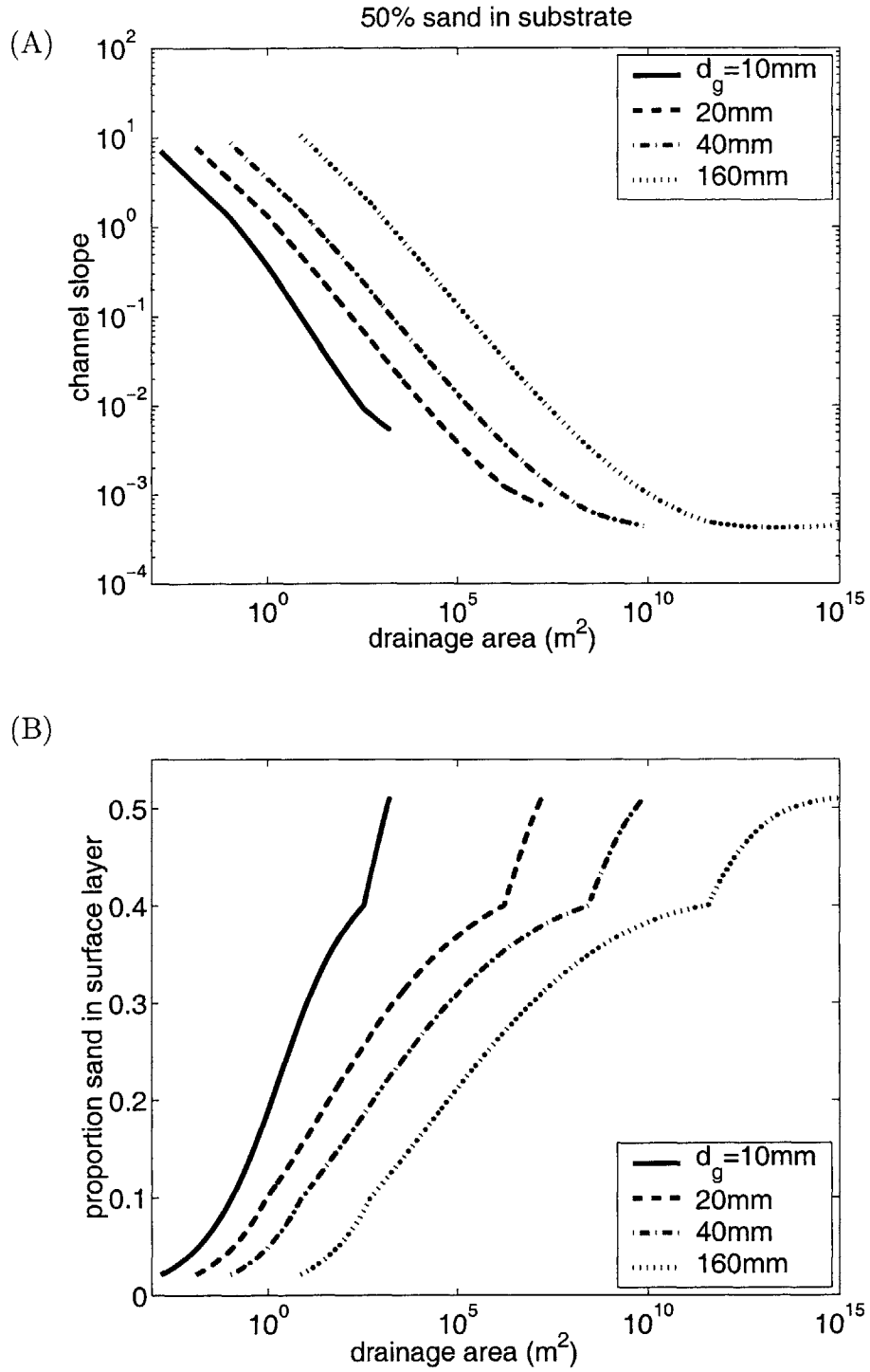

Figure 3-30: Sensitivity of equilibrium slope-area relationship (A) and surface texture-area relationship (B) to the gravel grain size. Wilcock (2001) equations are used. (Uplift rate = 0.1mm/yr; Precipitation rate = 1m/yr falling over 100 days; d_s = 1.5mm)

$f_{sub} = 50\%$	d_g=10mm	d_g=20mm	d_g=40mm	d_g=160mm
$f_s < 0.1$	0.42	0.42	0.42	0.42
$0.1 < f_s < 0.4$	0.64	0.50	0.47	0.45
$f_s > 0.4$	0.33(0.29)	0.21(0.16)	0.12(0.10)	0.02
$0.1 < f_s < 0.2$	0.58	0.51	0.50	0.48
$0.2 < f_s < 0.3$	0.66	0.53	0.50	0.48
$0.3 < f_s < 0.4$	0.64	0.46	0.40	0.35

Table 3.3: Sensitivity of concavity values (θ) to gravel-grain size in different parts of the network ($f_{sub} = 0.50$, d_s=1.5mm, uplift rate is 0.1mm/yr, and precipitation rate is 1m/yr falling over 100 days). All concavity values are calculated over the same surface texture range (minimum $f_s = 0.02$, maximum $f_s = 0.51$), except for those in parentheses, which are calculated to the largest surface sand content possible given the parameters.

entrain sand increases with the gravel-grain size, but in the sand-dominated region τ_{cs} does not depend on the gravel-grain size. As discussed in the beginning of this chapter (section 3.2), we expect concavity to be linked to critical shear stress. However, here the same concavity results with different critical shear stress values (gravel-dominated region), but different concavities result in region where the critical shear stress values are the same (sand-dominated region).

3.6 Discussion and Conclusions

The equilibrium predictions of the slope-area relationship in homogeneous networks (spatially uniform critical shear stress) are unexpected in many ways. In the case when the critical shear stress in negligible, the equilibrium theory that we present predicts a convex channel network. This contradicts natural observations. However, when the critical shear stress is non-negligible and plays an important role in determining the sediment transport rate, concave channels result, as one would expect. In retrospect, it's not surprising that the equations do not predict realistic morphologies without a critical shear stress. All sediment transport equations are empirical fits to highly non-linear data that suggest the presence of a threshold. Applying them otherwise may be inappropriate.

Absolute channel slope and overall network concavity increase with critical shear stress in homogeneous landscapes. Except for the case without a threshold, channel concavity decreases with drainage area. Spatial changes in concavity are due to the competing terms in the slope-area relationship (equation 3.12).

The most unexpected result from the homogeneous theory is the insensitivity to uplift rate of the critical shear term in the slope-area relationship (equation 3.12). Without a critical shear stress term, equilibrium slopes behave as expected - they increase with increasing uplift rate and decrease with increasing precipitation rate. In actuality, it would be impossible for slopes to stay static with changes in uplift rate; higher uplift rates require higher transport rates, and in the homogeneous model, slope is the only variable, and therefore must increase with uplift rate. However, this extreme prediction by the end-member case helps us to understand some of the sensitivity we see in the heterogeneous examples.

Both of the heterogeneous models that we explored predict that changes in grain size, and therefore changes in critical shear stress, play an important role in determining the equilibrium morphology of the landscape. Predicted equilibrium networks are always concave-upward with decreasing median grain size or sand content downstream. Channel slope and concavity are linked to the surface texture as predicted by the homogeneous model. When comparing between networks, the channel slope is steeper (for a given drainage area) when the median grain size of the substrate is larger (e.g. figure 3-17). This makes sense because the threshold is larger and therefore steeper slopes are required to move the sediment. The regions of the network with the smallest median grain size (or largest sand content) have the least concave channels.

A larger precipitation rate results in less steep channels with a coarser texture using the heterogeneous models. This result is intuitive. A higher precipitation rate results in a larger discharge throughout the network. At equilibrium, the network still has to transport the same load, and therefore the slopes decrease to compensate for the increase in discharge. A coarser grain size could be described as armoring, which reduces transport rates under higher flow conditions.

The most surprising prediction by the heterogeneous models is the relationship between equilibrium slopes and uplift rate. Using the Meyer-Peter Müller model, equilibrium slopes generally stay the same or increase with uplift rate, but in some cases there are small parts of the network in channel slopes actually decrease with increasing uplift rate. Using the Wilcock model, slopes can increase, remain the same, or decrease with uplift rate. Counter-intuitive changes in slope are a result of changes in surface texture. In the surprising case in which equilibrium channel slopes decrease with increasing uplift rates, surface texture changes more than compensate for the required increase in transport rates, causing channel slopes to decrease. Buffington and Montgomery (1999) discussed the link between sediment supply and surface texture, however its impact on surface slopes in this study is quite surprising.

There are some limitations to these predictions. We do not consider sediment delivery from the hillslopes and its influence on the grain-size distribution. In a gently rolling topography, one might imagine that only fine material is being washed off the hillslopes. While in an landscape with steep hillslopes, bigger boulders and gravel could be fed into the channel from the surrounding hillslopes. This will obviously affect the grain-size distribution of sediment on the bed and could have important implications for equilibrium slopes.

For example, rapidly uplifting topographies are often associated with steep hillslopes where landslides and debris flows occur. Most likely these would fill a channel up with coarse material. On the other hand, our model predicts that the surface material becomes finer with increasing uplift rates in order to transport more material. This could be considered a counter-intuitive result if more landslides occur in rapidly uplifting areas and feed the channel with course material. Our model may not be appropriate in these regions which are probably more controlled by incision into bedrock, rather than transport of sediment. However, the link between hillslopes and channels should not be ignored. Numerical models are a good tool for exploring these questions.

The results presented in this chapter highlight the important role of sediment grain size in determining transport rates. When the threshold for entrainment is

ignored, unrealistic concavities result. Downstream changes in grain size, which lead to downstream changes in critical shear stress, are intimately linked with changes in channel slope. Further, the mutual adjustment of both channel slope and surface texture to a change in forcing can lead to unexpected results. At the very least, our study suggests that one should not ignore the important role of surface texture in alluvial networks.

Chapter 4

Transients in Transport-Limited Alluvial River Networks

4.1 Motivation and Background

Past climatic and tectonic conditions could highly affect the morphology of the landscape we see today. If boundary conditions have been changing fast enough so that erosion rates cannot keep pace, then the landscape is not in equilibrium and inferring future or past changes can be difficult. In this work, we use a numerical model to investigate the effects of a change in uplift rate (or similarly a change in base-level fall) and a change in climate on the erosion patterns in an alluvial network. We focus on the link between channel bed texture and slope during the transient response. We address the following questions: How do changes in climate affect erosion and deposition in a river network? Can past climates be inferred from the texture of alluvial deposits? and How do channels respond to a change in base-level due to sea-level rise and fall or changes in tectonics?

A number of numerical modeling studies have investigated the transient form of alluvial channels. Snow and Slingerland (1987) looked at adjustments in the channel profile using a 1-D model. In the three cases examined - evolution from a straight, convex, and concave initial profile - the initial conditions are quickly erased, and the transient channel reaches a shape that is similar to the final profile. Willgoose

(1994) investigated the decline in catchment relief of a homogeneous transport-limited drainage network in response to a cessation in uplift rate. He found that the initial response is dominated by a reduction in catchment relief, but that the network quickly transitions to a declining state in which the channel form does not change. In fact, when scaled appropriately, the transitional form of the slope-area relationship is indistinguishable from the equilibrium form. Whipple and Tucker (2002) showed that channel concavity also remains constant during a transition from low- to high-uplift rate (in a homogeneous transport limited network). The initial response to an increase in uplift rate is at the outlet, but the upper parts of the network begin to respond before the lower parts have reached their new equilibrium slopes; resulting in the characteristic slope-area relationship.

Tucker (2003) added some complexity to the erosion processes by including both a threshold for sediment transport (critical shear stress) and a model for floods of variable magnitude. The presence of variable storms and a transport threshold implies that not all storms result in erosion. Under these conditions, he explored the transient form of an eroding escarpment. Without a threshold, channels are smooth and convex as the plateau erodes away. However, the topography is rougher and channels are concave when there is a threshold for sediment entrainment.

Baldwin et al. (2003) explored the factors which control the time of response in post-orogenic decay. They began using a detachment-limited stream power model model and found that this model produces response time-scales that are relatively short compared to the believed life-time of mountain belts. However, they found that the presence of a detachment threshold increases response times 20-fold. Other complications in response, such as the transition to a transport-limited regime as channels became inundated with sediment also increased response time.

A number of numerical modeling studies have explored the impacts of climate change on erosion and deposition (e.g. Rinaldo et al. (1995); Tucker and Slingerland (1997); Howard (1999); Coulthard et al. (2000)). Although these studies have different focuses, generally they show that a wetter climate (wetter refers to different things in different studies) leads to increased erosion in the headwaters and expansion of the

drainage network, resulting in an increase in sediment discharge and aggradation at larger drainage areas .

For example Rinaldo et al. (1995) used a self-organization model which lowers slopes to their threshold value (no deposition occurs), to investigate whether climate oscillations leave a distinct signature on the landscape. Climate change is modeled through changes in critical shear stress; humid periods correspond to low critical shear stress values and arid periods correspond to high critical shear stress values. When the climate is wet, predicted drainage density is high, and when the climate is dry, drainage density is low. Network response to climate change is asymmetrical, suggesting a complex response in the landscape as climate varies.

Response to climate change using a landscape evolution model was also studied by Tucker and Slingerland (1997). Their model includes both a threshold for detachment and transport of sediment. Changes in storm frequency, storm intensity and critical shear stress were considered. The responses from an increase in runoff intensity or a decrease in critical shear stress were similar; both resulted in a rapid increase in drainage density and deposition in the main channel. On the other hand, when runoff intensity decreased or critical shear stress increased, the response was much slower, as drainage density decreased. Sinusoidal variation in runoff intensity produced a punctuated response in denudation rates (short periods of rapid erosion) and an asymmetrical response in drainage density. Further, landscape response depended on the period of variation. Again, these results highlight the complex response within a drainage network due to changes in climate.

Regardless of the exact perturbation in forcing, thresholds for entrainment appear to be a key factor in landscape response. We explore the impact of thresholds in disequilibrium networks by allowing the surface texture, and therefore the critical shear stress, to vary in space and time. Changes between one equilibrium network to another are modeled.

4.2 Transient Response Using a Multiple Grain-Size Model

We use the CHILD model and the sediment transport relationships (equations 3.26 and 3.27) and critical shear stress data (figure 3-21) presented by Wilcock (1998, 2001) to model sediment transport rates in a sand and gravel mixture. Erosion and deposition in all numerical simulations is limited by the amount of sediment that the channel can transport.

In the previous chapter of this thesis, we presented a model to predict the equilibrium slope-area relationship and surface texture-area relationship. The equilibrium numerical results using the CHILD model agree with the equilibrium predictions (similar to the results of Gasparini et al. (2003) using the GOLEM model (e.g. Tucker and Slingerland (1996)). However, transitions from one equilibrium state to another are not necessarily intuitive from the equilibrium conditions. Changes in surface texture add an extra degree of freedom to network response, as opposed to adjustments in channel slope only.

The network response to an increase in uplift rate and precipitation rate (separate experiments) is examined here. The flux boundary conditions are the same in all of the experiments. We use a synthetic square drainage network that has no-flux boundaries on all four sides, with a single corner outlet through which water and sediment can pass out of the network. The point downstream from the outlet has a constant elevation of zero and the entire network is uplifted at the same rate. Precipitation is uniform spatially and throughout the duration of a numerical experiment. The network referred to as the 50% sand network has a substrate composition of 50% 16mm gravel and 50% 0.5mm sand. The network referred to as the 10% sand network has a substrate composed of 90% 40mm gravel and 10% 1.5mm sand. The substrate composition is uniform in space in both networks. The texture of the surface layer can adjust to changes in slope and fluvial discharge, and if deposition occurs, sediment layers will form above the substrate. In these experiments, an active layer depth of 3m is used. The average cell size for the numerical experiments is $2,500m^2$, and the

total domain size is $1.4x10^6m^2$.

All experiments start and end with concave channels in which the surface sand content increases downstream (Chapter 3 of this thesis; Gasparini et al. (1999); Gasparini et al. (2003)). In the 50% sand network, the initial equilibrium network contains less sand in the surface layer than in the substrate. On the contrary, the lower parts of the 10% sand network initially contain more sand in the surface layer than in the substrate. The relationship between the surface texture and substrate texture is important to keep in mind while examining the transient response because as erosion rates increase, more of the substrate material is incorporated into the surface layer.

4.2.1 Response to an Increase in Uplift Rate

In this section we illustrate the response of channel slopes and surface texture to a step increase in uplift rate. When the drainage network reaches its new equilibrium state, erosion rates have increased throughout the network. However, during the transient evolution, erosion rates both increase and decrease. We illustrate the response of the 50% sand network and the 10% sand network to a five-fold increase in uplift rate (from 0.1mm/yr to 0.5mm/yr). The patterns illustrated by both numerical experiments follow the same trends.

4.2.1.1 50% Sand Network

Figure 4-1A illustrates the equilibrium slope-area relationship for the low (dashed line) and high (solid line) uplift rates. Similarly, the equilibrium surface texture-area relationships are shown in figure 4-1B. The equilibrium lines are obtained using the iterative method described in chapter 3 of this thesis. The data from the numerical equilibrium networks are also shown in figure 4-1 as circles which overlap the equilibrium lines. All cases explored using the equilibrium iterative model (chapter 3) predict that the surface sand content increases with uplift rate. The change in equilibrium channel slope in this example is somewhat surprising. The higher uplift case has a smaller equilibrium concavity; slopes are steeper in the larger drainage areas

near the outlet and shallower in the smaller drainage areas. Just from these equilibrium results, we already know that the transition between uplift rates will not be a simple rise in slopes throughout the network.

The initial equilibrium topography of the 50% sand network, shaded by the texture of the surface layer, is illustrated in figure 4-2. In this figure, darker colors contain more sand (versus gravel) and therefore are finer. Initially, the surface layer does not contain any of the finest material in the range of the color bar (black). The surface contains less sand than the subsurface throughout the numerical experiment.

The increase in uplift rate is felt first at the outlet and propagates up through the network (figure 4-3), as expected (e.g. Whipple and Tucker (2002); Tucker (2003)). The surface texture becomes much finer near the outlet, both in the main channel and in points surrounding the main channel (darker shading near outlet in figure 4-3A). 4,000 years after the uplift increase (figure 4-3A), the upper reaches of the network have yet to respond to the increase in uplift rate and there is no change in their surface texture. The elevations of the upper parts of the network have increased because the slopes in the lower parts of the network have increased.

By the time shown in figure 4-3B, the surface of the entire network contains more sand than it did initially. In this example, we expect the surface texture to be finer in equilibrium, so this change in not entirely unexpected. As a general pattern, surface sand content increases downstream in the network, even during the transient.

The exact change in surface texture in response to the increase in uplift rate is partly a result of the texture of the material replenishing the surface layer (the substrate material). Everywhere in the network, the initial equilibrium surface texture contains less sand than the substrate (figure 4-1B). So one might expect that an increase in erosion rate alone would cause the sand content of the surface layer to increase. However, if the erosion rates of both sand and gravel were to increase at the same rate, the surface texture would not change during the transient response.

Because the sand and gravel erosion rates respond differently during the transient, the surface texture changes. We define the sand erosion ratio as the ratio of the local sand erosion rate to the local total erosion rate, $\frac{\partial z_s}{\partial z_{total}}$. (The total erosion rate is the

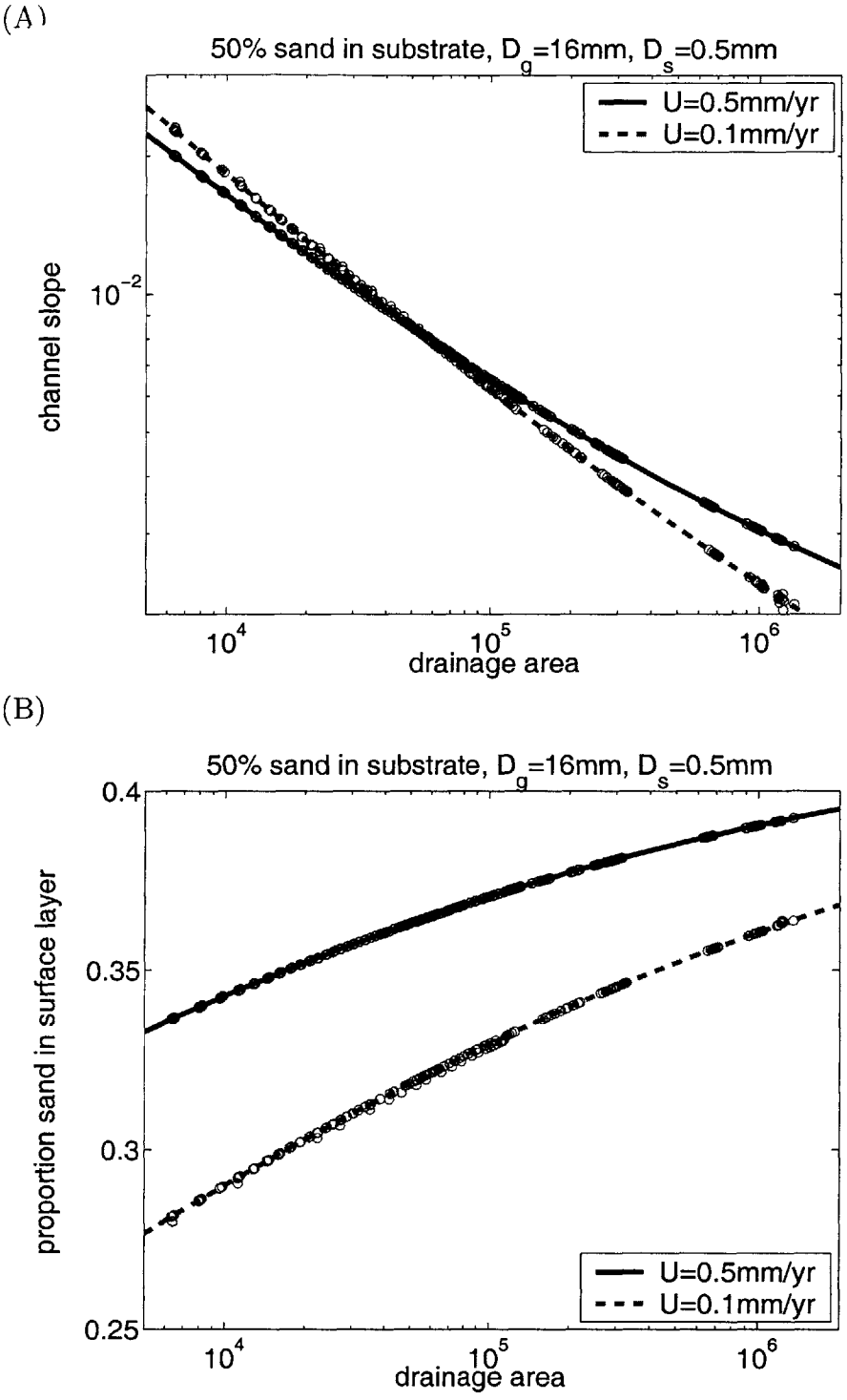

Figure 4-1: Expected equilibrium slope-area relationship (A) and surface texture-area relationship (B) for the initial condition (U=0.1mm/yr) and increased uplift rate (U=0.5mm/yr) for the 50% sand network. Solutions from iterative model described in chapter 3. Data from equilibrium networks are also shown as circles.

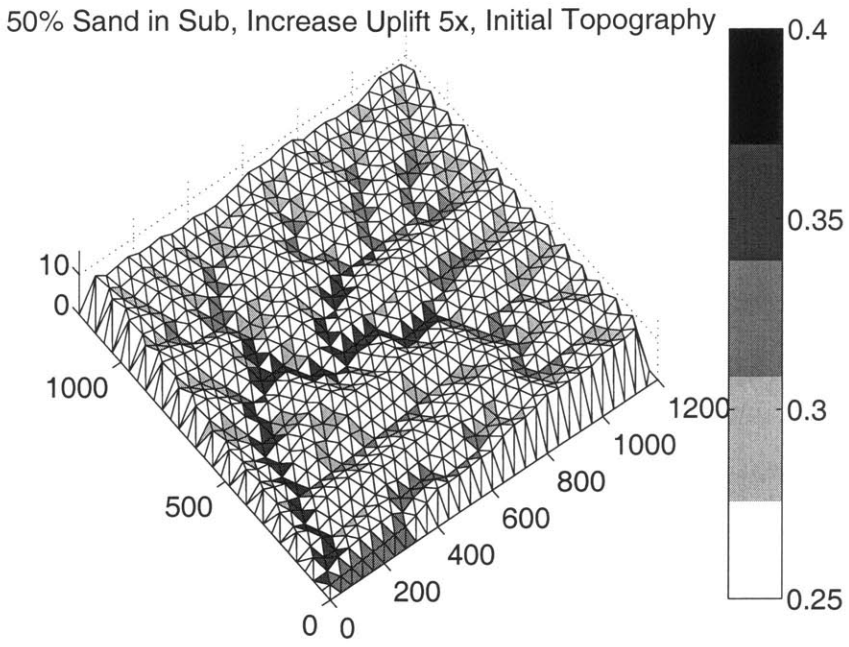

Figure 4-2: Initial equilibrium topography, shaded by surface texture. Darker shades contain more sand (vs. gravel) and are therefore finer. (Substrate contains 50% sand, D_g=16mm, D_s=0.5mm, U=0.1mm/yr) Note that the texture and elevation scale are the same in the next two figures.

sum of the sand and gravel erosion rates, equation 2.9.) In this example, because the substrate material is composed of 50% sand, at equilibrium, the sand erosion ratio is 0.5. Figures 4-4A, B, and C illustrate the sand erosion ratio across the topography at three different times after the uplift rate increase. In these figures, yellow represents the equilibrium sand erosion ratio. When this value drops, it means that the ratio of sand erosion to gravel erosion drops from its equilibrium value. As a result, more gravel than sand is removed from the surface. This alone would result in a finer surface, however, in this case the change in surface sand content is exacerbated by the relatively sandier material supplying the surface from below.

Changes in the sand erosion ratio start near the outlet and move up the network (figures 4-4A, B, and C). The initial decrease in the sand erosion ratio (figure 4-4) results in a sandier surface near the outlet 4,000 years after the uplift increase (figure 4-3A). By 6K, the sand erosion ratio has increased in the lower parts of the network, in some places to higher than its equilibrium value, while the upper parts

(A)

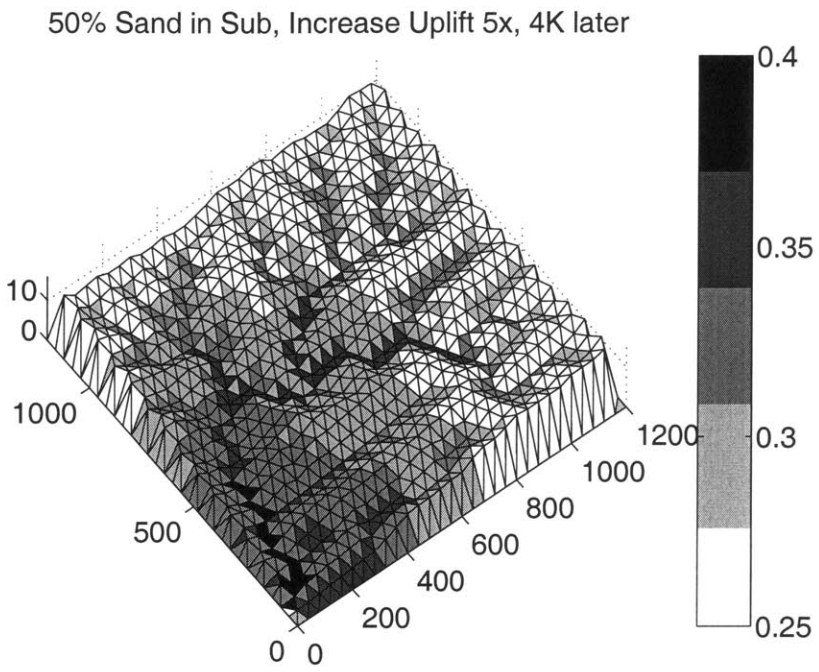

(B)

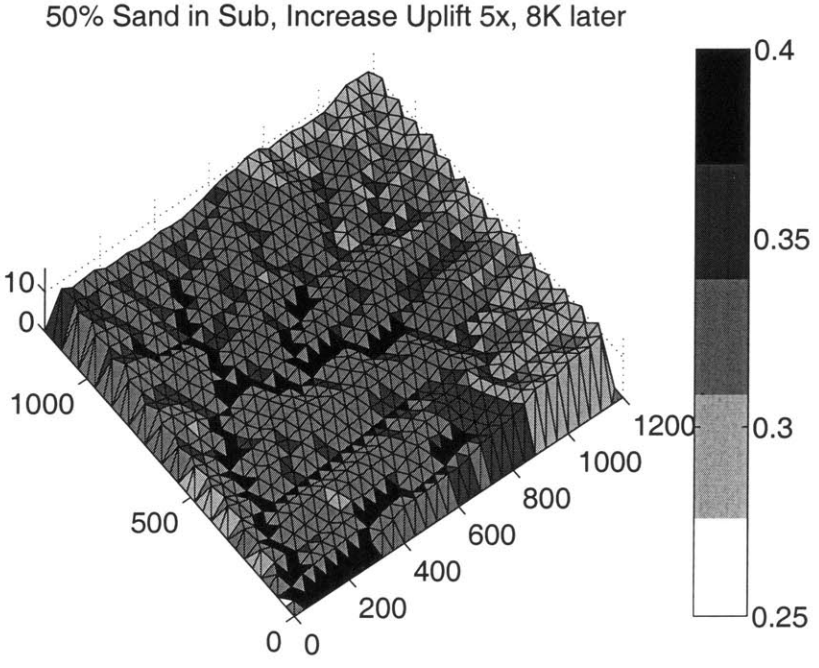

Figure 4-3: Response of topography and surface texture (initial condition from previous plot) to a five-fold increase in uplift rate at 4,000 (A) and 8,000 (B) years after the increase in uplift rate.

of the network still have a relatively low sand erosion ratio. The increase in the sand erosion ratio in the lower parts of the network, causing more sand to be eroded relatively to gravel, results in a decrease in the surface sand content in some areas around the outlet by 8K (figure 4-3B).

(A)

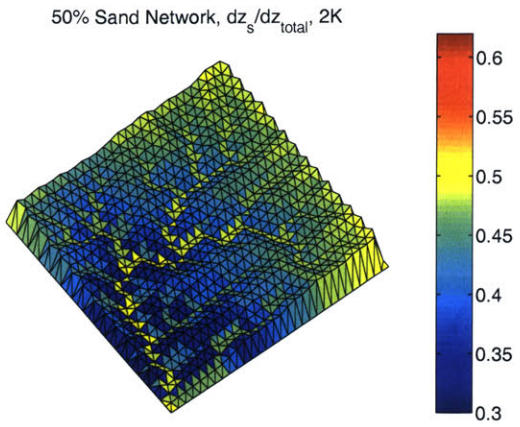

(B)

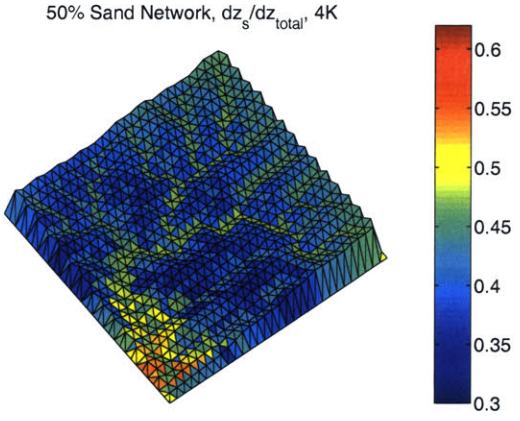

(C)

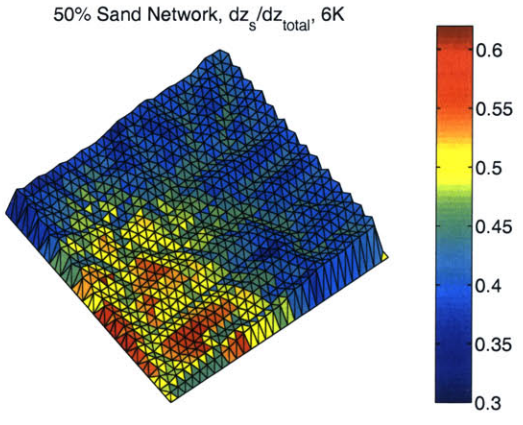

Figure 4-4: Topography of the 50% sand network shaded by the ratio of the local sand erosion rate to the local total erosion rate (sand erosion ratio) at 2,000 (A), 4,000 (B), and 6,000 (C) years after the increase in uplift rate. In these figures, yellow is the equilibrium sand erosion ratio.

We focus now on the response in the main channel to highlight some of these results. Figure 4-5 illustrates the initial changes in main channel elevation (A) and slope (B) in the 50% sand network. Initially, slopes increase throughout the main channel in response to the increase in uplift rate (figure 4-5B). Slopes near the outlet rise more than those in the upper parts of the main channel. This is not so surprising given that channel slopes will actually decrease at lower drainage areas when they reach their new equilibrium values. In the last two time slices shown in this figure, slopes everywhere in the main channel have increased above their new equilibrium value. The local over-steepening in the channel between $4x10^4$ and $5x10^4m^2$ that occurs 8,000 years after the increase in uplift rate (see dotted line in figure 4-5) is due to a network capture above this location. (This is not a result of unstable numerics; we have run the model multiple times with different time-steps and the same rearrangement always occurs.)

Figure 4-6 illustrates the initial response of surface texture and total erosion rates (plotted as the ratio of total erosion rate to new uplift rate) in the main channel. As already illustrated by the sand-topographies (figures 4-2 and 4-3), the surface texture becomes finer everywhere in response to the uplift increase (figure 4-6A). Even though channel slopes have over-steepened above their new equilibrium value by 8,000 years, the channel surface still contains more gravel (less sand) than it will when it reaches its new equilibrium condition. Total erosion rates increase throughout the main channel but most rapidly near the outlet. The local increase in channel slope downstream (between $4x10^4$ and $5x10^4m^2$) at 8K years (figure 4-5B) corresponds to the local downstream decrease in erosion rate (between $4x10^4$ and $5x10^4m^2$) in figure 4-6B. Erosion rates temporarily decrease locally in response to the increase in sediment load from the network rearrangement.

Given that slopes over-steepen throughout the main channel, they must come back down. The fall in slopes is accompanied by a decrease in channel elevations (figure 4-7A). In order for slopes to decrease, the total erosion rate needs to surpass the uplift rate (figure 4-8B). In the upper reaches of the channel, the erosion rate reaches a value of almost double its new equilibrium rate. When erosion rates reach

(A)

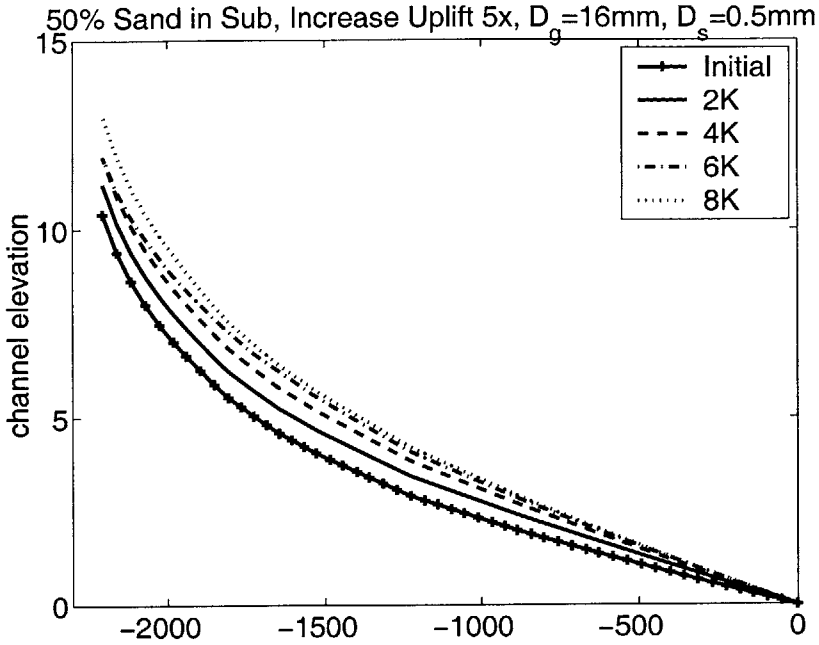

(B)

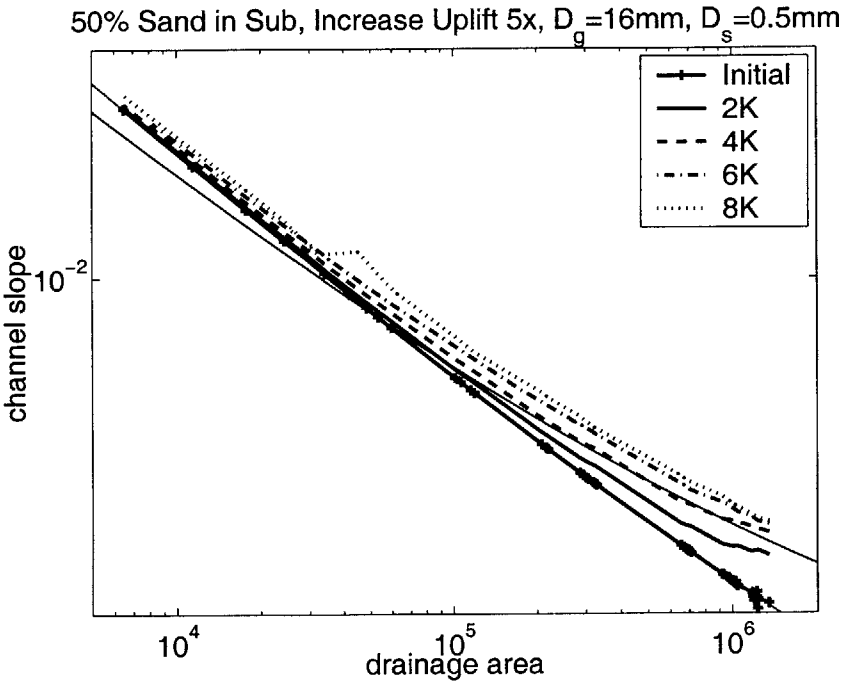

Figure 4-5: Initial changes in main channel elevation (A) and channel slope (B) in response to a five-fold increase in uplift rate using the Wilcock sediment transport model. The thin lines that run through the plot are the equilibrium solutions for the low uplift rate (shallower at the outlet) and high uplift rate (steeper at the outlet, shallower at low drainage areas).

(A)

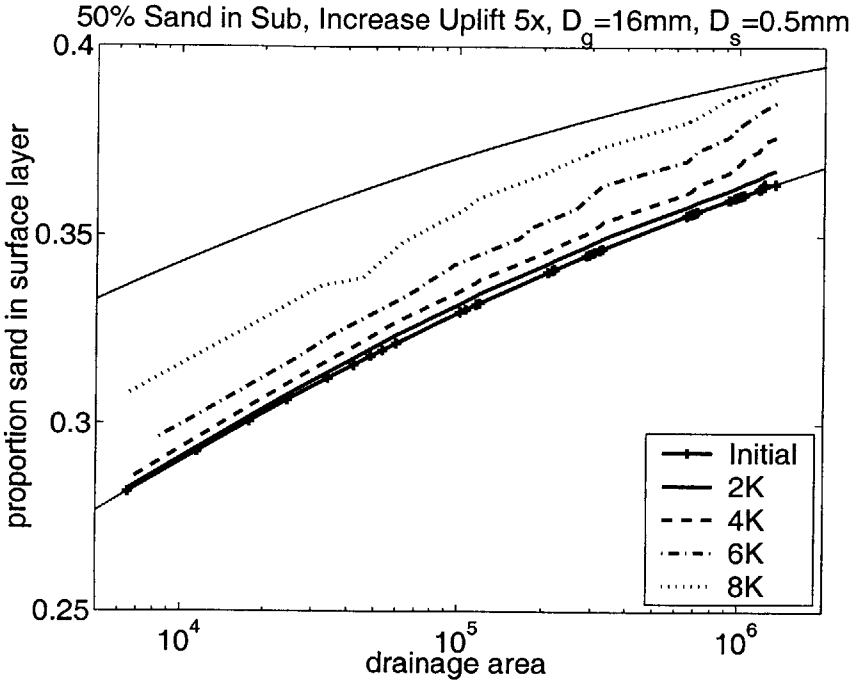

(B)

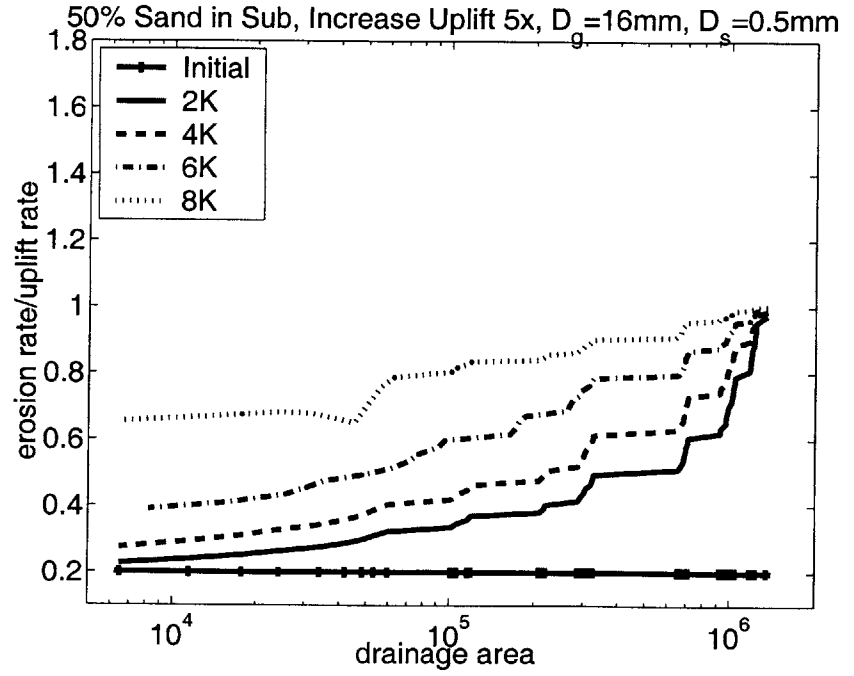

Figure 4-6: Changes in surface texture (A) and total erosion ratio (B) in response to a five-fold uplift increase using the Wilcock sediment transport rate. The total erosion ratio is one when the new equilibrium is reached. It begins at 0.2 because the the uplift rate has increase by five times. (The equilibrium texture solutions for the low and high uplift rate are shown as the thin lower and upper lines running through the texture plot, respectively.)

their highest values throughout the main channel (at 12K, the dashed line in figure 4-8B), the channel surface also contains the greatest amount of sand (figure 4-8A). Given that the surface sand content is between 10% and 40%, the critical shear stress to entrain both sand and gravel is decreasing with increasing sand content (chapter 3, figure 3-21). This change in surface texture allows for the high erosion rates, even though channel slopes have decreased. During the period between 8K and 12K, channel slopes have switched from rising to falling in the main channel (solid line with bars to dashed line in figure 4-7B), but surface sand content is still increasing (same style lines in figure 4-8A). Just as channel slopes over-steepened, the surface sand content surpasses its new value. However, channel slopes begin to fall before the surface sand content begins to decrease.

The network is very nearly in equilibrium by the last time (16K) shown in figures 4-7 and 4-8. Changes in channel slope and profile are imperceptible after this time. The surface sand content drops slightly below its new equilibrium value and then settles. This adjustment of surface texture causes total erosion rates in the main channel to drop slightly below their equilibrium value and then to settle.

4.2.1.2 10% Sand Network

Equilibrium slope-area and surface texture-area relationships for the 10% sand network are shown in figure 4-9. There is almost no change in equilibrium channel slopes with uplift rate using these parameters (figure 4-9A). Channel slopes only change in higher drainage areas, where they increase. Surface sand content increases everywhere with uplift rate (figure 4-9B). An important difference between this example and the previous example (50% sand network) is that in most of the main channel the surface layer contains more sand than the substrate layer.

The initial topography shaded by surface sand content is illustrated in figure 4-10. It is only a coincidence that the equilibrium 10% sand and 50% sand networks look the same. Both evolve independently and network patterns can be highly variable (Ijjasz-Vasquez et al. 1992).

The response in the 10% sand network is similar to that in the 50% sand network.

(A)

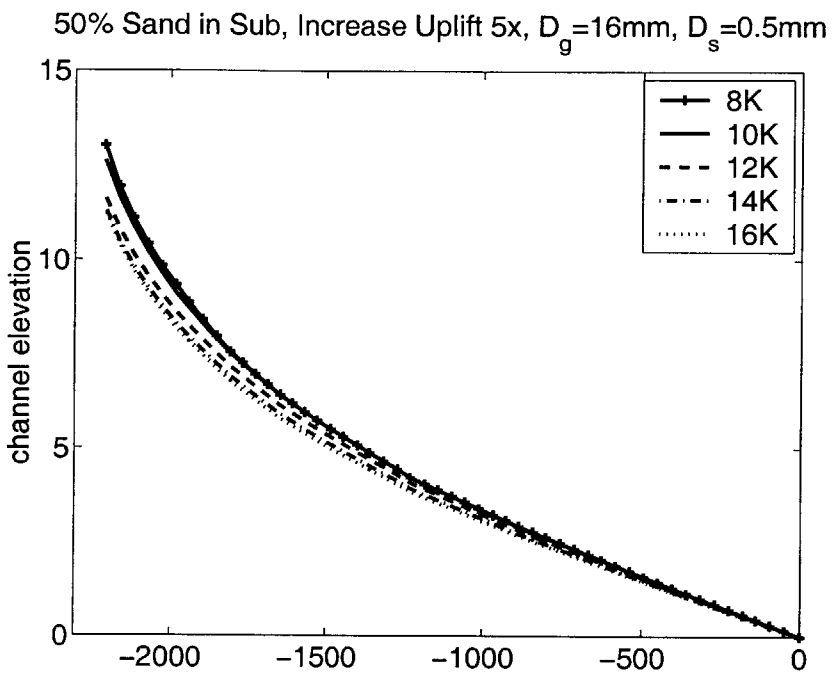

(B)

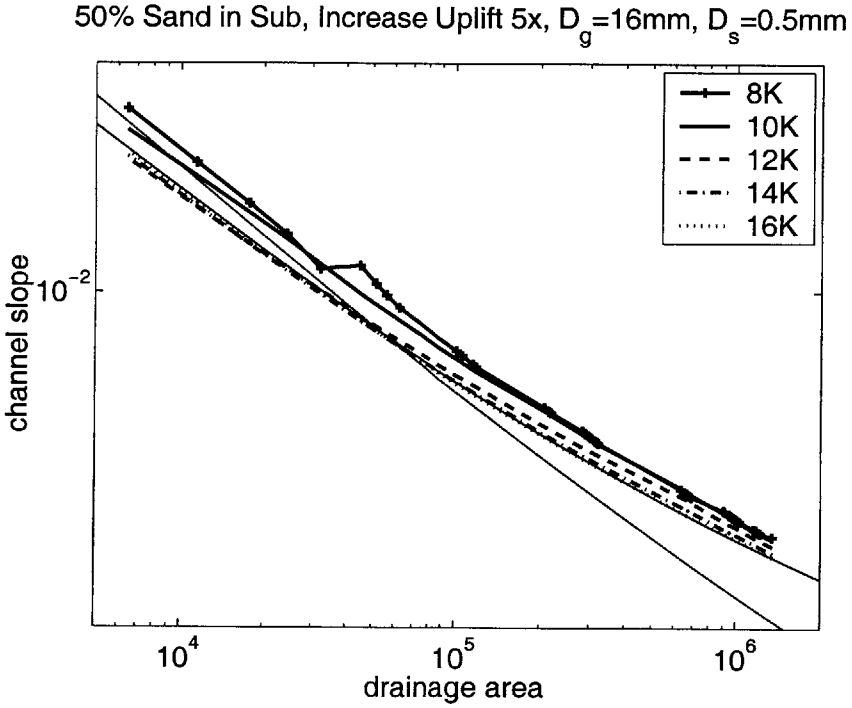

Figure 4-7: Later changes in main channel elevation (A) and channel slope (B) in response to a five-fold increase in uplift rate using the Wilcock sediment transport model. The thin lines that run through the plot are the equilibrium solutions for the low uplift rate (shallower at the outlet) and high uplift rate (steeper at the outlet, shallower at low drainage areas).

(A)

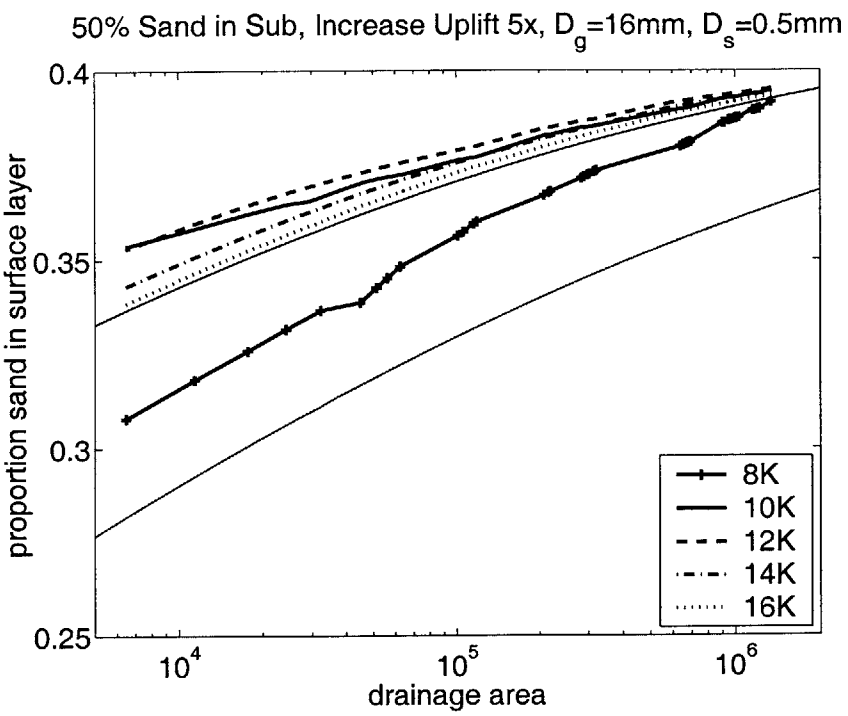

(B)

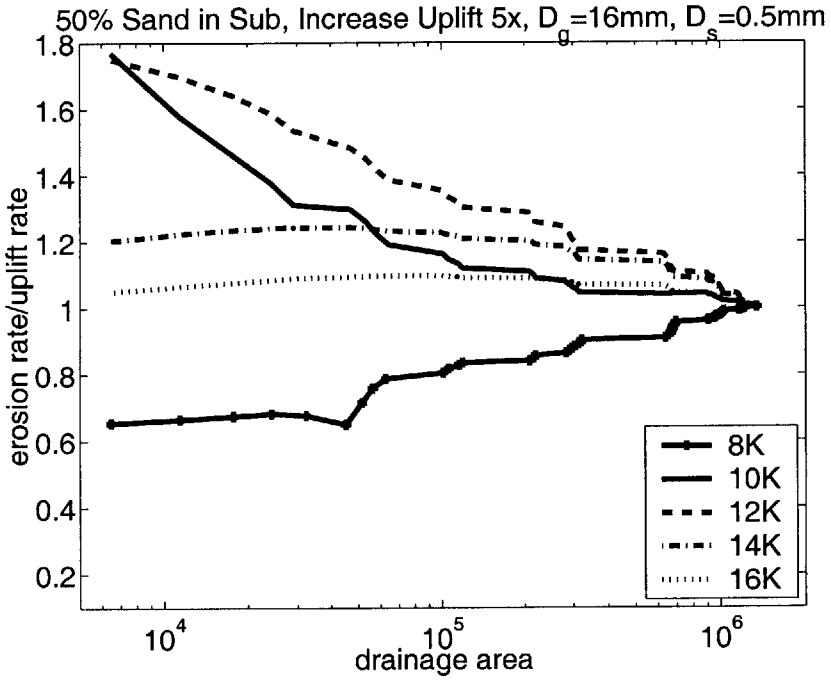

Figure 4-8: Later changes in surface texture (A) and erosion ratio (B) in response to a five-fold uplift increase using the Wilcock sediment transport rate. (The equilibrium texture solutions for the low and high uplift rate are shown as the thin lower and upper lines running through the texture plot, respectively.)

(A)

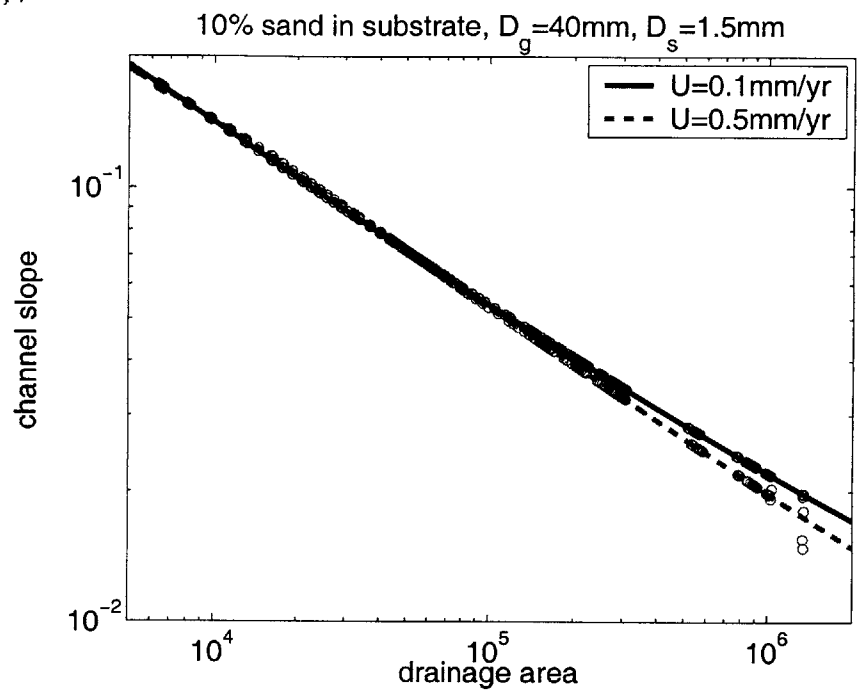

(B)

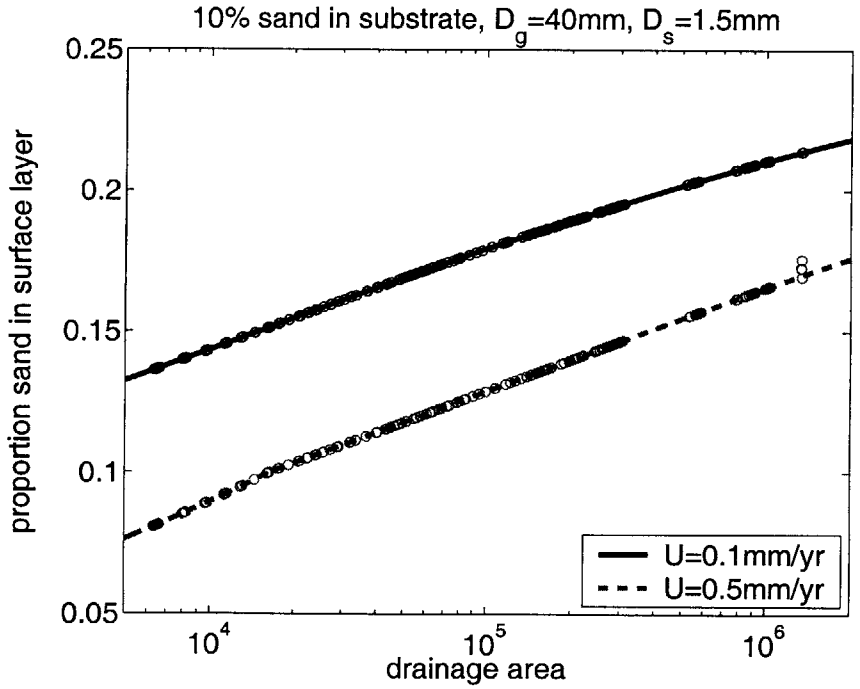

Figure 4-9: Predicted equilibrium slope-area relationship (A) and surface texture-area relationship (B) for the initial condition (U=0.1mm/yr) and increased uplift rate (U=0.5mm/yr) in 10% sand network. Solutions from iterative model described in chapter 3. Note that data from equilibrium numerical networks are also shown as circles.

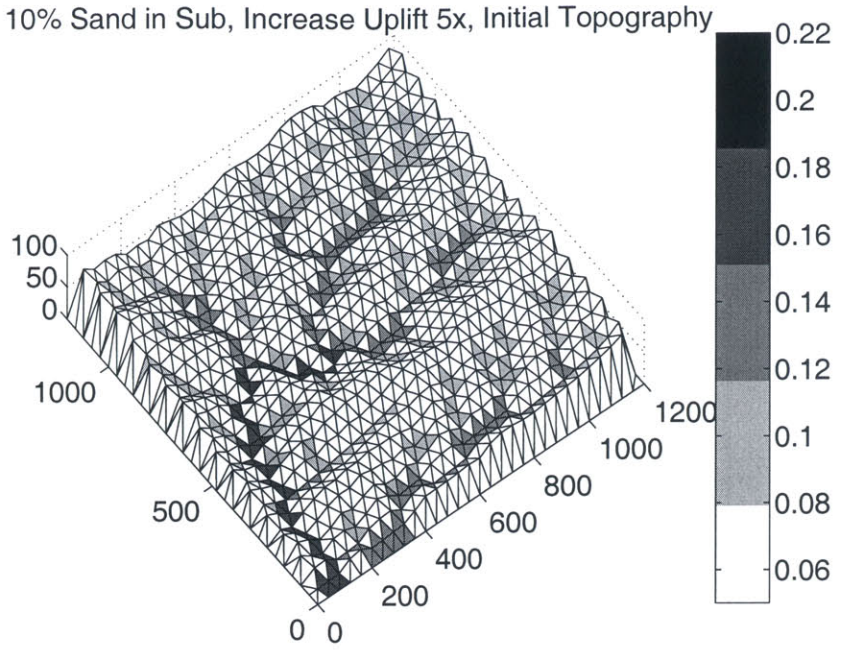

Figure 4-10: Initial equilibrium topography, shaded by surface texture. (Substrate contains 10% sand, D_g=40mm, D_s=1.5mm, U=0.1mm/yr) Darker shades contain more sand (vs. gravel) in the surface layer, and are therefore finer. Note that elevation and texture scale remain the same in the next two figures.

Surface sand content increases, first near the outlet and later moving up through the network (figures 4-11A and B). 30,000 years after the increase in uplift rate, the surface texture is finer almost everywhere in the network (figure 4-11A). 60,000 years after the uplift increase, the surface sand content has increased almost everywhere from the 30K time slice, however points surrounding the lower parts of the main channel contain less sand than they did at 30K. This time-varying response in different parts of the drainage network results in a complex change in the texture of the incoming sediment load at different parts of the network.

The pattern of slope and elevation change in the main channel of the 10% sand network is also similar to the previous example (figure 4-12). Slopes are an order of magnitude larger in the 10% sand network, due to the larger grain size and smaller sand content of the substrate (chapter 3). Initially slopes increase everywhere, although the steeper slopes of the 10% and network take more time to rise than those in the 50% sand network. 10,000 years after the increase in uplift rate, the slopes in

(A)

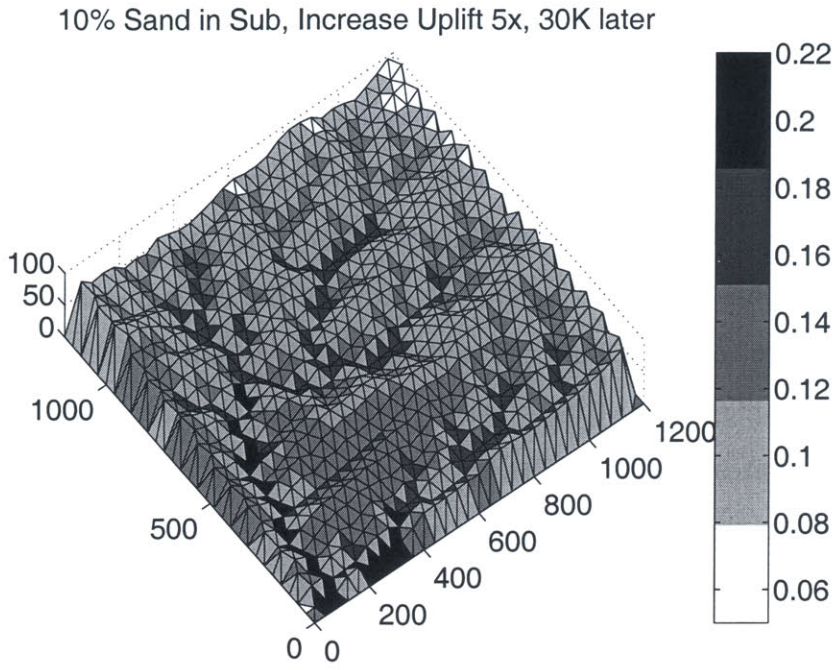

(B)

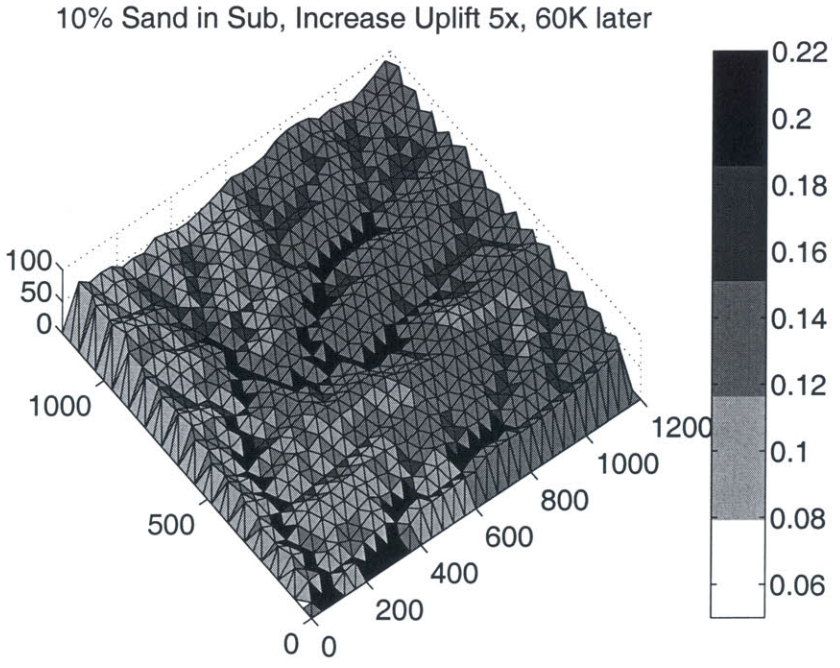

Figure 4-11: Response of the topography and surface texture to a five-fold increase in uplift rate 30,000 (A) and 60,000 (B) years later (initial condition shown in figure 4-10). Note that the response is from the outlet up the network.

the main channel have increased to reach a state that is almost identical to the new equilibrium condition; in fact this time slice is not even detectable in figure 4-12B because it overlaps the high uplift equilibrium solution line (running through the plot). However, the surface texture at 10K has barely changed from its initial state (solid line in figure 4-13B). By 40K, slopes in the main channel have over-steepened and stabilized (30K and 40K profiles are nearly identical, figure 4-12), and surface texture is very close to its new equilibrium value in the main channel. Total erosion rates are very close to equilibrium throughout the main channel as well (figure 4-13B).

One might expect that initially the surface texture would become coarser as total erosion rates rise, because the material supplying the surface layer (substrate material) is coarser than the surface layer in most parts of the main channel. Even though the total erosion rate is rising, the sand erosion ratio is dropping. Because the sand erosion ratio drops during the transient response, more gravel is eroded away than sand, leaving behind a sandier surface. We saw a similar pattern in the 50% sand network.

Figure 4-14 illustrates the sand erosion ratio across the topography at two different times. Given the color scale used in these figures, the initial topography would be completely yellow (not shown), because the sand erosion ratio would be 10% of the total erosion rate everywhere. At 10K (figure 4-14A), most parts of the topography have a sand erosion ratio of less than 10% (shaded blue or green) resulting in a finer surface. At 30K (figure 4-14B), far from the outlet, the sand erosion ratio is still less than 10% (green and blue shades), but in some points surrounding the lower parts of the main channel the sand erosion ratio has increased (yellow and orange). The surface sand content of points surrounding the lower part of the main channel stabilizes and will begin to fall again.

(A)

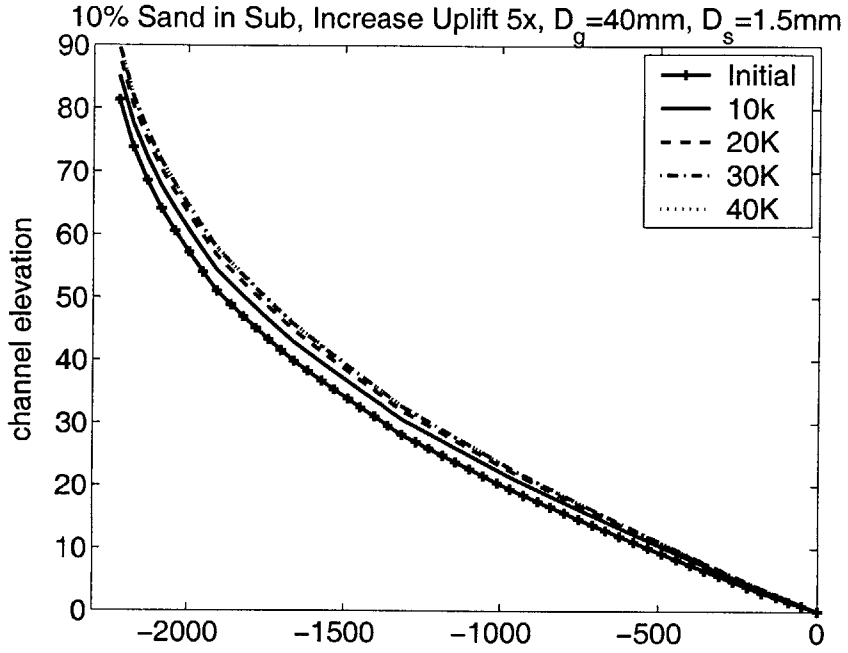

(B)

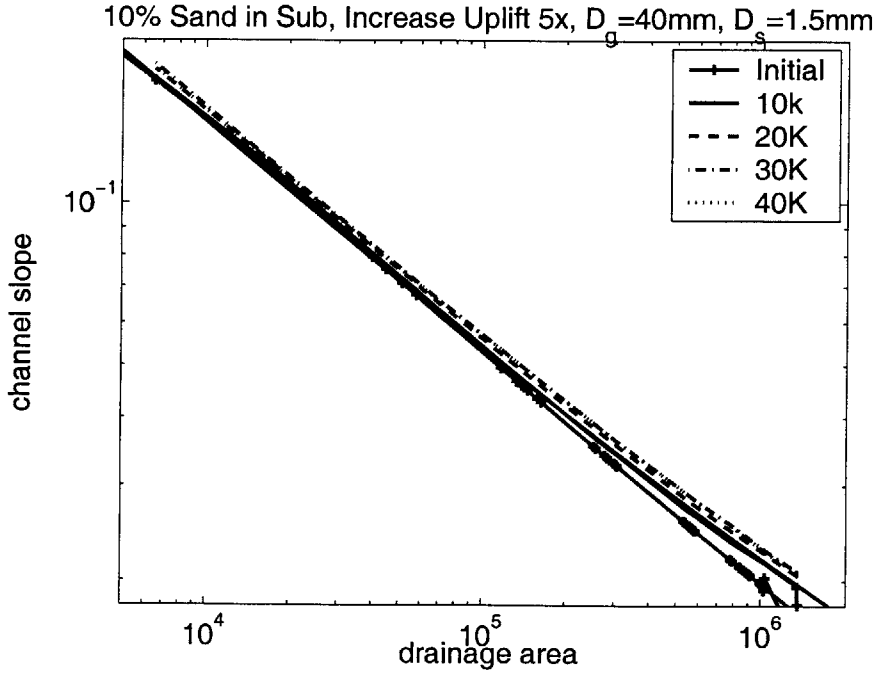

Figure 4-12: Initial changes in main channel elevation (A) and channel slope (B) in response to a five-fold increase in uplift rate using the Wilcock sediment transport model. (The line that runs through the plot is the equilibrium solution for the higher uplift rate. The equilibrium line for the low uplift rate overlaps the initial condition.)

(A)

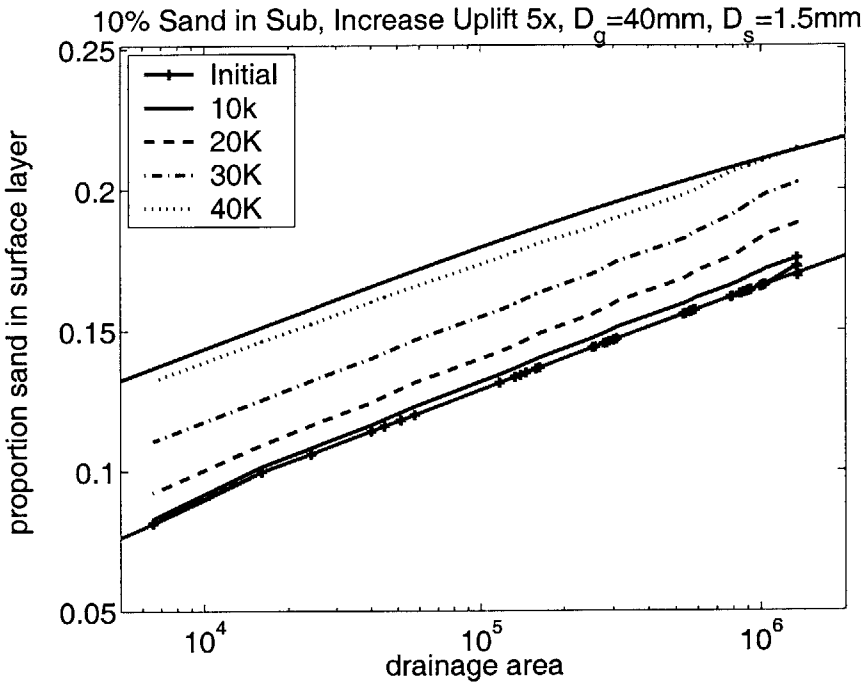

(B)

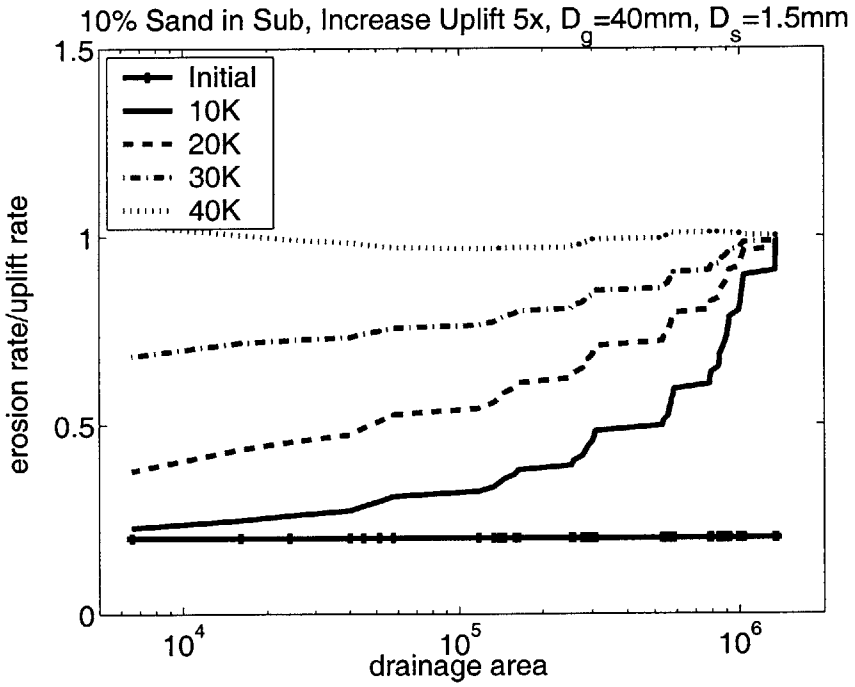

Figure 4-13: Initial changes in surface texture (A) and total erosion ratio (with respect to the new uplift rate) (B) in response to a five-fold uplift increase using the Wilcock sediment transport rate. (The equilibrium texture solutions for the low and high uplift rate are shown as the lower and upper lines running through the texture plot, respectively.)

(A)

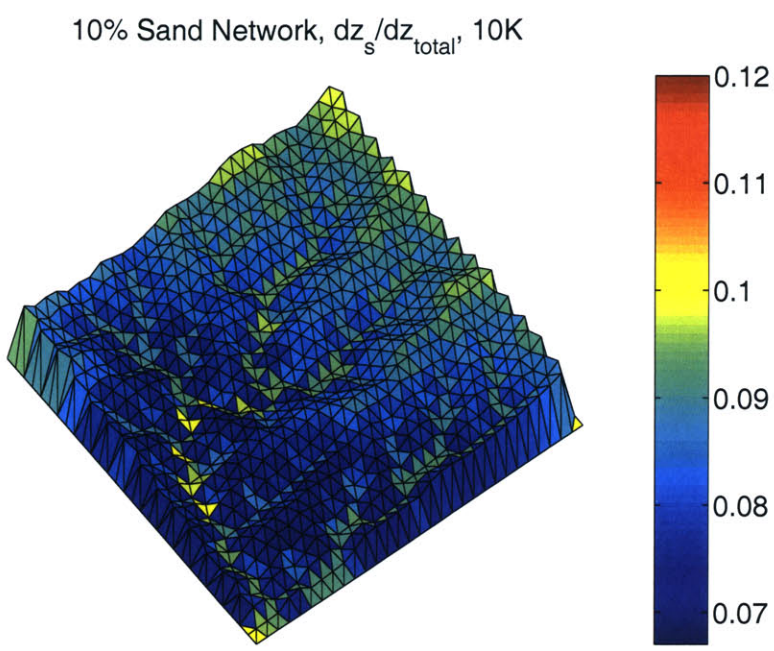

(B)

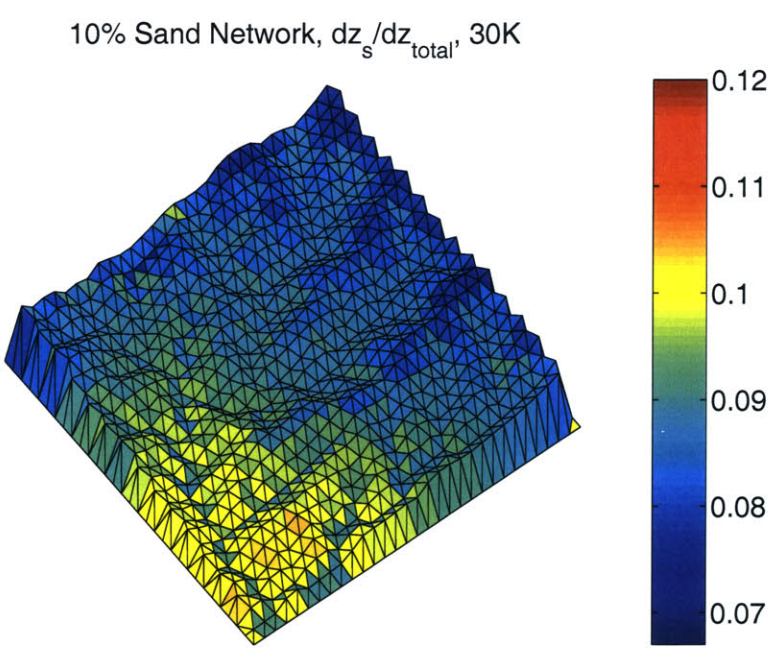

Figure 4-14: Topography of the 10% sand network shaded by the ratio of the local sand erosion rate to the local total erosion rate (sand erosion ratio).

After 40K, slopes decline to their new equilibrium values (figure 4-15) while both surface sand content and total erosion rates in the main channel rise until 60K and then start to fall (figure 4-16). This pattern of falling slopes in the main channel while surface sand content and total erosion rates are still rising is similar to that in the 50% sand network.

After 80K, the erosion rates in the 10% sand network actually drop below equilibrium values, but only slightly, and then rise back up. On the scales used in figures 4-12 - 4-16, the change in surface texture and channel slope after 80K is not noticeable.

4.2.2 Transient Response to an Increase in Precipitation Rate

We now examine the response in the 50% sand network to an increase in precipitation rate from 1m/yr to 1.5m/yr. The same initial condition is used here as was for the uplift experiment with the 50% sand network. Uplift rate remains constant in the following simulation. The precipitation rate increases instantaneously and remains at the same higher rate for the entire duration of the experiment.

The entire network feels the change in precipitation as soon as it occurs, resulting in immediate changes across the network as opposed to the response in the uplift experiments which was from the outlet up. The numerics of this experiment are much more sensitive and require much smaller time-steps for stability than required in the uplift perturbation experiments. We initially use a time-step of 0.0005 years ($\approx$ 0.2 days), and increase this time-step by ten-fold after the first 1,000 years of the model run. We ran the same simulation multiple times with different time-steps. After 100 years a 0.0005yr time-step and a 0.005yr time-step converge to the same result and remain the same. The same stability testing was used in the uplift experiments, and an initial time-step of 0.02 years was sufficient for the 50% sand uplift experiment. The 10% sand network required a smaller time-step for the uplift experiment (0.005yrs). Because of computational limitations, we could not generate stable results from the 10% network when increasing precipitation.

In general, a higher precipitation rate will result in an equilibrium surface texture which contains less sand (chapter 3). However, the transition from one equilibrium to

(A)

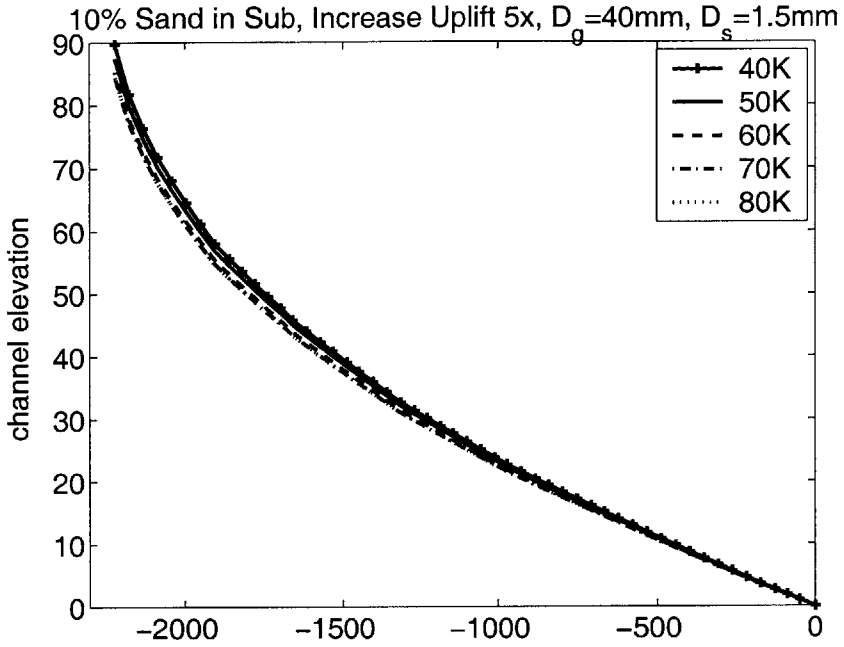

(B)

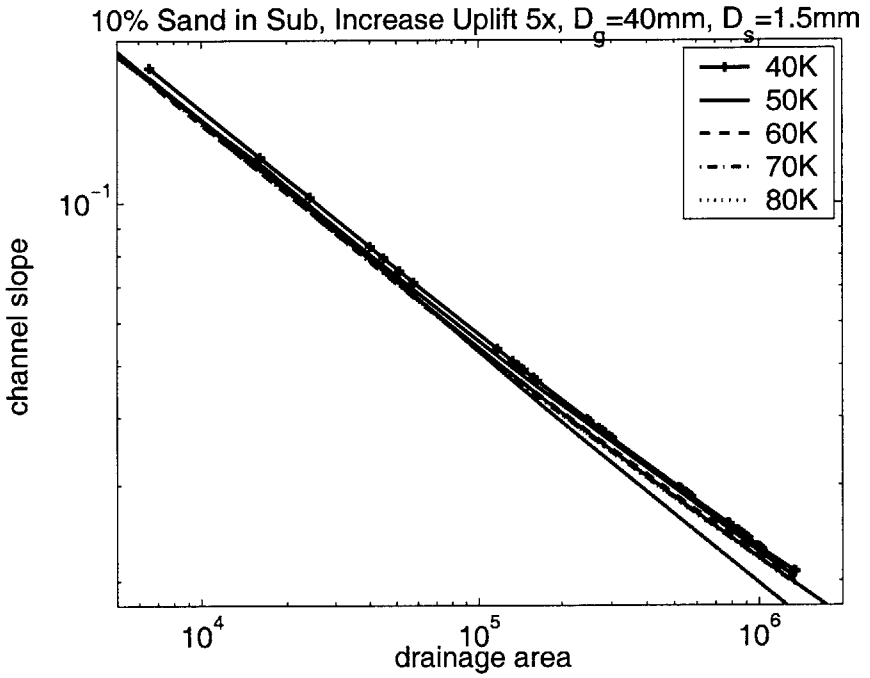

Figure 4-15: Later change in main channel elevation (A) and channel slope (B) in response to a five-fold increase in uplift rate using the Wilcock sediment transport model. (The lower and upper lines running through the plot are the equilibrium solution for the low and high uplift rate, respectively. These solutions overlap at the lower drainage area parts of the plot.)

(A)

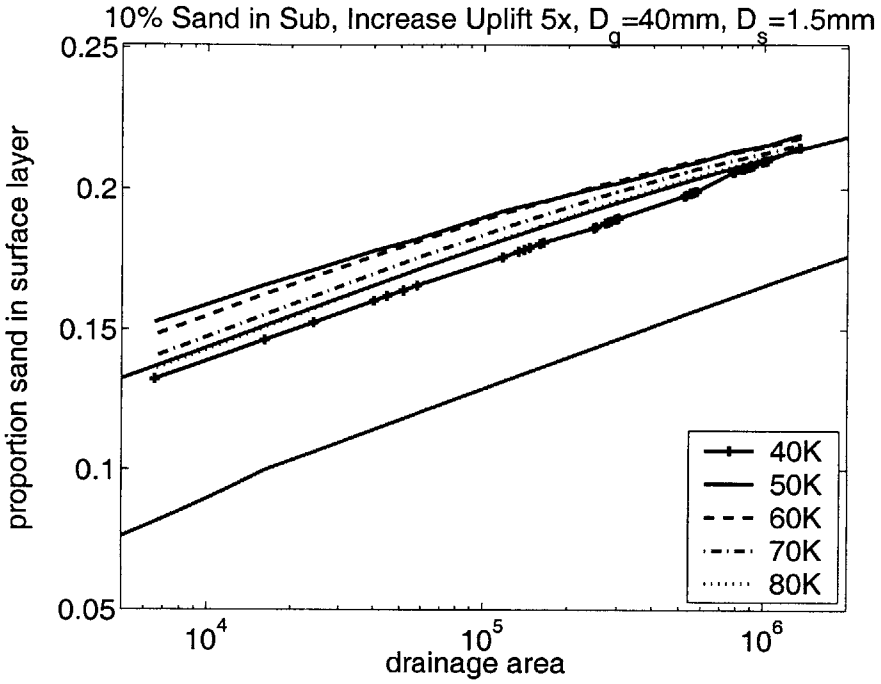

(B)

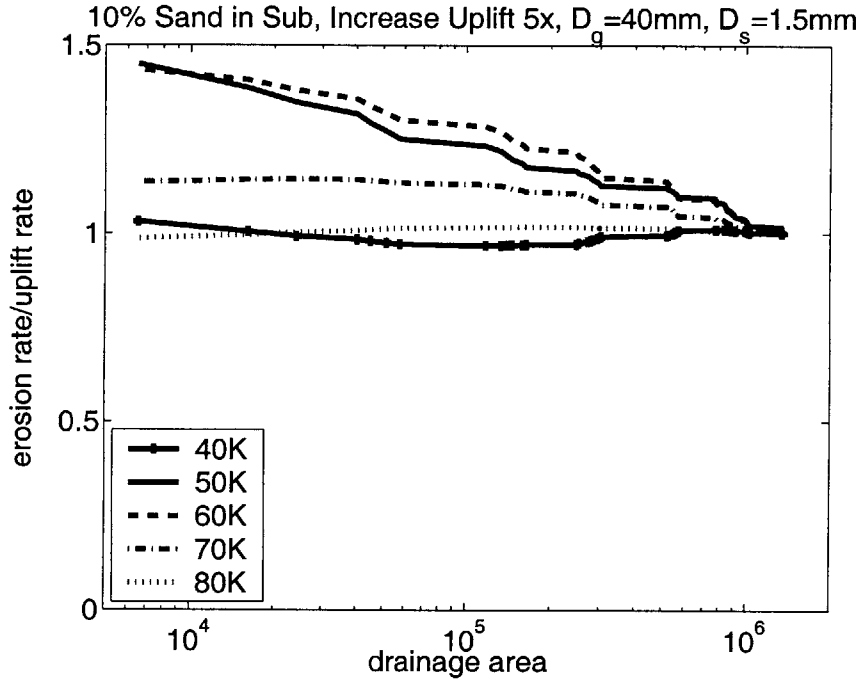

Figure 4-16: Later changes in surface texture (A) and total erosion ratio (with respect to the new uplift rate) (B) in response to a five-fold uplift increase using the Wilcock sediment transport rate. (The equilibrium texture solutions are shown for the low and high uplift rate as the lower and upper lines running through the texture plot, respectively.)

another is not so straightforward. In our numerical experiment, the initial response to an increase in precipitation rate is for the surface sand content to increase in the headwaters and decrease at larger drainage areas (figure 4-17A). The changes are subtle, but the pattern is worth noting. There is deposition in the lower part of the main channel immediately following the precipitation increase (figure 4-17B). A value of -6 on figure 4-17B implies 0.6mm/yr of deposition, in this case over 100 years. Note the upper part of the main channel is eroding at a relatively high rate with respect to equilibrium erosion values. This is the region in which the surface sand content is increasing.

Figures 4-18A, B, and C illustrate the erosion response throughout the network. In the areas shaded white in this figure, both sand and gravel are being eroded; in the gray areas, gravel is deposited while sand is still eroded from the bed, and in the black areas both sand and gravel are deposited. (There is no case in which gravel is eroded and sand is deposited.) In the uppermost parts of the network, there is no incoming sediment load. Erosion rates are calculated as the difference between the incoming sediment load and the local transport rate. As a result of the precipitation increase, fluvial discharge increases and the channel can transport more gravel and sand (white regions). The sediment load increases downstream faster than the transport rate. The channel begins to deposit gravel first (gray regions). Moving further downstream, even the sand content of the load is too high, and both sand and gravel are deposited (black regions). After 100 years, (figure 4-18A) a large part of the network is depositing both sand and gravel. In the lowest parts of the network, only gravel is deposited. In this region, there has been a slight increase in slope (not illustrated), which increases the sand-transport rate enough so that sand is not deposited. However, because gravel is still being deposited lower down in the channel, the surface sand content decreases (figure 4-17A). By 200 years, deposition in the lower parts of the channel (figure 4-17B) has caused further steepening of slopes and the region in which both sand and gravel are deposited has decreased from the 100 year time slice. 400 years after the increase in precipitation, there is still some deposition of gravel (figure 4-18C), but with the exception of one point, there is no

deposition of sand.

1,000 years after the increase in precipitation, there is erosion of both sand and gravel throughout the network. This remains the case hereafter, with one local exception due to network rearrangement (not illustrated). We can now look at the sand erosion ratio, as we did in the uplift experiments. (The sand erosion ratio has no meaning when deposition is occurring.) Figure 4-19 illustrates the sand erosion ratio 1,000 years after the increase in precipitation rate. The yellow regions correspond to an equilibrium value of 0.5. Gravel erosion rates are still high in the upper parts of the network, leading to a low sand erosion ratio (blue or green in figure 4-19). The sand erosion ratio is at or near the equilibrium value in most of the main channel, and there is very little change in surface texture at this time (compare dash-dot and dotted lines in figure 4-17A).

(A)

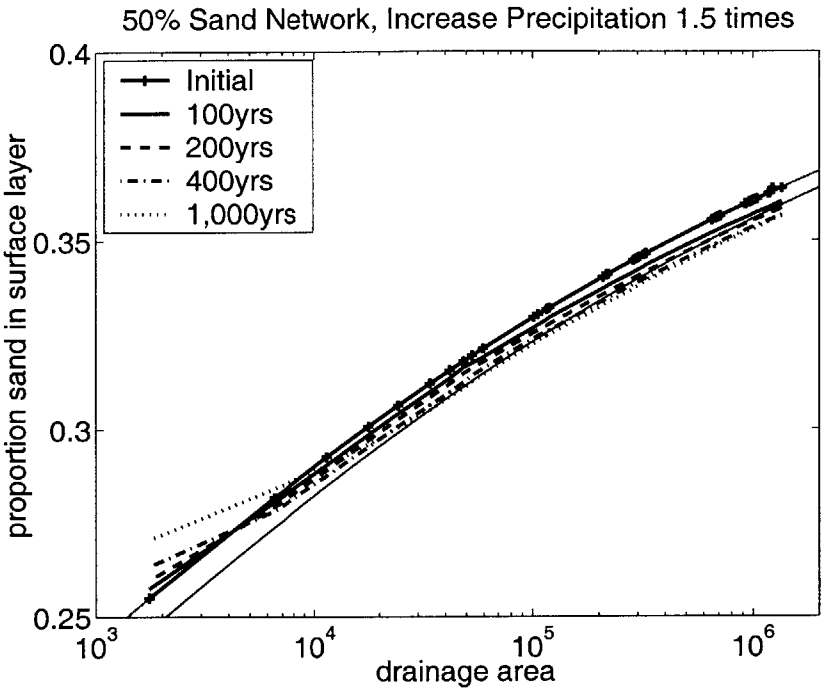

(B)

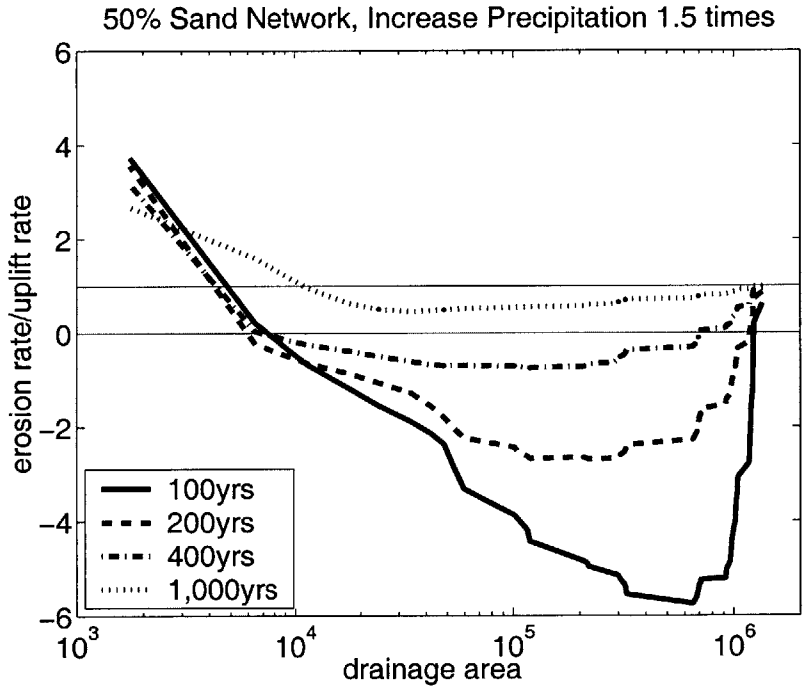

Figure 4-17: Initial changes in surface texture (A) and total erosion ratio (with respect to the uplift rate) (B) in response to a 1.5-fold increase in the precipitation rate using the Wilcock sediment transport rate. The equilibrium texture solutions are shown for the low and high precipitation rate as the upper and lower lines running through the texture plot, respectively. The upper horizontal line in the erosion plot represents the equilibrium erosion rate. The lower horizontal line marks the difference between erosion (above) and deposition (below). Note that the change in times between the lines is not equal.

(A)

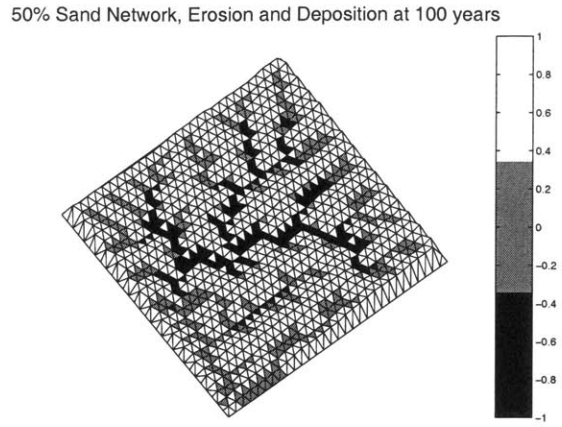

(B)

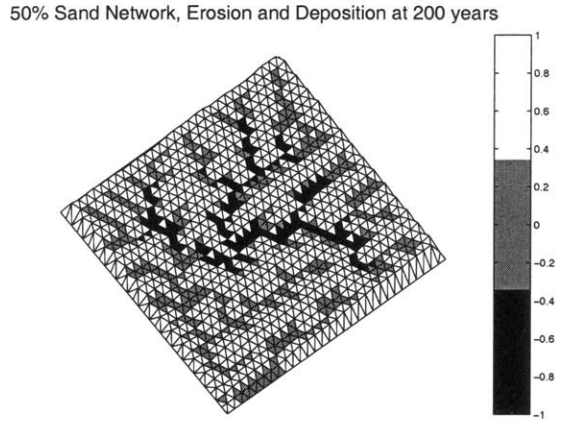

(C)

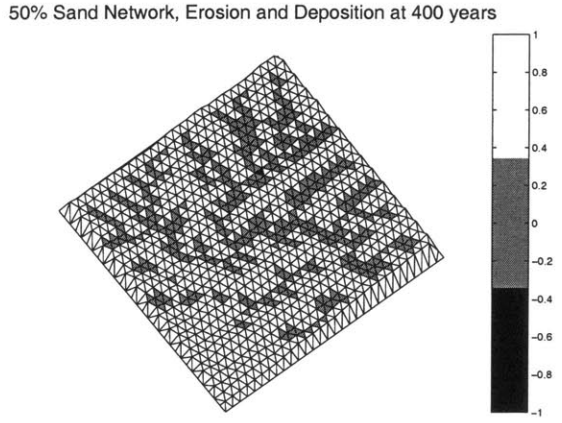

Figure 4-18: Locations of erosion and deposition across the network 100 years (A), 200 years (B), and 400 years (C) after the increase in precipitation rate. White represents total erosion; gray represents erosion or transport of sand, but deposition of gravel; and black represents deposition of both sand and gravel. (Note the color bar scale is arbitrary.)

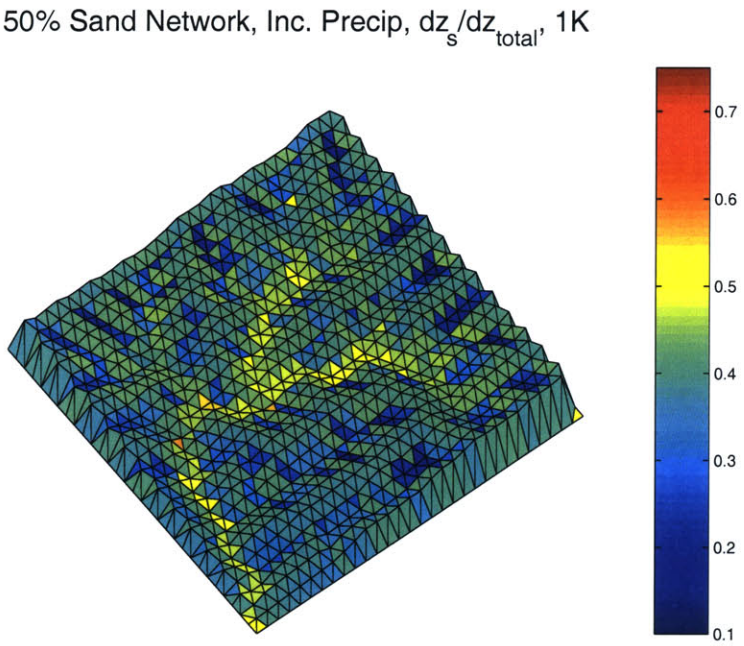

Figure 4-19: Sand erosion ratio 1,000 years after the increase in precipitation. Note that erosion of both grain sizes is occurring across this topography; only the relative rate of erosion varies.

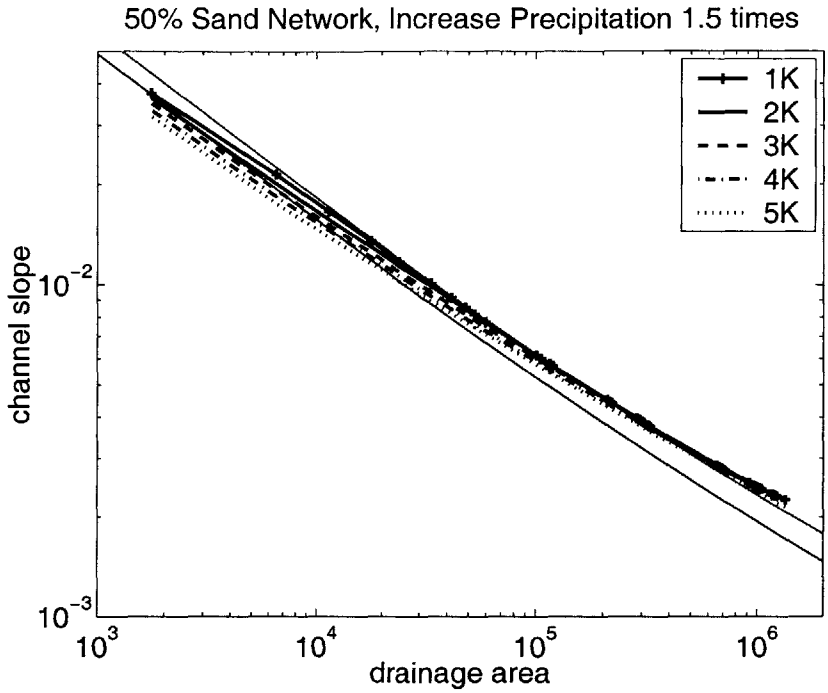

Figure 4-20: Changes in channel slope beginning 1,000 years after the increase in precipitation rate. The equilibrium channel slope (from the iterative model) for the low and high precipitation rate are the upper and lower thin lines, respectively, running through the plot.

There is a noticeable difference in channel slopes after 1,000 years (figure 4-20). Slopes in the upper parts of the network have decreased and continue to decrease due to the increase in erosion rates. Slopes in the lower parts of the main channel have increased from deposition, but they begin to fall at this point. Erosion rates continue to rise after 1,000 years (figure 4-21B) even though slopes are decreasing. In the lower parts of the channel, slopes must decline because they have over-steepened. In the upper parts of main channel slopes are also too steep at 1K, but the increased erosion rate drops them below their new equilibrium value by 3K, and they continue to fall after this time (figure 4-20). By 3K, the surface sand content throughout the main channel is higher than the equilibrium value (figure 4-21A), enabling erosion rates that are higher than their equilibrium value on slopes that are shallower than their equilibrium steepness.

The main channel experiences a number of transitions between 5,000 and 9,000

(A)

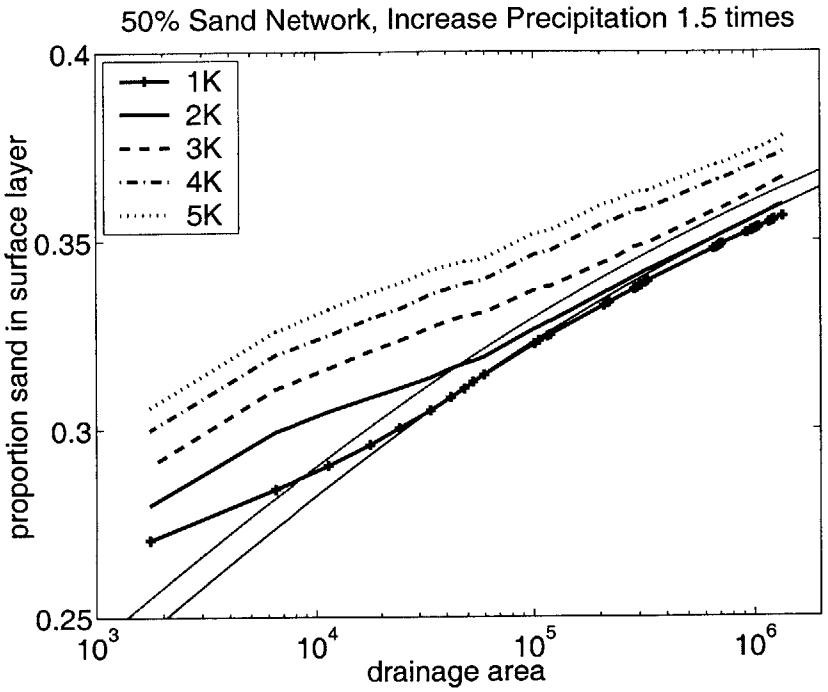

(B)

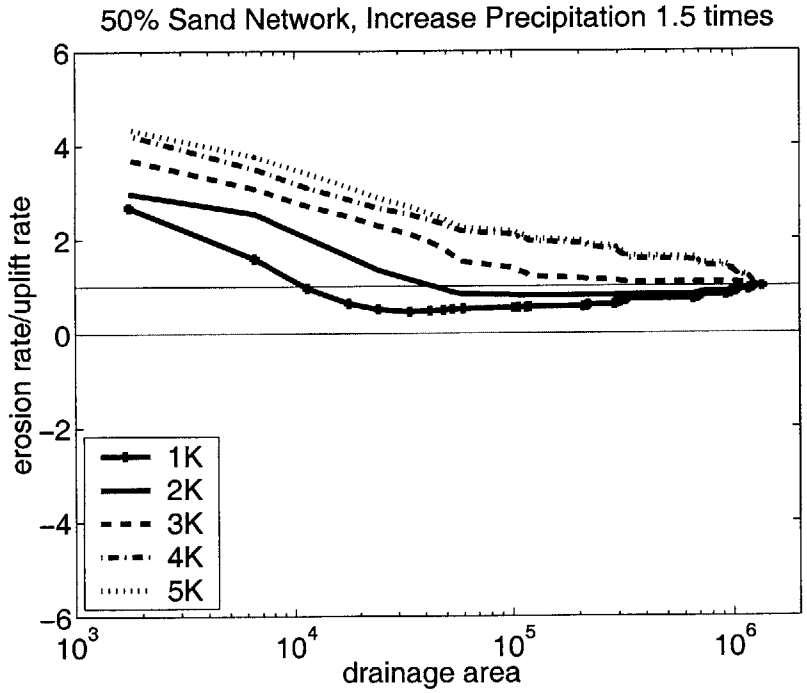

Figure 4-21: Later changes in surface texture (A) and total erosion ratio (with respect to the uplift rate) (B) in response to a 1.5-fold increase in the precipitation rate using the Wilcock sediment transport rate. The equilibrium texture solutions are shown for the low and high precipitation rate as the upper and lower lines running through the texture plot, respectively.

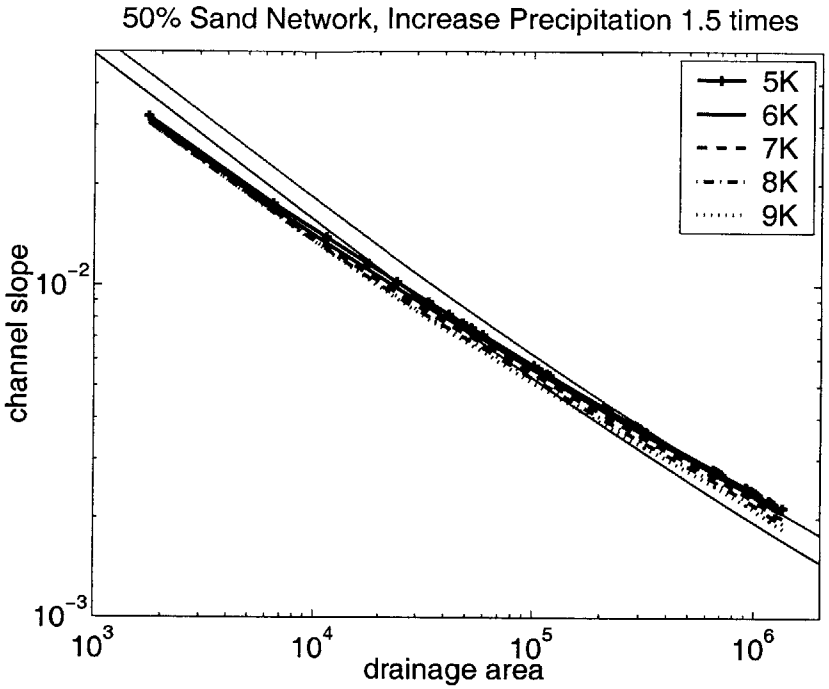

Figure 4-22: Changes in channel slope beginning 5,000-9,000 years after the increase in precipitation rate. The equilibrium channel slope (from the iterative model) for the low and high precipitation rate are the upper and lower thin lines, respectively, running through the plot.

years after the increase in precipitation. The surface sand content increases, stabilizes, and later decreases (figure 4-23A). The trend in texture changes reverses first in the upper parts of the main channel and slowly the lower parts catch-up. A decline in channel slope (figure 4-22) and total erosion rate (figure 4-23B) accompany the decline in surface sand content. As channel slopes decline, the erosion rate of gravel declines as well. The sand erosion ratio increases, causing the surface sand content to decline. The sand erosion ratio by 9K is above 0.5 almost everywhere in the network (figure 4-24)

(A)

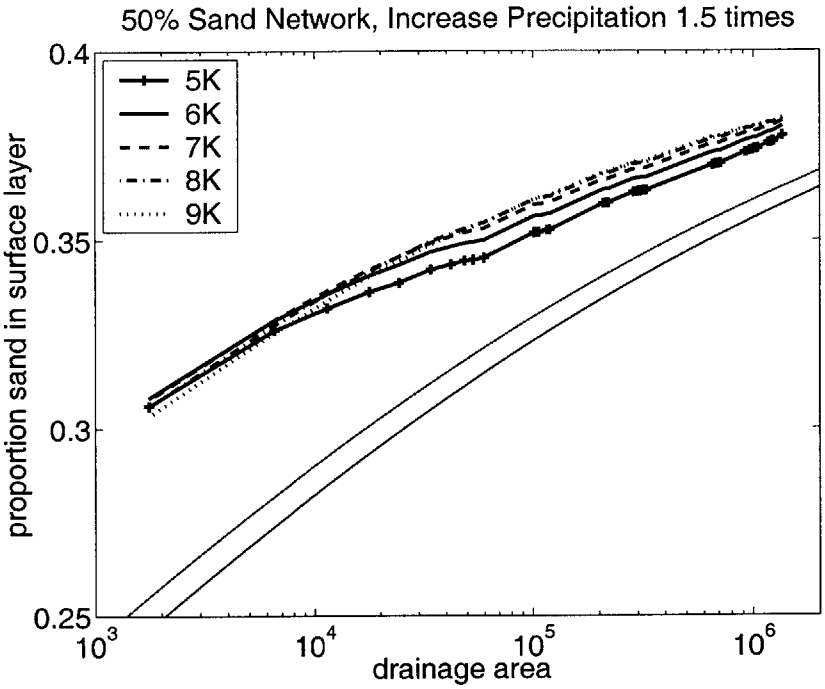

(B)

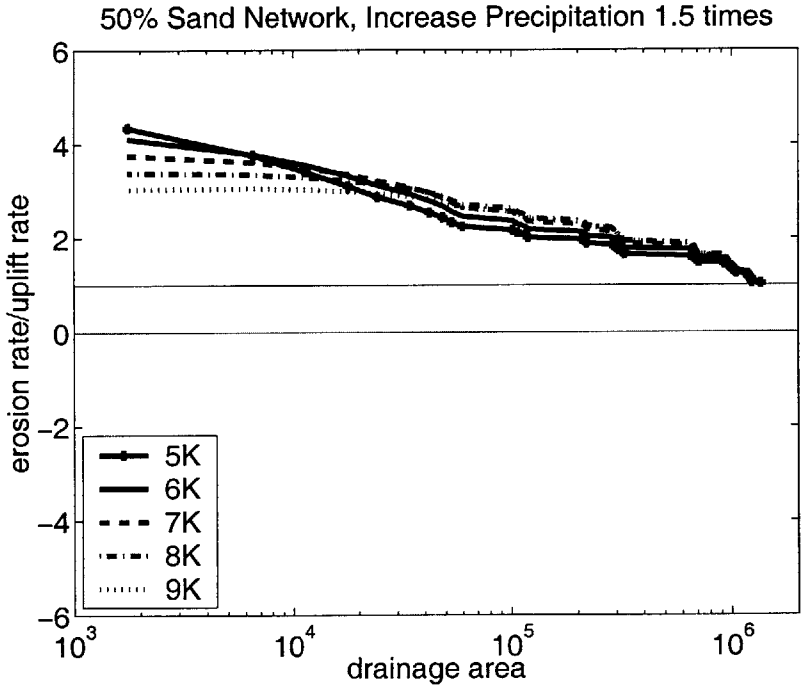

Figure 4-23: Later changes in surface texture (A) and total erosion ratio (with respect to the uplift rate) (B) in response to a 1.5-fold increase in the precipitation rate using the Wilcock sediment transport rate. The equilibrium texture solutions are shown for the low and high precipitation rate as the upper and lower lines running through the texture plot, respectively.

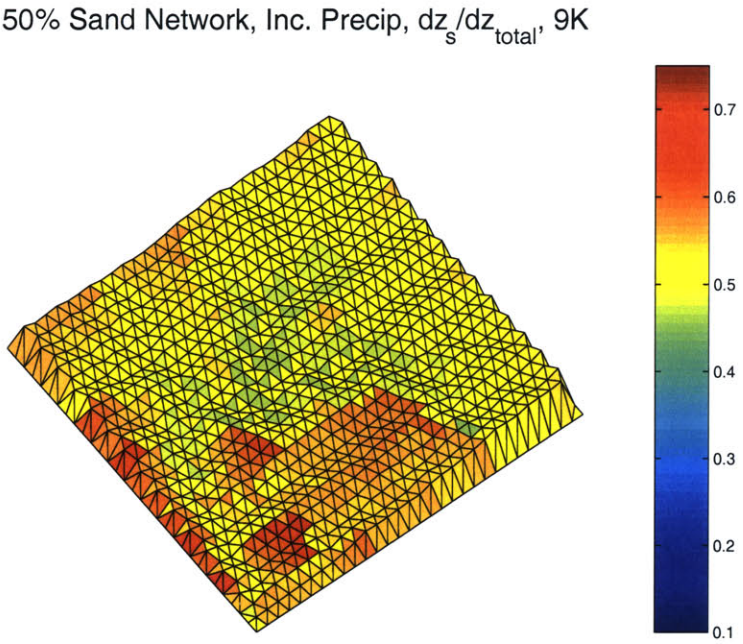

Figure 4-24: Sand erosion ratio 9,000 years after the increase in precipitation. Note that erosion of both grain sizes is occurring across this topography; only the relative rate of erosion varies.

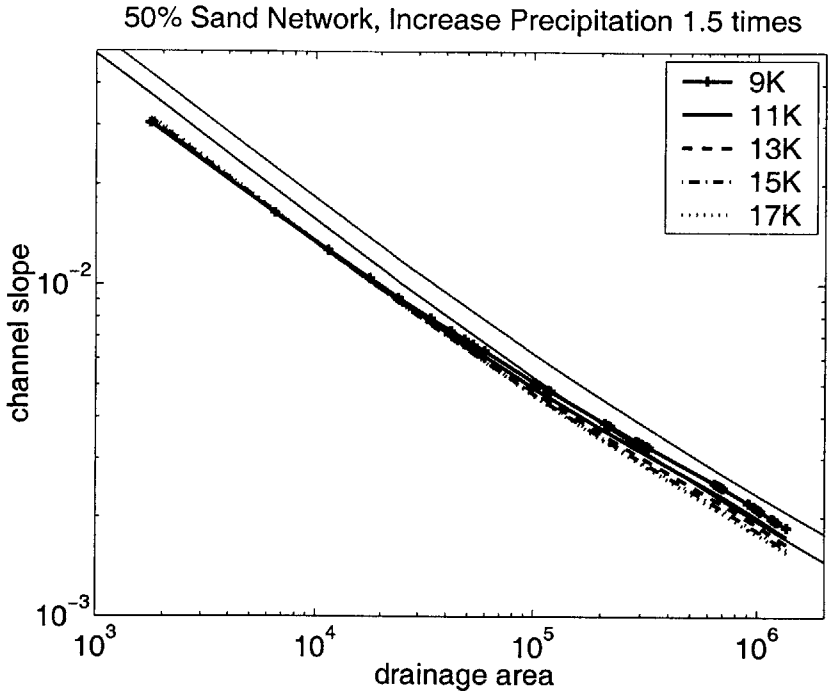

Figure 4-25: Changes in channel slope beginning 9,000-17,000 years after the increase in precipitation rate. The equilibrium channel slope (from the iterative model) for the low and high precipitation rate are the upper and lower thin lines, respectively, running through the plot.

Although total erosion rates are declining everywhere in the main channel by 9K, they still remain above the equilibrium rate. Many parts of the channel have already shallowed to below their new equilibrium value, and those that haven't yet will eventually (figure 4-25). The high surface sand content enables the high erosion rates (figure 4-26), even though slopes are below their new equilibrium values. Erosion rates dip slightly below their new equilibrium values and then rise again as a result of the under-steepening of slopes (not shown.)

The variable erosion rates throughout the network result in a reduction in channel concavity during the transient. Relatively high erosion rates in the upper parts of the channel, in comparison with lower erosion rates or deposition in the lower parts of the channel are responsible for the lower concavity. However, the main channel profile remains smooth throughout the transient. We do not illustrate any of the profiles here because the changes are small and don't stand-out very well.

(A)

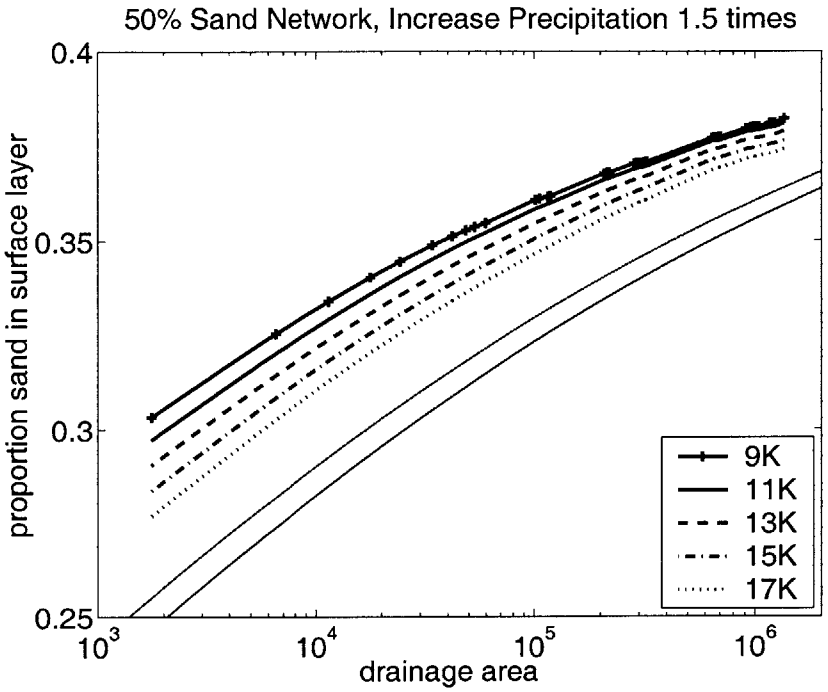

(B)

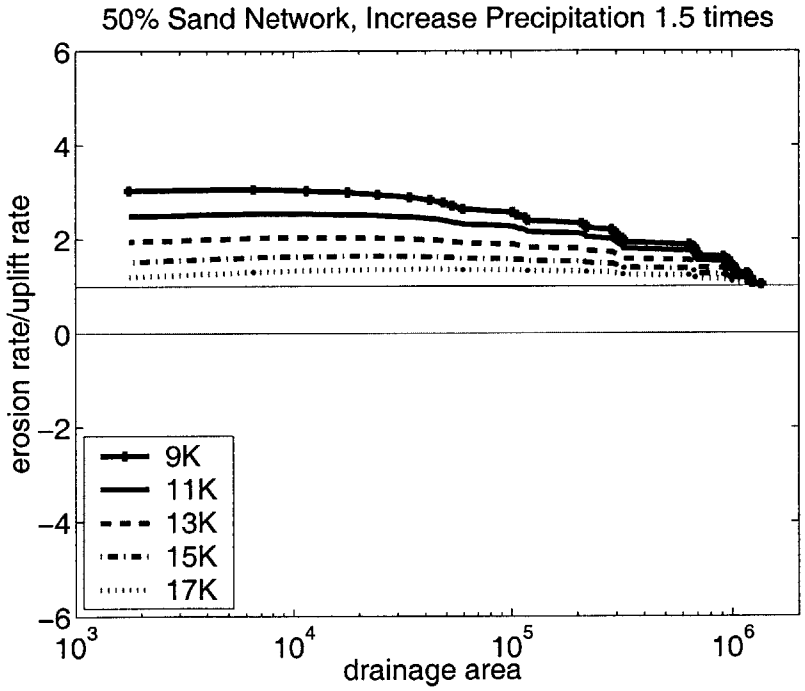

Figure 4-26: Later changes in surface texture (A) and total erosion ratio (with respect to the uplift rate) (B) in response to a 1.5-fold increase in the precipitation rate using the Wilcock sediment transport rate. The equilibrium texture solutions are shown for the low and high precipitation rate as the upper and lower lines running through the texture plot, respectively.

4.3 Discussion

4.3.1 Change in Uplift Rate

Previous numerical studies of transport limited networks predict that channel slopes increase in response to an increase in uplift rate, and decrease in response to a decrease in uplift rate (Willgoose (1994); Whipple and Tucker (2002)); local areas of deposition can cause short deviations from this pattern, but these are the overall trends. In these studies, channel slopes are the sole variable responsible for changing the erosion rate. The novelty of the experiments presented here is that both surface texture and channel slope can adjust, as opposed to channel slope alone. This fairly simple expansion of the model results in significant changes in network response. Surface texture and channel slopes adjust at different rates throughout the network. There is a significant period of time during which channel slopes decrease in response to an increase in uplift rate. Although the channel profile remains relatively smooth during the transition (barring exceptions from network rearrangement as in figure 4-5), channel concavity does change.

Key to the results presented are the spatial changes in surface texture during disequilibrium. The relative rate of erosion of sand versus gravel is responsible for these variations in surface sand content. Exact changes in texture are sensitive to the texture of material that replenishes the surface from below and the depth of the surface layer; these are both boundary conditions in the numerical model. From the two examples illustrated in this chapter, we have shown that similar changes in surface texture can result from an increase in uplift rate even when the boundary conditions (substrate texture) are very different. We acknowledge that the details of the response may be sensitive to the texture boundary condition, but the complex trends are probably not. Changes in the relative rates of erosion of different grain sizes should always result in transient changes in surface texture causing a complex response in channel slopes.

At equilibrium, the model results have been shown to be insensitive to the depth of the surface layer, as long as it is deeper than the depth of erosion during a single

time-step (Gasparini 1998). During the transient, we expect that a shallower active layer could create more extreme changes in surface texture. After erosion, the surface layer is replenished with material from below. When the texture of material eroded is different from the texture of the material replenishing the surface layer, changes in surface texture result. If a larger depth of material is being eroded, then the surface texture will be highly influenced by the material replenishing it. We use a surface layer depth of three meters, and one might expect that with this depth, surface texture changes would be unnoticeable. However, significant changes still occur. Most likely the results we show would be more extreme with a smaller active layer depth.

Although the changes in the relative erosion rates of sand and gravel in these example are subtle, and the resulting surface texture changes could differ depending on boundary conditions, the important lesson from these numerical simulations is that when both surface texture and channel slope can respond to a change in uplift rate, network response is more complex. Changes in surface texture, channel slope, and erosion rates in the main channel integrate conditions throughout the network. Erosion rates depend not only on the texture and volume of material which can be transported, but on the texture and volume of material carried into the channel from upstream. Channel response to a change in forcing is complicated by the different inputs in space and time, resulting in slopes which both rise and fall, and channel material which both coarsens and fines, all in response to a single change in forcing. These remarkable trends, and not necessarily the absolute values of surface sand content, are the key result of these numerical simulations.

4.3.2 Change in Precipitation Rate

The sedimentary response in channels to changes in climate remains an open research question. It seems impossible to investigate fluvial deposits without trying to infer something about the climatic conditions while they were being laid down (e.g. Schumm (1968); Knox (1972); Costa (1978); Knox (1983); Blum and Valastro (1989); Sugai (1993); Arbogast and Johnson (1994); Fuller et al. (1998); Reid et al. (1999)). Vegetation responds to climate change and influences sediment load (e.g.

Huntington (1924); Bryan (1928); Slaymaker (1990); Prosser et al. (1994); Wilcox et al. (1996); Mulligan (1998); Howard (1999)); the sediment load is also sensitive to changes in flood magnitude (e.g. Baker (1977); Tucker and Slingerland (1997); Bourke and Pickup (1999); Molnar (2001)). We have ignored much of the natural complexity, focusing solely on changes in texture and integrated network changes.

Previous studies have recognized that the response of the main channel to a change in climate is not isolated from the tributaries and hillslopes feeding it (e.g. Schumm (1973); Butzer (1980); Rinaldo et al. (1995); Tucker and Slingerland (1997)), leading to a different response in space and time which can vary depending on the initial state. The idealization of our numerical simulations illustrate this concept as well. Erosion rates in response to a change in precipitation vary both spatially and temporally. The upper parts of the network erode more rapidly than the lower parts of the network, and are more likely to erase past information stored in the sedimentary record. However, because the sediment load downstream increases, resulting in periods of deposition, some parts of the network may be more likely to contain information about the past than others. These numerical results confirm and strengthen the hypothesis that scientists can not ignore the complex erosional response throughout a network in response to climate change (Summerfield 1991).

Changes in surface texture resulting from a change in climate further the notion of complexity in channel response. Blum and Valastro (1989) found that the Pedernales River, Texas, was carrying a coarser sediment load during more humid conditions 1,000 years ago, while the current climate is more arid and the sediment load is finer. They also point out that other studies have observed the opposite trend, that coarser-grained sediment loads occur during arid periods. We believe the numerical results presented here are a great illustration of how tricky relations between climate and channel texture can be. In response to a single change in precipitation rate, the surface coarsens and fines. One might interpret the result of climate change differently depending on which deposits were preserved or the period of time since climate change occurred. Given these results, we question whether a one-to-one relationship exists between climate and texture of the channel bed and sediment load. Even with uniform

boundary conditions and a well-organized initial network, the response of surface texture to a single change in precipitation is highly complex.

In all of the sensitivity experiments here, one can imagine further complexity if the network was not initially in equilibrium and if the substrate and erosion processes varied throughout the network. It's also possible that further complexity in the processes could dampen the changes in surface texture and erosion rates (Bras et al. 2003). We also make the assumption that the hydraulic geometry relationships do no vary in disequilibrium. This assumption is supported by Wolman (1955), who found that these relationships did not vary between streams at grade and aggrading and degrading channels. However, transient adjustments in channel width, roughness and cross-sectional area could affect the transient results we have shown for both changes in uplift and climate (Stark and Stark (2001); Chitale (2003)).

4.4 Conclusions

Allowing for changes in surface texture has some surprising effects on transient network response. The exact values of surface sand content or channel slope are not the critical result of this study, but rather the trends in how they vary. The numerical experiments presented here remind the reader to use caution when interpreting network response to a change in forcing. Channel slopes might rise and fall in response to an increase in uplift rate or precipitation rate. Our study emphasizes the variables other than channel slope can dampen or enhance channel response. Further, channel response might look very different at different locations in the network and at different times. Finally, the results highlight the influence of the network structure during transient conditions; changes in the main channel can not be isolated from variations in the tributaries feeding it.

Chapter 5

Sensitivity of Bedrock Rivers to Sediment-Flux-Dependent Erosion Equations

5.1 Introduction

In many regions, bedrock channels form an important link in the landscape by transporting sediment eroded off the hillslopes to the lower alluvial reaches of a drainage network. As sediment moves through these channels, it may play a critical role in determining the rate of fluvial incision into bedrock. Gilbert (1877) discussed the processes responsible for bedrock incision, but only recently has much attention been focused on this problem. Field and flume studies have investigated the different controls on bedrock incision (e.g. Foley (1980); Gardner (1983); Wohl (1993); Wohl and Ikeda (1997); Hancock et al. (1998); Whipple, Hancock and Anderson (2000); Whipple, Snyder and Dollenmayer (2000); Sklar and Dietrich (2001); Hartshorn et al. (2002)). Numerical models have also considered bedrock erosion, using mostly the stream-power equation to calculate incision rates (e.g. Howard (1994); Rosenbloom and Anderson (1994); Stock and Montgomery (1999); Snyder et al. (2002)). However, some studies suggest that stream power alone may not adequately describe the

processes controlling the morphology of bedrock channels (e.g. Howard et al. (1994); Sklar and Dietrich (1998); Snyder et al. (2003b); Tomkin et al. (2003)); considerations such as thresholds, local grain size and downstream sorting, sediment delivery and transport rates are among those variables which may play important roles in channel evolution. With these ideas in mind, we investigate fluvial incision into bedrock using the CHILD numerical landscape evolution model.

We explore the control of different erosion processes on the equilibrium and transient morphology of bedrock rivers. All of the examples here consider channels in which erosion is limited by the amount of material that can be detached from the bed, although the detachment capacity may be governed by transport capacity. A number of different erosion equations are explored that represent different erosion processes including (1) the force that running water imparts as shear stress on the bed of a channel, (2) the role of sediment entrained in the flow to wear down bedrock, and (3) the role of sediment in covering the bedrock to protect it from bedrock erosion. No hillslope processes are considered in the numerical experiments, implying a system in which sediment supply from the hillslopes keeps pace with the fluvial system.

All of the different formulations produce very similar equilibrium channel morphologies, indicating that equilibrium form may not be the best indicator of the dominant erosion process. However, equilibrium form may vary in unexpected ways to climate change depending on the dominant erosion process.

Transient conditions can result which resemble equilibrium conditions, do not contain knickpoints, and/or appear to be the result of an opposite shift in forcing. These surprising transient states result from using very simplified sediment transport laws (erosion thresholds are ignored) and climate states (a single storm rate, storm duration, and inter-storm duration are used in all cases).

5.2 Equilibrium Conditions

Following Whipple and Tucker (2002), we start by expressing the rate of erosion into bedrock (E_d) as

$$E_d = Kf(Q_s)A^m S^n, \tag{5.1}$$

where K is an erodibility parameter which depends on factors such as lithology, climate, and channel properties (e.g. Stock and Montgomery (1999)); $f(Q_s)$ embodies the importance of sediment load in eroding the channel bed (Q_s is the volumetric rate of incoming sediment - referred to as Q_s^{in} in earlier parts of this thesis). We will often refer to the product of K and $f(Q_s)$, or to $f(Q_s)$ alone as the erodibility. A is the upstream drainage area; S is channel slope; and m and n are conventionally considered to be positive constants which can be derived from physical channel properties (e.g. Howard et al. (1994); Whipple and Tucker (1999); others too), although recent studies suggest that in some cases m and n may not be positive (Tomkin et al. (2003); Sklar (2003)). In this study we will always use positive values for m and n. The rate of change in elevation ($\frac{\partial z}{\partial t}$) is given by:

$$\frac{\partial z}{\partial t} = U - E_d. \tag{5.2}$$

In all cases considered here the uplift rate, U, is considered to be spatially uniform. When the landscape reaches dynamic equilibrium, or steady-state, elevations are no longer changing in time, leading to the following equilibrium condition:

$$U = E_d. \tag{5.3}$$

Following from equations 5.1 and 5.3, the common expression for equilibrium channel slope (e.g. Howard (1980); Howard et al. (1994); Moglen and Bras (1995); Whipple and Tucker (1999)); Snyder et al. (2000)) can be written somewhat incompletely as,

$$S = \left(\frac{U}{Kf(Q_s)}\right)^{\frac{1}{n}} A^{-\theta}, \tag{5.4}$$

where

$$\theta = \frac{m}{n}. \tag{5.5}$$

Equation 5.4 is a bit non-conventional because it includes the $f(Q_s)$ term. The different forms of $f(Q_s)$ are given in later sections. Because $f(Q_s)$ includes channel slope, equation 5.4 is somewhat more complicated than it first appears. However, in some cases it is useful to think of channel slope as inversely proportional to both K and the value of $f(Q_s)$ (assuming, as we do, that n is positive).

In all examples we use values of m and n so that $\theta = 0.5$. The value of θ, or the concavity index, has been studied by numerous researchers (e.g. Hack (1957); Flint (1974); Tarboton et al. (1991); Tucker and Whipple (2002)), and $\theta = 0.5$ is an average representative value for many landscapes.

In the following sections we describe different forms of the erosion equation (5.1) and the equilibrium form predicted by each equation.

5.2.1 Stream-Power Model

Significant attention has been given to the stream-power model (see Whipple and Tucker (1999) for an overview). The stream-power rule can be derived from physical relations and assumes that the bedrock erosion rate is proportional to either bed shear stress or unit stream power. There is no dependence on sediment flux in detachment-limited channels, implying that $f(Q_s) = 1$. In this case, the equilibrium relationship (equation 5.4) reduces to:

$$S = \left(\frac{U}{K}\right)^{\frac{1}{n}} A^{-\theta}. \tag{5.6}$$

This work does not concentrate on the stream-power model and it will not be discussed at length. However, because it is so widely applied (e.g. Seidl and Dietrich (1992); Rosenbloom and Anderson (1994); Tucker and Slingerland (1996); Stock and Montgomery (1999); Roe et al. (2002); Snyder et al. (2002)), we only wish to remind the reader of its equilibrium sensitivity with respect to uplift rate and climate (contained in K) as point of reference for the other results presented in this chapter.

From equation 5.6 it is easily seen that equilibrium channel slopes increase with

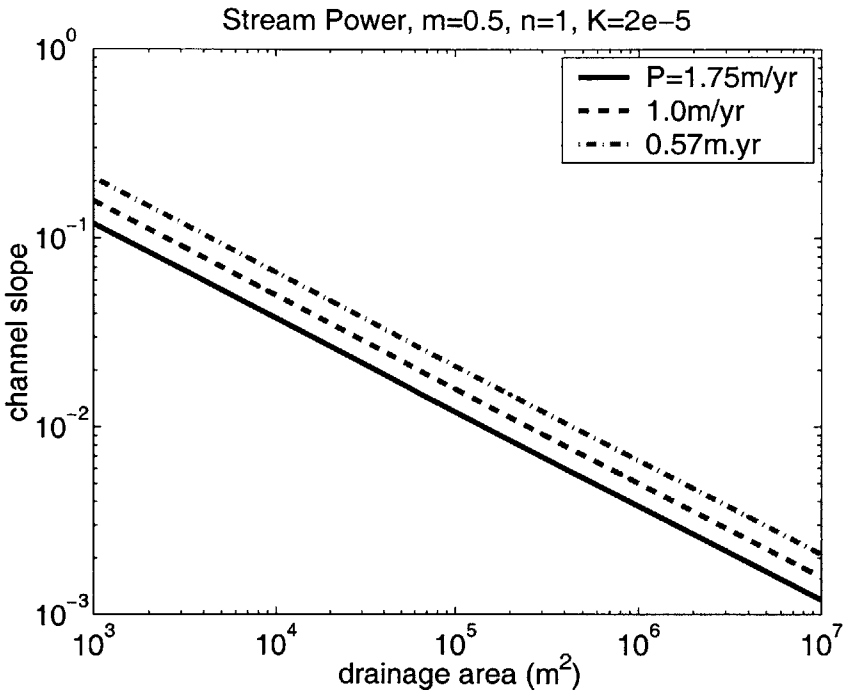

Figure 5-1: Sensitivity to precipitation rate of the equilibrium stream-power slope-area relationship.

uplift rate, or more specifically, $S \propto U^{1/n}$. The sensitivity of channel slopes to uplift rate decreases with increasing values of n (Snyder et al. 2000).

Precipitation is considered to be contained in the value of K in equations 5.1 (and 5.6). If one assumes that fluvial discharge increases linearly with drainage area ($Q \propto A$), it follows that $K \propto P^m$, where P is the precipitation rate (Whipple and Tucker 1999). Therefore, the stream power rule predicts that equilibrium channel slopes are shallower in drainage basins with higher rainfall rates (Figure 5-1).

5.2.2 Almost-Parabolic Model

In this section we consider the role of sediment flux ($f(Q_s)$) in eroding bedrock, using a model very similar to the relationship described by Whipple and Tucker (2002). Gilbert (1877) was the first to observe that sediment flux plays an important role in channel incision. Recently, researchers have returned back to Gilbert's ideas (e.g. Slingerland et al. (1997); Sklar and Dietrich (1998); Sklar and Dietrich (2001)).

The basic premise is sediment carried in the load can enhance erosion as it impacts the channel bed, causing wear. Gilbert (1877) stated that sediment can effectively erode the bed when the sediment load is well below the sediment transport capacity. However, as the sediment load increases (in relation to the carrying capacity) the sediment begins to cover the bed and protect it from erosion. We describe this dual role of sediment in enhancing and inhibiting erosion through the $f(Q_s)$ factor in equation 5.1.

Following the model presented by Sklar and Dietrich (1998), Whipple and Tucker (2002) described a parabolic form of $f(Q_s)$ as a function of the ratio of $\frac{Q_s}{Q_c}$, where Q_c is the sediment transport capacity. In the relationship used by Whipple and Tucker (2002) $f(Q_s)$ increases from 0 to 1.0 as $\frac{Q_s}{Q_c}$ increases from 0 to 0.5 (sediment enhances erosion) and $f(Q_s)$ decreases from 1.0 to 0 as $\frac{Q_s}{Q_c}$ increases from 0.5 to 1.0 (sediment covers the bed). The function used in this study for $f(Q_s)$ is the same as that used by Whipple and Tucker (2002) except we slightly adapt the function so that erosion can still take place when there is there is no sediment load, theoretically through processes other than wear by sediment, such as plucking or solution (e.g. see Wohl (1993); Hancock et al. (1998); Wohl (1998); Whipple, Hancock and Anderson (2000), for a discussion of bedrock erosion processes). This assumption is also made partly as a boundary condition to avoid infinite slopes (Whipple and Tucker 2002).

The above description of the $f(Q_s)$ function translates into the following equations: when $\frac{Q_s}{Q_c} > 0.1$ (from Whipple and Tucker (2002),

$$f(Q_s) = 1 - 4\left(\frac{Q_s}{Q_c} - 0.5\right)^2, \tag{5.7}$$

and when $\frac{Q_s}{Q_c} < 0.1$,

$$f(Q_s) = 2.6\left(\frac{Q_s}{Q_c}\right) + 0.1. \tag{5.8}$$

Figure 5-2 illustrates this relationship. In this chapter, we describe the sediment transport capacity using a very simple function (in comparison with those used in

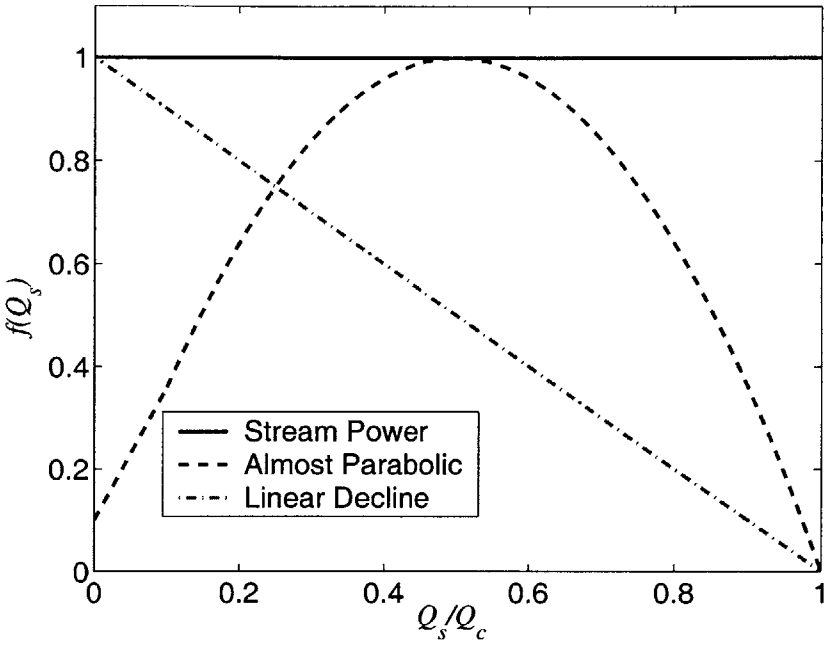

Figure 5-2: Dependency of three different erosion equations on the ratio of sediment load to sediment carrying capacity.

Chapter 3 and 4).

$$Q_c = K_t A^{mt} S^{nt}. \tag{5.9}$$

In this simplified form of the sediment transport equation, there is some range in the value used for mt. (nt is always assumed to be 1.) Generally, one expects there to be a threshold for sediment entrainment which is sensitive to grain size variations, and equation 5.9 does not contain a threshold. From the discussion in chapter 3, we expect that if the values of mt and nt are chosen based on a shear stress model, unrealistic equilibrium concavities will result without a threshold. However, in order to generate realistic concavity values without including the complicating effects of grain-size variation (e.g. Snow and Slingerland (1987); Pizzuto (1995); Sinha and Parker (1996); Gasparini et al. (2003)), the value of mt can be increased (Howard 1980). In all examples we use either $mt = 1.3$ or $mt = 1.5$ to create channels with realistic concavities.

Using equations 5.7, 5.8 and 5.9 in the equilibrium slope-area relationship (equa-

tion 5.4) and making the equilibrium assumption that $Q_s = \beta UA$ (β represents the fraction of the sediment load that is bedload, and here is always considered to be 1.0), we can solve for the almost-parabolic slope-area relationship. These results were shown by Whipple and Tucker (2002) and we have added to their solution the slope-area relationship in the linear region of the almost-parabolic model ($\frac{Q_s}{Q_c} < 0.1$).

For the case when $n = 1$ and $nt = 1$ the equilibrium relations are as follows:

When $\frac{Q_s}{Q_c} > 0.1$,

$$S = \frac{\frac{\beta U}{K_t} A^{1-mt}}{1 - \frac{K_t}{4K\beta} A^{mt-m-1}}, \tag{5.10}$$

and when $\frac{Q_s}{Q_c} < 0.1$,

$$S = \frac{10U}{K} A^{-m} - \frac{26\beta U}{K_t} A^{1-mt}. \tag{5.11}$$

For the case when $n = 2$ and $nt = 1$ the equilibrium relations are as follows: When $\frac{Q_s}{Q_c} > 0.1$,

$$S = \frac{K_t}{4K\beta} A^{mt-m-1} + \frac{\beta U}{K_t} A^{1-mt}, \tag{5.12}$$

and when $\frac{Q_s}{Q_c} < 0.1$,

$$S = \frac{-13\beta U}{K_t} A^{1-mt} + 5\sqrt{\left(\frac{2.6\beta U}{K_t} A^{1-mt}\right)^2 + \frac{0.4U}{K} A^{-m}}. \tag{5.13}$$

Similarly to the stream-power model (e.g. Whipple and Tucker (1999)), equilibrium channel slopes increase with uplift rate using the almost-parabolic model (equations 5.10-5.13). When $n = 1$, slopes vary directly with uplift rate. The equilibrium relationship for $\frac{Q_s}{Q_c}$ is given by

$$\frac{Q_s}{Q_c} = \frac{\beta UA}{K_t A^{mt} S^{nt}}. \tag{5.14}$$

In the special case when $n = 1$ and $S \propto U$, the equilibrium value of $\frac{Q_s}{Q_c}$ does not very with uplift rate and therefore $f(Q_s)$ also does not vary with uplift rate.

Generally, one might expect the role of sediment flux on channel incision rates ($f(Q_s)$) to vary throughout the drainage network. In fact, this is the key point of

using an incision rule such as the almost-parabolic model, otherwise an equation with a constant erodibility, such as the stream-power model, applies. However, in the special case where $mt = 1.5$ (and $\frac{m}{n} = 0.5$), $f(Q_s)$ does not vary downstream. In this case, the equilibrium slope-area relationships for the almost-parabolic model (equations 5.10- 5.13) all predict that $S \propto A^{-0.5}$. It follows under these conditions from the equilibrium expression for $\frac{Q_s}{Q_c}$ (equation 5.14) that $\frac{Q_s}{Q_c}$ is constant in space and therefore $f(Q_s)$ is constant in space.

Figure 5-3A illustrates the sensitivity of equilibrium slopes to uplift rate when $n = 1$ and $mt = 1.3$. There is a slight curvature in these slope-area plots. This is easily seen when comparing the solid line in figure 5-3A with the thin dotted line, which is the stream-power equilibrium slope-area relationship for the same K, m, and n values. The variable concavity produced using the almost-parabolic model is due to downstream changes in $\frac{Q_s}{Q_c}$ and therefore $f(Q_s)$ (figure 5-3B). Because $n = 1$, $f(Q_s)$ does not vary with uplift rate, and all of the $f(Q_s)$ lines in figure 5-3B plot on top of each other.

When $n = 2$, equilibrium slopes increase with uplift rate, but not linearly (equations 5.12- 5.13). Sensitivity of equilibrium channel slope to uplift rate is illustrated in figure 5-4. In this example, equilibrium slopes predicted by the almost-parabolic model are less sensitive to uplift rate than those predicted by the stream-power model. With the parameters and uplift rates used in figure 5-4, $\frac{Q_s}{Q_c}$ increases with increasing uplift rate (figure 5-5). Because $\frac{Q_s}{Q_c} < 0.5$, the increase in $\frac{Q_s}{Q_c} < 0.5$ causes $f(Q_s)$ to increase as well (figure 5-5). Because erodibility is increasing with uplift rate through the $f(Q_s)$ term, slopes do not vary as much as they do using the stream-power model. Further increases in uplift rate push $\frac{Q_s}{Q_c}$ to values greater than 0.5 and cause $f(Q_s)$ (figure 5-5) to decrease with increasing uplift rate, magnifying the effect of an increase in uplift rate on equilibrium slopes (figure 5-6).

We expect that equilibrium channel slopes should decrease with increasing precipitation rate, given equation 5.4 and the discussion based on the stream-power model. In order to describe equilibrium sensitivity to climate, we need to include the precipitation rate in the expression for $f(Q_s)$ and, more specifically, in the value

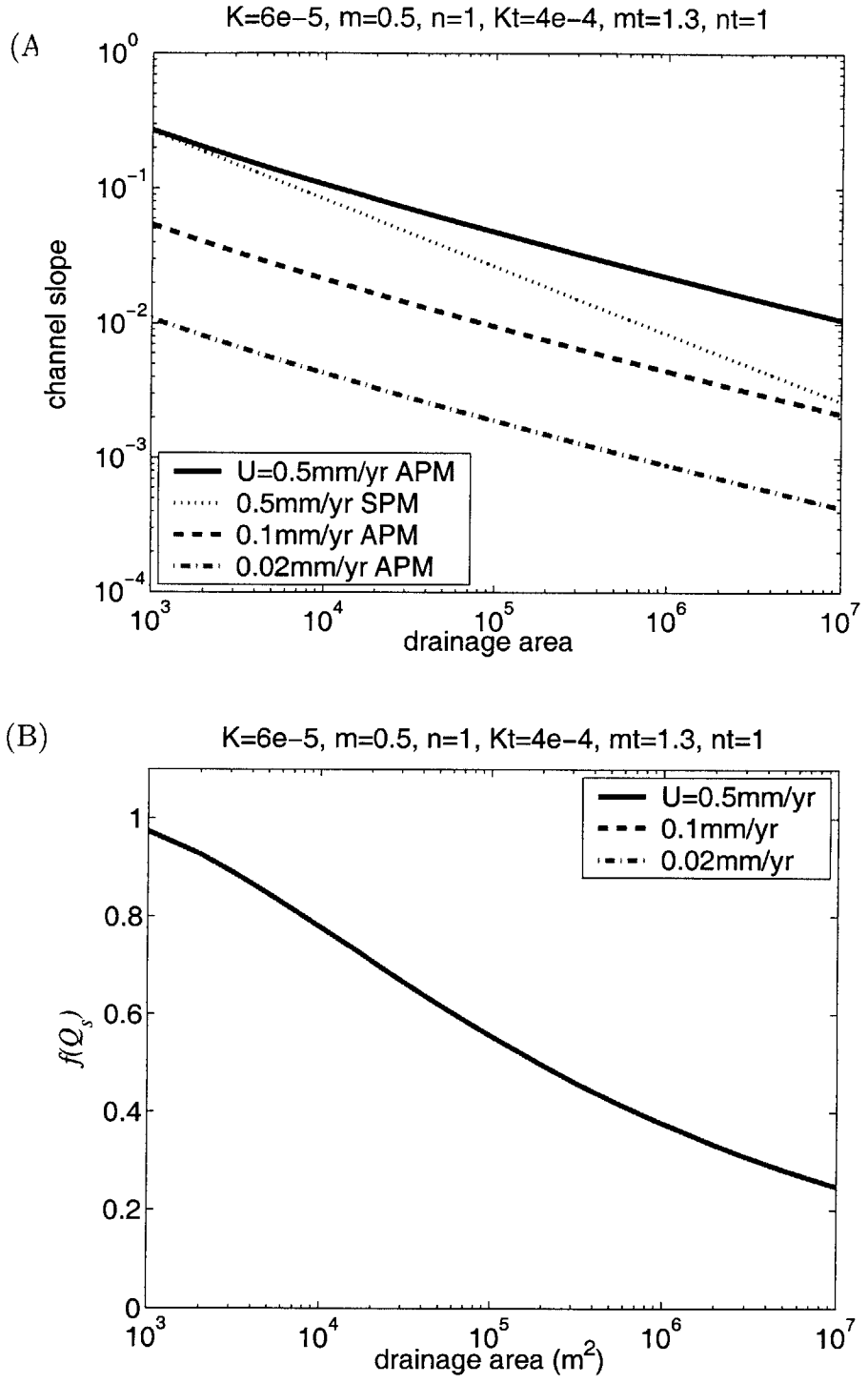

Figure 5-3: Sensitivity of equilibrium slope-area relationship (A) and $f(Q_s)$ value (B) to different uplift values (see legend - APM = almost parabolic model, SPM = stream-power model). $f(Q_s)$ values only apply to the almost parabolic rule.

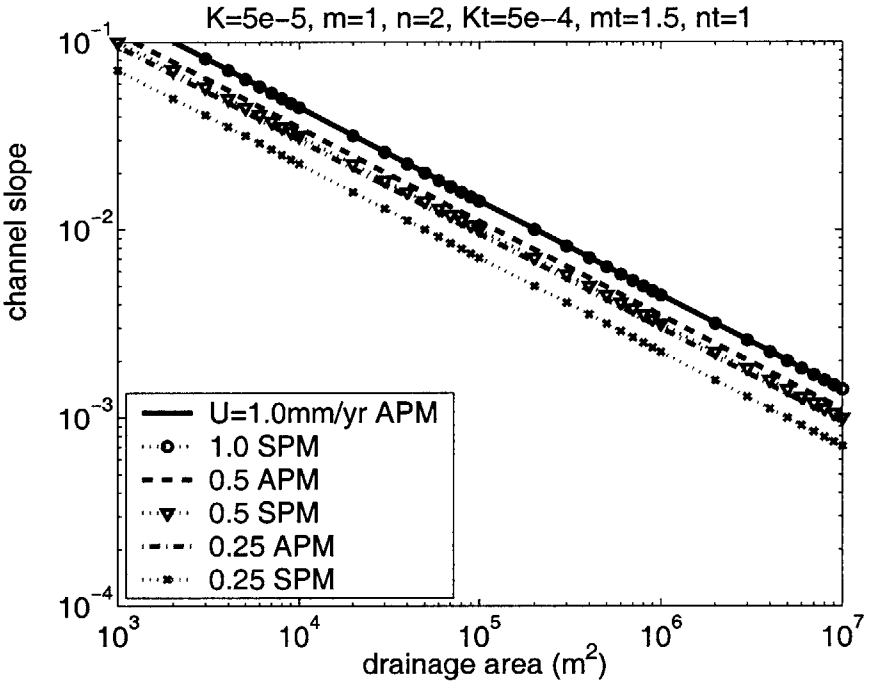

Figure 5-4: Equilibrium slope-area sensitivity to uplift rate using the almost parabolic model (APM) and stream power model (SPM) with same K, m and n values. Note that in the case of $U = 1mm/yr$, $f(Q_s) \approx 1$ (given these parameters), and therefore the almost-parabolic model and stream-power model predict exactly the same relationship.

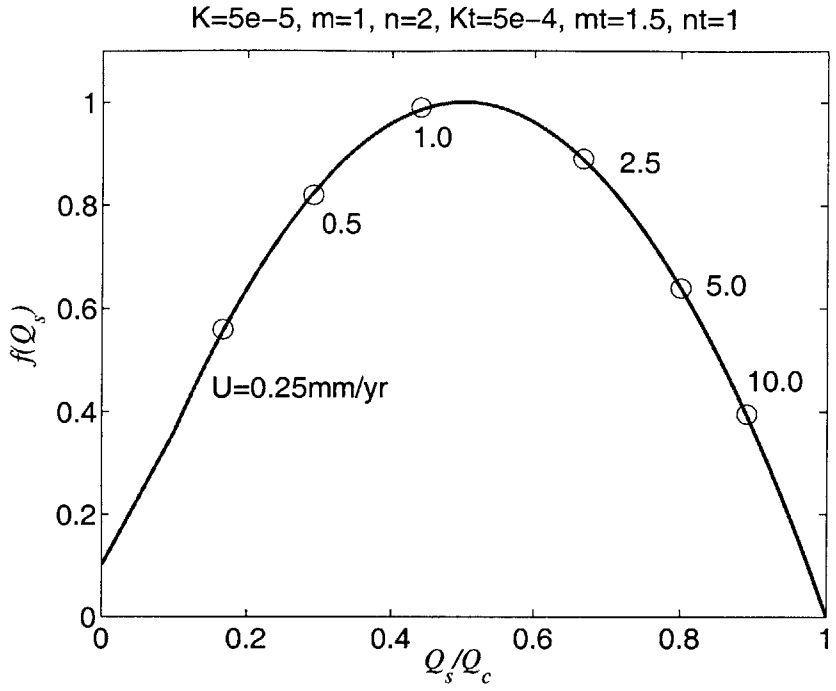

Figure 5-5: Sensitivity of equilibrium $f(Q_s)$ and $\frac{Q_s}{Q_c}$ values to different uplift rates using the almost-parabolic model. Note that because $mt = 1.5$, $f(Q_s)$ does not change with drainage area.

of K_t in the transport equation. Using the almost-parabolic model, the equilibrium relationship between channel slope and K_t (equations 5.10- 5.13) is more complex than the relationship between channel slope and K. It is therefore critical to define a reasonable way in which K_t varies with precipitation rate. This is not as straightforward as assuming $K \propto P^m$ as we did for the stream-power model. (We continue to make this assumption about K in this section.) The relationship between K_t and P is not as obvious because we are using a highly simplified version of the sediment transport equation (equation 5.9). The analysis in chapter 3 shows that there are two important terms in the sediment transport equation, the bed shear stress term which varies with $P^{0.9}$ and the critical shear stress term, which varies with $P^{0.43}$ (expanding equation 3.11). The simplified version of the sediment transport equation used in this chapter ignores the threshold term, but in some ways we include the effects of a threshold by increasing the value of mt (Howard 1980). The net result is that we are left without an easily translatable relationship between K_t and P. From the analysis

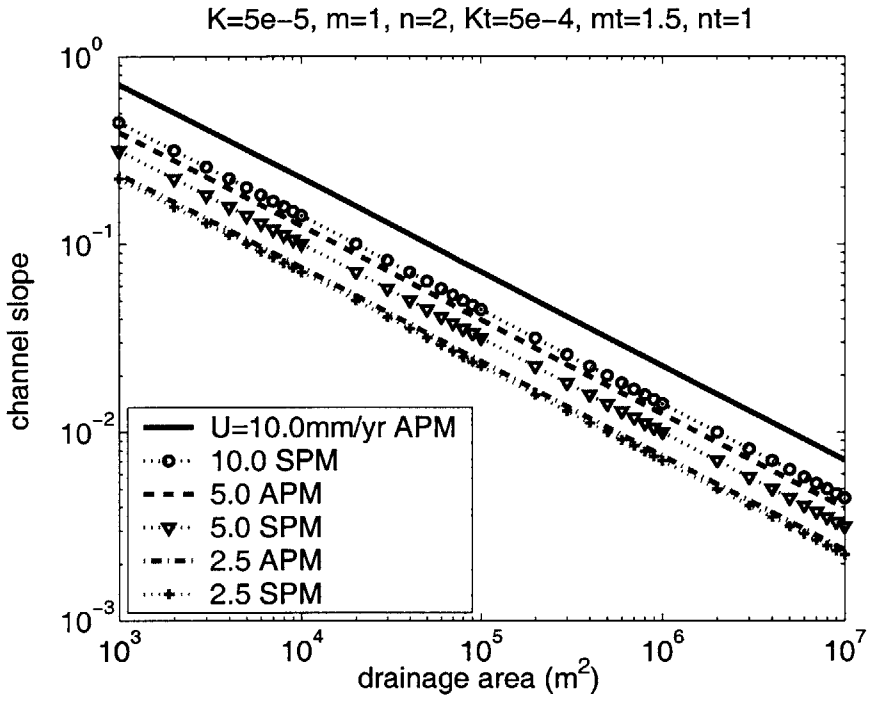

Figure 5-6: Sensitivity of the equilibrium slope-area relationship using both the almost-parabolic model (APM) and the stream-power model (SPM) to different uplift rates. The only difference between this figure and figure 5-4 is that the magnitude of uplift rate is larger here. Note that when $U = 2.5$mm/yr, $f(Q_s)$ is close to unity, and therefore the SPM and APM predict nearly the same equilibrium solution.

in chapter 3 we will assume that $K_t \propto P^{mp}$ where mp varies between 0.5 and 1.

Not surprisingly, this relationship is critical in determining the sensitivity of equilibrium slopes to precipitation rate using the almost-parabolic model. When the precipitation rate varies, the equilibrium sediment load does not (βUA remains constant). Given that Q_s remains constant with precipitation rate, $f(Q_s)$ adjusts to changes in precipitation rate by adjusting the value of Q_c. Variations in $f(Q_s)$ can enhance the decrease in slopes resulting from an increase in precipitation rates, or alternatively, they may counter-act the change in slopes.

In the first case considered we assume that $K_t \propto P^{1.0}$ (similar to the bed shear stress term from equation 3.11), and an increase in precipitation significantly changes the value of $\frac{Q_s}{Q_c}$. From past studies, we expect channel slopes to decrease with precipitation rate (e.g. Tucker and Bras (1998); Whipple et al. (1999); Bonnet and Crave (2003)). Figure 5-7 illustrates a counter-intuitive example of slope changes with precipitation rate. In this example, the steepest equilibrium slopes are produced with the largest precipitation rate, while the two smaller precipitation rates produce almost identical slopes. This is all due to changes in Q_c with precipitation rate. In this example, the increase in precipitation causes an decrease in $\frac{Q_s}{Q_c}$ (figure 5-8). Because $\frac{Q_s}{Q_c} < 0.5$ for all three cases illustrated in figure 5-7, the decrease in $\frac{Q_s}{Q_c}$ with increasing precipitation rate (figure 5-8) causes a decrease in $f(Q_s)$ (figure 5-8). This decrease in $f(Q_s)$ counteracts the increase in K with precipitation. As one might expect, in cases where the conditions are such that $\frac{Q_s}{Q_c} > 0.5$, an increase in precipitation rate actually causes $f(Q_s)$ to increase (figure 5-9B) and slopes decrease even more with increasing precipitation rate than expected from the stream-power model (figure 5-9A).

Alternatively, if we assume that $K_t \propto P^{0.5}$ (similar to the critical shear stress term from equation 3.11), we find that Q_c, and therefore $f(Q_s)$, are not nearly as sensitive to changes in precipitation rate. Because $f(Q_s)$ does not vary with precipitation rate and therefore cannot compensate for changes in precipitation rate, equilibrium slopes adjust as expected and increase with decreasing precipitation rate (figure 5-10A).

Given the analysis in chapter 3, we expect that the actual relationship between K_t and precipitation will depend on the sediment composition of the channel bed. If the

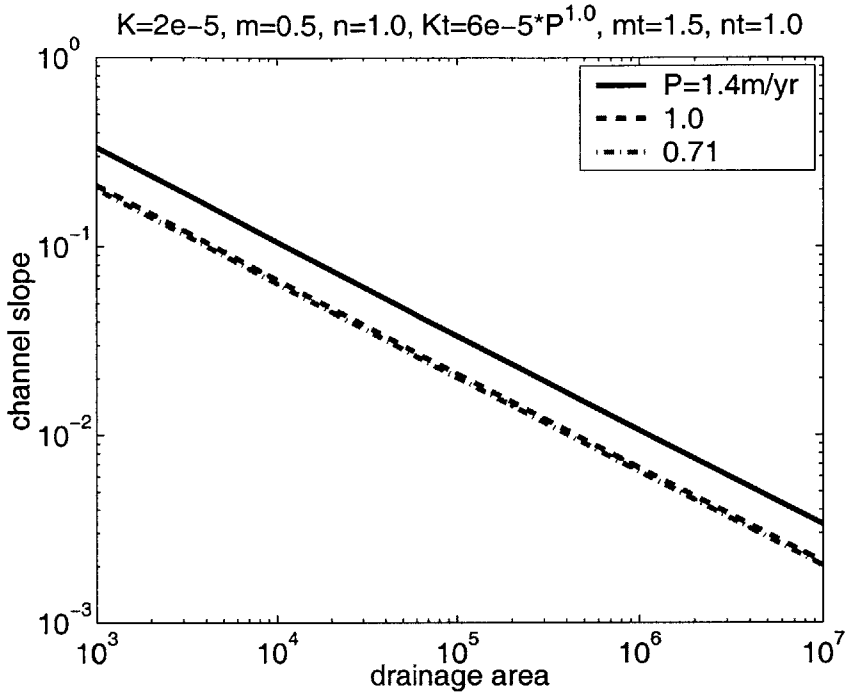

Figure 5-7: Slope-area sensitivity to precipitation rate using the almost-parabolic model and assuming that $K_t \propto P^{1.0}$.

grain-sizes are larger, the critical shear stress term should dominate and $f(Q_s)$ will probably be less sensitive to changes in precipitation rate. However, a less simplified sediment-transport model would give better insights into the relationship between $f(Q_s)$ and precipitation, or fluvial discharge. We do not carry out such an analysis here.

5.2.3 Linear-Decline Model

As an alternative method to the almost-parabolic model, we explore a generalized version of the under-capacity model described by Beaumont et al. (1992) and Kooi and Beaumont (1994). The linear-decline rule assumes that as the sediment load increases (with respect to the sediment transport capacity), more energy is required to transport sediment, so less energy is available to expend on erosion of the bed.

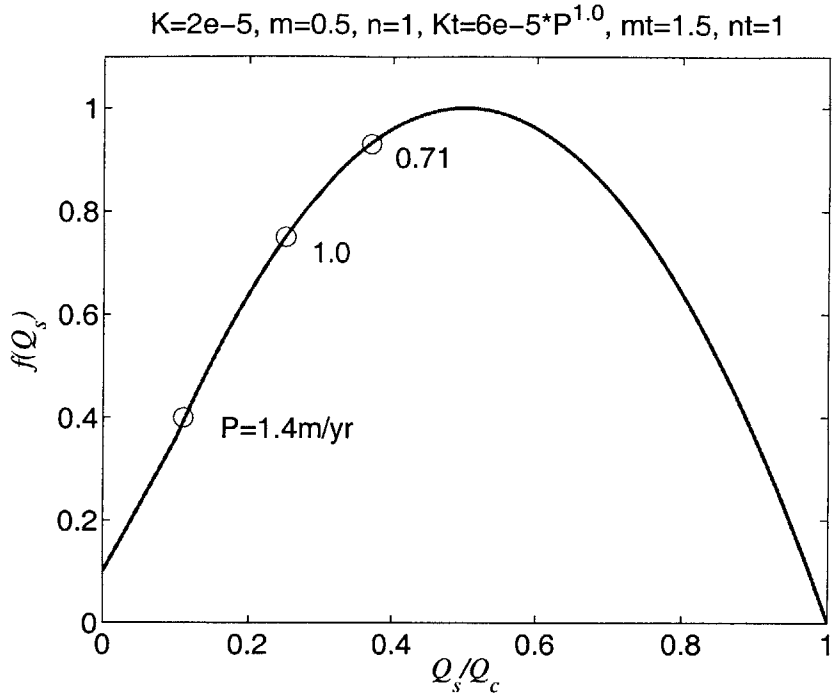

Figure 5-8: Sensitivity of equilibrium $f(Q_s)$ and $\frac{Q_s}{Q_c}$ values to different precipitation rates, assuming that $K_t \propto P^{1.0}$ (almost-parabolic model).

Here we use the model described by Whipple and Tucker (2002) (figure 5-2):

$$f(Q_s) = 1 - \frac{Q_s}{Q_c}. \tag{5.15}$$

Using the same equilibrium assumption for sediment load as in the previous section ($Q_s = \beta U A$) and the same sediment transport equation ($Q_c = K_t A^{mt} S^{nt}$) the equilibrium slope-area relationships described by Whipple and Tucker (2002) can be derived: when $n = 2$ and $nt = 1$,

$$S = \frac{\beta U}{2K_t} + \sqrt{\left(\frac{\beta U}{2K_t} A^{1-mt}\right)^2 + \frac{U}{K} A^{-m}}, \tag{5.16}$$

and when $n = 1$ and $nt = 1$,

$$S = \frac{U}{K} A^{-m} + \frac{\beta U}{K_t} A^{1-mt}. \tag{5.17}$$

It is clear from equations 5.16 and 5.17 that sensitivity of equilibrium slopes to

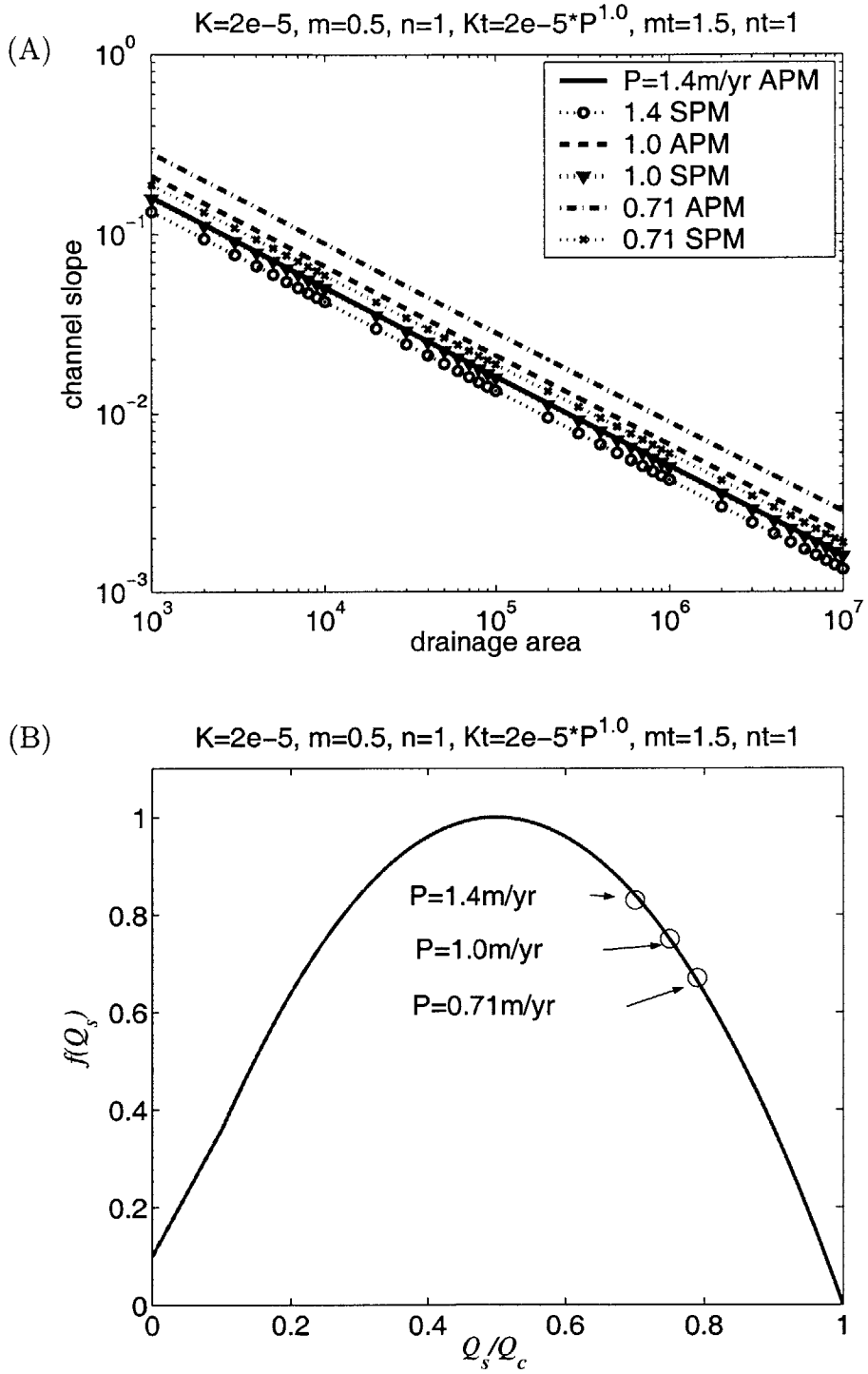

Figure 5-9: Sensitivity of equilibrium slope (A) and $f(Q_s)$ and $\frac{Q_s}{Q_c}$ values (B) to different precipitation rates, assuming that $K_t \propto P^{1.0}$ (almost-parabolic model - note change in K_t from previous example). Here the equilibrium slope values predicted from the stream-power model are shown for comparison. Note that the slope solution for P=1.4 APM overlaps the slope solution for P=1.0 SPM.

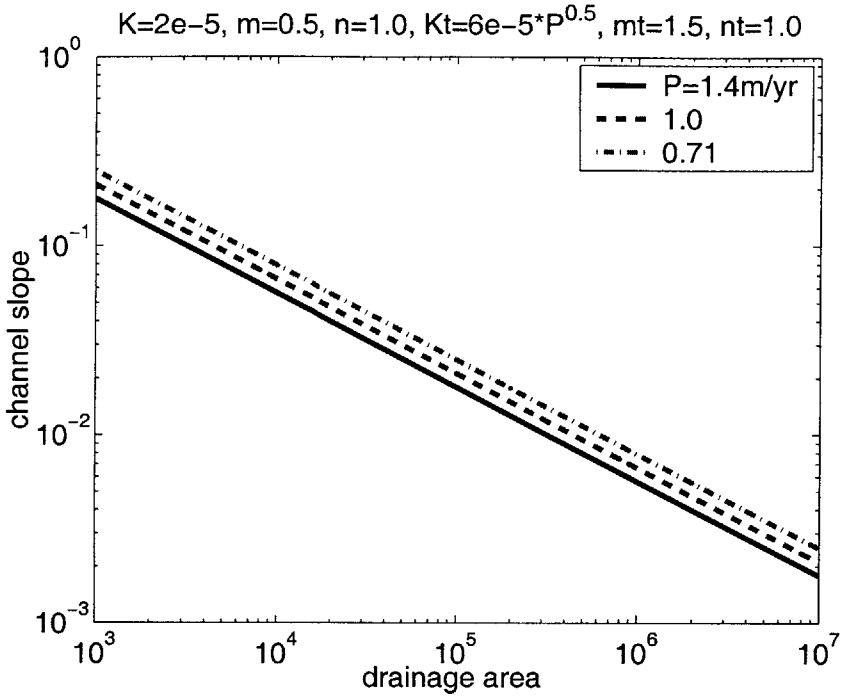

Figure 5-10: Sensitivity of equilibrium slope-area relationship to different precipitation rates, assuming that $K_t \propto P^{0.5}$ (almost-parabolic model).

both uplift rate and precipitation rate (contained in K and K_t) is as expected from the stream-power model. That is, equilibrium slopes increase with increases in uplift rate and equilibrium slopes decrease with increases in precipitation rate (assuming only that K_t increases with precipitation rate).

Similar to the almost-parabolic model, when $mt = 1.5$ the value of $f(Q_s)$ remains constant throughout the network and channel concavity is constant. This is not the case when $mt \neq 1.5$. Further, when $n = 1$ and $mt = 1.5$, $f(Q_s)$ does not change with uplift rate.

5.2.4 Wear Model

The last sediment flux erosion model that we explore is the wear model described by Parker (2002). Both Slingerland et al. (1997) and Sklar and Dietrich (1998) have discussed similar models which consider the wear of saltating particles on the channel bed. These models consider factors such as the saltation length of particles, sediment

grain size on the bed, the number of times a particle hits the channel bed (of given area over a period of time) and sediment cover (protection) of the bed. All of these factors can lead to a somewhat complicated erosion rule, especially when a threshold for sediment transport is considered.

The sediment flux term given by Parker (2002) which describes wear of the bed can be written as:

$$f(Q_s) = \frac{Q_s}{W}\left(1 - \frac{Q_s}{Q_c}\right), \tag{5.18}$$

where W is channel width. In Parker's model $m = n = 0$ and therefore the erosion rate is written as:

$$E_d = \beta K \frac{Q_S}{W}\left(1 - \frac{Q_s}{Q_c}\right). \tag{5.19}$$

Making the same assumptions as we did in previous sections ($Q_s = \beta\ UA$, $Q_c = K_t A^{mt} S^{nt}$) and further, $W \propto A^{0.5}$, we can derive the equilibrium slope-area relationship for the wear model in equation 5.19:

$$S = \left(\frac{\beta U}{K_t}\right)^{\frac{1}{nt}} A^{\frac{1-mt}{nt}} \left(1 - \frac{A^{-0.5}}{\beta K}\right)^{\frac{-1}{nt}} \tag{5.20}$$

In keeping with the previous sections, we only consider the case in which $nt = 1$. For small values of drainage area, equation 5.20 grows infinitely large. Similarly, the value of K can not be too small, otherwise slopes quickly explode (figure 5-11). However, if K is large, this leads to transport-limited conditions. At large drainage areas, the wear model always predicts the same slope-area relationship as the transport-limited slope. The equilibrium channel slope reaches the transport slope at smaller drainage areas for larger K values (figure 5-11).

There is no parameter set which predicts a constant concavity with this model. At large drainage areas, the average channel concavity increases with the value of mt (figure 5-12). The wear model predicts that in equilibrium slopes increase with uplift rate (figure 5-13) at the same rate as predicted by a simple transport-limited model (Whipple and Tucker 2002).

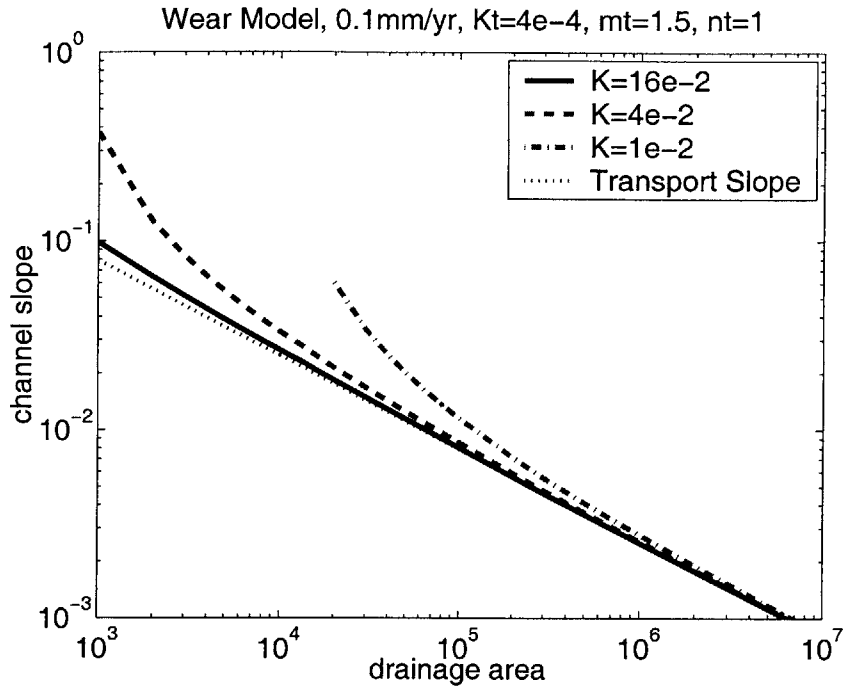

Figure 5-11: Sensitivity of the wear model equilibrium slope-area relationship to the value of K (see equation 5.20). (U =0.1mm/yr) The equilibrium transport slope does not depend on K and is therefore the same for all examples (dotted line).

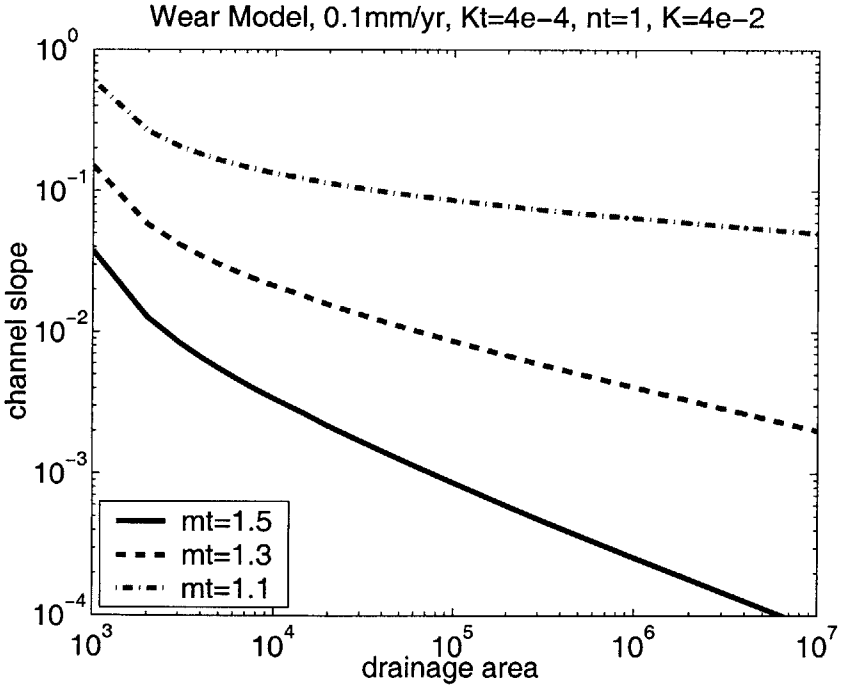

Figure 5-12: Sensitivity of the equilibrium wear model slope-area relationship to the value of mt (see equation 5.20). (U =0.1mm/yr)

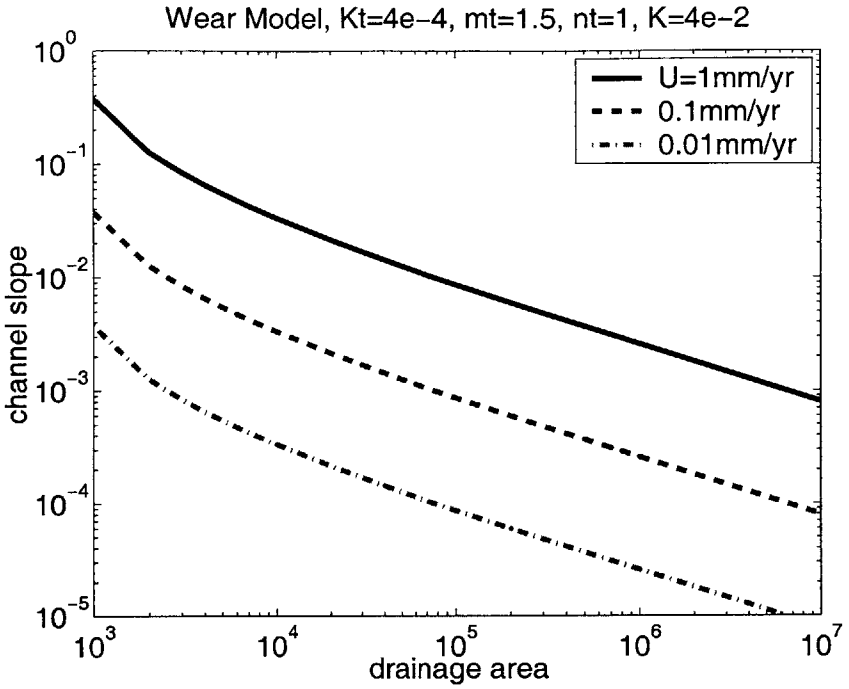

Figure 5-13: Sensitivity of the equilibrium wear model slope-area relationship to uplift rate (see equation 5.20).

5.3 Transient Behavior using the Stream-Power Model

Detachment limited channels controlled by the stream-power model have been shown to respond to a change in uplift rate by locally increasing or decreasing channel slopes to the new equilibrium value, and this response propagates upstream as knickpoint (Howard et al. (1994); Whipple and Tucker (1999); Niemann et al. (2001); Whipple and Tucker (2002)). Because this result has already been shown, we illustrate this concept with only one figure so that the reader can compare with later results (figure 5-14).

5.4 Transient Behavior using the Almost-Parabolic Model

In this section we discuss changes in the channel network in response to a single step increase in uplift rate when the almost-parabolic model controls erosion rate. The initial condition for each experiment is an equilibrium drainage network. In the first

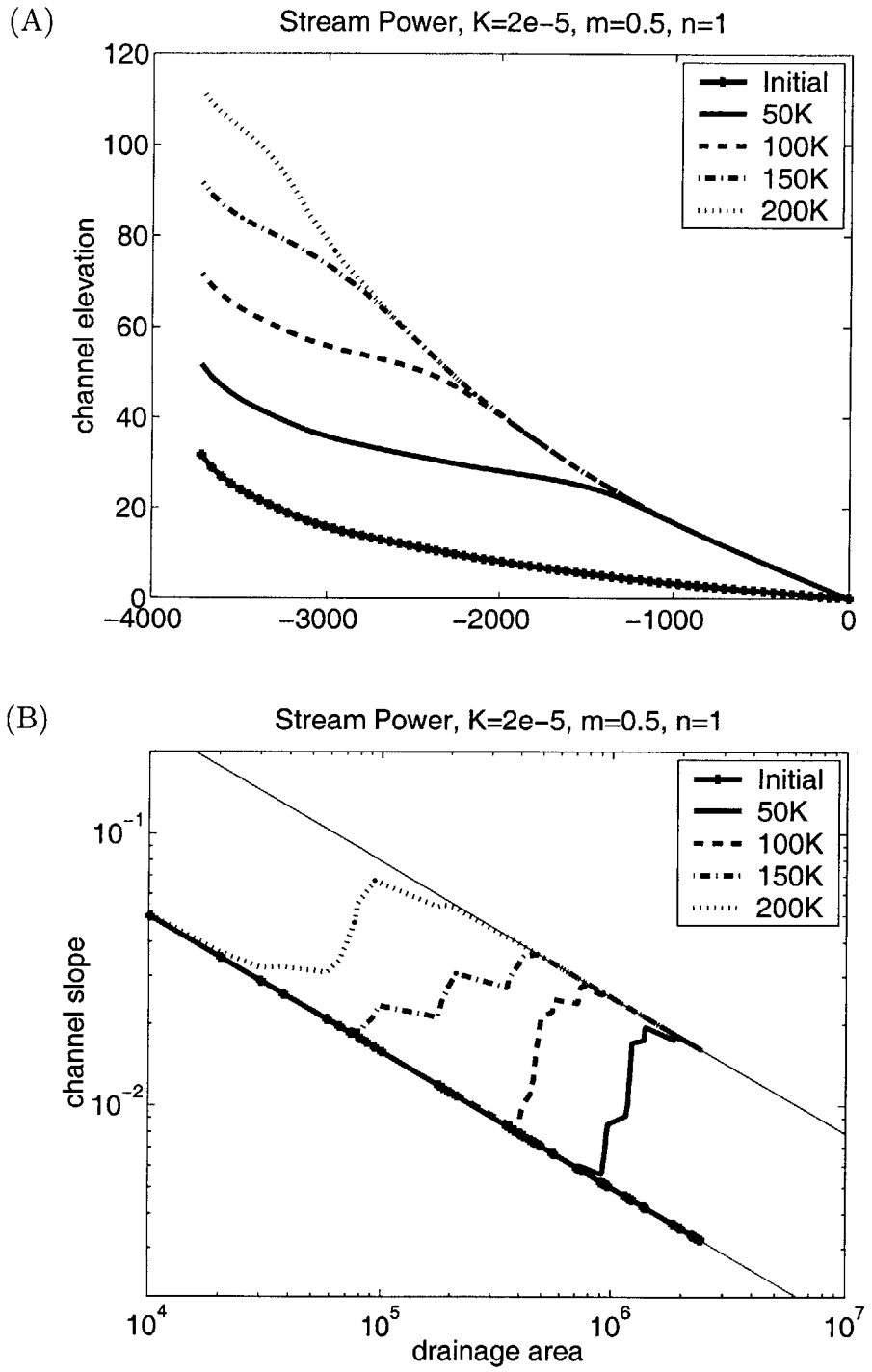

Figure 5-14: Change in main channel elevation (A) and channel slope (B) in response to a five-fold increase in uplift rate using the stream-power model. (The thin lines running through the slope-area plot are the equilibrium relationships.)

three experiments the same initial drainage network is used, but the change in the uplift rate varies between the experiments. The results show that the same network can react very differently depending on the magnitude of the perturbation. In the last experiment discussed, we illustrate the transient response using a different parameter set (namely, $n = 2$ versus $n = 1$ in the first three experiments). The response of channel slopes in the last example is surprisingly complex. While reading this section it is important to keep in mind that a network controlled by the stream-power model responds directly to an increase in uplift rate, sending a knickpoint through the network that raises channel slopes/elevations to their new equilibrium values.

We expect equilibrium channel slopes to increase with uplift rate (equations 5.10 and 5.12), regardless of the parameter values in the almost-parabolic erosion equation. In the first three examples, $n = 1$ and $mt = 1.5$ and, therefore, in equilibrium $f(Q_s)$ is uniform throughout the network and insensitive to changes in uplift rate. (In the $n = 1$ example, the equilibrium value of $\frac{Q_s}{Q_c}$ is 0.75.) This "simplest" case seems like a simple choice for investigating the transient response. However, so far the theory presented only predicts the equilibrium outcome and says nothing about how a drainage network transitions from one equilibrium state to another. Even though $f(Q_s)$ values may not vary between equilibrium states, they are not constant as the network responds to a change in forcing, leading to some very curious results.

Figure 5-15 shows the response of main channel elevations (A) and slopes (B) to a two-fold increase in uplift rate. The initial response looks very much like a knickpoint traveling up the network as one would expect from the stream-power model (Whipple and Tucker (2002)). However the knickpoint does not increase channel elevations all the way up to their new equilibrium values. After the knickpoint has swept up the main channel, elevations and slopes continue to gradually increase everywhere (figure 5-16A and B), similar to transitions in a transport-limited channel (Whipple and Tucker (2002)).

Note that the initial equilibrium slope-area relationship in figure 5-15 deviates in the smaller drainage areas from the predicted slope-area relationship. The deviation in the smaller drainage areas is a boundary condition of the model. The predicted

slope-area relationship (plotted in figure 5-15) assumes that $Q_s = \beta UA$, but this is not the case at points which only drain themselves and have no incoming sediment load ($Q_s = 0$). These points are still eroding at the uplift rate when equilibrium is reached, but their value of $f(Q_s)$ differs from that predicted using $Q_s = \beta UA$, and therefore their slope values also differ from those predicted assuming $Q_s = \beta UA$. This boundary condition affects the predicted slopes in the upper-most reaches of the network in all of the examples using the almost-parabolic model.

The combination response illustrated by figures 5-15 and 5-16, where initially a knickpoint propagates up the network and later slopes increase throughout the network to their final values, is similar to the mixed-channel response illustrated by Whipple and Tucker (2002). In their example, they choose the erosion parameters so that the equilibrium profile of the transport-limited and stream-power detachment limited channels are exactly the same. Their results show that the transient response to an increase in uplift rate has tendencies of both types of channels, depending on when changes in sediment load become important and the response switches from stream-power style to transport-style. The almost-parabolic model is not the same as the mixed-channel model used by Whipple and Tucker (2002), but variations in sediment load are also responsible for the results produced in both studies. We elaborate on this later.

An important change in the nature of network response occurs when the increase in uplift rate is amplified to three-fold (versus two-fold in the last example). A three-fold increase in uplift rate also causes channel slopes to step-up knickpoint style to a value less than their new equilibrium value (figure 5-17B). Surprisingly though, slopes actually *decrease* after the initial increase and channel elevations come down (figure 5-17A). After the initial increase and decrease in slopes (at a point), channel slopes rise uniformly up to their new equilibrium values in a transport-limited manner as they did in later times in the two-fold uplift case (figure 5-18).

A four-fold increase in uplift rate is even more dramatic. Following the increase in uplift rate, the knickpoint (figures 5-19A and 5-20A) actually increases slopes above their new equilibrium values (figures 5-19B and 5-20B). In response to this

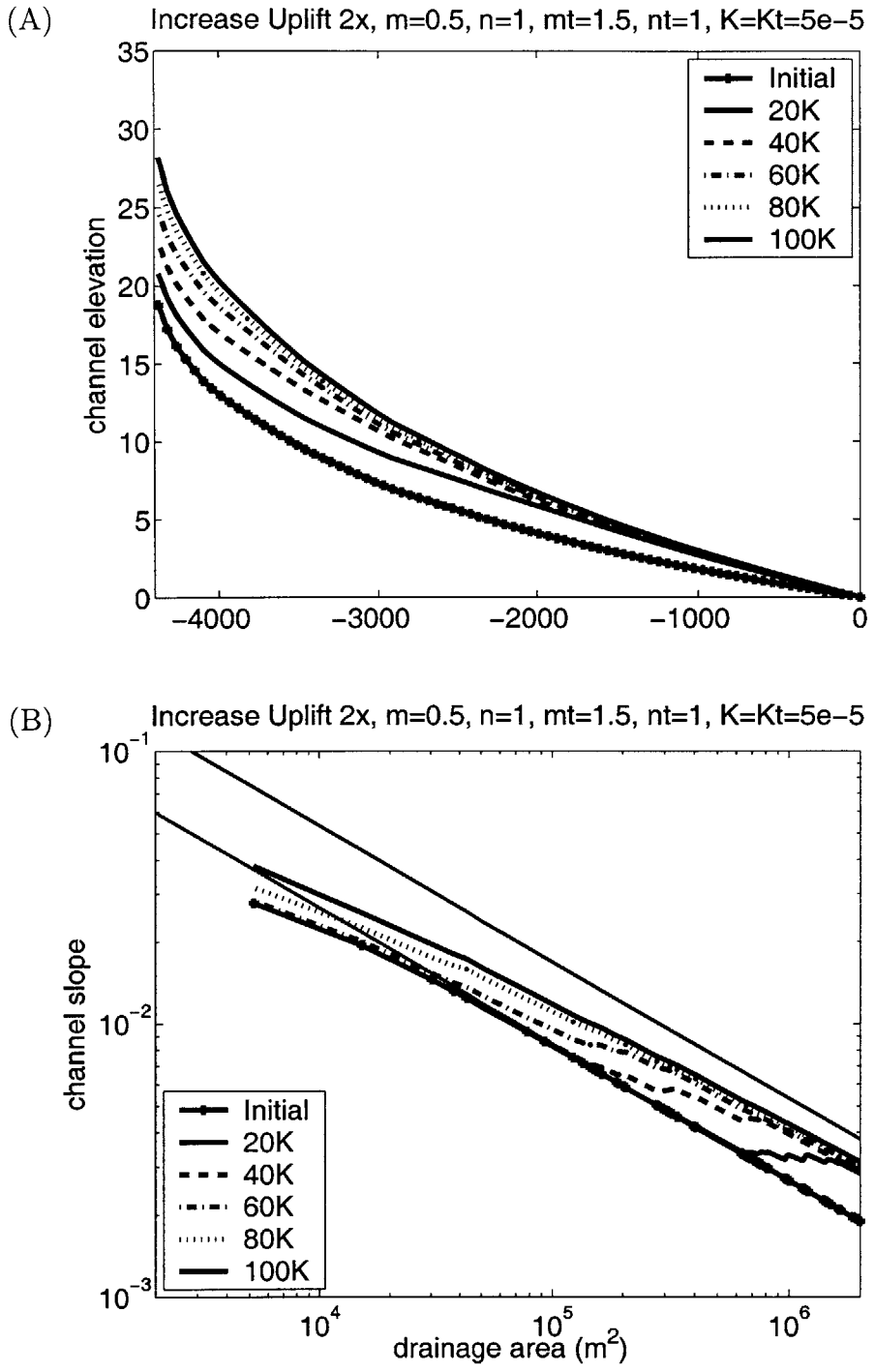

Figure 5-15: Initial change in main channel profile (A) and channel slope (B) in response to a two-fold increase in uplift rate using the almost parabolic sediment flux rule. (The lines running through the slope-area plot are the equilibrium relationships for old (lower) and new (upper) uplift rates.)

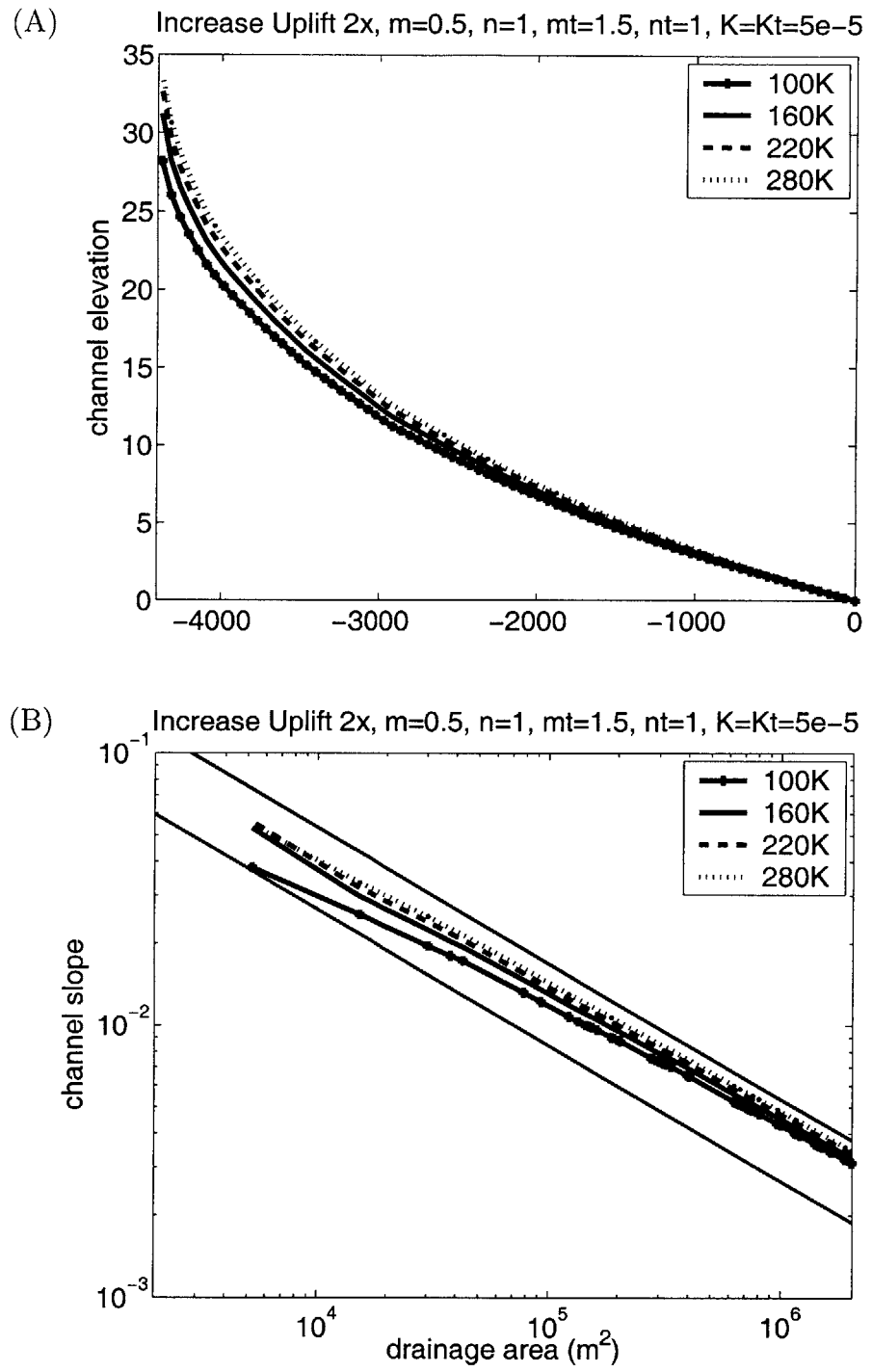

Figure 5-16: Later change (following figure 5-15) in main channel profile (A) and channel slope (B) in response to a two-fold increase in uplift rate. (The lines running through the slope-area plot are the equilibrium relationships for old (lower) and new (upper) uplift rates.)

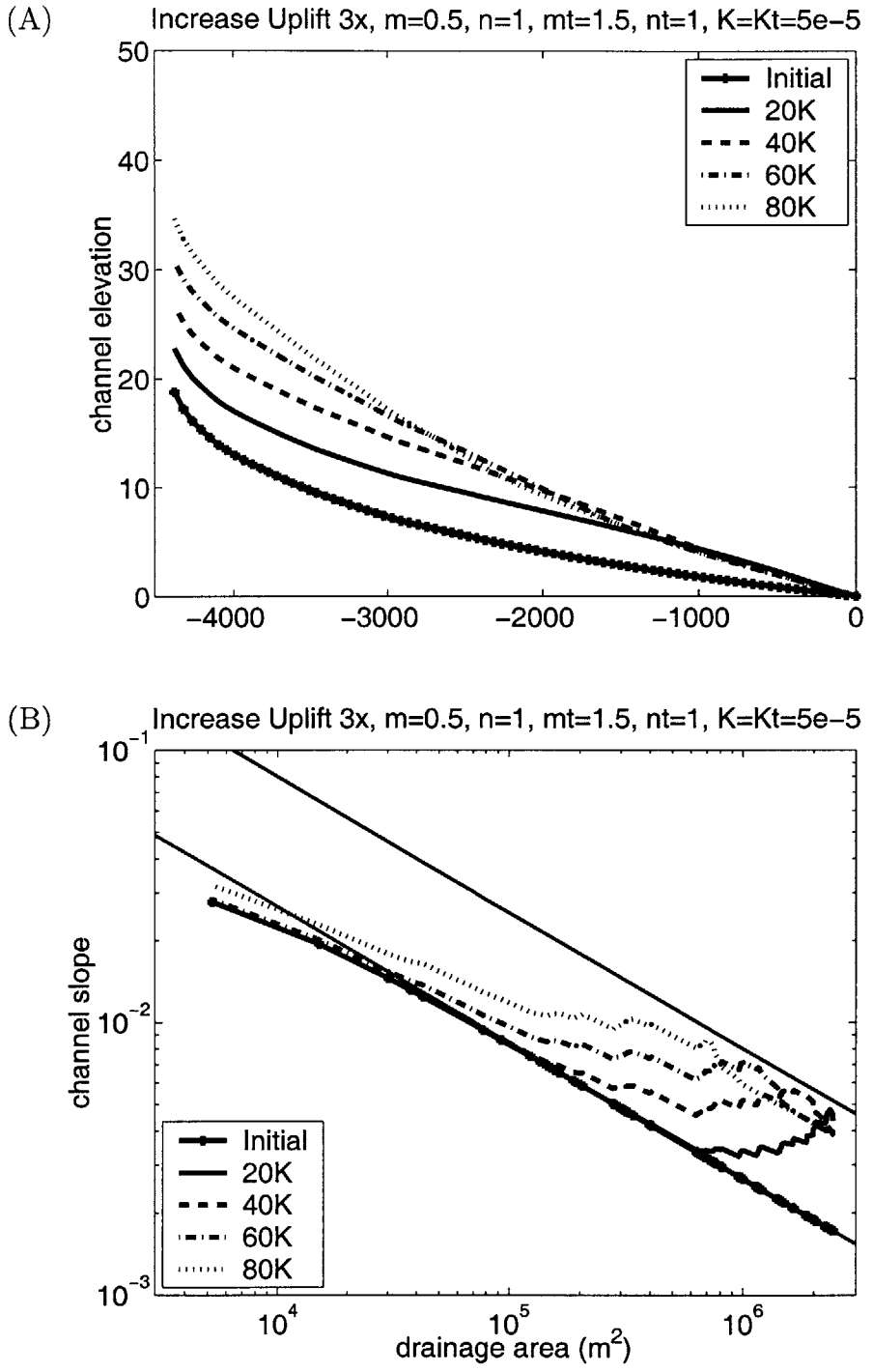

Figure 5-17: Initial change in main channel profile (A) and channel slope (B) in response to a three-fold increase in uplift rate. (The lines running through the slope-area plot are the equilibrium relationships for old (lower) and new (upper) uplift rates.)

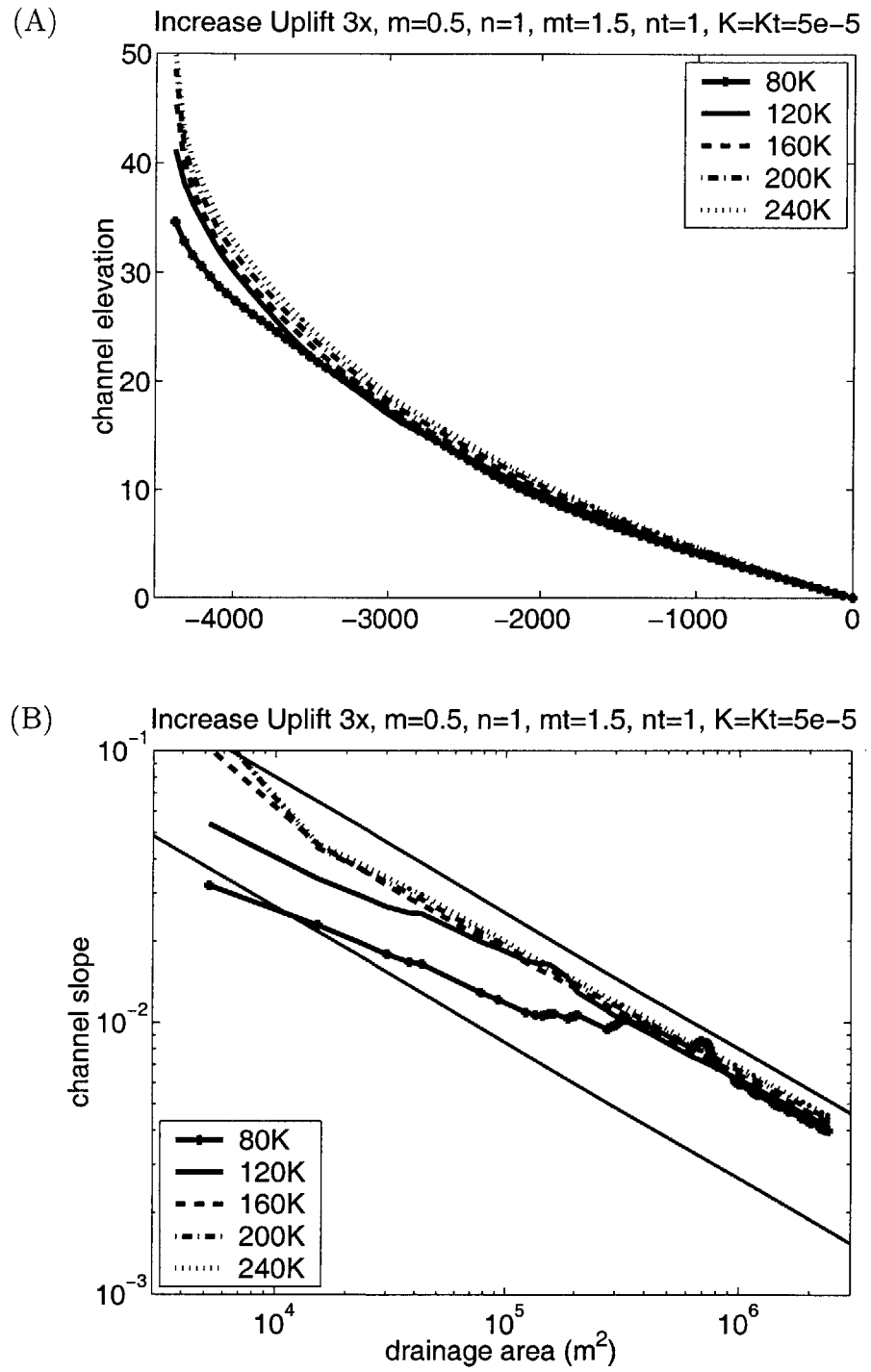

Figure 5-18: Later change (following figure 5-17) in main channel profile (A) and channel slope (B) in response to a three-fold increase in uplift rate. (The lines running through the slope-area plot are the equilibrium relationships for old (lower) and new (upper) uplift rates.)

overshooting of slopes above their new equilibrium value, channel elevations must subsequently be reduced. The result is much more dramatic than in the previous example because slopes first overshoot their new equilibrium values, later drop down below their new equilibrium value, and finally must rise again (not shown). This overshooting and undershooting creates a dramatic whiplash-like response in channel profiles (figure 5-20A). In all cases tested, the same over-steepening of slopes occurs with higher values of U_{new} leading to more exaggerated whiplash-like response in channel profile (figures 5-19A and 5-20A).

The complex response in channel slopes produced from a single increase in uplift rate is all the result of changes in sediment load and its effects on erodibility ($f(Q_s)$). Initially, the response to an increase in uplift rate is felt only at the outlet. The rest of the points in the network continue to erode at the old equilibrium uplift rate (Whipple and Tucker 1999). (U_{old} is used to refer to the original smaller uplift rate in this discussion.) Figure 5-21 illustrates the pattern in erosion rates across the topography; shaded is according the ratio of the erosion rate to the new uplift rate (U_{new}). This example is from the four-fold uplift increase experiment, therefore points which are eroding at the old uplift rate have an erosion ratio of 0.25 (shaded white in this figure). Points eroding at the new equilibrium value have an erosion ratio of 1.0 (shaded dark gray in this figure). Light gray points have just started to respond to the change in uplift rate, while black points are eroding faster than the new uplift rate. (There are no black points in figure 5-21.) Figure 5-21 shows that points near the outlet respond first, while the rest of the network continues to erode at the same old value. (This pattern is the same regardless of the magnitude of change in uplift rate.) As time moves on, erosion rates increase as a wave moving up the network (figures 5-21B and C). In figures 5-21B and C, the black points are eroding faster than the new uplift rate (causing channel elevations to be reduced in figure 5-20A), and their erosion ratio will eventually reduce back to unity.

Because the points in the upper reaches of the network are eroding at the same original value (U_{old}), there is no change in the amount of sediment that they send downstream. Therefore, initially there is no change in the sediment load received by

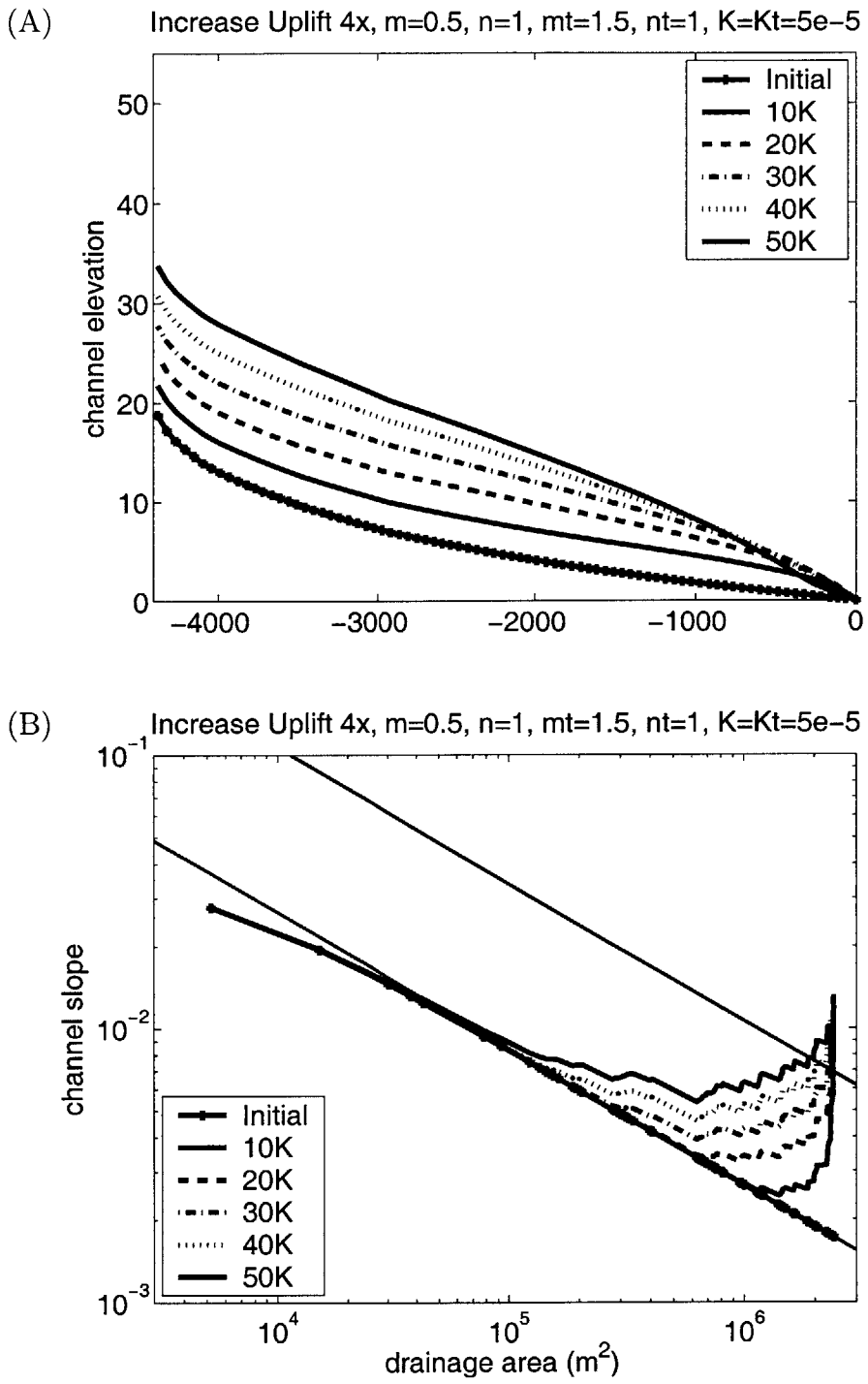

Figure 5-19: Initial change in main channel profile (A) and channel slope (B) in response to a four-fold increase in uplift rate. (The lines running through the slope-area plot are the equilibrium relationships for old (lower) and new (upper) uplift rates.)

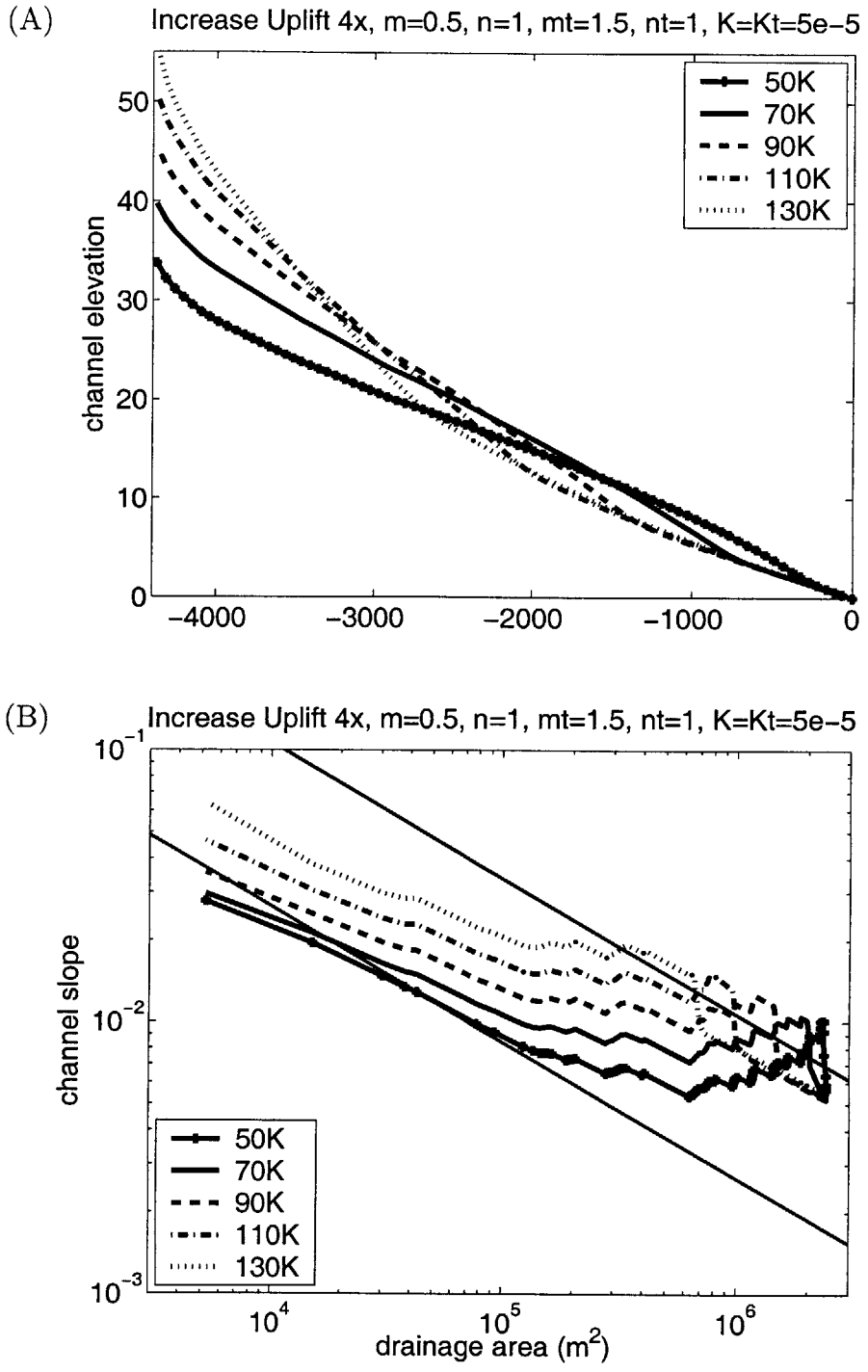

Figure 5-20: Later change (following figure 5-19) in main channel profile (A) and channel slope (B) in response to a four-fold increase in uplift rate. (The lines running through the slope-area plot are the equilibrium relationships for old (lower) and new (upper) uplift rates.)

the outlet point. However the outlet point feels the increase in uplift rate and adjusts its slope to erode at the higher rate of U_{new}. The outlet point adjusts its slopes based on the old sediment load. This can lead to overshooting of slopes, as the profiles in figures 5-19 and 5-20 illustrate.

As stated above, the outlet point needs to erode at the new uplift rate. Initially, the incoming sediment load at the outlet (or any point) does not change, but the slope can adjust, changing the value Q_c, and furthermore, the value of $f(Q_s)$. This results in the following equation for the interim erosion rates at the outlet:

$$U_{new} = Kf(Q_s)_t A^m S_t^n, \tag{5.21}$$

where $f(Q_s)_t$ and S_t are the transient values of $f(Q_s)$ and S in response to the uplift increase. Rearranging equation 5.21, we obtain an expression for S_t as a function of $f(Q_s)_t$:

$$S_t = \left(\frac{U_{new}}{Kf(Q_s)_t}\right)^{\frac{1}{n}} A^{\frac{-m}{n}}. \tag{5.22}$$

In order to describe the transient channel slope, we need to describe $f(Q_s)_t$. We have already predicted that the value of Q_s at the outlet remains at its old equilibrium value of $\beta U_{old} A$ (initially). On the other hand, we expect slopes to rise in response to an increase in uplift rate, resulting in larger values of Q_c (equation 5.9). As a result, $\frac{Q_s}{Q_c}$ will decrease. But what affect does this have on $f(Q_s)_t$?

The response of $f(Q_s)_t$ will depend on the initial value of $\frac{Q_s}{Q_c}$. Figure 5-22 is a schematic of the expected response of $f(Q_s)_t$ based on the examples from this section. The equilibrium value of $\frac{Q_s}{Q_c}$ in these examples is 0.75 (for both U_{new} and U_{old}). More important than the actual value of $\frac{Q_s}{Q_c}$ is that $\frac{Q_s}{Q_c} > 0.5$. Therefore a decrease in $\frac{Q_s}{Q_c}$ (as expected) will initially cause $f(Q_s)_t$ to rise (first part of solid arrow-line in figure 5-22). If $\frac{Q_s}{Q_c}$ is reduced to a value smaller than 0.5, the value of $f(Q_s)_t$ will decline (second part of solid arrow-line in figure 5-22). If $\frac{Q_s}{Q_c}$ is reduced far enough, the value of $f(Q_s)_t$ can decrease below the equilibrium value of $f(Q_s)$, leading to a transient slope value which is greater than the new equilibrium slope value (equation 5.22). In the case when $\frac{Q_s}{Q_c} \leq 0.5$ initially, any reduction in $\frac{Q_s}{Q_c}$ will cause $f(Q_s)_t$ to decrease

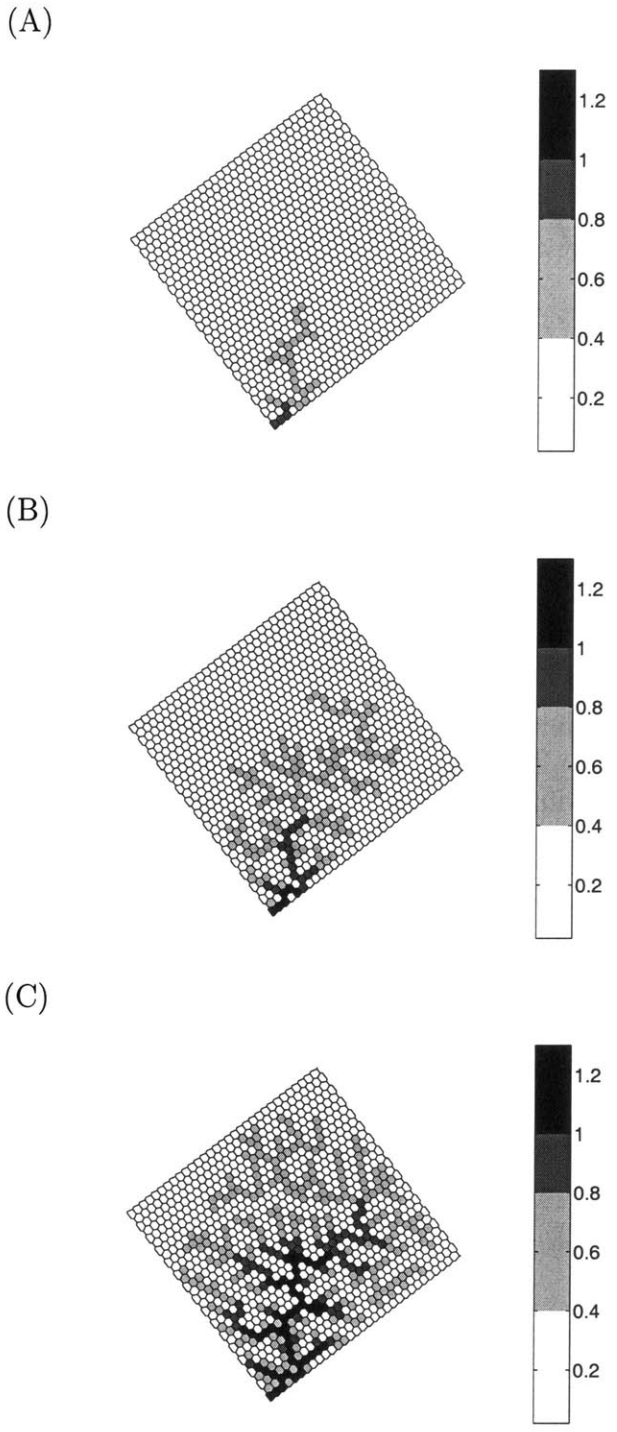

Figure 5-21: Response of erosion rates across the landscape 10K (A), 30K (B), and 60K (C) years after increasing the uplift rate by four-fold using the almost-parabolic model. Shading is by the ratio of erosion rate to new uplift value, so a value of 0.25 corresponds to the old erosion rate. The black values are areas eroding faster than the new equilibrium erosion rate.

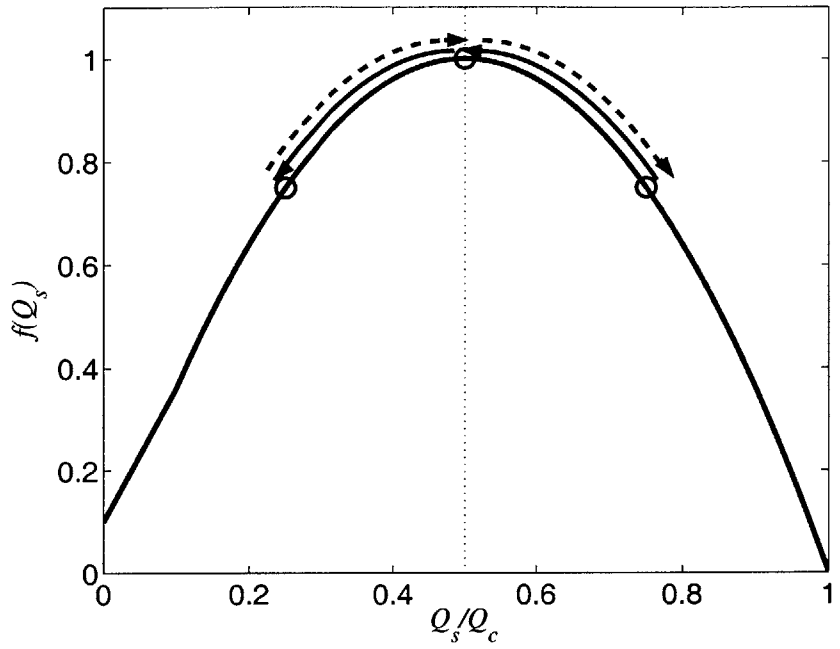

Figure 5-22: Cartoon example of how an increase in uplift rate changes $f(Q_s)$ using the almost-parabolic model. The solid arrow-line indicates the initial response of $f(Q_s)$, and the dotted arrow-line indicates the later response.

(starting at the top or left side of the hump in figure 5-22).

The decrease in $\frac{Q_s}{Q_c}$ results in the following expression for the transient value of $f(Q_s)$ when $\frac{Q_s}{Q_c} > 0.1$:

$$f(Q_s)_t = 1 - 4\left(\frac{\beta U_{old} A}{K_t A^{mt} S_t^{nt}} - 0.5\right)^2, \tag{5.23}$$

and when $\frac{Q_s}{Q_c} < 0.1$:

$$f(Q_s)_t = 2.6\left(\frac{\beta U_{old} A}{K_t A^{mt} S_t^{nt}}\right) + 0.1. \tag{5.24}$$

Combining equation 5.22 with either equation 5.23 or 5.24, we obtain an equation for the predicted value of S_t. When $n = 1$ and $nt = 1$: $\frac{Q_s}{Q_c} > 0.1$,

$$S_t = \frac{\frac{\beta U_{old}}{K_t} A^{1-mt}}{1 - \frac{U_{new} K_t}{4\beta U_{old} K} A^{mt-m-1}}, \tag{5.25}$$

and $\frac{Q_s}{Q_c} < 0.1$,

$$S_t = \frac{10U_{new}}{K}A^{-m} - \frac{26\beta U_{old}}{K_t}A^{1-mt}. \tag{5.26}$$

When $n = 2$ and $nt = 1$: $\frac{Q_s}{Q_c} > 0.1$,

$$S_t = \frac{K_t U_{new}}{4K\beta U_{old}}A^{mt-m-1} + \frac{\beta U_{old}}{K_t}A^{1-mt}, \tag{5.27}$$

and $\frac{Q_s}{Q_c} < 0.1$,

$$S_t = \frac{-13\beta U_{old}}{K_t}A^{1-mt} + 5\sqrt{\left(\frac{2.6\beta U_{old}}{K_t}A^{1-mt}\right)^2 + \frac{0.4U_{new}}{K}A^{-m}}. \tag{5.28}$$

Equations 5.25 - 5.28 predict the initial change in slope before the sediment load starts to increase. The transient slope value predicted from these equations can be compared with the new equilibrium slope value (predicted using U_{new} and equations 5.10 - 5.13) in order to predict cases where the transient slope will over-shoot its new equilibrium value. In the case when initially $\frac{Q_s}{Q_c} < 0.1$, the transient slope will always be greater than the new equilibrium slope (compare equation 5.11 using U_{new} as the uplift value with equation 5.26, or similarly compare equations 5.13 and 5.28). This is because $f(Q_s)$ will always initially decrease with an increase in uplift rate. When $\frac{Q_s}{Q_c} > 0.1$ initially, whether or not S_t is greater than the new equilibrium slope depends on the the initial value of $\frac{Q_s}{Q_c}$ and the magnitude of change in $\frac{Q_s}{Q_c}$. If $\frac{Q_s}{Q_c} < 0.5$ to start, transient slopes will always over-steepen because $f(Q_s)$ will always initially decrease with an increase in uplift rate. However, when $\frac{Q_s}{Q_c} > 0.5$ initially, the magnitude of change in uplift rate determines whether or not transient slopes over-steepen. This last scenario ($\frac{Q_s}{Q_c} > 0.5$ initially) is the case with the two examples we have presented.

The transient slope equations give an accurate prediction of the results we see. In the case of a two-fold increase in uplift rate (figures 5-15 and 5-16), $f(Q_s)_t = 1$. Because $f(Q_s) = 0.75$ initially, S_t is less than the new equilibrium slope value (equation 5.22), and as a result, transient slopes only increase. In the example with a two-fold uplift increase, $\frac{Q_s}{Q_c}$ decreases initially to 0.5, but it never falls below 0.5 or, in

other words, goes over the hump in figure 5-22. This causes slopes to rise initially, but to a value less than their new equilibrium value (figure 5-15B). Slopes then remain static for a period before rising again to their equilibrium value (figure 5-23B). The lag in the time of response from the upper parts of the network results in interim stabilization of slopes (roughly between 10^3 and 10^4 years). Later, when sediment load increases, and therefore $\frac{Q_s}{Q_c}$ increases and $f(Q_s)$ decreases, slopes rise even further (figure 5-16B). In this example, erosion rates never overshoot their new equilibrium values (figure 5-23C).

In the case of a three-fold increase in uplift rate, the predicted transient slope is exactly equal to the new equilibrium slope. This is because the equilibrium value of $f(Q_s)$ is exactly the same as $f(Q_s)_t$, although the value of $\frac{Q_s}{Q_c}$ decreases (schematic in figure 5-22). Figure 5-24 illustrates the response over time of $f(Q_s)$ (A) and channel slope (B) at the outlet and two other points upstream. Initially slopes at the outlet increase while the transient value of $f(Q_s)$ remains larger than the initial value (even though it both increases and decreases). $\frac{Q_s}{Q_c}$ is decreasing almost until 10^4 years, even though $f(Q_s)$ is rising and falling in this period. The fall in $f(Q_s)$ before 10^4 years is because $f(Q_s)$ is pushed onto the left side of the hump in figure 5-22. When $\frac{Q_s}{Q_c}$ starts to increase again, $f(Q_s)$ starts to rise again (at $\approx 10^4$ years), and the slope at the outlet begins to decrease. The transient slope at the outlet does not reach its new equilibrium value before it starts to decrease again as predicted by the value of S_t from equation 5.25. The prediction of S_t is based on no change in the incoming sediment flux. In actuality, the slopes never have time to rise to the predicted value before the value of Q_s at the outlet starts to increase. This is apparent from the rise in $f(Q_s)$ at points upstream of the outlet that begins before the outlet reaches its minimum $f(Q_s)$ value (figure 5-24A). Here erosion rates essentially increase to their new equilibrium value, although there is a slight overshooting in the upper parts of the network (figure 5-24C).

For the four-fold uplift increase case, $\frac{Q_s}{Q_c}$ is pushed to below its initial value of 0.75 even further than it was in the three-fold case. Equation 5.25 predicts slopes to rise above their new equilibrium value, as was illustrated in figures 5-19B and 5-20B.

(A)

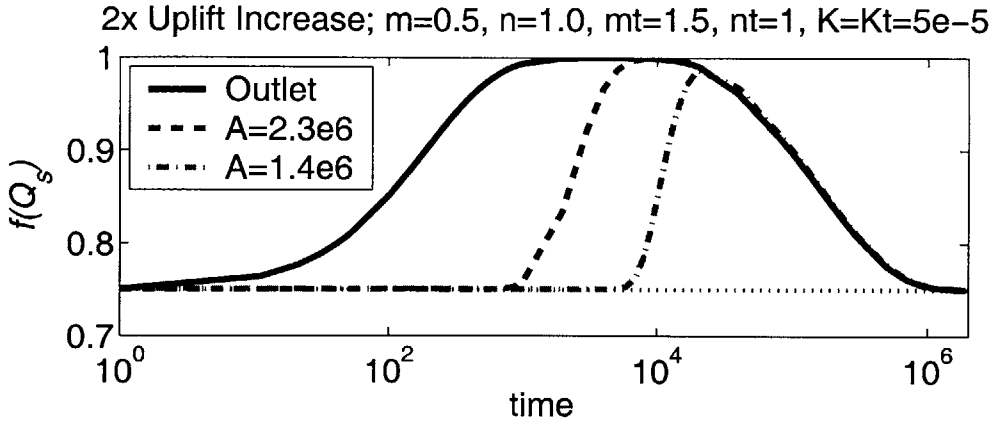

(B)

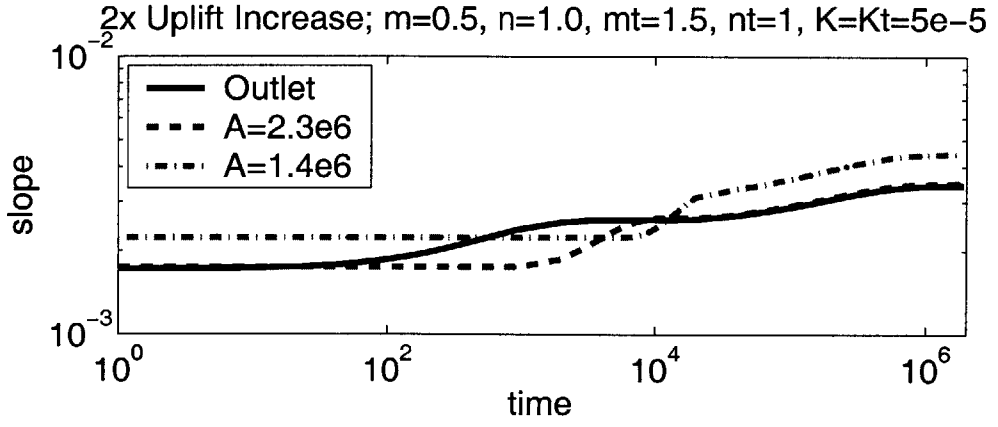

(C)

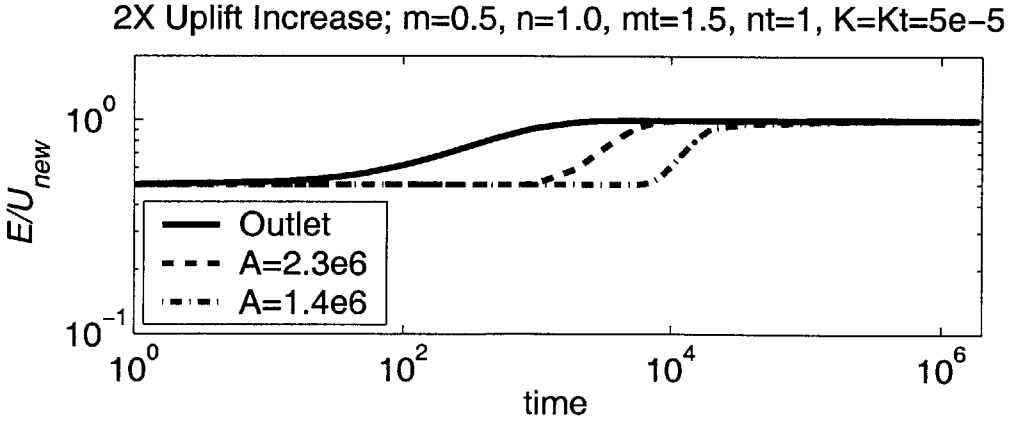

Figure 5-23: Response over time of $f(Q_s)_t$ (A) channel slope (B) and erosion ratio (C) at three different points in response to a two-fold increase in uplift rate using the almost-parabolic model.

(A)

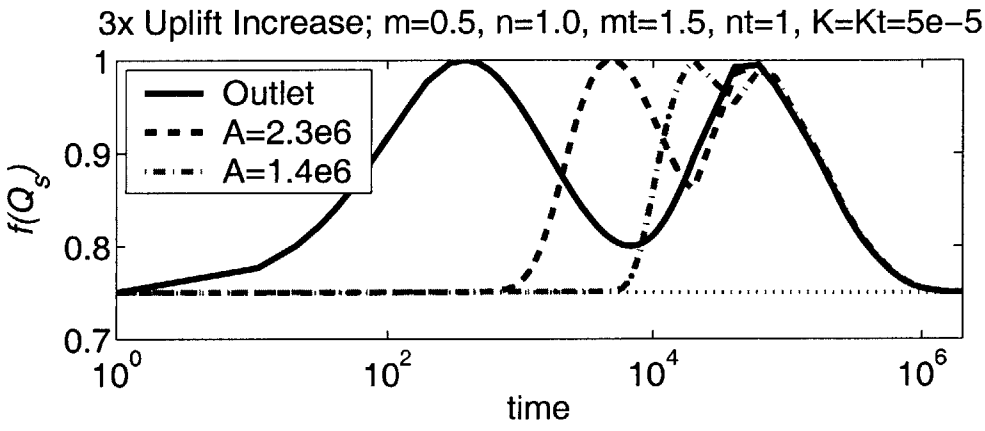

(B)

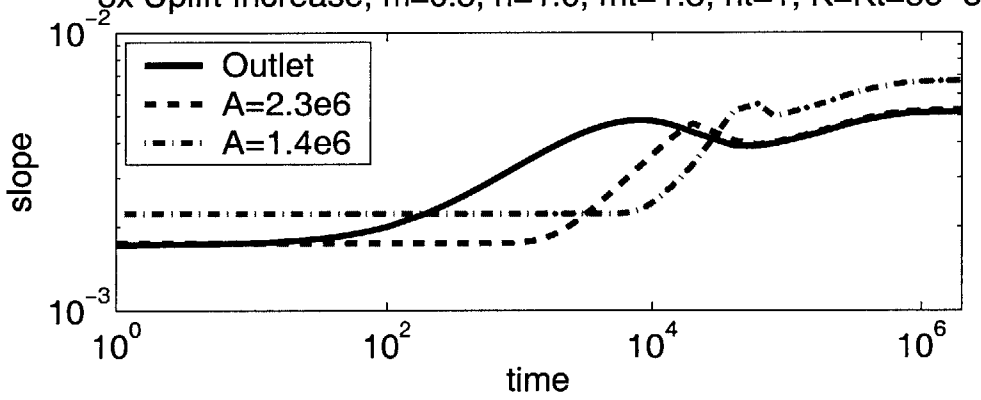

(C)

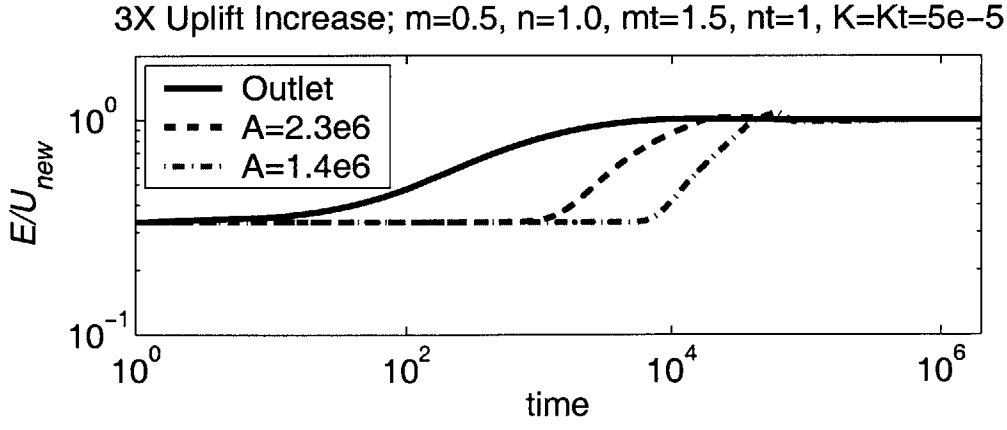

Figure 5-24: Response over time of $f(Q_s)_t$ (A) channel slope (B) and erosion ratio (C) at three different points in response to a three-fold increase in uplift rate using the almost-parabolic model.

Changes in $f(Q_s)$ through time at the outlet and two points upstream are illustrated in figure 5-25A. As slope increases at the outlet through time (figure 5-25B) $f(Q_s)$ rises and then falls (figure 5-25A) as the value of $\frac{Q_s}{Q_c}$ is steadily decreasing (not illustrated). This initial rise and fall in $f(Q_s)$ is the pushing over the hump in figure 5-22. Once the upper parts of the network start to respond and the sediment-flux starts to increase, erosion rates rise above their new equilibrium value (figure 5-25C) and slopes begin to decrease.

The pattern is similar in upstream points. Changes in $f(Q_s)$ are dampened at the upstream points. Because $f(Q_s)$ does not drop as low in the upstream points, but the slopes still increase, this allows for the erosion ratio to vary more than it does at the outlet. There is some loss of information upstream. The outlet point and points near to the outlet feel the boundary condition more closely and are more tied to it, while points higher upstream feel the change later. Upstream points are not bounded to immediately adjust their slopes to erode at U_{new}, and therefore a lag in information sent upstream or misinformation through the over-shooting of slopes, leads to more freedom in the transient erosion rates upstream.

As stated earlier, when the equilibrium value of $\frac{Q_s}{Q_c} \leq 0.5$, an increase in uplift rate will always result in an initial decrease in $f(Q_s)$ (starting at the top of the hump, or to the left of it, in figure 5-22). We performed a number of numerical experiments where the initial and final values of $\frac{Q_s}{Q_c}$ are less than 0.5 (not illustrated), and the slopes always over-steepened, regardless of the magnitude of increase in uplift rate.

We illustrate one more transient example. In this last case, we increase the uplift rate five times, using parameter values of $mt = 1.5$ and $n = 2$ (versus $n = 1$ in the previous examples). With these parameters, in equilibrium $f(Q_s)$ does not vary in space, but its equilibrium value increases with uplift rate. The initial knickpoint response is more pronounced in this example (figure 5-26) than it was for the previous example with an uplift increase of 4x and $n = 1$. In this example, slopes over-steepen and remain over-steepened (instead of quickly dropping) as the knickpoint passes up the network; this response looks deceptively similar to a stream-power response. The main difference here is that the slopes have over-steepened above their new

(A)

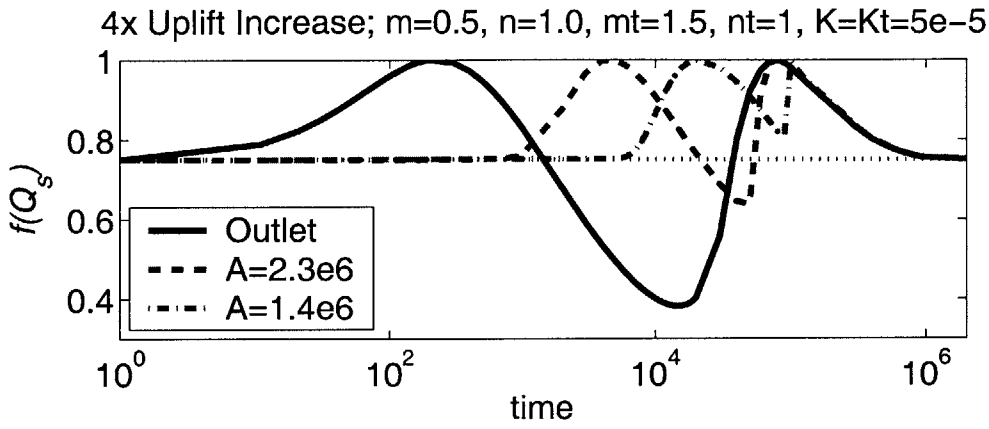

(B)

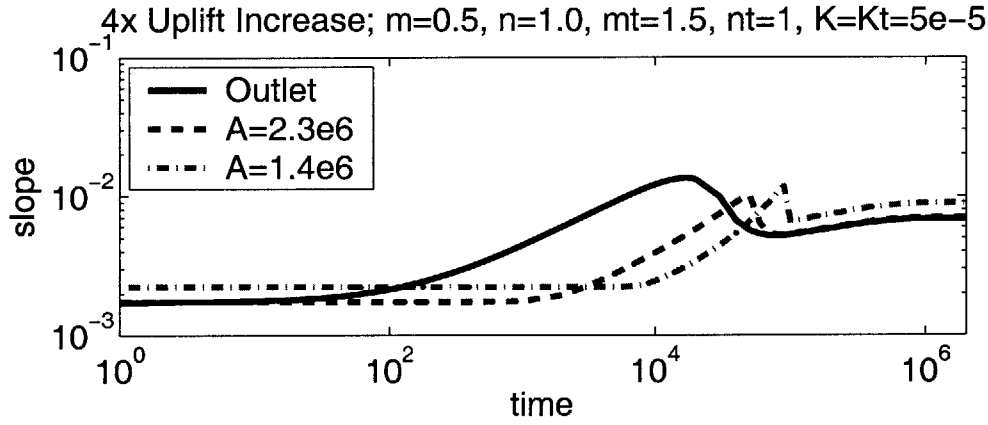

(C)

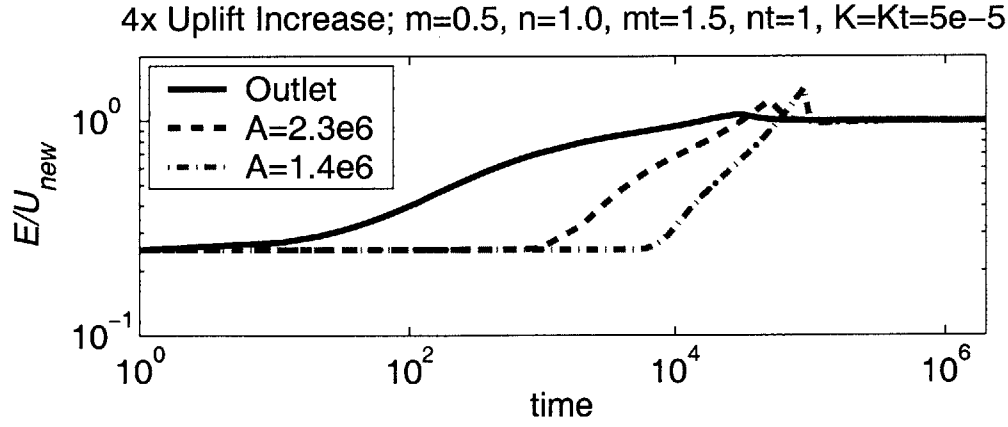

Figure 5-25: Response over time of $f(Q_s)_t$ (A) channel slope (B) and erosion ratio (C) at three different points in response to a four-fold increase in uplift rate using the almost-parabolic model.

equilibrium values. Eventually, slopes need to be reduced, and this begins to happen while slopes are still steepening in the upper reaches of the network (figure 5-27). There is a transient period during which there is no longer evidence of a knickpoint in the profiles or in the slope-area data, and on first glance, it might be difficult to detect that these are temporary conditions (dash-dot and dotted lines in figure 5-27A and B). The dash-dot line in figure 5-27B has a concavity of 0.64. This isn't much greater than the equilibrium value of 0.5 but worth noting.

This example turns out to be very dramatic. First slopes over-steepen above their new equilibrium value (figure 5-26B) then they under-steepen (figure 5-27B) and then they over-shoot again (figure 5-28B). This oscillatory behavior is the result of a single increase in uplift rate. As erosion rates respond at different times throughout the network (figure 5-30B), the sediment flux sent downstream both increases and decreases in time (figure 5-30A). At a point, changes in slope are always in phase with changes in $f(Q_s)$ (figure 5-29), however $f(Q_s)$ is not uniformly increasing and decreasing throughout the network, leading to the very complex response in erosion rates and sediment loads.

Erosion rates at the outlet rise to the new equilibrium value and remain stable (figure 5-30B). The outlet is always able to adjust its slope to accommodate the incoming sediment flux and maintain the new higher erosion rate. However, points upstream from the outlet do not instantly adjust and their erosion rate varies more (figure 5-30B). Note that peaks in sediment flux at different points are just barely off in time in this example (figure 5-30A), but this lag in response is able to produce very complex results.

Tucker and Whipple (2002) also point out that the transient response is highly dependent on the value of n using the stream-power model, which controls the dependence on slope of the speed of an erosion wave through the network. This certainly contributes to some of the differences in response between the two examples with the almost-parabolic model using $n = 1$ and $n = 2$. However, the dependence on sediment flux adds further complication.

Many more numerical experiments were performed than could be presented here.

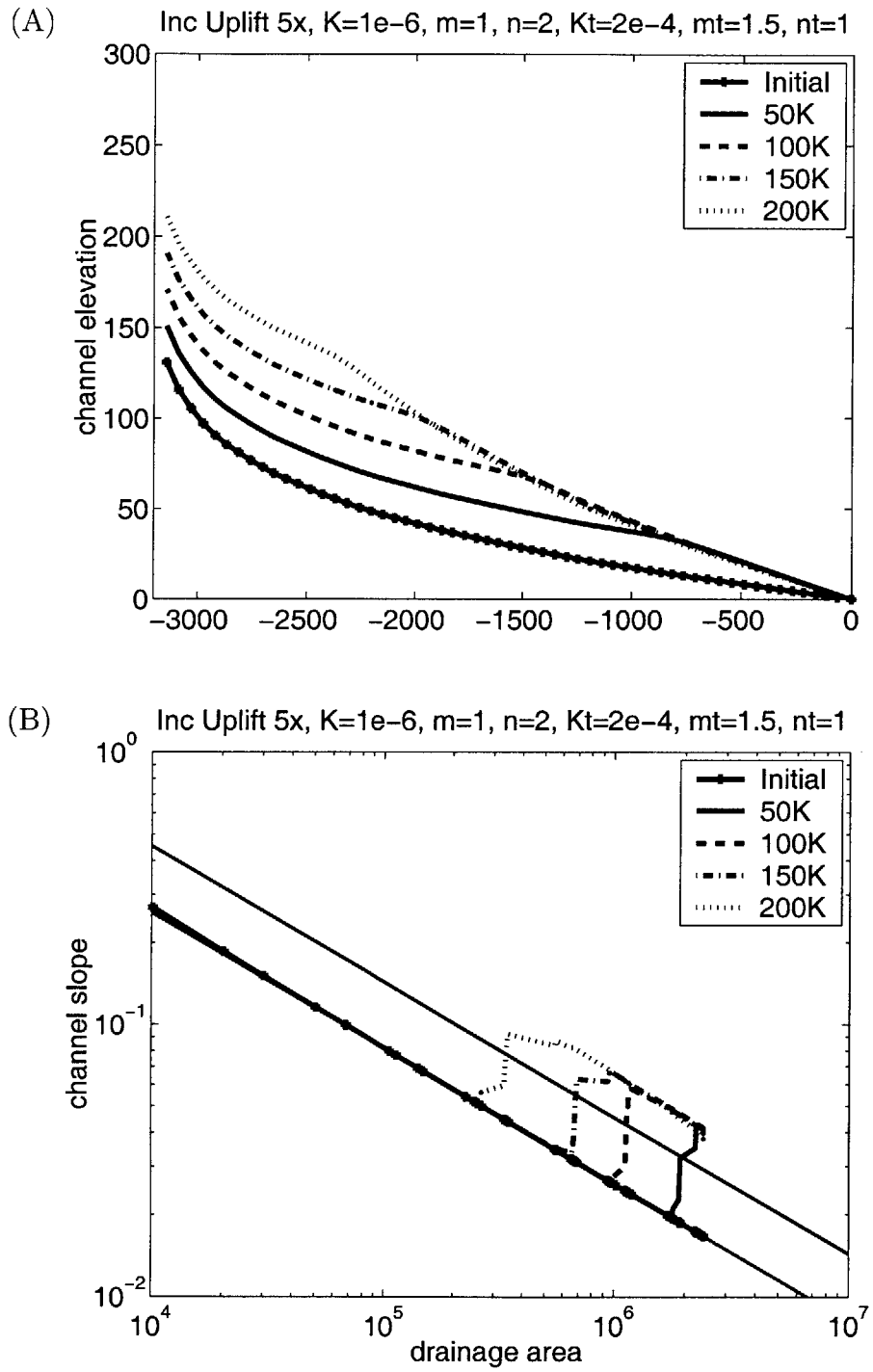

Figure 5-26: Using almost-parabolic model, change in main channel profile (A) and channel slope (B) in response to a 5x increase in uplift rate ($n = 2$). (The lines running through the slope-area plot are the equilibrium relationships for old (lower) and new (upper) uplift rates.)

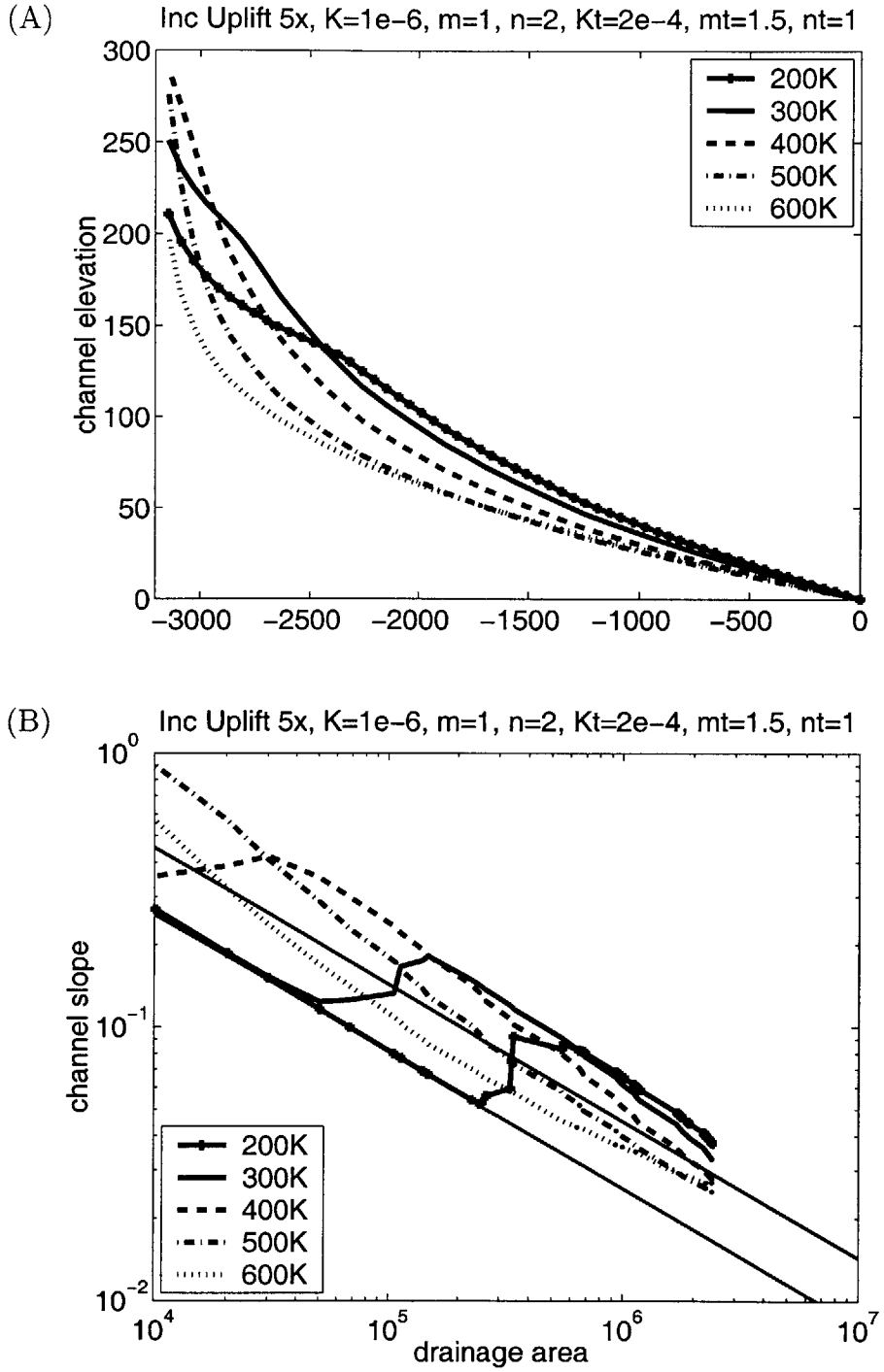

Figure 5-27: Using almost-parabolic model, later response in main channel profile (A) and channel slope (B) in response to a 5x increase in uplift rate ($n = 2$). (The lines running through the slope-area plot are the equilibrium relationships for old (lower) and new (upper) uplift rates.)

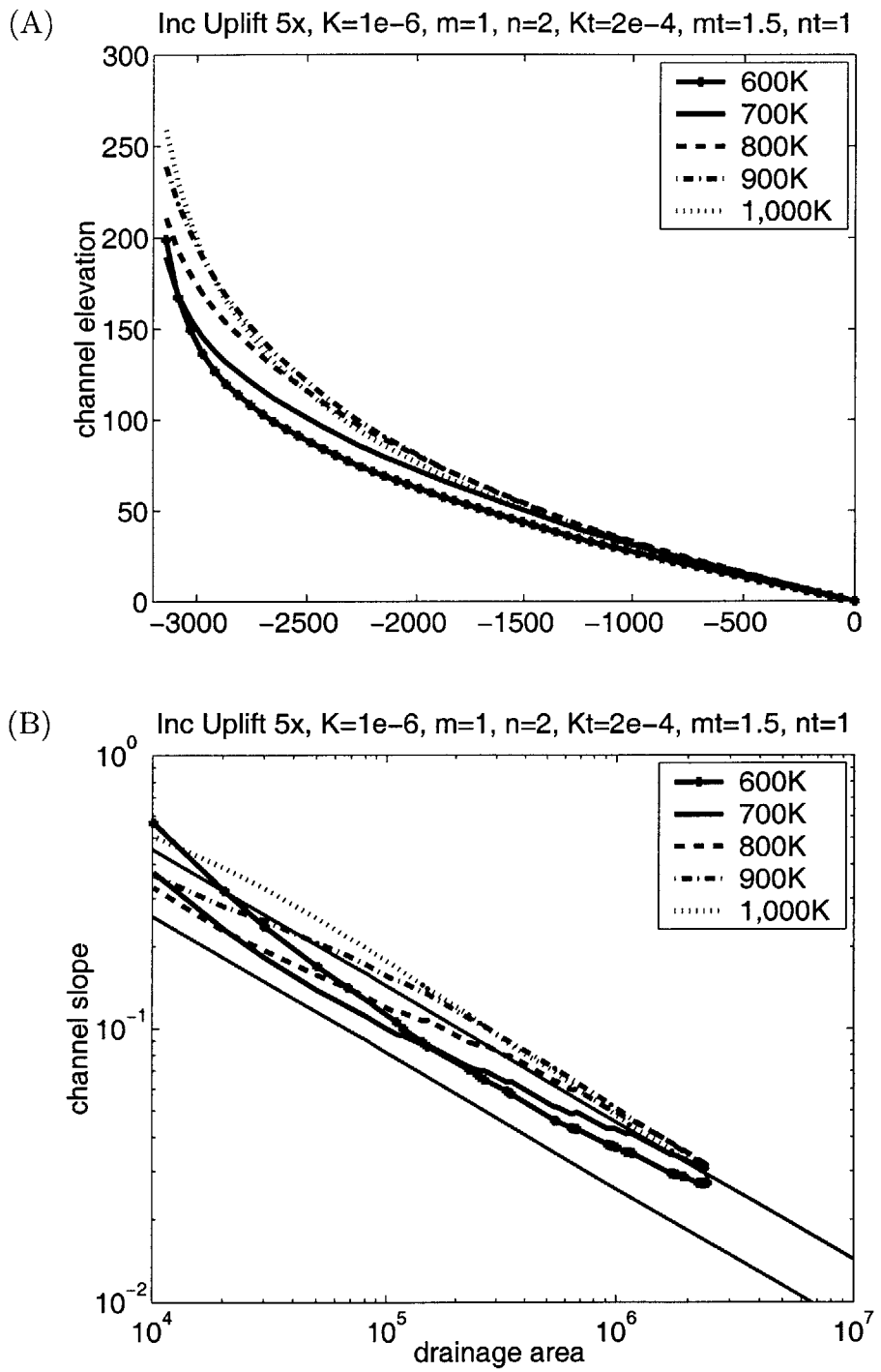

Figure 5-28: Using almost-parabolic model, even later response in main channel profile (A) and channel slope (B) in response to a 5x increase in uplift rate ($n = 2$). (The lines running through the slope-area plot are the equilibrium relationships for old (lower) and new (upper) uplift rates.)

(A)

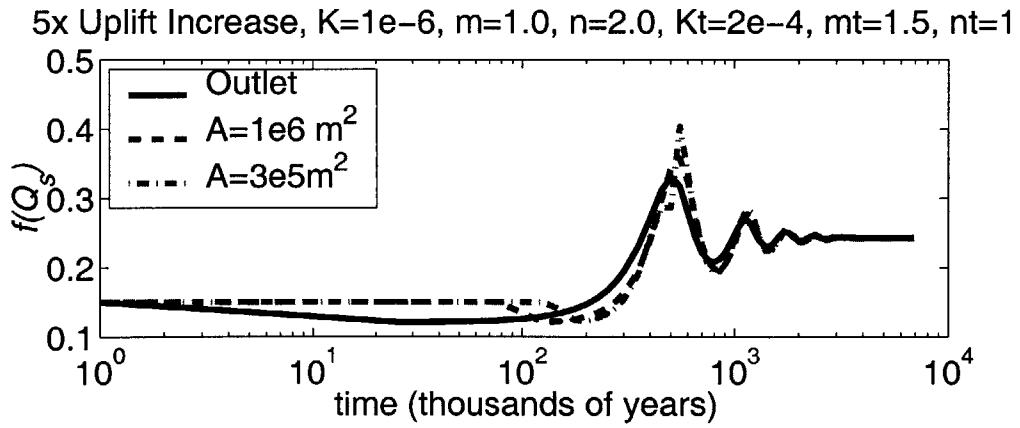

(B)

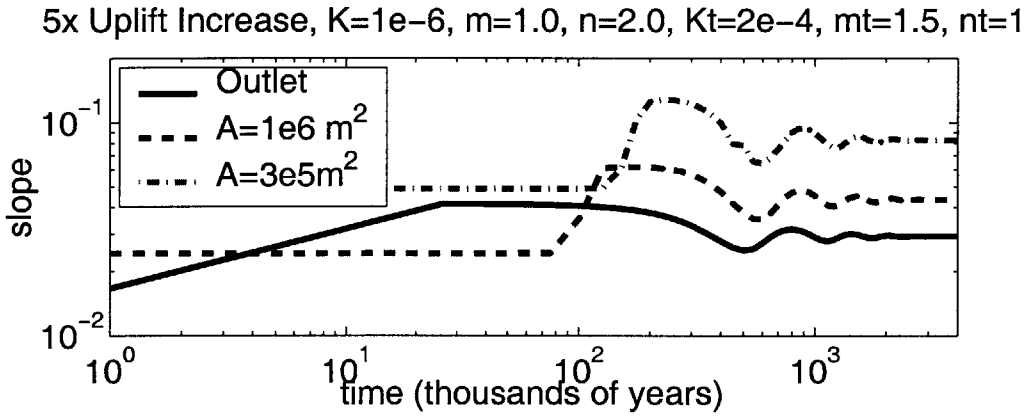

Figure 5-29: Response over time of $f(Q_s)_t$ (A) and channel slope (B) at three different points in response to a five-fold increase in uplift rate using the almost-parabolic model and $n = 2$.

(A)

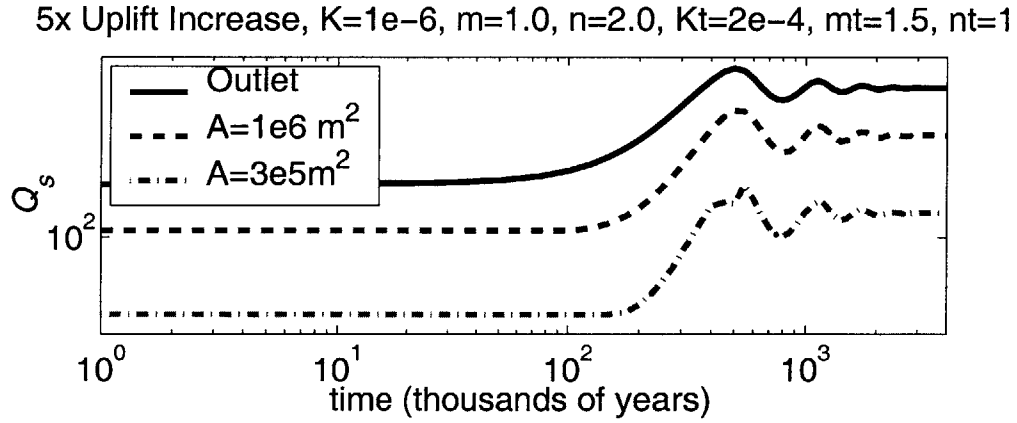

(B)

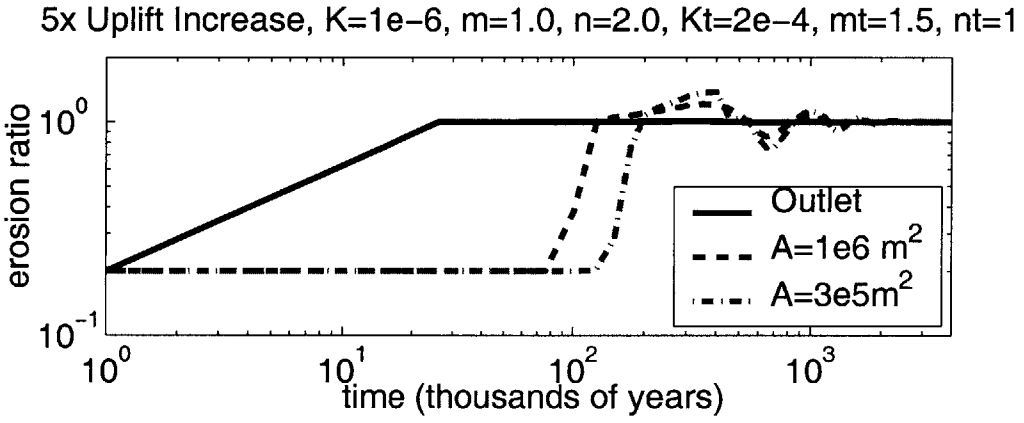

Figure 5-30: Response over time of Q_s (A) and erosion rate (B) at three different points in response to a five-fold increase in uplift rate using the almost-parabolic model and $n = 2$.

We have explored network response to both increases and decreases in uplift rate over a wide range of parameter space. The details of the response obviously differ, but the examples in this section capture all of the most interesting patterns that we observe in transient networks using the almost-parabolic model. We do not show any illustrations of network response to a decrease in uplift rate. The results are similar but opposite in direction.

5.5 Transient Behavior using the Linear-Decline Model

In this section, we discuss an example of channel network response to an increase in uplift rate using the linear-decline sediment flux erosion model. Changes in uplift rate are felt first at the outlet and then propagate upstream (in a similar fashion to the almost-parabolic model and stream-power model). The linear-decline model does not predict over-steepening of channel slopes during transitions from a low to high uplift rate.

Figure 5-31 illustrates the initial response in main channel elevations (A) and slopes (B) in response to a five-fold increase in uplift rate. Initially a knickpoint sweeps upstream. However, channel slopes increase to a value less than their new equilibrium value (figure 5-31B). Once the knickpoint passes a point, channel elevations still continue to rise. This leads to a later response in which slopes are rising everywhere throughout the network (figure 5-32). This combination-type response is similar to the two-fold uplift increase example using the almost-parabolic model and the mixed-channel response of threshold channels described by Whipple and Tucker (2002). The response illustrated in figures 5-31 and 5-32 is also due to the lag in sediment flux.

As was the case with the almost-parabolic model, the sediment flux at the outlet can be assumed to stay constant while channel slope rises to accommodate for the increase in uplift rate. Given that the channel slope rises but sediment flux remains the same, the value of $\frac{Q_s}{Q_c}$ declines in response to an increase in uplift rate. With

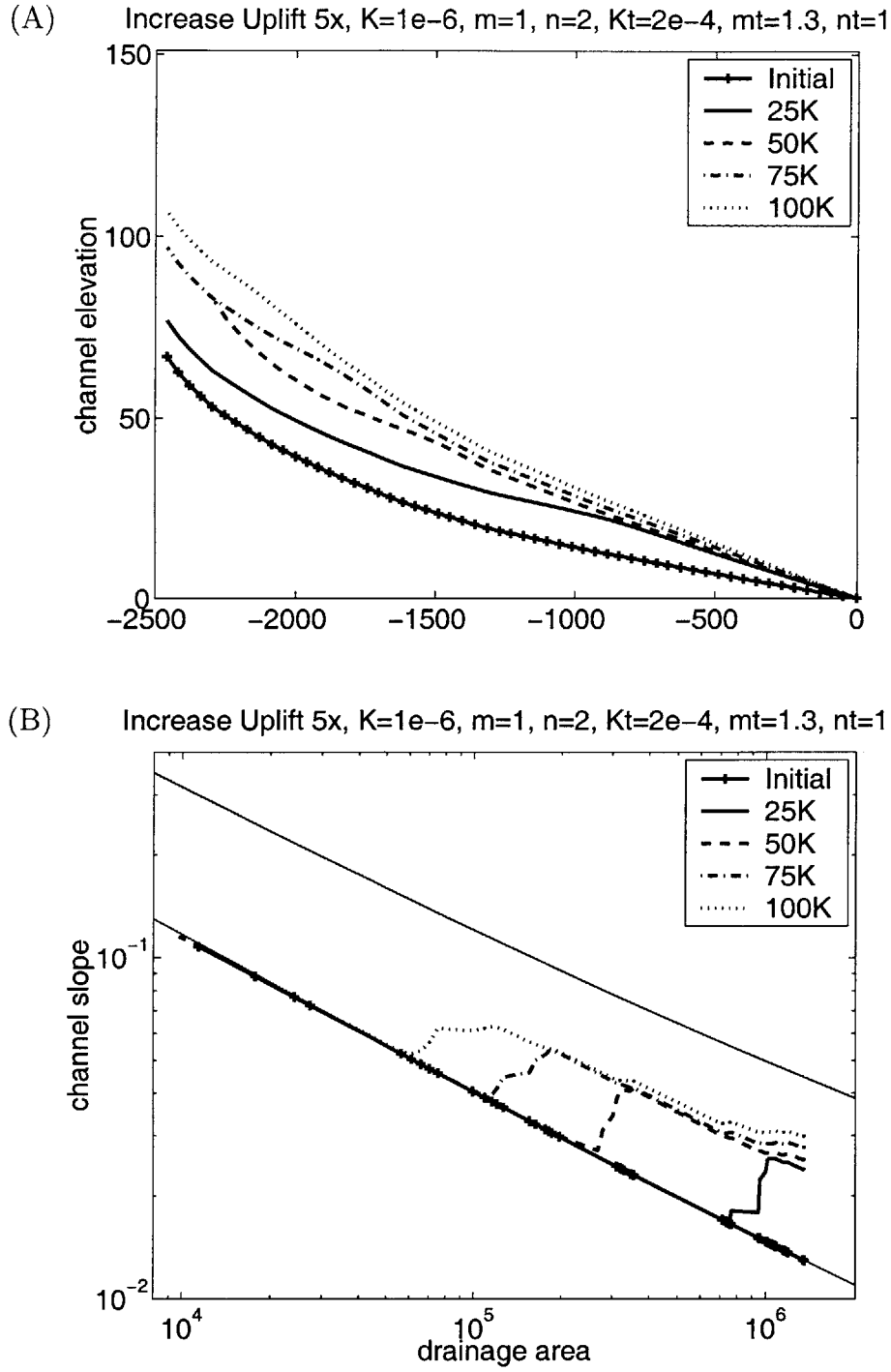

Figure 5-31: Using linear-decline erosion rule, change in main channel profile (A) and channel slope (B) in response to a 5x increase in uplift rate. (The lines running through the slope-area plot are the equilibrium relationships for old (lower) and new (upper) uplift rates.) The temporary shortening of the profile ant 50K is due to network rearrangement.

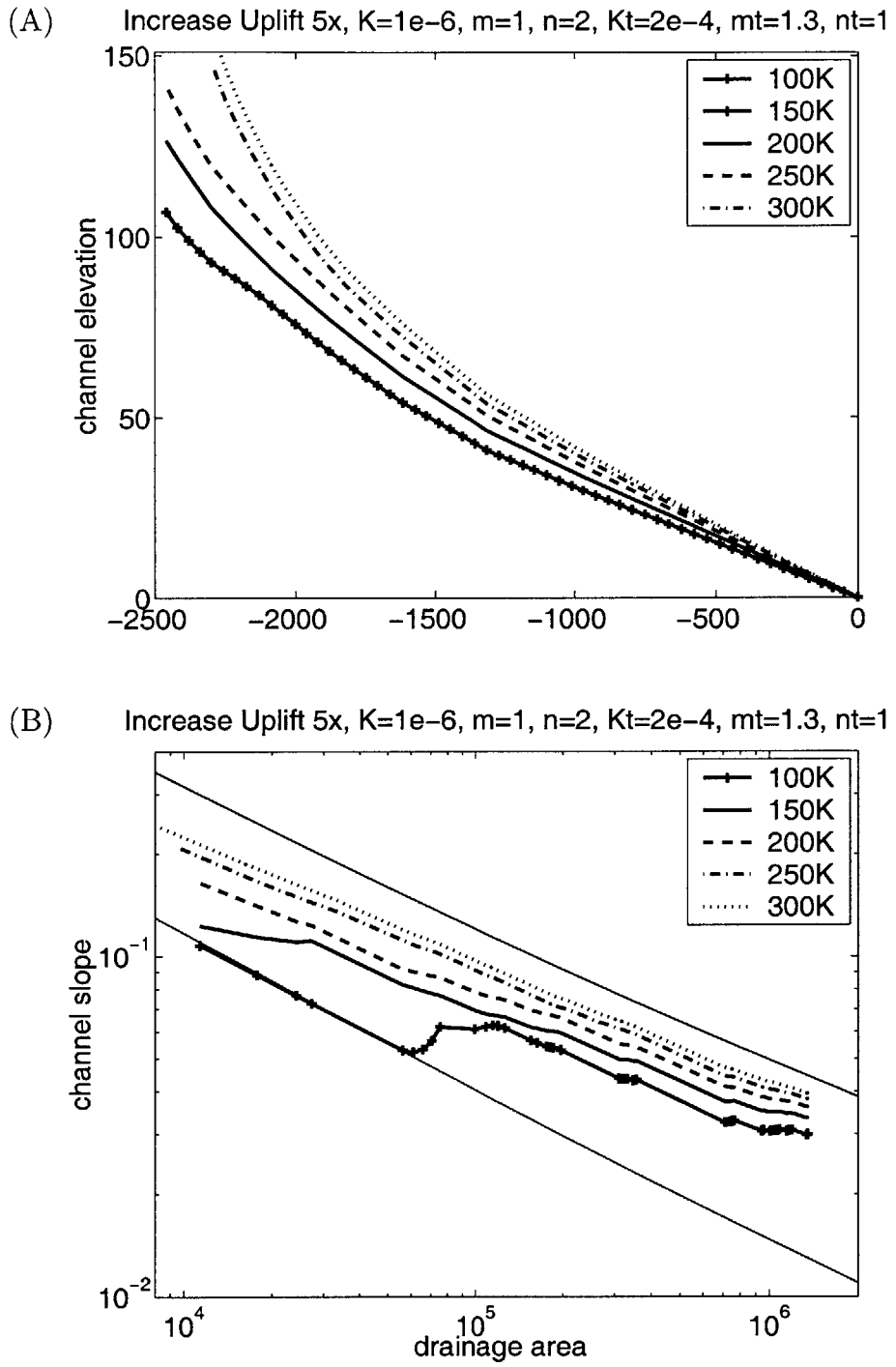

Figure 5-32: Using linear-decline erosion rule, change in main channel profile (A) and channel slope (B) in response to a 5x increase in uplift rate (later time from previous figure). (The lines running through the slope-area plot are the equilibrium relationships for old (lower) and new (upper) uplift rates.)

the linear-decline model, $f(Q_s)$ has nowhere to go but up as $\frac{Q_s}{Q_c}$ declines (figure 5-2 and equation 5.15), so we don't expect channel slopes to ever overshoot their new equilibrium value.

The increase in $f(Q_s)$ at the outlet (and two other points upstream) is shown in figure 5-33A. Channel slopes increase (figure 5-33B) while sediment load remains the same (not shown), causing $f(Q_s)$ to rise (figure 5-33A). Once the sediment load starts to respond, $f(Q_s)$ starts to decline and slopes continue to rise. As illustrated by figure 5-33 the response at upstream points lags the response at the outlet. The points upstream from the outlet adjust more freely than the outlet does, and erosion rates vary more upstream (figure 5-33C). The dash-dot line in figure 5-33 illustrates that for a very short period (approximately 50K-70K years) $f(Q_s)$ declines while channel slope does not keep pace, causing erosion rates to slightly decrease.

5.6 Transient Behavior using the Wear Model

We performed a series of experiments testing the sensitivity of the wear erosion rule (equation 5.19) to changes in uplift rate. This erosion rule predicts that when $Q_s = 0$ the erosion rate will be zero. This causes a boundary condition problem for points which only drain themselves. (Normally these points would be hillslopes, but we are not modeling hillslope processes here.) To avoid boundary condition problems, at points with no upstream neighbors the erosion rate is always calculated assuming transport-limited conditions. (These points have a sediment influx of zero.)

The initial response to a 5-fold increase in uplift rate using the wear model is illustrated in figure 5-34. There is some steepening at the outlet while the upper-most slopes remain the same, but it is not solely a local steepening, as with a knickpoint. During the later transient response (figure 5-35), slopes are increasing almost uniformly throughout the network and the profile is relatively smooth. These conditions could easily be mistaken for equilibrium. Interestingly, the concavity of the network is reduced during the transient in comparison with the old and new equilibrium values ($\theta = 0.41$ during the transient and $\theta = 0.55$ in equilibrium, for the region shown).

(A)

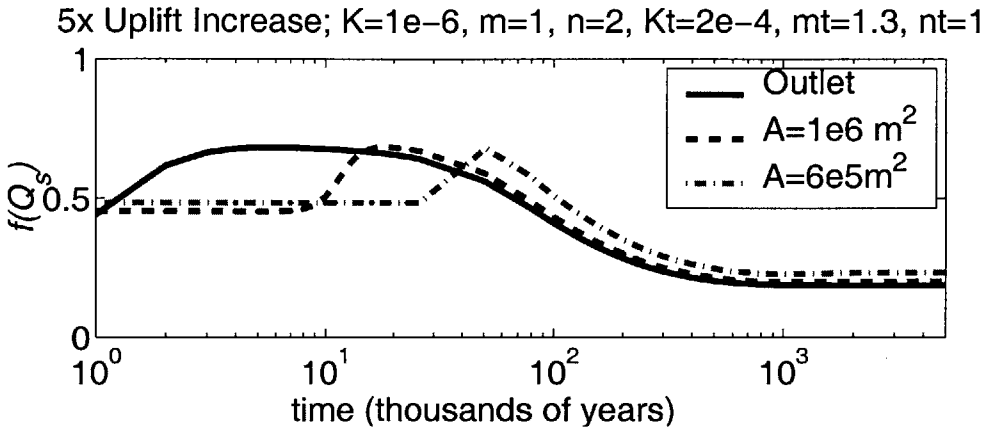

(B)

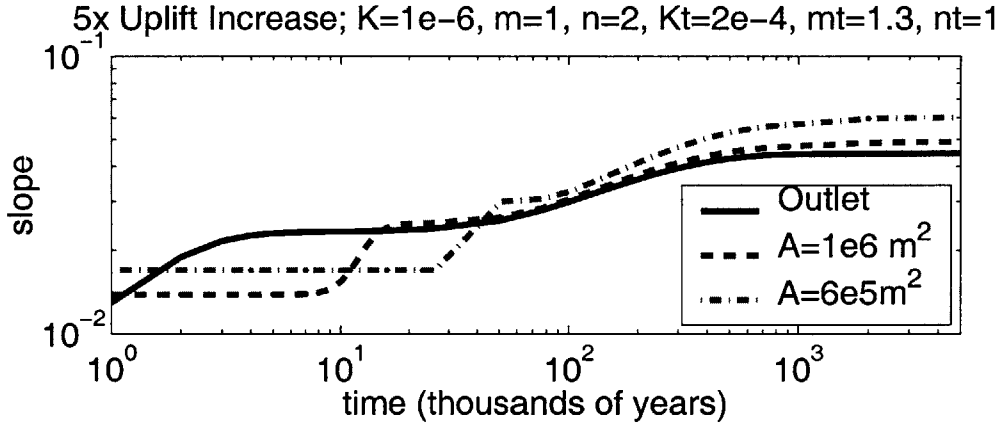

(C)

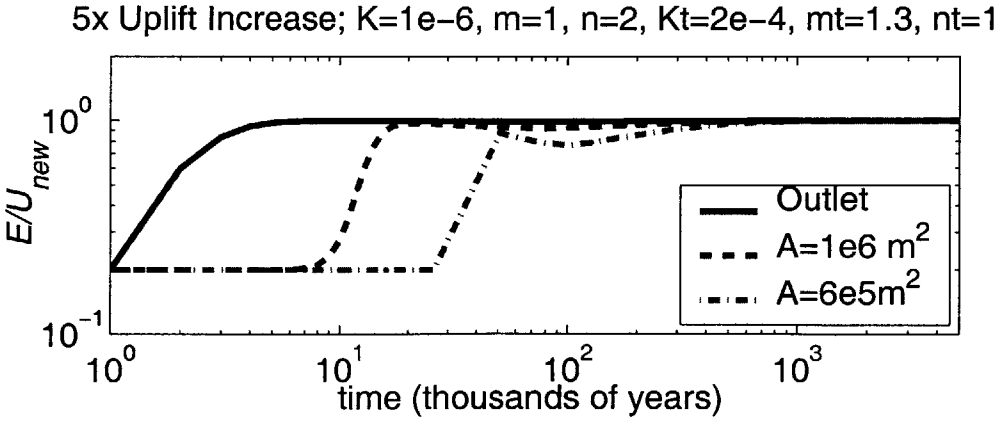

Figure 5-33: Response over time of $f(Q_s)_t$ (A) channel slope (B) and erosion ratio (C) at three different points in response to a five-fold increase in uplift rate using the linear-decline model.

Note that slopes in the small drainage areas deviate from the predicted equilibrium value initially (figure 5-34); this is due to the boundary condition that $Q_s = 0$, causing these points to be transport-limited, and therefore follow a different model.

Figure 5-36 illustrates the response of sediment load (A) and the ratio of sediment load to transport rate ($\frac{Q_s}{Q_c}$) (B) at three different points through time. Initially, and throughout the response, $\frac{Q_s}{Q_c}$ remains very close to one and slopes are very close to transport-limited slopes. As with the other transient responses explored, the sediment load does not respond immediately to the change in uplift rate, although the outlet does immediately adjust its erosion rate to the new uplift rate (figure 5-37A) by adjusting its slope (figure 5-37B). Slopes at the outlet, and throughout the network, continue to rise as the sediment load adjusts. In this example, the value of $\frac{Q_s}{Q_c}$ decreases and increases (figure 5-36B), but channel slopes and erosion rates (figure 5-37A and B) only increase.

We can derive an expression for the predicted transient response in slope at the outlet to see if any over-steepening of slopes will occur using the wear model. Assuming that the sediment load into the outlet does not change and that initially only slopes adjust to an increase in uplift rate (which seems reasonable given figure 5-36A), the following transient slopes are predicted:

$$S_t = \left(\frac{U_{old}}{K_t}\right)^{\frac{1}{nt}} A^{\frac{1-mt}{nt}} \left(1 - \frac{U_{new}}{U_{old}K} A^{-0.5}\right)^{\frac{-1}{nt}} . \tag{5.29}$$

Comparing this equation with the equilibrium slope-area equation for the wear rule (equation 5.20) we can calculate the ratio of the transient slope to the new equilibrium slope ($\frac{S_t}{S_{new}}$). When $\frac{S_t}{S_{new}} > 1$, we predict that transient slopes will over-steepen. The factor of increase in uplift rate to produce over-steepening depends on (1) U_{old} (2) K and (3) drainage area at the outlet. The over-steepening effect does not depend on either mt or K_t. As noted in the discussion of the equilibrium behavior of the wear model, there is a limited range of reasonable K values using this model, so there is a limit in the range of parameters we could reasonably investigate. Given the size of the simulated drainage networks (basin drainage area in these simulations is $2.4x10^6 m^2$),

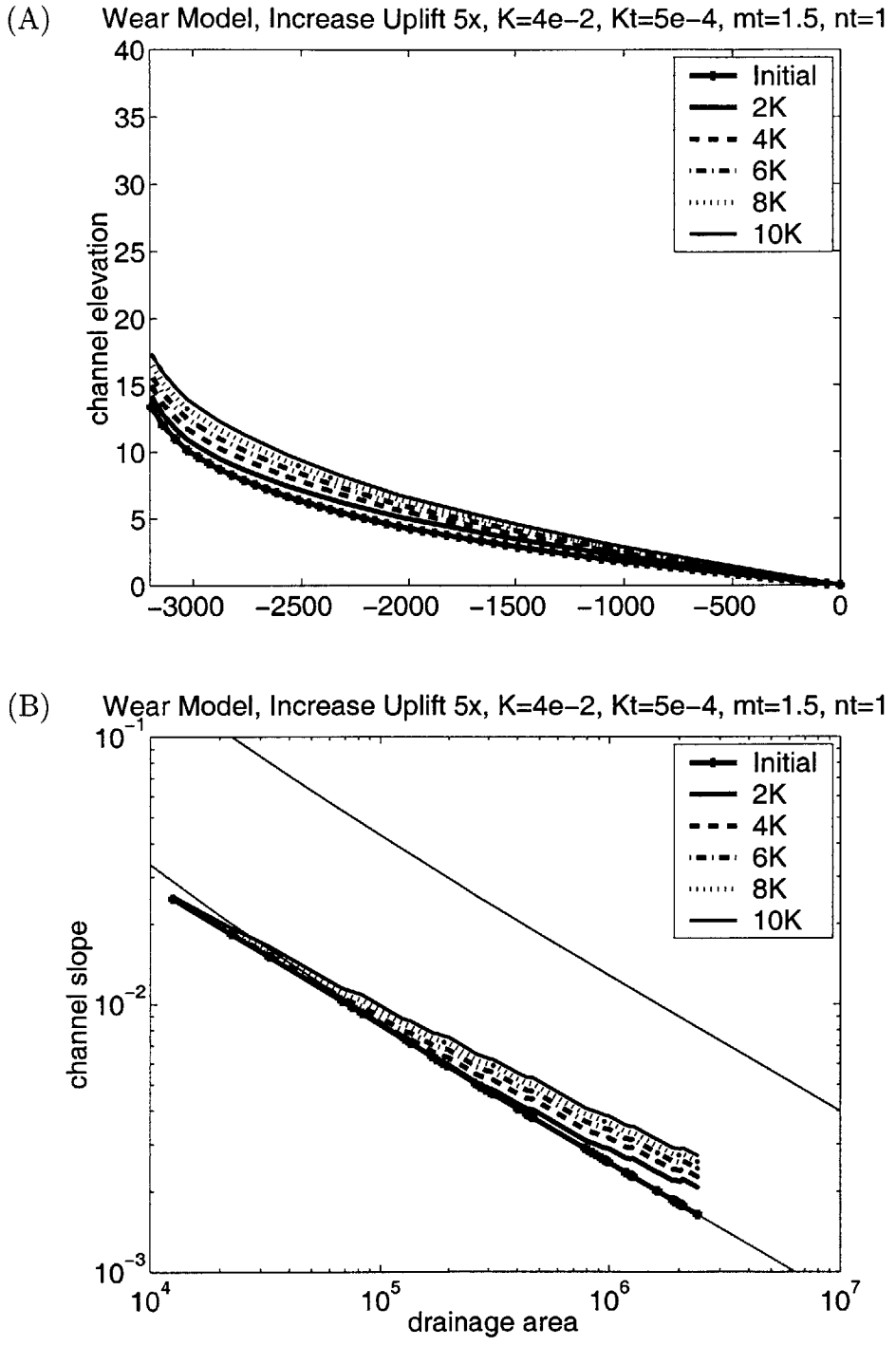

Figure 5-34: Using the wear model, change in main channel profile (A) and channel slope (B) in response to a 5x increase in uplift rate. The thin lines running through the slope-area plot are the old (lower) and new (upper) equilibrium solutions.

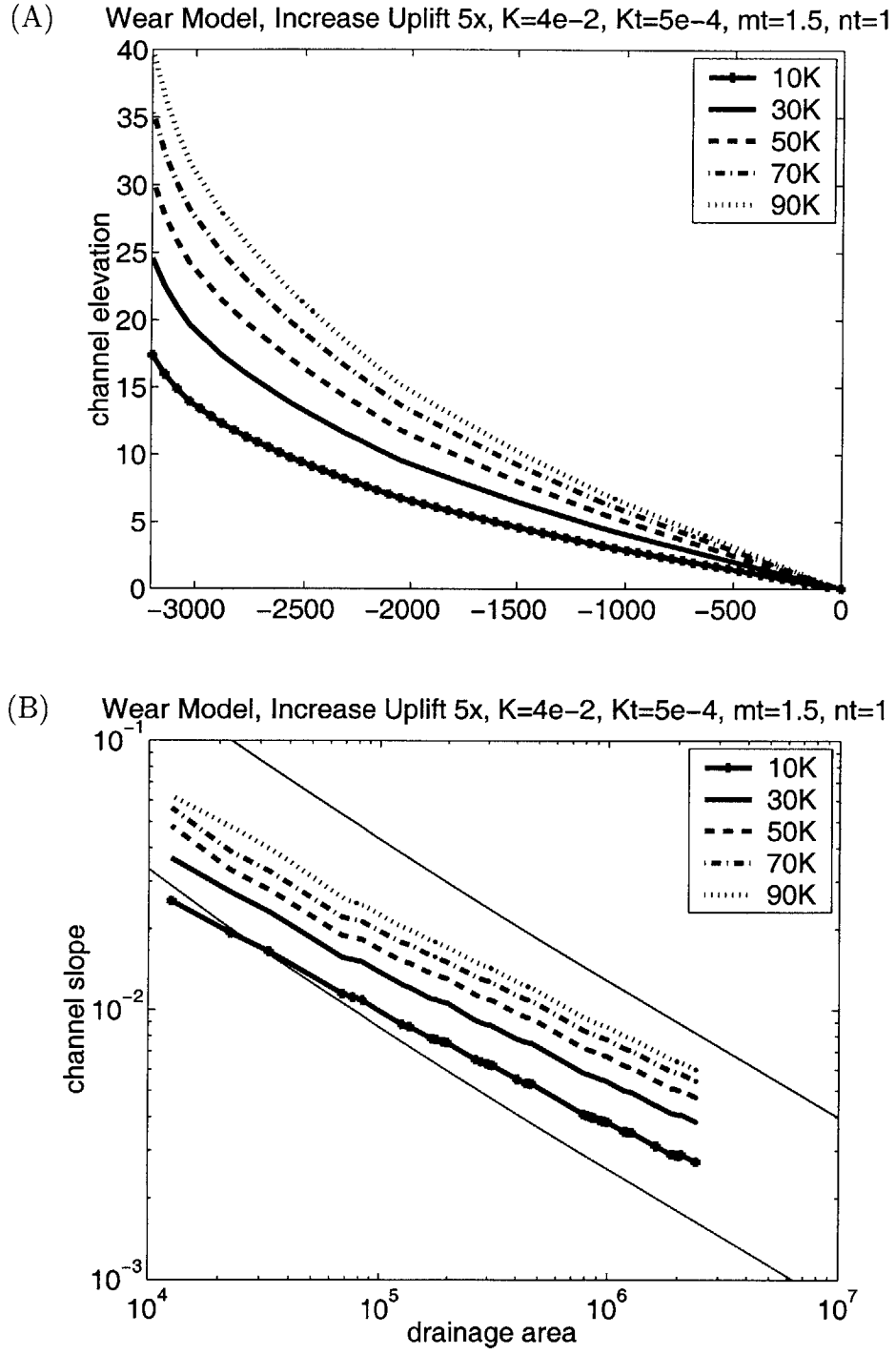

Figure 5-35: Using the wear model, change in main channel profile (A) and channel slope (B) in response to a 5x increase in uplift rate. The thin lines running through the slope-area plot are the old (lower) and new (upper) equilibrium solutions.

(A)

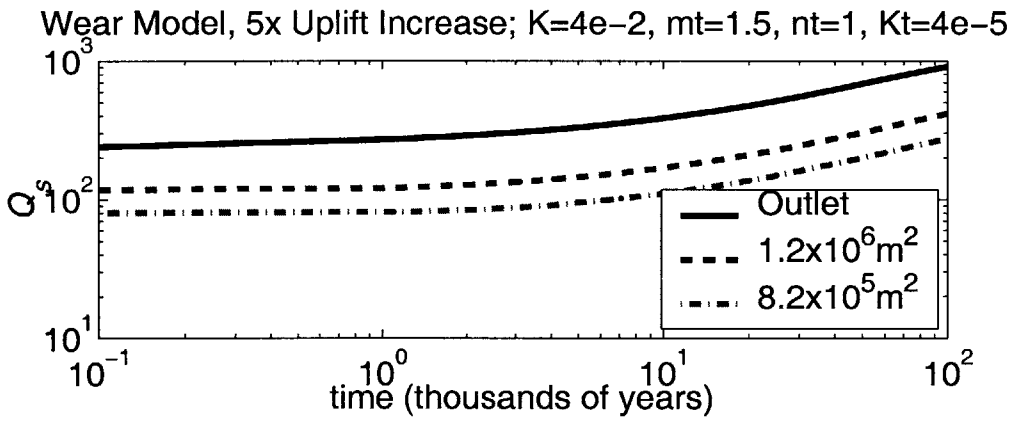

(B)

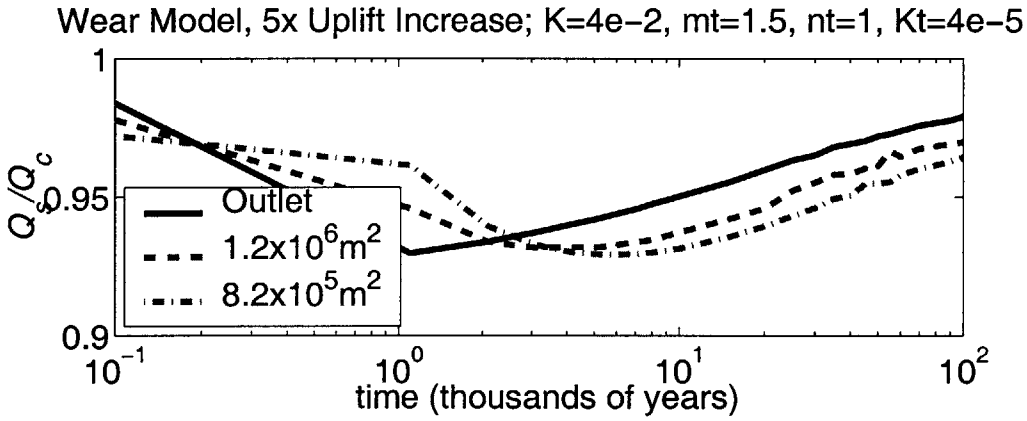

Figure 5-36: Response over time of Q_s (A) and $\frac{Q_s}{Q_c}$ (B) at three different points in response to a five-fold increase in uplift rate using the wear model. (Note that there are no points between 0.1 and 1K years). The initial values are plotted as time=10^{-1}.

(A)

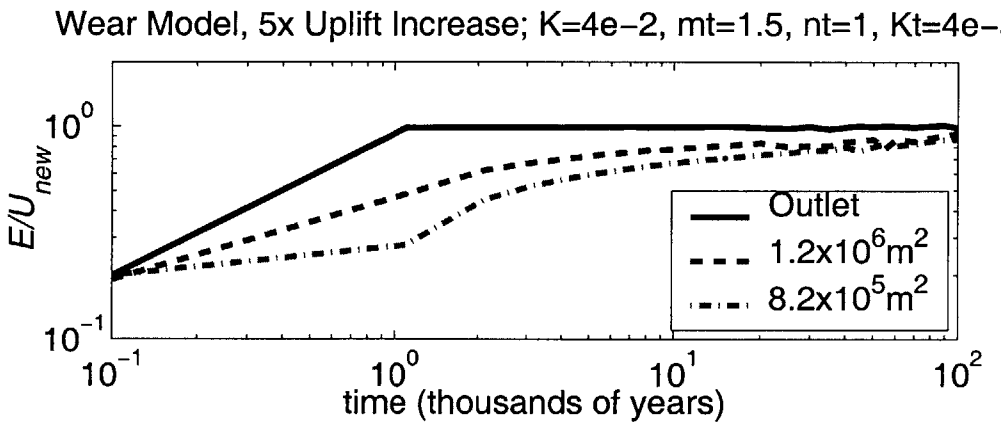

(B)

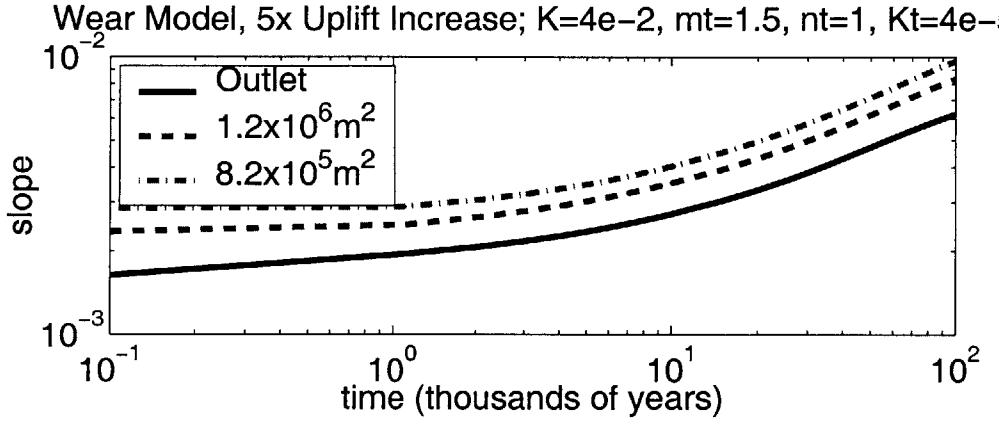

Figure 5-37: Response over time of erosion rate (A) and channel slope (B) at three different points in response to a five-fold increase in uplift rate using the wear rule. (Note that there are no points between 0.1 and 1K years).

the smallest increase in uplift rate to produce over-steepening was a 13-fold increase (using reasonable K values). The required increase in uplift rate to produce over-steepening increases with the drainage area of the network and is almost insensitive to the old uplift rate.

Given the parameters used in the example illustrated in figures 5-34 - 5-37, a predicted over-steepening would require a 55-fold increase in uplift rate. Such an increase is highly unlikely, but we performed the numerical experiment to test the prediction. Using the same parameters as the first example, but this time increasing uplift rate by 60 times (just to be safe) some reduction in slopes does occur. However, the results are not nearly as dramatic as the whiplash-effect produced using the almost-parabolic model.

Figure 5-38 illustrates the initial profile response to a drastic 60x increase in uplift rate. A knickpoint sweeps up the network, increasing slopes to a value less than their new equilibrium value. By 5,000 years, there is some reduction in slopes (roughly between drainage areas of $4x10^5 - 8x10^5 m^2$). However, there is no dramatic decrease in channel elevations - slopes downstream continue to rise. As the channel continues to adjust (figure 5-39) the knickpoint continues to sweep upstream with some lowering of slopes below the knickpoint, and slopes near the outlet continue to rise. The region just below the knickpoint has an increased channel concavity. This behavior continues through time (figure 5-40). After the knickpoint has completely swept through the network, the slopes continue to rise everywhere in the network to their new equilibrium value (transport-limited style).

The pattern of change in Q_s and $\frac{Q_s}{Q_c}$ through time at a point is similar in both the 5-fold (figure 5-36) and 60-fold (not illustrated) uplift increase cases. In the 60x case, $\frac{Q_s}{Q_c}$ decreases more drastically (to values of less than 0.5); both channel slopes and erosion rates increase and decrease, but not nearly as drastically as with the almost-parabolic model.

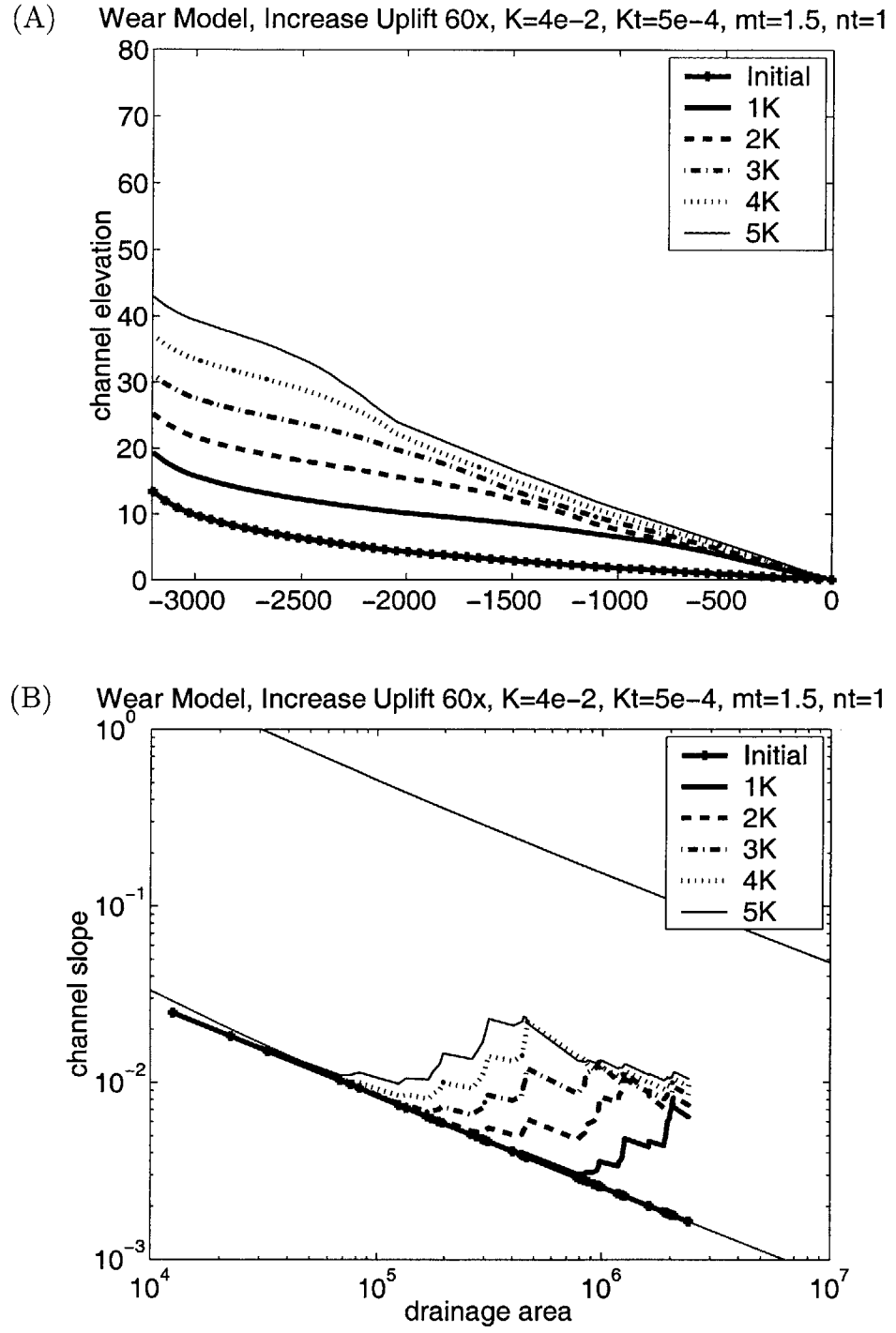

Figure 5-38: Using the wear model, change in main channel profile (A) and channel slope (B) in response to a 60x increase in uplift rate. The thin lines running through the slope-area plot are the old (lower) and new (upper) equilibrium solutions.

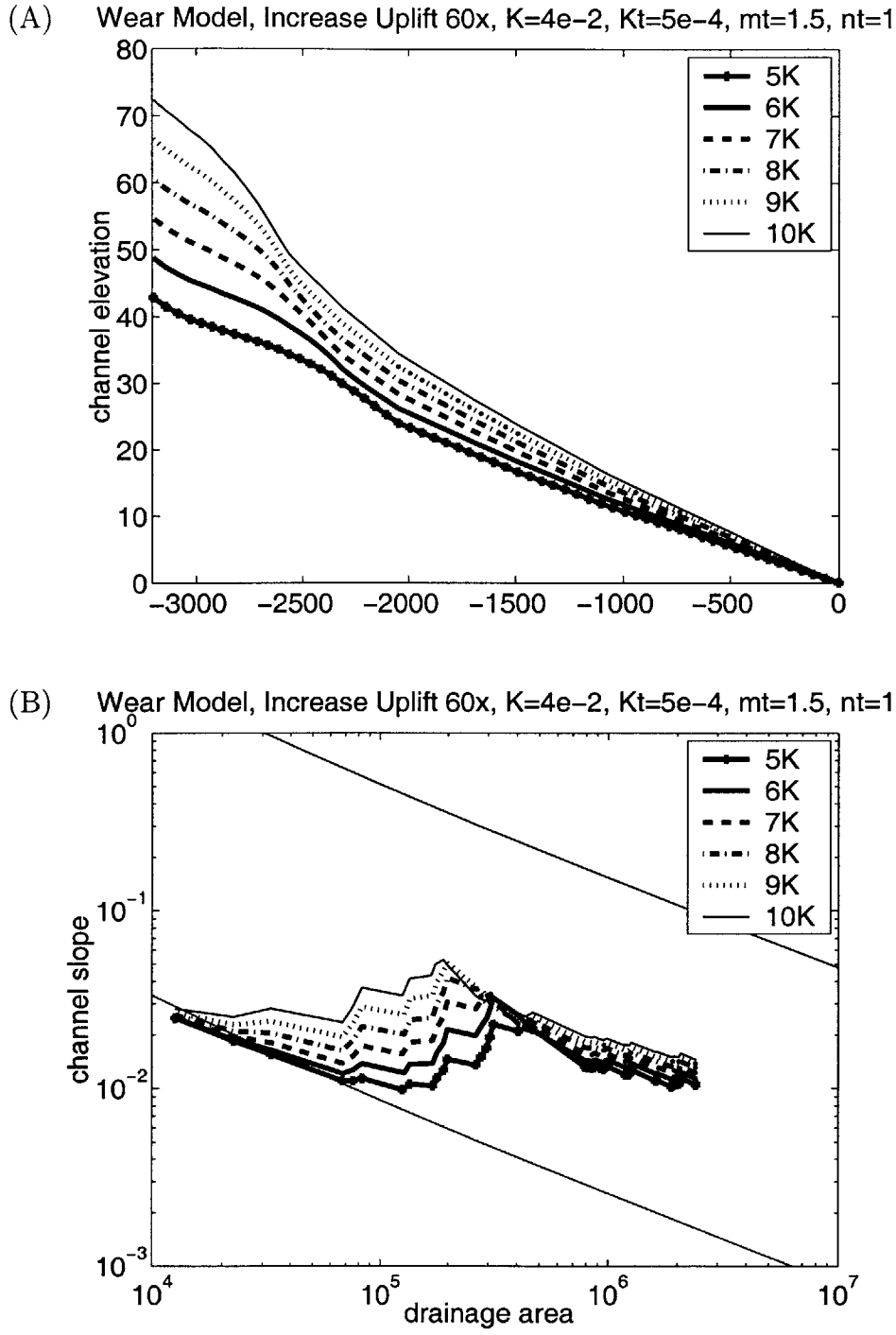

Figure 5-39: Using the wear model, change in main channel profile (A) and channel slope (B) in response to a 60x increase in uplift rate. The thin lines running through the slope-area plot are the old (lower) and new (upper) equilibrium solutions. (Later time from previous plot.)

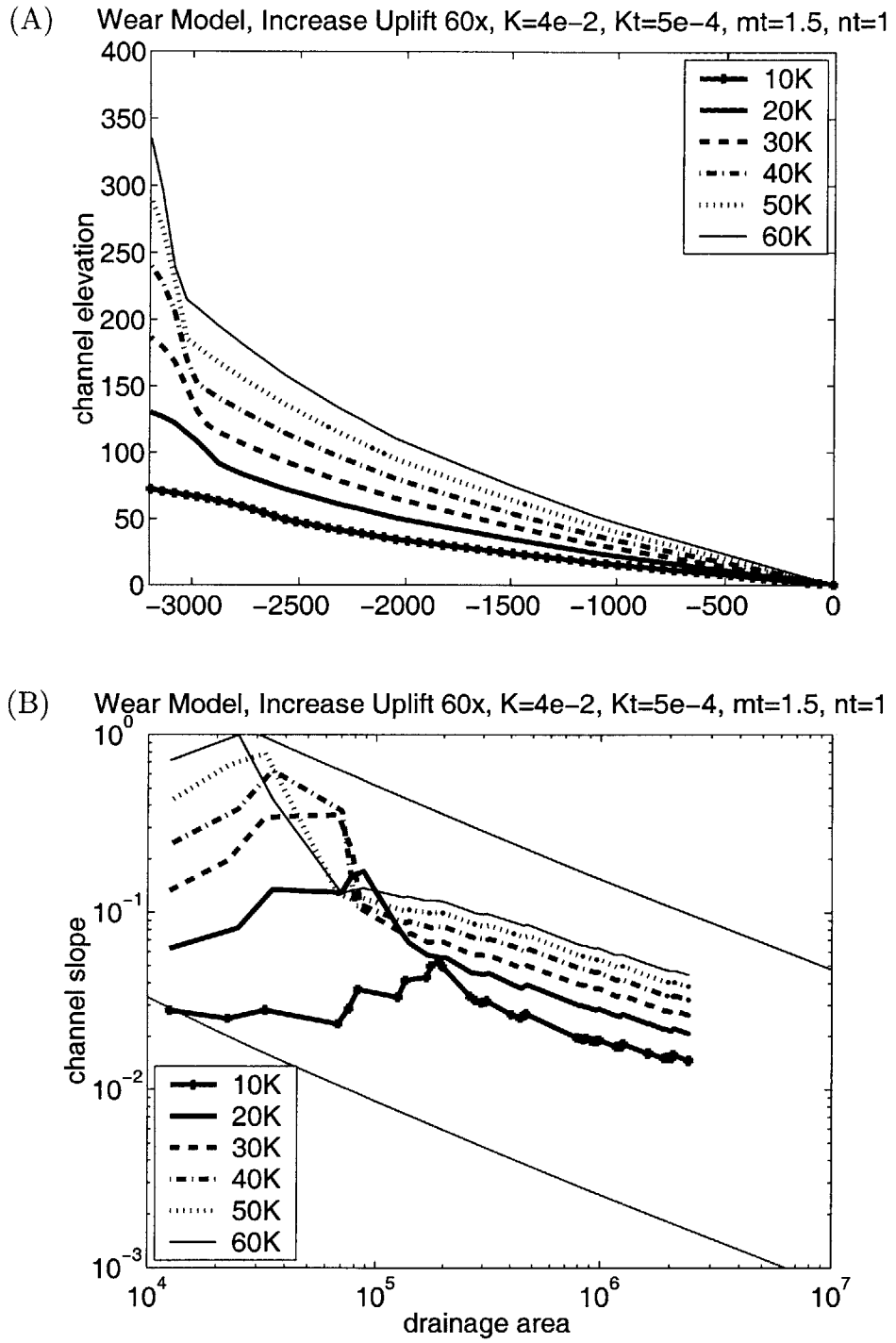

Figure 5-40: Using the wear model, change in main channel profile (A) and channel slope (B) in response to a 60x increase in uplift rate. The thin lines running through the slope-area plot are the old (lower) and new (upper) equilibrium solutions. (Later time from previous plot, note the change in scale on channel elevation plot.)

5.7 Discussion

Equilibrium network morphology is fairly similar with all of the models explored here. Including spatial variations in erodibility (through changes in $f(Q_s)$) results in spatially variable concavity. The variations in concavity are all within the range of those observed in actual rivers and are not very remarkable. However, the influence of sediment flux has some interesting and unexpected controls on equilibrium channel slopes. Using the almost-parabolic model, changes in uplift rate can enhance or dampen changes in equilibrium channel slopes through variations in sediment supply. Furthermore, equilibrium channel slopes may change in unexpected ways to climate when one considers the increased capacity to transport sediment under higher flow conditions.

The sensitivity of equilibrium channel slopes depends significantly on the parameters in the erosion equation. Natural landscapes show significant scatter in these parameters, and they are highly dependent on the model used. For example, Stock and Montgomery (1999) estimated that the value of K in the stream-power model by setting the value of m and n. In streams in Japan and California, K varied by up to two orders of magnitude within a given lithology, and by as much as five orders of magnitude between lithologies. Estimates made in the Oregon Coast Range of the ratio of m/n ranged from 0.8 to 12.9 (Seidl and Dietrich 1992). Snyder et al. (2003b) found that when they considered thresholds and stochastic storms in their erosion model of channels in Northern California, their estimated value of n dropped from 3.8 to 1.

The sensitive equilibrium behavior of the almost-parabolic model indicates that variable erodibility, here modeled through the ratio of sediment flux to sediment transport rate, can have important implications on equilibrium and transient sensitivity. Other variables, such as thresholds and stochastic storms may be as important and add complications that should be considered.

The remarkable transient results using the almost-parabolic model could have important implications when interpreting the landscape. If a channel is cutting ver-

tically as well as laterally, periods of incision can leave behind a strath terrace. In some of the examples presented here, the channel went through periods of both rising and falling in response to a single increase in uplift rate. If the different periods of channel incision were recorded in fluvial terraces, they could be interpreted the response to multiple changes in forcing (Hancock and Anderson 2002). Furthermore, if the decline in channel slopes was recorded in strath terraces, it would probably be associated with a decline in uplift rate and not an increase (Pazzaglia et al. 1998). Channel slopes decline over a significant period of time in some of our experiments as a result of an increase in uplift rate. This decline in slopes could be very misleading if such a record was left in the landscape.

With all three of the sediment flux models, there are periods during the transient in which the channel profile is relatively smooth. One might mistakingly interpret the channel to be at grade, given the lack of knickpoints or notable disequilibrium. This could lead to incorrect interpretations of values such as K and θ.

The transient response to a change in uplift rate is very sensitive to the erosion rule. Whipple and Tucker (2002) illustrated the differences between stream-power detachment-limited channels, transport-limited channels, and mixed channels (a combination of the two). We have expanded on these results using three different sediment-flux erosion models. The key difference between the stream-power model and the rest of the examples here is that the stream-power model is not sensitive to changes upstream. The sediment-flux term represents a variable erodibility that can respond to changes throughout the network. Allowing for a variable erodibility in both space and time can alter network adjustments from the model of a single knickpoint propagating upstream.

Knickpoints have been observed in many channels, so why not stick with the stream-power model? Because knickpoints aren't always the whole story. For example, Blythe et al. (2000) suggest that there has been an acceleration in uplift rate in the San Gabriel Mountains, California, over the last 3Ma. In these drainages, we have observed many higher-order channels that have knickpoints and exposed bedrock. However, landslides are inundating the upstream parts of the drainages

with sediment, and erosion rates appear to be limited by the transport and wear of large boulders. It is likely that the stream-power model could not fully capture transients in such a case.

There are a number of limitations in our model. We do not consider landslides, and this could be an important omission. In essence, our models assumes that sediment delivery from the hillslopes keeps pace with fluvial erosion. If hillslopes adjust over long time scales, this could be an important oversimplification (Fernandes and Dietrich 1997). Episodic inputs of sediment to the channel from landslides or debris flows should have interesting consequences on channel evolution using a sediment-flux erosion model. Furthermore, although we have made some improvements by allowing channel erodibility to respond to a change in uplift rate (as opposed to channel slope only), we do not consider other variables, such as grain size, hydraulic roughness, and channel width. Snyder et al. (2003a) found that channel width did not vary between regions of different uplift rates, but few studies have been made on the adjustment of channel form to uplift rates, leaving room for further investigation.

5.8 Conclusions

We have explored three different models which include sediment flux as an important variable in setting erosion rates. In all cases, equilibrium produces concave channels. Concavity varies in the network due to changes in erodibility, however all models produce reasonable values. Sensitivity of the network to an increase in uplift rate can be dampened or enhanced when the increase in sediment flux is considered. Changes in precipitation rate can also have a complex affect on equilibrium slopes because the sediment transport rate increases with fluvial discharge. Exact changes in channel slope with precipitation depend on the details of the sediment transport model, and a simple sediment transport model is applied in this study.

Transient network response is very sensitive to the applied erosion model. Knickpoint propagation is the sole method for a network to respond to an uplift rate increase using the stream-power model. Using the linear decline model, an increase

in uplift rate can result initially in a knickpoint propagating through the network which does not, however, raise slopes to their new equilibrium values; at later times channel slopes rise throughout the network. The wear model, responds in a similar manner to a transport-limited model; slopes rise throughout the network and there is no knickpoint. Only in the most extreme perturbations will a knickpoint result using the wear model. The almost-parabolic model produces the most surprising transients. Channel slopes can oversteepen initially due to the lag in response of the sediment flux. This can cause a complex pattern of increase and decreasing elevations, both in time and space.

In all of the models, there are periods in which the channel profile is relatively smooth. At these times, one could easily mistake the channel to be at steady state, however the transient concavity and channel slopes vary from their equilibrium values. Declining slopes in response to an increase in uplift rate could leave a very deceptive mark in the landscape. This study highlights that complexities in the total network response may have an important influence on the transient state of the main channel in fluvial bedrock networks.

Chapter 6

Summary and Future Work

6.1 Summary

This study focuses on two very different types of fluvial environments, alluvial and bedrock rivers, but in both cases two important results hold. (1) Steady-state channel networks are concave under a wide range of fluvial erosion processes. However, when variables other than channel slope control erosion rates, the sensitivity of equilibrium channel slopes can change. (2) Transient conditions in response to a shift in boundary conditions are a result of changes in the network as a whole.

We explored the equilibrium sensitivity of the slope-area and texture-area relationships using two different models for sediment transport of grain-size mixtures: the Meyer-Peter and Müller equation (1948) using the Komar (1987) hiding function and the Wilcock (2001) sand and gravel model. Both of these models predict downstream fining and concave channels in equilibrium. Changes in surface texture are linked to changes in channel slope, and in general, finer surfaces have shallower slopes and less concave channels. Under wetter conditions (modeled as higher precipitation rate and, therefore, higher fluvial discharge values across the network), equilibrium slopes are shallower and the surface texture is coarser (or contains more gravel). This is not surprising since the shallower slopes and coarser surface both counteract the increase in fluvial discharge. However, equilibrium sensitivity to uplift rate or, equivalently, base-level lowering rate, is not as straightforward. In some cases, adjustments in sur-

face texture actually allow for shallower slopes in higher uplift conditions; there are also examples in which slope change is negligible or slopes increase with uplift rate as expected. The mutual adjustment of both surface texture and channel slope is critical in determining sediment transport rates and the results predict that it is possible for the surface texture to absorb changes in boundary conditions, rather than the slope.

Some unexpected results are also produced using the heterogeneous sediment-transport model to explore network response to a change in forcing. When the uplift rate is increased (or the base-level lowering rate is increased), the initial response in the network starts at the outlet and moves upstream, as expected. However, slopes over-steepen initially, because the surface texture is adjusting more slowly. Channel slopes begin to decline throughout the main channel while the surface sand content is still increasing and eventually increases to above its new equilibrium value. Both channel slope and surface texture over-adjust to the change in uplift rate, causing periods of decline which would usually be associated with a decrease in uplift rate.

In response to an increase in precipitation rate, the heterogeneous model also predicts very complex results. The entire network responds immediately to a change in precipitation rate. Selective erosion and deposition cause the sand content in the upper parts of the network to increase initially, while lower down in the network, deposition of gravel coarsens the surface. After the initial response, the network begins to erode again everywhere, and the surface sand content increases and, eventually, decreases again. During the transient, network concavity is reduced because of the large rates of incision in the upper parts of the network. In general slopes are decreased everywhere, and in some parts of the network, slopes eventually need to steepen again. All of this complexity results from a single change in precipitation rate.

When sediment flux is considered as a variable driving and/or inhibiting erosion rates in bedrock rivers, some differences in equilibrium morphology result from predictions made using the standard stream-power model. Inclusion of sediment flux essentially allows for spatial variability in the erodibility. In some cases, this leads to curvature in the slope-area plots, or spatially variable concavity. However, natural variability in other parameters that control incision rate could hide the changes in

network concavity, as they are not that extreme. There are some differences in the sensitivity of equilibrium slopes to changes in boundary conditions when the sediment flux is considered. For example, changes in uplift rate, resulting in higher equilibrium sediment-flux values, can enhance or dampen changes in erodibility using the almost parabolic model. This same model also predicts, in some cases, that an increase in precipitation rate, resulting in larger sediment transport rates can result in no change in equilibrium slopes. This result is very sensitive to the sediment transport model used.

The transient response to an increase in uplift rate is highly sensitive to the incision model. The linear-decline model predicts knickpoint propagation initially and steadily increasing slopes throughout the network at later times. The wear model predicts that elevations throughout the network will slowly increase; an increase and decrease in slopes can occur in the most extreme conditions. The almost-parabolic model produces the most dynamic response of all three models explored. Because increases in sediment flux can both increase and decrease erodibility, and because there is a lag in response of the upper parts of the networks, an increase in uplift rate can result in both increasing and decreasing slopes in the main channel. The nature of the response depends both on model parameters and the magnitude of change in uplift rate. With all three models, there are periods during the transient in which the profile is relatively smooth, but the concavity of the network is different (higher or lower) than its equilibrium value.

The results highlight that a single model of cause and effect may not apply to fluvial networks. Deposits of fine material do not necessarily correspond to more arid conditions. Decreasing channel slopes could be temporary and may not imply an overall decrease in erosion rates. Changes in variables other than channel slope can dampen or enhances the response of channel slope. There are many factors controlling erosion rates in rivers, and one needs to consider them all before making an interpretation about the conditions leading to the present morphology of a river network.

6.2 Future Work

There are a number of ways to expand upon the work presented in this thesis. Below are just a few avenues for future research.

1. In chapter 3 we find that changes in surface bed texture can result in shallower channel slopes with higher transport rates at equilibrium. In all of the results presented, the ratio between bed shear stress and critical shear stress varies downstream. This model differs from that proposed by Parker (Parker (1978); Parker (1979)) in which the ratio of bed shear stress to critical shear stress remains constant, and channel geometry adjusts downstream. With such a model, it remains to be seen whether or not texture changes would compensate for the required increase in sediment-transport rate. This area should be explored.

2. We use a very simple model for rainfall, that is we only model a single storm intensity and duration. Variable storm intensities could be important omission from this work. If larger storms do all the work, the channel could be armored with a coarser surface layer that inhibits erosion during smaller storms, even on steeper slopes. Because we use only a single storm intensity, we can not capture these dynamics. In fact, Tucker and Slingerland (1997) found that storm intensity is the important climatic variable. This avenue could be easily explored because CHILD already contains a stochastic rainfall model.

3. In all of this work, we ignore sediment delivery from the hillslopes to the channels. Most likely, hillslope processes add an important degree of complexity which shouldn't be ignored. The results presented using the multiple grain-size model in chapters 3 and 4 assume that the distribution of grain sizes coming off the hillslopes is the same as that transported in the channel. However, it's very possible that the hillslopes are feeding the channel with coarser material from processes such as landslides or with finer material carried through sheet wash. The grain-size distribution of hillslope material could also change in response to a change in boundary conditions and could counter-act the results we pre-

dicted. For example, one might expect a faster uplifting network to experience more landslides, which feed the channels with coarser material. However our results predict that the equilibrium surface texture will become finer in an environment with higher erosion rates. The link between hillslopes and the river network might change these results.

4. The link between hillslopes and channels may also be a critical omission in the study of bedrock rivers in chapter 5. The erosion models we used consider sediment load to be an important variable in determining incision rates into bedrock. Therefore incision rates could be very sensitive to the amount of sediment fed into the channels from the hillslopes. One could imagine that the stochastic nature of hillslopes processes such as landslides could leave an interesting mark in the landscape, causing periods of minimal erosion when the channel is clogged with sediment after a landslide and possibly later periods of enhanced erosion when more sediment is sent downstream acting as tools. These dynamics deserve further attention.

5. Stark and Stark (2001) point out that many variable can respond to a change in boundary conditions. In both the bedrock- and alluvial-channel transient experiments, we do not allow channel geometry to respond to the required changes in erosion rate due to faster uplift rates. It's possible that channels narrow and deepen in response to higher uplift rates, creating local areas of faster incision rates with less adjustments in channel slope. This could greatly affect our results, and a physically based model for changes in channel geometry in response to changes in uplift rate or base-level lowering rate would be an important addition to our model. This area requires further field and laboratory attention.

6. Both Sklar (2003) and Parker (2002) consider much more complicated transport models in their bedrock incision model than we used in this study. Their model accounts for variable grain sizes. We have ignored these details in bedrock channels, and it is well worth exploring. The link between sediment delivery

from the hillslopes to the channels could have important implications not just on the total sediment flux but also on the grain size of sediment being fed into the channels.

References

Adams, J. (1985). Large-scale tectonic geomorphology of the Southern Alps, New Zealand, *in* M. Morisawa and J. T. Hack (eds), *Tectonic Geomorphology*, Publications in Geomorphology, State University of New York, Binghamton, N.Y., pp. 105–128.

Andrews, E. D. (1983). Entrainment of gravel from naturally sorted riverbed material., *Geological Society of America Bulletin* **94**: 1225–1231.

Arbogast, A. and Johnson, W. (1994). Climatic implications of the Late Quaternary alluvial record of a small drainage basin in the Central Great Plains, *Quaternary Research* **41**: 298–305.

Ashida, K. and Michiue, M. (1972). Study on hydraulic resistance and bedload transport rate in alluvial streams, *Transactions, Japan Society of Civil Engineering* **206**: 59–69.

Bagnold, R. A. (1980). An empirical correlation of bedload transport rates in flumes and natural rivers, *Proc. R. Soc. London, Ser. A, 372*, pp. 453–473.

Baker, V. (1973). Erosional forms and processes from the catastrophic Pleistocene Missoula floods in eastern washington, *in* M. Morisawa (ed.), *Fluvial Geomorphology*, Publications in Geomorphology, State University of New York, Binghamton, N.Y., pp. 123–148.

Baker, V. (1977). Stream-channel response to floods, with examples from central Texas, *Geological Society of America Bulletin* **88**: 1057–1071.

Baldwin, J., Whipple, K. and Tucker, G. (2003). Implications of the shear stress river incision model for the timescale of postorogenic decay of topography, *Journal of Geophysical Research* **108**.

Beaumont, C., Fullsack, P. and Hamilton, J. (1992). Erosional control of active compressional orogens, *in* K. McClay (ed.), *Thrust Tectonics*, Chapman and Hall, New York, pp. 1–18.

Bernet, M., Zattin, M., Garver, J., Brandon, M. and J.A., V. (2001). Steady-state exumation of the European Alps, *Geology* **29**: 35–38.

Blum, M. D. and Valastro, S. (1989). Response of the Pedernales River of Central Texas to late Holocene climate change, *Annals of the Association of American Geographers* **79**(3): 435–456.

Blythe, A., Burbank, D., Farley, K. and Fielding, E. (2000). Structural and topographic evolution of the central Transverse Ranges, California from apatite fission-track, (U-Th)/He and digital elevation model analyses, *Basin Research* **12**: 97–114.

Bonnet, S. and Crave, A. (2003). Landscape response to climate change: Insights from experimental modeling and implications for tectonic versus climatic uplift of topography, *Geology* **31**(2): 123–126.

Bourke, M. and Pickup, G. (1999). Fluvial form variability in arid central Australia, *in* A. Miller and A. Gupta (eds), *Varieties of Fluvial Form*, John Wiley & Sons Ltd, pp. 249–271.

Bras, R., Tucker, G. and Teles, V. (2003). Six myths about mathematical modeling in geomorphology, *in* P. Wilcock and R. Iverson (eds), *Prediction in Geomorphology*, American Geophysical Union, pp. 63–79.

Braun, J. and Sambridge, M. (1997). Modelling landscape evolution on geological time scales: a new method based on irregular spatial discretization, *Basin Research* **9**: 27–52.

Bridge, J. and Dominic, D. (1984). Bed load grain velocities and sediment transport rates, *Water Resources Research* **20**(4): 476–490.

Bryan, K. (1928). Historic evidence on changes in the channel of the Rio Puerco, a tributary of the Rio Grande in New Mexico, *Journal of Geology* **36**: 265–282.

Buffington, J. and Montgomery, D. (1999). Effects of sediment supply on surface textures of gravel-bed rivers, *Water Resources Research* **35**: 3523–3530.

Butzer, K. (1980). Holocene alluvial sequences: Problems of dating and correlation, *in* R. Cullingford, D. Davidson and J. Lewin (eds), *Timescales in geomorphology*, John Wiley & Sons, Ltd., London, pp. 131–142.

Carling, P. (1983). Threshold of coarse sediment transport in broad and narrow natural streams, *Earth Surface Processes and Landforms* **8**: 1–18.

Chitale, S. (2003). Modeling for width adjustment in alluvial rivers, *Journal of hydraulic engineering* **129**: 404–407.

Chow, V. (1959). *Open-channel hydraulics*, McGraw-Hill.

Church, M. (1985). Bed load in gravel-bed rivers: Observed phenomena and implications for computation., Canadian Society for Civil Engineering Annual Conference.

Collins, D. (2002). *Modeling the effects of vegetation-erosion coupling on landscape evolution*, Master's thesis, Massachusetts Institute of Technology. 171 p.

Costa, J. (1978). Holocene stratigraphy in flood frequency analysis, *Water Resources Research* **14**: 626–632.

Coulthard, T. J., Kirkby, M. J. and Macklin, M. G. (2000). Modelling geomorphic response to environmental change in an upland catchment, *Hydrological Processes* **14**(11-12): 2031–2045.

Cui, Y., Parker, G. and Paola, C. (1996). Numerical simulation of aggradation and downstream fining, *Journal of Hydraulic Research* **34**(2): 185.

Day, T. J. (1980). A study of initial motion characteristics of particles in graded bed material, current research, part a, *Technical Report 80-1A*, Geological Survey of Canada.

Du, C. (1996). An algorithm for automatic delaunay triangulation of arbitrary planar domains, *Advances in Engineering Software* **27**: 21–26.

Eagleson, P. (1978). Climate, soil, and vegetation: 2. the distribution of annual precipitation derived from observed storm sequences, *Water Resources Research* **14**: 713–721.

Egiazaroff, I. (1965). Calculation of nonuniform sediment concentrations, *Journal of the Hydraulics Division, American Society of Civil Engineers* **91**: 225–247.

Einstein, H. (1950). The bedload function for sediment transport in open channel flows., *Technical Bulletin 1026*, United States Department of Agriculture, Soil Conservation Service, Washington, D.C.

Ellis, M. A., Densmore, A. L. and Anderson, R. S. (1999). Development of mountainous topography in the Basin Ranges, USA, *Basin Research* **11**: 21–41.

Emmett, W. (1980). A field calibration of the sediment-trapping characteristics of the Helley-Smith bedload sampler, *USGS Professional Paper* **1139**.

Emmett, W., Myrick, R. and Martinson, H. (1985). Hydraulic and sediment-transport data, East Fork River, Wyoming, *Open-File Report 85-486*, USGS.

Emmett, W., Myrick, R. and Meade, R. (1980). Field data describing the movement and storage of sediment in the East Fork River, Wyoming, Part 1. River hydraulics and sediment transport, 1979, *Open-File Report 80-1189*, USGS.

Engelund, F. and Fredsoe, J. (1976). A sediment transport model for straight alluvial channels, *Nordic Hydrology* **7**: 293–306.

Fernandes, N. and Dietrich, W. (1997). Hillslope evolution by diffusive processes: the timescale for equilibrium adjustments, *Water Resources Research* **33**: 1307–1318.

Fernandez Luque, R. and van Beek, R. (1976). Erosion and transport of bedload sediment, *Journal of Hydraulic Research* **14**(2): 127–144.

Flint, J. J. (1974). Steam gradient as a function of order, magnitude, and discharge, *Water Resources Research* **10**(5): 969–973.

Foley, M. (1980). Bed-rock incision by streams, *Geological Society of America Bulletin* **91**: 2189–2213.

Fuller, I., Macklin, M., Lewin, J., Passmore, D. and Wintle, A. (1998). River response to high-frequency climate oscillations in southern Europe over the past 200 k.y., *Geology* **26**(3): 275–278.

Gardner, T. (1983). Experimental study of knickpoint and longitudinal profile evolution in cohesive, homogeneous material, *Geological Society of America Bulletin* **94**: 664–672.

Gasparini, N. M. (1998). *Erosion and deposition of multiple grain sizes in a landscape evolution model*, Master's thesis, Massachusetts Institute of Technology.

Gasparini, N. M., Tucker, G. E. and Bras, R. L. (1999). Downstream fining through selective particle sorting in an equilibrium drainage network, *Geology* **27**(12): 1079–1082.

Gasparini, N., Tucker, G. and Bras, R. (2003). Network-scale dynamics of grain-size sorting: implications for downstream fining, stream-profile concavity and drainage basin morphology, *Earth Surface Processes and Landforms* . in Press.

Gilbert, G. K. (1877). Report of the geology of the Henry Mountains, *Technical report*, U.S. Geological Survey, Rocky Mountain Region. 160p.

Hack, J. T. (1957). Studies of longitudinal stream profiles in Virginia and Maryland, *United States Geological Survey Professional Papers* **294-B**: 45–97.

Hammond, F., Heathershaw, A. and Langhorne, D. (1984). A comparison between Shields' threshold criterion and the movement of loosely packed gravel in a tidal channel, *Sedimentology* **31**: 51–62.

Hancock, G. and Anderson, R. (2002). Numerical modeling of fluvial strath-terrace formation in response to oscillating climate, *Geological Society of America Bulletin* **114**: 1131–1142.

Hancock, G., Anderson, R. and Whipple, K. (1998). Beyond power: Bedrock river incision process and form, *in* K. Tinkler and E. Wohl (eds), *Rivers Over Rock: Fluvial Processes in Bedrock Channels*, American Geophysical Union, pp. 35–60.

Hartshorn, K., Hovius, N., Dade, W. and Slingerland, R. (2002). Climate-driven bedrock incision in an active mountain belt, *Science* **297**: 2036–2038.

Hoey, T. B. and Ferguson, R. I. (1997). Controls of strength and rate of downstream fining above a river base level, *Water Resources Research* **33**(11): 2601–2609.

Hovius, N., Stark, C., Chu, H. and Lin, J. (2000). Supply and removal of sediment in a landslide-dominated mountain belt: Central Range, Taiwan, *Journal of Geology* **108**: 73–89.

Howard, A. (1980). Thresholds in river regimes, *in* D. Coates and J. Vitek (eds), *Thresholds in Geomorphology*, Allen and Unwin, pp. 227–258.

Howard, A. (1997). Badland morphology and evolution: interpretation using a simulation model, *Earth Surface Processes and Landforms* **22**: 211–227.

Howard, A. D. (1994). A detachment-limited model of drainage basin evolution, *Water Resources Research* **30**: 2261–2285.

Howard, A. D. (1999). Simulation of gully erosion and bistable landforms, *in* S. E. Darby and S. Andrew (eds), *Incised river channels; processes, forms, engineering and management*, J. Wiley, pp. 277–299.

Howard, A., Seidl, M. and Dietrich, W. (1994). Modelling fluvial erosion on regional to continental scales, *Journal of Geophysical Research* **99**(B7): 13971–13986.

Huntington, E. (1924). *The Climatic Factor as Illustrated in Arid America*, Carnegie Institution Publication. 192 pgs.

Ijjasz-Vasquez, E. J., Bras, R. L. and Moglen, G. E. (1992). Sensitivity of a basin evolution model to the nature of runoff production and to initial conditions, *Water Resources Research* **28**(10): 2733–2741.

Knox, J. (1972). Valley alluviation in Southwestern Wisconsin, *Annals of the association of American geographers* **62**(3): 401–410.

Knox, J. (1983). Responses of river systems to Holocene climates, *in* H. Wright and S. Porter (eds), *Late Quaternary Environments of the United States: Volume 2, The Holocene*, University of Minnesota Press, Minneapolis, pp. 26–41.

Komar, P. D. (1987). Selective grain entrainment by a current from a bed of mixed sizes: a reanalysis., *Journal of Sedimentary Petrology* **57**(2): 203–211.

Kooi, H. and Beaumont, C. (1994). Escarpment evolution on high-elevation rifted margins: Insights derived from a surface processes model that combines diffusion, advection, and reaction, *Journal of Geophyscial Research* **99**(12): 12191–12209.

Kuhnle, R. (1992). Fractional transport rates of bedload on Goodwin Creek, *in* P. Billi, R. Hey, C. Thorne and P. Tacconi (eds), *Dynamics of Gravel-bed Rivers*, John Wiley and Sons Ltd.

Kuhnle, R. A. (1993). Incipient motion of sand-gravel sediment mixtures., *Journal of Hydraulic Engineering* **119**(12): 1400–1415.

Lancaster, S. (1998). *A nonlinear river meandering model and its incorporation in a landscape evolution model*, PhD thesis, Massachusetts Institute of Technology.

Leopold, L. B. and Maddock, T. (1953). The hydraulic geometry of stream channels and some physiographic implications, *United States Geological Survey Professional Paper* **252**: 1–57.

Leopold, L. B., Wolman, M. G. and Miller, J. P. (1964). *Fluvial Processes in Geomorphology*, Dover Publications.

Li, Y. (1976). Denudation of Taiwan island since the Pliocene epoch, *Geology* **4**: 105–107.

Liew, P., Hsieh, M. and Lai, C. (1990). Tectonic significance of Holocene marine terraces in the Coastal Range, eastern Taiwan, *Tectonophysics* **183**: 121–127.

Lisle, T. (1989). Sediment transport and resulting deposition in spawning gravels, north coastal California, *Water Resources Research* **25**(6): 1303–1319.

Mackin, J. (1948). Concept of the graded river, *Geological Society of America Bulletin* **59**: 463–512.

Meyer-Peter, R. and Müller, R. (1948). Formulas for bedload transport, *Proceedings 2nd Meeting International Association of Hydraulic Research*, Stockholm, pp. 39–64.

Milhous, R. T. (1973). *Sediment transport in a gravel-bottomed stream.*, PhD dissertation, Oregon State University.

Miller, S., Slingerland, R. and Kirby, E. (2002). Landscape evolution in orogens with significant lateral advection of rock: Insights from numerical simulations of fault-bend folds, *Eos, Transactions of the American Geophysical Union* **83**. Fall Meeting Supplement.

Moglen, G. and Bras, R. (1995). The effect of spatial heterogeneities on geomorphic expression in a model of basin evolution, *Water Resources Research* **31**(10): 2613–2623.

Molnar, P. (2001). Climate change, flooding in arid environments, and erosion rates, *Geology* **29**: 1071–1074.

Montgomery, D. and Gran, K. (2001). Downstream variations in the width of bedrock channels, *Water Resources Research* **37**: 1841–1846.

Morisawa, M. (1968). *Streams: their dynamics and morphology*, McGraw-Hill Book Company.

Mulligan, M. (1998). Modelling the geomorphological impact of climatic variability and extreme events in a semi-arid environment, *Geomorphology* **24**: 59–78.

Niemann, J., Gasparini, N., Tucker, G. and Bras, R. (2001). A quantitative evaluation of playfair's law and its use in testing long-term stream erosion models, *Earth Surface Processes and Landforms* **26**(12): 1317–1332.

Paola, C. and Seal, R. (1995). Grain size patchiness as a cause of selective deposition and downstream fining, *Water Resources Research* **31**(5): 1395–1407.

Parker, G. (1978). Self-formed rivers with stable banks and mobile bed: Part II, the gravel river, *Journal of Fluid Mechanics* **89**: 127–148.

Parker, G. (1979). Hydraulic geometry of active gravel rivers., *Journal of Hydraulics Division, American Society of Civil Engineering* **105**(HY9): 1185–1201.

Parker, G. (1990). Surface-based bedload transport relation for gravel rivers, *Journal of Hydraulic Research* **28**: 417–436.

Parker, G. (1991). Selective sorting and abrasion of river gravel. I: Theory, *Journal of Hydraulic Engineering* **117**(2): 131–149.

Parker, G. (1997). Explaining the half-power dependence of bankfull river width on bankfull discharge, *Eos, Transactions of the American Geophysical Union* **78**. Fall Meeting Supplement.

Parker, G. (2002). Somewhat less random notes on bedrock incision. Unpublished.

Parker, G. and Klingeman, P. C. (1982). On why gravel bed streams are paved., *Water Resources Research* **18**(5): 1409–1423.

Parker, G., Klingeman, P. C. and McLean, D. G. (1982). Bedload and size distribution in paved gravel-bed streams., *Journal of the Hydraulics Division, Proceedings of the American Society of Civil Engineers* **108**(HY4): 544–571.

Pazzaglia, F., Garner, T. and Merritts, D. (1998). Bedrock fluvial incision and longitudinal profile development over geologic time scales determined by fluvial terraces, *in* K. Tinkler and E. Wohl (eds), *Rivers Over Rock: Fluvial Processes in Bedrock Channels*, American Geophysical Union, pp. 207–235.

Pizzuto, J. E. (1995). Downstream fining in a network of gravel-bedded rivers, *Water Resources Research* **31**: 753–759.

Prosser, I., Chappell, J. and Gillespie, R. (1994). Holocene valley aggradation and gully erosion in headwater catchments, Sout-Eastern Highlands of Australia, *Earth Surface Processes and Landforms* **19**: 465–480.

Reid, I., Laronne, J. and Powell, D. (1999). Impact of major climate change on coarse-grained river sedimentation: a speculative assessment based on measured flux, *in* A. Brown and T. Quine (eds), *Fluvial Processes and Environmental Change*, John Wiley & Sons Ltd, pp. 105–115.

Rinaldo, A., Dietrich, W., Rigon, R., Vogel, G. and Rodriquez-Iturbe, I. (1995). Geomorphological signatures of varying climate, *Nature* **374**: 632–635.

Roe, G., Montgomery, D. and Hallet, B. (2002). Effects of orographic precipitation variations on the concavity of steady-state river profiles, *Geology* **30**(2): 143–146.

Rosenbloom, N. and Anderson, R. (1994). Hillslope and channel evolution in a marine terraced landscape, santa cruz, california, *Journal of Geophysical Research* **99**: 14013–14029.

Schumm, S. (1968). River adjustment to altered hydrologic regime - Murrumbidgee River and paleochannels, Australia, *Professional Paper 598*, US Geological Survey.

Schumm, S. (1973). Geomorphic thresholds and complex response of drainage systems, *in* M. Morisawa (ed.), *Fluvial Geomorphology*, Publications in Geomorphology, State University of New York, Binghamton, NY, pp. 299–310.

Seidl, M. and Dietrich, W. (1992). The problem of channel erosion into bedrock, *Catena Supplement* **23**: 101–124.

Shields, A. (1936). Application of similarity principles and turbulence research to bedload movement. *mitteilungen der preussischen versuchsanstalt für wasserbau und schiffbau*, Berlin, *W. M. Keck Laboratory of Hydraulics and Water Resources Report 167*, California Institute of Technology, Pasadena, Ca. Ott, W. P., and Uchelen, J. C., translators, 43p.

Sinha, S. K. and Parker, G. (1996). Causes of concavity in longitudinal profiles of rivers, *Water Resources Research* **32**(5): 1417–1428.

Sklar, L. (2003). *The influence of grain size, sediment supply and rock strength on rates of river incision into bedrock*, PhD thesis, University of California, Berkeley.

Sklar, L. and Dietrich, W. (2001). Sediment and rock strength controls on river incision into bedrock, *Geology* **29**: 1087–1090.

Sklar, L. and Dietrich, W. E. (1998). River longitudinal profiles and bedrock incision models: Stream power and the influence of sediment supply, *in* K. J. Tinkler and E. E. Wohl (eds), *Rivers Over Rock: Fluvial Processes in Bedrock Channels, Geophysical Monograph*, Vol. 107, American Geophysical Union, Washington, D.C., pp. 237–260.

Slaymaker, O. (1990). Climate change and erosion processes in mountain regions of Western Canada, *Mountain Research and Development* **10**(2): 171–182.

Slingerland, R., Willett, S. and Hennessey, H. (1997). A new fluvial bedrock erosion model based on the work-energy principle, *Eos, Transactions of the American Geophysical Union* **78**. Fall Meeting Supplement F299.

Snow, R. S. and Slingerland, R. L. (1987). Mathematical modeling of graded river profiles, *Journal of Geology* **95**: 15–33.

Snyder, N. P., Whipple, K. X., Tucker, G. E. and Merritts, D. J. (2000). Landscape response to tectonic forcing: Digital elevation model analysis of stream profiles in the Mendocino triple junction region, northern California, *GSA Bulletin* **112**(8): 1250–1263.

Snyder, N., Whipple, K., Tucker, G. and Merritts, D. (2002). Interactions between onshore bedrock-channel incision and nearshore wave-base erosion forced by eustasy and tectonics, *Basin Research* **14**: 105–127.

Snyder, N., Whipple, K., Tucker, G. and Merritts, D. (2003a). Channel response to tectonic forcing: Analysis of stream morphology and hydrology in the Mendocino triple junction region, norther California, *Geomorphology* **53**: 97–127.

Snyder, N., Whipple, K., Tucker, G. and Merritts, D. (2003b). Importance of a stochastic distribution of floods and erosion thresholds in the bedrock river incision problem, *Journal of Geophysical Research* **108**.

Stark, C. and Stark, G. (2001). A channelization model of landscape evolution, *American Journal of Science* **301**: 486–512.

Sternberg, H. (1875). Untersuchungen über längen- und querprofil geschiebeführender flüss, *Zeitschrift für Bauwesen* **25**: 483–506.

Stock, J. and Montgomery, D. (1999). Geologic constraints on bedrock river incision using the stream power law, *Journal of Geophysical Research* **104**: 4983–4993.

Sugai, T. (1993). River terrace development by concurrent fluvial processes and climatic changes, *Geomorphology* **6**: 243–252.

Summerfield, M. (1991). *Global Geomorphology*, Longman Scientific & Technical, Essex, England.

Tarboton, D., Bras, R. and Rodriquez-Iturbe, I. (1991). On the extraction of channel networks from digital elevation data, *Hydrological Processes* **5**: 81–100.

Tarboton, D. G., Bras, R. L. and Rodriguez-Iturbe, I. (1989). The analysis of river basins and channel networks using digital terrain data, *Technical Report 326*, Massachusetts Institute of Technology, Ralph M. Parsons Laboratory.

Teles, V., Capolongo, D. and Bras, R. (2002). A physically-based model for rainfall-triggered landslides at a regional scale, *Proceedings of the European Geophysical Society* **EGS02-A-03808**.

Tomkin, J., Brandon, M., Pazzaglia, F., Barbour, J. and Willett, S. (2003). Quantitative testing of bedrock incision models for the Clearwater River, NW Washington state, *Journal of Geophysical Research* . in press.

Tucker, G. (2003). Drainage basin sensitivity to tectonic and climatic forcing: implications of a stochastic model for the role of entrainment and erosion thresholds, *Earth Surface Processes and Landforms* . in press.

Tucker, G. E. and Bras, R. L. (1998). Hillslope processes, drainage density, and landscape morphology, *Water Resources Research* **34**(10): 2751–2764.

Tucker, G. E. and Slingerland, R. L. (1996). Predicting sediment flux from fold and thrust belts, *Basin Research* **8**: 329–349.

Tucker, G. E. and Slingerland, R. L. (1997). Drainage basin responses to climate change, *Water Resources Research* **33**(8): 2031–2047.

Tucker, G, E. and Whipple, K. (2002). Topographic outcomes predicted by stream erosion models: Sensitivity analysis and intermodel comparison, *Journal of Geophysical Research* **107**.

Tucker, G., Lancaster, S., Gasparini, N. and Bras, R. (2001). The channel-hillslope integrated landscape development model (child), *in* R. Harmon and W. Doe (eds), *Landscape Erosion and Evolution Modeling*, Kluwer Academic/Plenum Publishers, pp. 349–388.

Tucker, G., Lancaster, S., Gasparini, N., Bras, R. and Rybarczyk, S. (2001). An object-oriented framework for distributed hydrologic and geomorphic modeling using triangulated irregular networks, *Computers and Geosciences* **27**: 959–973.

van Niekerk, A., Vogel, K. R., Slingerland, R. L. and Bridge, J. S. (1992). Routing of heterogeneous sediments over movable bed: Model development, *Journal of Hydraulic Engineering* **118**(2): 246–261.

Whipple, K. (2001). Fluvial landscape response time: how plausible is steady-state denudation?, *American Journal of Science* **301**: 313–325.

Whipple, K. (n.d.). Bedrock rivers and the geomorphology of active orogens. in review.

Whipple, K., Hancock, G. and Anderson, R. (2000). River incision into bedrock: Mechanics and relative efficacy of plucking, abrasion, and cavitation, *Geological Society of America Bulletin* **112**: 490–503.

Whipple, K., Snyder, N. and Dollenmayer, K. (2000). Rates and processes of bedrock incision by the Upper Ukak River since the 1912 Novarupta ash flow in the Valley of Ten Thousand Smokes, Alaska, *Geology* **28**: 835–838.

Whipple, K. X., Kirby, E. and Brocklehurst, S. H. (1999). Geomorphic limits to climate-induced increases in topographic relief, *Nature* **401**: 39–43.

Whipple, K. X. and Tucker, G. E. (1999). Dynamics of the stream-power river incision model; implications for height limits of mountain ranges, landscape response timescales, and research needs, *Journal of Geophysical Research, B, Solid Earth and Planets* **104**: 17661–17674.

Whipple, K. X. and Tucker, G. E. (2002). Implications of sediment-flux dependent river incision models for landscape evolution, *Journal of Geophysical Research, B, Solid Earth and Planets* **107**(2).

Wilcock, P. I. (2001). Toward a practical method for estimating sediment-transport rates in gravel-bed rivers, *Earth Surface Processes and Landforms* **26**: 1395–1408.

Wilcock, P. R. (1998). Two-fraction model of initial sediment motion in gravel-bed rivers, *Science* **280**: 410–412.

Wilcock, P. R. and McArdell, B. W. (1993). Surface-based fractional transport rates: mobilization thresholds and partial transport of a sand-gravel sediment., *Water Resources Research* **29**(4): 1297–1312.

Wilcox, B., Pitlick, J., Allen, C. and Davenport, D. (1996). Runoff and erosion from a rapidly eroding pinyon-juniper hillslope, *in* M. Anderson and S. Brooks (eds), *Advances in Hillslope Processes*, Vol. 1, John Wiley & Sons Ltd., pp. 61–77.

Willgoose, G. (1994). A physical explanation for an observed area-slope-elevation relationship for catchments with declining relief, *Water Resources Research* **30**: 151–159.

Willgoose, G., Bras, R. L. and Rodriquez-Iturbe, I. (1991). Results from a new model of river basin evolution, *Earth Surface Processes and Landforms* **16**: 237–254.

Wilson, K. (1966). Bedload transport at high shear stresses, *Journal of Hydraulic Engineering* **92**(6): 49–59.

Wohl, E. (1993). Bedrock channel incision along Piccanniny Creek, Australia, *Journal of Geology* **101**: 749–761.

Wohl, E. (1998). Bedrock channel morphology in relation to erosional processes, *in* K. Tinkler and E. Wohl (eds), *Rivers Over Rock: Fluvial Processes in Bedrock Channels*, American Geophysical Union, pp. 133–151.

Wohl, E. and Ikeda, H. (1997). Experimental simulation of channel incision into a cohesive substrate at varying gradients, *Geology* **25**: 295–298.

Wolman, M. G. (1955). The natural channel of brandywine creek pennsylvania, *Professional Paper 271*, United States Geological Survey.

Yalin, M. S. (1963). An expression for bedload transportation, *Journal of Hydraulics Division, American Society of Civil Engineering* **89**(HY3): 221–250.

Yatsu, E. (1955). On the longitudinal profile of the graded river, *American Geophysical Union Transactions* **36**(4): 655–663.